DYNAMIC MECHANICAL BEHAVIOR OF MAGNESIUM ALLOYS UNDER SHOCK LOADING CONDITION

A Thesis Submitted to the College of
Graduate Studies and Research
In Partial Fulfillment of the Requirements
For the Degree of Doctor of Philosophy
In the Department of Mechanical Engineering
University of Saskatchewan
Saskatoon

By
Hamed Asgari Moslehabadi

PERMISSION TO USE

In presenting this thesis in partial fulfilment of the requirements for a postgraduate degree from the University of Saskatchewan, I agree that the Libraries of this University may make it freely available for inspection. I further agree that permission for copying of this thesis in any manner, in whole or in part, for scholarly purposes may be granted by the professors who supervised my thesis work or, in their absence, by the Head of the Department or the Dean of the College in which my thesis work was done. It is understood that any copying or publication or use of this thesis or parts thereof for financial gain shall not be allowed without my written permission. It is also understood that due recognition shall be given to me and to the University of Saskatchewan in any scholarly use which may be made of any material in my thesis.

Requests for permission to copy or to make other use of material in this thesis in whole or part should be addressed to:

Head of the Department of Mechanical Engineering
57 Campus Dr.
University of Saskatchewan
Saskatoon, Saskatchewan (S7N 5A9)

ABSTRACT

The use of magnesium and its alloys, as the lightest structural materials, to decrease the weight, improve the fuel efficiency and reduce the greenhouse gas emissions has significantly increased in the automotive and aerospace industries in recent years. However, magnesium alloys are commonly used as die casting products. The current application of wrought magnesium alloy products is limited because of their poor ductility at room temperature due to the formation of a strong texture and restricted active deformation modes in wrought magnesium products. Moreover, to support the application of magnesium alloys in automobile and airplane components, their dynamic mechanical response must be determined to evaluate their behavior during impact events such as car crash and bird strike in airplanes. Therefore, in this research study, the dynamic mechanical behavior of magnesium alloys at high strain rates was investigated. The effects of initial texture, composition, strain rate and grain size on the deformation mechanism were also determined.

Split Hopkinson Pressure Bar was used to investigate the dynamic mechanical behavior of the magnesium alloys. Texture analysis on the alloy prior and after shock loading was done using X-ray diffraction. Scanning electron microscopy was used to study the microstructural evolution in the alloys before and after shock loading. Chemical analysis and phase identification were done by energy dispersive spectroscopy and X-ray diffraction analysis, respectively. Additionally, twinning type and distribution was determined by means of orientation imaging microscopy whereas dislocation types and distribution was determined using transmission electron microscopy. A visco-plastic self-consistent simulation was used to corroborate the experimental textures and possible deformation mechanisms.

The dynamic mechanical behavior of cast AZ and AE magnesium alloys with different chemistries was investigated at strain rates ranging between 800 to 1400 s^{-1} to determine the effects of composition on the response of the alloys to shock loading. It was found that an increase in the aluminum content of the AZ alloys increased the volume fraction of β-$Mg_{17}Al_{12}$ and Al_4Mn phases, strength and strain hardening but, on the other hand, decreased the ductility and twinning fraction, particularly extension twinning fraction, for all the investigated strain rates. In addition, increasing the strain rate resulted in considerable increase in strength of the alloys. Texture measurements showed that shock loading of the AE alloys resulted in development of a stronger (00.2) basal

texture in samples with higher content of yttrium at the investigated strain rates. Increasing the yttrium content of the cast AE alloys decreased twinning fraction but increased dislocation density and volume fraction of the Al_2Y second phase. As a result, the tensile strength and ductility of the alloys increased which is an interesting result for high-strain rate applications of AE alloys in comparison to AZ alloys.

The dynamic mechanical behavior of rolled AZ31B and WE43 magnesium alloys were also studied at strain rates ranging between 600 to 1400 s^{-1}. A strong (00.2) basal texture was observed in all shock loaded AZ31B samples. It was also observed that increasing the strain rate led to an increase in strength and ductility, but to a decrease in twinning fraction. A high degree of mechanical anisotropy was found for all investigated strain rates so that the lowest strength was registered for the samples cut along the direction parallel to the rolling direction. Furthermore, it was found that at high strain rates, fine-grained AZ31B alloy exhibits better ductility and strength compared to coarse-grained alloy. However, the hardening rate of coarse-grained alloy was higher.

In the case of rolled WE43 alloy, it was found that the strength and ductility increased and twinning fraction decreased with increase in strain rate. Furthermore, another effect of increase in strain rate was the higher activation of pyramidal <c+a> slip systems. In addition, degree of stress and strain anisotropy is low particularly at higher strain rates, which is mainly related to the weak initial texture of the samples due to the presence of rare earth elements. Furthermore, strength and ductility were found to decrease with increasing grain size, while twinning fraction, activity of double and contraction twins and strain hardening rate increase with increasing grain size. In both AZ31B and WE43 alloy, the presence of <c+a> dislocations was confirmed at high strain rates using ‘g.b’ analysis confirming activation of pyramidal <c+a> slip systems during dynamic shock loading.

ACKNOWLEDGMENTS

My immense thanks go to all of the following:

My supervisors, Prof. Jerzy Szpunar and Prof. Akindele Odeshi, for their endless patience and understanding that carried me through my PhD program and I wish to express my gratitude for their insights and comments that helped me sharpen my research skills. I feel very fortunate for being one of their graduate students.

My PhD advisory committee members, Prof. Qiaoqin Yang, Prof. Ikechukwuka Oguocha and Prof. Leon Wegner for their constructive comments and discussions.

Prof. Eva Olsson, for her valuable support and comments during the time I spent at Chalmers University of Technology in Sweden.

Faculty and staff members of Department of Mechanical Engineering at University of Saskatchewan, especially Prof. James Bugg and Prof. Reza Fotouhi, for their support and attention.

Faculty and staff members of Department of Applied Physics at Chalmers University of Technology, especially Dr. Lunjie Zeng and Dr. Stefan Gustafsson, for their friendly and effective help and support.

Auto21 and NSERC discovery grant program for financial support.

My friends and colleagues, at University of Saskatchewan and Chalmers University of Technology, for being helpful and creating such a pleasant working environment.

My adorable family, for their unconditional support and encouragement. I never could have done any of this without you.

Farideh, the love of my life and my best friend till the end, for her support and all the beautiful feelings, particularly when the tasks seemed overwhelming.

DEDICATION

I dedicate this thesis to my lovely wife and my beloved parents for their unconditional love and support.

TABLE OF CONTENTS

LIST OF TABLES

LIST OF FIGURES

ACRONYMS

RE	Rare Earth
SHPB	Split Hopkinson Pressure Bar
PF	Pole Figure
IPF	Inverse Pole Figure
IQ	Image Quality
TB	Twin Boundary
PSN	Particle Stimulated Nucleation
CRSS	Critical Resolved Shear Stress
VPSC	Visco Plastic Self Consistent
EDS	Energy Dispersive Spectroscopy
OIM	Orientation Imaging Microscopy
EBSD	Electron Backscattered Diffraction
SEM	Scanning Electron Microscope
TEM	Transmission Electron Microscope
BF	Bright Field
XRD	X-ray Diffraction

CHAPTER 1

INTRODUCTION

One of the promising solutions for global environmental and energy problems, such as global warming, greenhouse gas emissions and the exhaustion of fossil energy resources, is increased use of lightweight materials in the transportation industries. Mechanical properties of lightweight materials can be significantly modified without losing reliability by optimizing their microstructure in order to enhance their suitability for high performance structural applications. Increased use of magnesium alloys, as the well-known lightest structural material, can contribute to the weight reduction of transportation structures. In the automotive and aircraft industries, magnesium alloys have continued to attract increasing attention as a structural material with the aim of improving fuel economy, enhancing passenger safety and reducing greenhouse gas emissions.

Magnesium has a hexagonal closed packed crystallographic structure and the density of magnesium at room temperature is 1.74 g/cm^3 [1, 2]. Magnesium is available in large quantities in the earth and in seawater and can be extracted from several minerals such as dolomite and magnesite. Due to its lowest density among all structural metals, magnesium is widely used in various applications such as automotive, aerospace and aeronautics, electronics and communications [2-4].

High strength-to-density ratio, high damping capacity, good machinability and weldability of magnesium alloys make them appropriate candidates for applications where weight saving, fuel efficiency and environmental conservation are critical criteria, such as aircraft and automotive industries. Recently, the average magnesium usage in each vehicle in North America has increased considerably and more magnesium components are used in automotive industries [5]. Although magnesium is largely available, the usage of magnesium in the industry is limited and this element

is mainly used as an alloying addition to aluminum alloys. Also, a considerable percentage of magnesium usage is related to die casting of magnesium alloys, and a very restricted amount of magnesium is used in magnesium wrought products [6].

There are mainly two reasons for the low usage of magnesium alloy sheets. The first reason is the poor formability of magnesium and its alloys at low temperatures, which is attributed to the restricted active slip systems [1,2,3-7]. The second reason is a strong crystallographic texture which develops in wrought magnesium alloys during deformation processes such as rolling, which results in the low formability [1,2,3-8]. This basal texture will arrange most of the basal planes parallel to the sheet surface which is a difficult orientation for deformation along crystallographic c-axis of the unit cells. Due to the insufficient number of active slip systems at room temperature, it is not possible to accommodate the imposed strain along the normal direction of the sheet and premature fracture takes place. Although it is possible to increase the formability of magnesium alloys at high temperatures, hot forming of magnesium will significantly increase its production cost and is not economical.

Anisotropy is another result of the strong crystallographic texture in wrought magnesium alloys. In rolled magnesium sheets, the strong basal texture leads to an anisotropy in mechanical behavior. Mechanical anisotropy increases with increase in texture strength in magnesium sheets. This behavior can be ascribed to the activation of extension twins during the deformation of rolled magnesium sheets. One effective method to improve the formability of wrought magnesium alloys is to optimize or randomize the texture by addition of rare earth elements. The texture randomizing effect of rare earth elements may weaken the strong texture in wrought magnesium alloys, resulting in better mechanical properties of these alloys.

The main problem with magnesium and its alloys is therefore their low formability that should be improved. Besides, components made of magnesium alloys in the aerospace and automotive industries can be subjected to dynamic loading or high strain rate deformation. Considering the fact that the materials show a different mechanical behavior at high strain rates compared with low strain rate condition, it is necessary to understand the dynamic response of magnesium alloys, as influenced by such parameters as the initial texture, chemical composition, strain rate and grain size, under shock loading conditions.

Unfortunately, dynamic deformation behavior of magnesium alloys, particularly rare earth element containing magnesium alloys, has received relatively little attention and most of the studies

in the field of magnesium alloys are focused on the low strain rate deformation behavior of these alloys. Furthermore, to date, there is no systematic study in the literature about the texture development, microstructural evolution and deformation mechanism of magnesium alloys deformed under compressive shock loading conditions.

In this research study, high strain rate deformation behavior of magnesium alloys was investigated and effects of key parameters such as the initial texture, grain size, composition and strain rate, on the dynamic mechanical response and deformation mechanisms of magnesium alloys under shock loading conditions are determined. In addition, several characterization methods were used to analyze the texture formation and microstructural changes in magnesium alloys at high strain rates. The results of this project provide an in-depth understanding of the dynamic mechanical response and deformation mechanism of magnesium alloys subjected to high strain rates.

1.1. Objectives of the project

The overall goal of this research was to investigate the dynamic deformation behavior of magnesium alloys at high strain rates. Additionally, considering the facts that initial texture, composition, strain rate and grain size affect the deformation behavior of magnesium alloys under shock loading conditions, the specific objectives are outlined as follows:

1. Determine the effect of chemical composition and strain rate on the deformation behavior of cast magnesium alloys under shock loading conditions.
2. Determine the effects of initial texture, strain rate and grain size on the dynamic mechanical behavior of rolled magnesium alloys under shock loading conditions.
3. Determine the deformation mechanism(s) of magnesium alloys under shock loading conditions.

To fulfill the above-mentioned objectives, some cast and rolled magnesium alloys were selected, which are widely used in automotive and aerospace industries but for which there is very restricted information about their dynamic deformation behavior in the open literature.

The results of experimental investigations addressing the research objectives are published in reputable peer review journals and presented in Chapters 2, 3, 4, 5, 6 and 7:

In Chapter 2, the deformation behavior of three cast AZ magnesium alloys with variation in aluminum content is discussed in relation to texture formation, microstructural changes and mechanical response. The effects of strain rates on the dynamic response of three cast AZ alloys under shock loading are also presented and discussed. This manuscript is published in the journal: *Materials & Design*.

The results of the investigations on the deformation behavior of rare-earth element containing cast AE alloys are presented and discussed in Chapter 3. The effects of yttrium content and strain rates on the mechanical response and microstructural evolution in the AE alloys at high strain rates are also discussed. This manuscript is published in the journal: *Materials Science and Engineering A.*

In Chapter 4, the effects of initial texture and strain rate on the mechanical behavior and deformation mechanisms in rolled AZ31B alloy are discussed. This manuscript is published in the journal: *Materials Science and Engineering A*.

The effects of initial texture and strain rate on the dynamic mechanical behavior of rolled WE43 alloy and deformation mechanism are discussed in Chapter 5. This manuscript is published in the journal: *Materials & Design*.

In Chapter 6, the results of experimental investigations on the effects of grain size on the high strain-rate deformation behavior of rolled AZ31B alloy are discussed. This manuscript was submitted to the journal: *Materials Characterization*. It is currently under review.

The effects of grain size on the deformation behavior of rolled WE43 alloy under shock loading conditions are discussed in Chapter 7. This manuscript is published in the journal: *Materials Science and Engineering A.*

The conclusions drawn from experimental studies and suggestions for future work are outlined in Chapter 8.

In the next section, a brief literature review of related background about properties, deformation mechanisms and high strain rate deformation behavior of magnesium alloys is presented. It should be mentioned that in the introduction sections of Chapters 2 to 7, a literature survey for each part of this research is presented. To avoid repetition, therefore, this chapter does not include a detailed literature review.

1.2.Literature review

1.2.1. Magnesium Alloys: Properties and Application

Magnesium has a hexagonal closed packed (HCP) crystallographic structure. The lattice parameters of magnesium unit cell are: $a_1 = a_2 = 0.321$, $c = 0.521$, $c/a = 1.624$, $\alpha = \beta = 90°$ and $\gamma = 120°$. The atomic packing factor and coordination number of magnesium are 0.74 and 12, respectively. The density of magnesium at room temperature is 1.74 g/cm^3 which is very close to that of nylon and is the least for all engineering metals [1, 2]. High strength-to-density ratio, high specific stiffness, high damping capacity, good machinability, weldability and castability of magnesium alloys make them appropriate candidates particularly for automotive and aerospace industries which weight saving and fuel efficiency are very important criteria.

Magnesium alloys usually contain up to 8% Al with additions of Mn, Zn, Zr, Si, RE elements and Li. In general, there are three groups of magnesium alloys based on the chemical composition and alloying elements added to them [7]:

- Group 1: Mg-Mn (e.g. M1, M2 alloys); Mg-Al-Zn (e.g. AZ31 and AZ91 alloys); Mg-Zn-(Mn,Cu) (e.g. ZM21, ZC71 alloys).
- Group 2: Mg-Zn-Zr (e.g. ZK30 and ZK60 alloys); Mg-Zn-Re (e.g. ZE10 alloy); Mg-Y-RE-Zr (e.g. WE43 alloy); Mg-Th (e.g. HK31 and HZ11 alloy).
- Group 3: Mg-Li-Al (LA141 alloy).

After deformation, alloying elements in magnesium alloys can be classified into three groups [7]:

- Elements that increase both strength and formability of the alloy: Examples of strength-increasing alloying elements in the order of decreasing strengthening are Al, Zn, Ca, Ag, Ce and Th. Those elements that increase formability in the order their increasing effects on formability are Th, Zn, Ag, Ce, Ca and Al.
- Elements that increase formability but do not have considerable effect on the strength of the alloy: Examples include Cd, Ti and Li.
- Elements that increase the strength of the alloy but are detrimental for the formability such as Sn, Pb, Bi and Sb.

The current application of magnesium and its alloys is unfortunately restricted to the cast magnesium products due to their low production cost. Compared to cast products, wrought

magnesium alloys such as rolled or extruded magnesium alloys however exhibit better mechanical properties such as strength and ductility. They are therefore better candidates for use in automobile and airplane components, particularly where the ductility and strength are the key parameters. Unfortunately, a widespread application of wrought magnesium products is limited due to their low formability at low temperatures and the strong texture which develops in wrought magnesium alloys during deformation processes such as rolling (Fig. 1.1), resulting in high magnitude of plastic anisotropy [1,2,3-5,8].

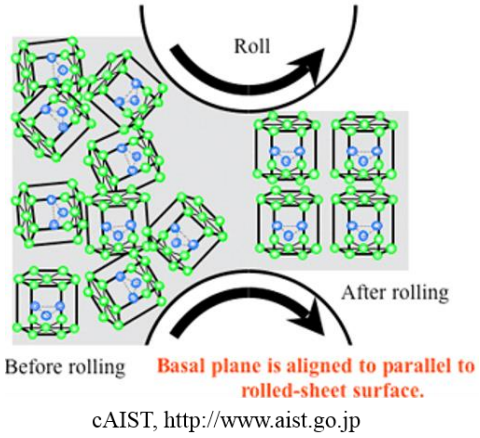

Fig. 1.1. Schematic of the formation of basal texture in rolled magnesium sheet [9].

Twin roll casting (TRC) has been shown to be an effective process to control the texture and microstructure of the magnesium sheets and includes casting and rolling in one processing step [10]. The strips which are produced by twin roll casting have a fine-grained microstructure and the texture can be changed by adjusting the casting and rolling conditions during twin roll casting. In general, there are two types of TRC which depends on the arrangement of the rolls: vertical and horizontal. The vertical TRC is usually used in steel industry and horizontal TRC is common in the nonferrous alloy industries such as magnesium and aluminum [10]. It should be mentioned that both vertical and horizontal TRC can be used for fabrication of magnesium alloy strips. Since it is relatively easy to control the uniformity of melt distribution in horizontal TRC, wide magnesium sheets can be produced by this method [11]. However, when fast casting and higher cooling rate is required, vertical TRC is used. Changing the casting and rolling speed in TRC may affect the texture and consequently the mechanical properties of the magnesium strip [11].

1.2.2. Deformation Mechanisms

1.2.2.1. Slip

As mentioned previously, the poor formability of magnesium alloys is related to the HCP crystal structure of magnesium, which has a limited number of active slip systems to accommodate the imposed strain. Based on the von Mises-Taylor criterion [12,13], a minimum of five active slip systems are required to avoid brittle fracture with minimal plastic deformation in magnesium alloys. In magnesium and its alloys, there are three possible Burgers vectors that can be activated on basal, prismatic and pyramidal planes during the deformation (Fig. 1.2). The main slip system in magnesium and its alloys is basal slip, which is the slip of dislocations with a $< 11\bar{2}0 >$Burgers vector on the close-packed (0001) planes. Other deformation modes that can be activated in magnesium are prismatic slip $\{1\bar{1}00\} < 11\bar{2}0 >$ and pyramidal slip $\{10\bar{1}1\} < 11\bar{2}0 >$. It should be mentioned that the critical resolved shear stress (CRSS) for the basal slip is very low (~0.5 MPa). However, the CRSS of non-basal slip modes such as pyramidal slip system is very high at low temperatures (< 200° C), implying that the activation of non-basal slip systems will be difficult at low temperatures [14-19]. The values of CRSS significantly decreases to low values at high temperatures as shown in Fig. 1.3. This decrease in the CRSS values at elevated temperatures occurs due to activation of new slip system to satisfy the minimum required in the von Mises-Taylor criterion. The activation of prismatic and pyramidal slips systems at elevated temperatures easies dislocation glide on these slip systems leading to increase in ductility and the material's ability to accommodate large strains before fracture. At low temperatures, the activation of prismatic and pyramidal slip systems is restricted to the vicinity of grain boundaries. Therefore, it can be possible to increase the formability of a magnesium alloy at low temperatures by grain refinement owing to the fact that activation of non-basal slip systems may be extended to the entire grain in a fine-grained alloy [20].

In single crystals of magnesium, basal slip is the dominant deformation mode at room temperature due to its very low CRSS. However, in polycrystalline magnesium and its alloys, the deformation behavior is different. This difference is mainly related to the presence of many grains which may have different orientations. Activation of basal slip can only offer two independent slip systems which is less than the required five deformation modes to satisfy von-Mises criterion. When von-Mises criterion is not fulfilled in the grains, strain is not accommodated and therefore,

dense pile ups of dislocations will occur at grain boundaries generating high stress concentrations that result in the activation of non-basal slip modes, fracture or twinning [16-21].

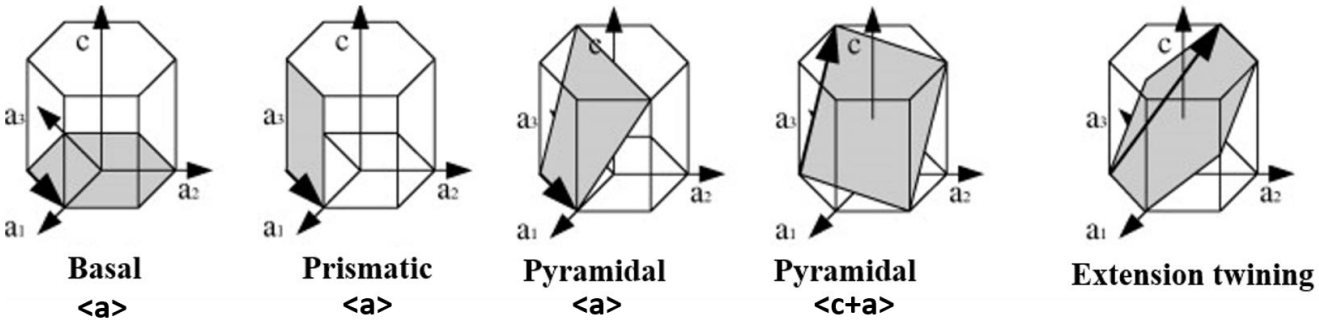

Fig. 1.2. Main (primary) deformation mechanisms in magnesium and its alloys [22].

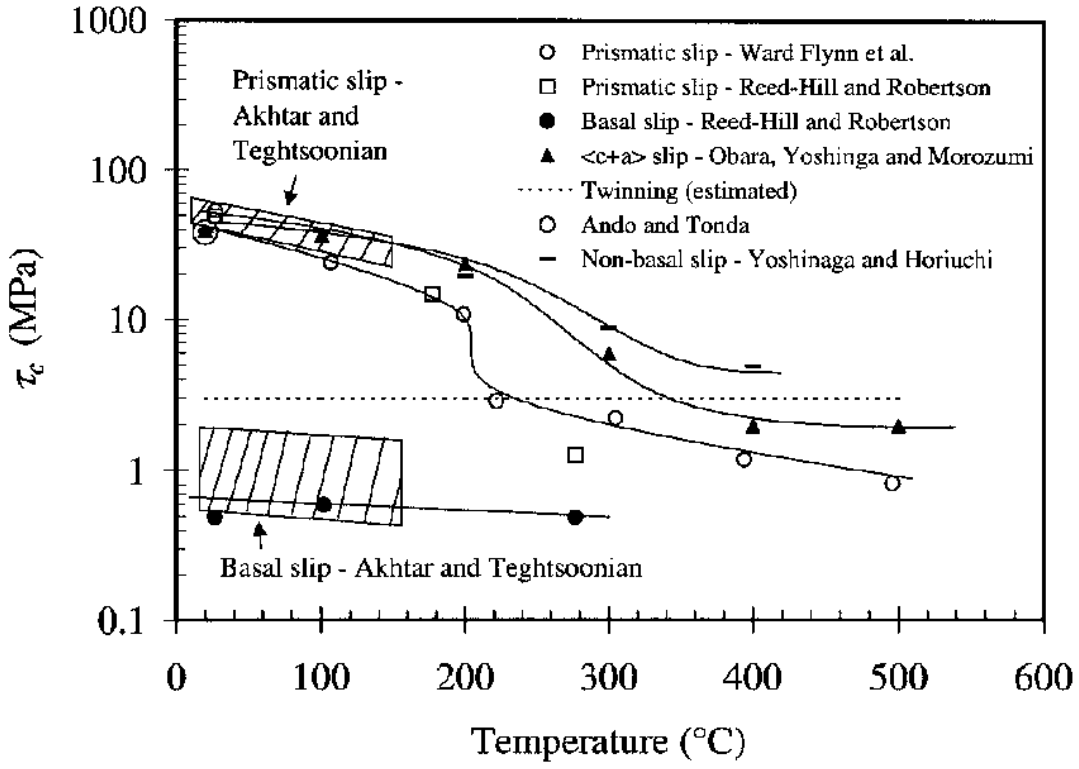

Fig. 1.3. The effect of deformation temperature on the CRSS value of slip systems in pure magnesium [23].

In some research, the activation of pyramidal slip system in magnesium alloys has been established at room temperature. For example, in an ECAE AZ31 magnesium alloy, with fine grains, considerable number of the total dislocations observed after a room temperature are of pyramidal type (<c+a> dislocations). The activation and presence of this high density of <c+a> dislocations were ascribed to the high level of grain boundary compatibility stress in the fine-grained structure [18]. The same phenomenon has been found by self-consistent modeling of plastic deformation in AZ31B alloy [24].

Considering the fact that <a> slip direction is perpendicular to the c-axis in HCP structure, <a> slip systems cannot accommodate any strain, including extension or contraction, along the c-axis. The only deformation modes which are able to accommodate strain along the c-axis are twinning or pyramidal <c + a> slip. However, at low temperatures, the pyramidal slip is not activated because of its high CRSS, and twinning is consequently the dominant deformation mechanism, resulting in extension or contraction along the c-axis [16-19].

1.2.2.2. Twinning

As a result of limited number of active slip systems in magnesium and its alloys, twinning becomes an important plastic deformation mode in in these materials. The three types of deformation twins observed in magnesium and magnesium alloys are: $\{10\bar{1}2\}$ extension (tension), $\{10\bar{1}1\}$ or $\{10\bar{1}3\}$ contraction (compression) and double twins [21, 25, 26]. Of these, $\{10\bar{1}2\}$ extension twin is the only one which accommodate extension strains parallel to the c-axis. In fact, $\{10\bar{1}2\}$ extension twin forms when a tensile stress is applied along a direction parallel to the c-axis or a compressive stress is applied in the normal direction to the c-axis. The CRSS of the extension twinning (2-3 MPa) is the smallest of those of the twinning systems in magnesium alloys, and it is only higher than that of basal slip. Therefore, it is activated easily at the early stages of deformation process and yielding behavior is affected by this twinning. One of the most important effects of the $\{10\bar{1}2\}$ extension twins is that they reorient basal planes by 86° about $< 1\bar{2}10 >$ axis, causing a significant change in the texture [21, 25, 26].

Contraction $\{10\bar{1}1\}$ or $\{10\bar{1}3\}$ twins, may accommodate contraction strain along c-axis. These twins are activated when a compressive stress is applied parallel to the c-axis or when tensile stress is applied perpendicular to the c-axis. Basal planes reorient by 56° about $< 1\bar{2}10 >$ axis by the activation of contraction twins [21, 25, 26]. The first in the occurrence of double twinning is the

reorientation of the matrix along $\{10\bar{1}1\}$ or $\{10\bar{1}3\}$ plane. In the next step, the twinned region may reorient along $\{10\bar{1}2\}$ plane. As a result, unfavorably oriented basal planes may assume a more favorable orientation for slip inside the twinned region. Double twinning, including $\{10\bar{1}1\}$-$\{10\bar{1}2\}$ and $\{10\bar{1}3\}$ - $\{10\bar{1}2\}$ twins, may reorient the basal planes at an angle of 38° and 22° from their original positions, respectively. It is worth noting that double twinning systems can accommodate contraction strain along the c-axis [21, 25, 26].

As mentioned, the CRSS of the extension twinning is very small and this system is activated very easily. For some other deformation modes, the CRSS values are reported by several authors [27-30] to be 0.5-0.8 MPa for basal slip , 45-81 MPa for pyramidal <c+a> slip and 76-153 MPa for contraction twinning. Twin boundaries can act as strong barriers to dislocation motion. Therefore, dense pile-ups of dislocations form behind the twin boundaries, resulting in generation of relatively high local stress concentrations at twin boundaries. This stress could be relieved by nucleation and growth of other types of twins or crack formation [31].

Some of the parameters affecting twinning in magnesium alloys include temperature, grain size and strain rate [32-34]. For example, it has been shown that the Hall-Petch slope of twinning is greater than the Hall-Petch slope of slip [33]. This suggests that a decrease in grain size can result in a larger increase in twinning stress than the stress required for slip activation. Therefore, reducing the grain size can lead to decrease in twinning activation. Therefore, twinning fraction is expected to be low in fine-grained alloys. Conversely, decreasing the temperature and increasing the strain rate will lead to the increase in twinning [32-34].

In general, activation and formation of different twinning systems during the deformation of magnesium and its alloys will result in tension-compression asymmetry [16, 20]. Therefore, to reduce the tension-compression asymmetry and improve the mechanical properties of magnesium alloys, the strong texture of wrought alloys should be weakened or randomized [35, 36]. One of the suitable methods to improve the texture of commercial magnesium alloys is the addition of rare earth elements such as yttrium (Y).

1.2.3. Rare Earth (RE) Addition to Mg Alloys

In conventional wrought magnesium alloys such as AZ31, the formability is very limited due to the strong basal texture which restrict the operation of basal and prismatic slip (Fig. 1.4(a)). In the texture of as-rolled magnesium sheet, is such that most of the grains are oriented such that their

basal poles are perpendicular to the sheet plane. The strong basal texture will place most of the grains in an orientation that makes deformation difficult, leading to a high yield stress, medium hardening rate and low ductility [37]. The textured sheets have a strong tension-compression strength asymmetry which is related to the polar nature of mechanical twinning. This tension-compression strength asymmetry is removed by randomizing the texture [38-40].

It is believed that addition of rare earth elements such as yttrium and neodymium to magnesium alloys can encourage the formation of a weak or random-like texture in the alloys [41-44]. The pole figure of the commercial magnesium alloys, such as AZ31B, shows a strong basal texture (Fig. 1.4 (a)). However, in the pole figure of rare earth containing magnesium alloys such as WE43, there is an angular distribution which is slightly broader toward RD. Also, there is a splitting of the basal poles by ±20 from ND toward RD (Fig. 1.4(b)). Recrystallization seems to play an important role in changing the texture of rare-earth containing magnesium alloys. Particle-stimulated nucleation (PSN) of recrystallization has been shown to be the main formation mechanism of the randomized texture of rare-earth containing magnesium alloys. Magnesium sheets with random or weak texture exhibit better formability and lower anisotropy [45].

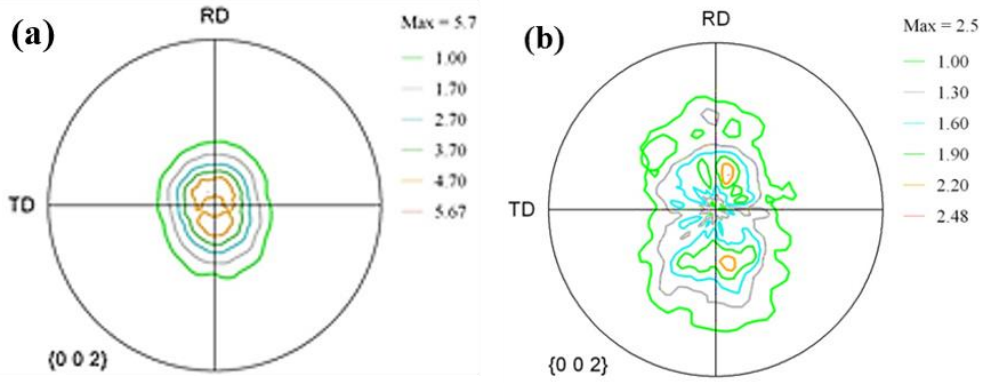

Fig. 1.4. (a) Strong basal texture of as-rolled AZ31B sheet and (b) weak (random-like) texture of the rare earth containing as-rolled WE43 magnesium sheet.

Agnew et al. [46] have ascribed the splitting of basal poles to the activation of <c+a> slip system, which results in a double-peak basal pole figure as shown in Fig. 1.4. Additionally, twinning has been considered as another mechanism that promotes the splitting of basal poles [47]. The texture-randomizing effect of rare earth additions would be attributed to the recrystallization behavior. The

texture which results from the recrystallization depends on both nuclei orientations and growth process. In general, four nucleation mechanisms have been proposed for magnesium alloys:

1. Nucleation of new grains at grain boundaries because of the significant deformation near grain boundaries in which the non-basal slip mechanisms may accommodate it. In this case, new grains are formed at the vicinity of the grain boundaries and results in the formation of a necklace-type microstructure. The original deformation texture is slightly affected by this mechanism [48, 49].
2. Coalescence of low angle boundaries due to the motion of subgrain boundaries, leading to the formation of high angle boundaries. Activation of non-basal slip systems may encourage this mechanism to occur. This mechanism is also not considered to be very effective in altering the deformation texture [50].
3. Variety of shear band types which are considered to be suitable sites for nucleation including the activation of basal slip in some poorly oriented grains that results in the formation of kink bands and also deformation twins. These bands can affect the overall texture of the material [50,51].
4. Particle-stimulated nucleation (PSN) can result from the generation of local inhomogeneity in the strain energy and orientation by particles. The particles may increase the driving force for recrystallization and serve as suitable sites for nucleation. PSN would result in more randomly oriented nuclei and consequently, a weaker or random-like texture will develop [41, 44].

1.2.4. High Strain Rate Deformation

The mechanical behavior of materials at high strain rates is different from that under low strain rate loading condition. This difference stems from the lack of equilibrium at high strain rates. In other words, the stress state of the material is near equilibrium in quasi-static loading whereas under shock loading condition, no equilibrium is established and deformation in material is generated by stress wave [52].

At the atomic scale, the wave can be considered as a series of successful collisions between neighboring atoms. Each atom is accelerated to a certain velocity and its momentum is totally or partially transmitted to the neighboring atom. The shape and velocity of the wave can be affected by mass, attraction and repulsion forces between atoms [53]. In general, there are two deformation

modes under dynamic shock loading condition. When the yield strength of the material is less than the stress wave magnitude, plastic deformation takes place. In contrast, only elastic deformation occurs when the magnitude of the stress wave is smaller than the yield strength of the material [53].

1.2.4. High Strain-rate Behavior of Magnesium Alloys

Most of the studies on magnesium alloys have been conducted using quasi-static loading to evaluate the mechanical properties. However, there are a few reports on the dynamic mechanical behavior some magnesium alloys under shock loading conditions. However, their deformation mechanisms at different strain rates have not been adequately studied. Several parameters affecting the mechanical behavior at high strain rates such as initial texture, temperature, strain rate and grain size, and their effects on the deformation behavior of magnesium alloys are not yet clearly understood. The results of some compression tests on AZ31 and AZ91 cast alloys indicated that the main deformation mechanism for strain rates lower than $0.1s^{-1}$ is dislocation creep. At higher strain rates, however, dislocation glide and twinning were reported to be the dominant deformation modes [54,55]. Tensile experiments on the aforementioned alloys for strain rate up to $10s^{-1}$ showed that tensile deformations are mainly governed by dislocation glides [56].

Some researchers have underscored the significant effects of strain rate on room temperature deformation of wrought AZ31 alloy [57]. The effect of temperature, however, has been reported to be less significant during high strain rate deformation of AZ31 alloy. This suggests that diffusion is not a rate-controlling factor at high strain rates. The effect of strain rate on the deformation of the AZ31 at room temperature was generation of more deformation twins in the samples deformed at low strain rates [57]. Formation of fewer twins at higher strain rate was ascribed to the flow localization. In another research, increasing strain rates from 0.01 to $10s^{-1}$ led to increased twin fraction at deformation temperature of 573K. At the strain rate of $10\ s^{-1}$ and temperature range of 473-673 K, it was found that twinning fraction decreased up to 573K but, with further increase in the temperature, twinning fraction drastically decreased [58].

As mentioned earlier, very few research studies have been done on the deformation of rolled magnesium alloys at high strain rates. High strain-rate compressive tests on AZ31B plate were conducted in different directions and at varying strain rates. A large magnitude of anisotropy was observed after the tests (Fig. 1.5). It was also found that the ductility increased with increasing the

strain rate when the load was applied in normal direction. However, the ductility decreased with increased strain rate when the loading was done in rolling and transverse directions [59].

Dynamic mechanical behavior of AZ31B-O sheets and the associated microstructural strain rates ranging from10^{-3} s^{-1} to 10^{3} s^{-1} in both tension and compression, and at different temperatures [60]. It was observed that a strong mechanical anisotropy existed even at high temperatures (up to 400°C), (Fig. 1.6). Additionally, tension-compression asymmetry was observed at high temperatures (Fig. 1.6). At low strain rates, however, tension-compression asymmetry nearly disappeared at temperatures higher than 200°C [60]. This behavior could be attributed to the activation of non-basal slip modes at elevated temperature during mechanical loading at low strain rates. [58]. In a study performed by Barnett et al. [57] on the deformation behavior of AZ31 alloy, a transition from twinning to slip mechanism was observed at low strain rates. They found that decrease in grain size promotes transition from twinning to slip whereas decrease in temperature has an opposite effect.

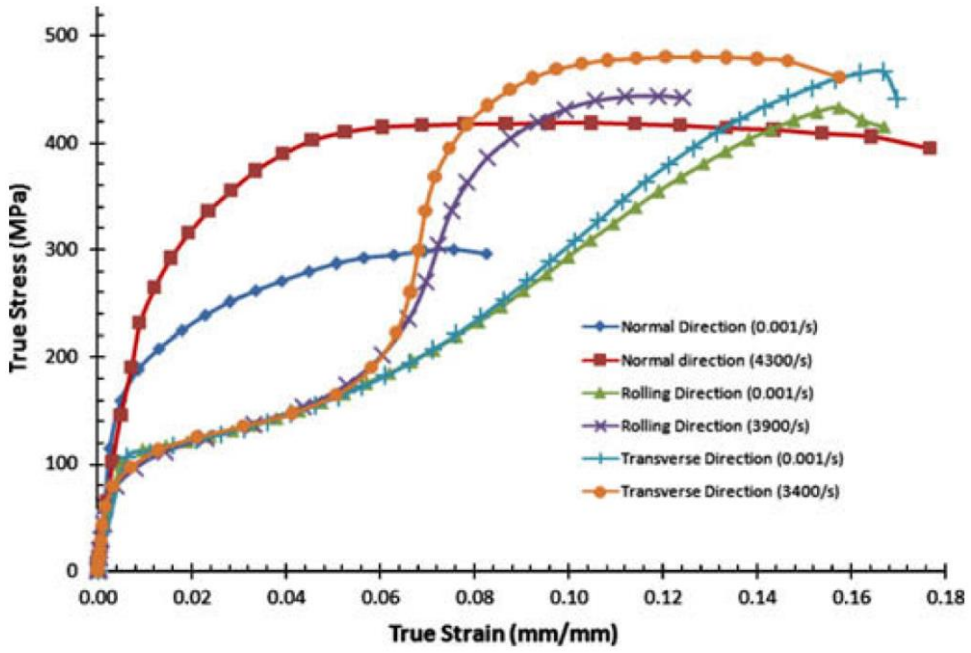

Fig. 1.5. Compressive true stress-strain curves of AZ31B at different strain rates and loading directions
[59].

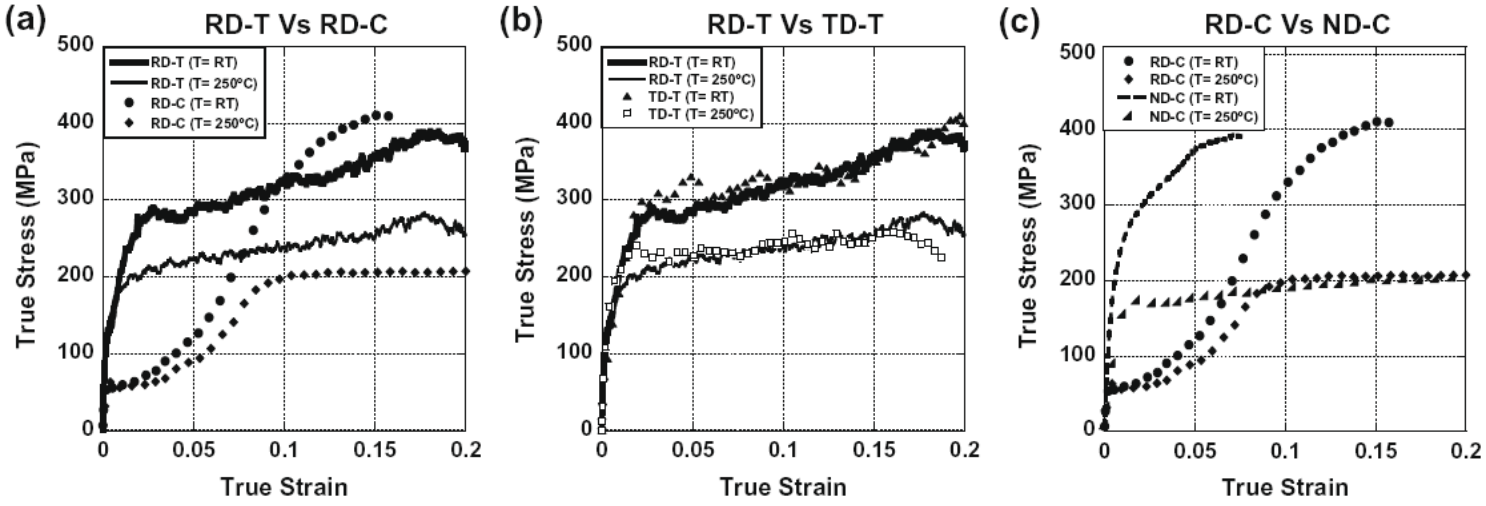

Fig. 1.6. True stress–true strain curves for the tests performed at high strain rate ($10^3 s^{-1}$) at room temperature and at 250 °C in different loading directions: (a) RD-T vs. RD-C,(b) RD-T vs. TD-T, and(c) RD-C vs. ND-C. (RD: rolling direction, TD: transverse direction, ND: normal direction, T: tensile, C: compression) [60].

References

[1] Holloway CE, Melnik M. Magnesium compounds: Classification and analysis of crystallographic and structural data. Journal of Organometallic Chemistry 1994; 465:1-63.

[2] Eliezer D, Aghion E, Froes FH. Magnesium science, technology and applications. Advanced Performance Materials 1998; 5:201-212.

[3] Li Q. Mechanical properties and microscopic deformation mechanism of polycrystalline magnesium under high-strain-rate compressive loadings. Materials Science and Engineering A 2012; 540:130-134.

[4] Korla R, Chokshi AH. Strain-rate sensitivity and microstructural evolution in a Mg–Al–Zn alloy. Scripta Materialia 2010; 63: 913-916.

[5] Cole GS. Issues that influence magnesium's use in the automotive industry. Materials Science forum 2003; 419-422:43-50.

[6] Paramsothy M, Tan XH, Chan J, Kwok R, Gupta M. Al2O3 nanoparticle addition to concentrated magnesium alloy AZ81: Enhanced ductility. Journal of Alloys and Compounds 2012; 545:12–18.

[7] Xu Y, Hu LX, Sun Y. Hot deformation behavior and microstructure evolution of as-cast AZ91D magnesium alloy without pre-homogenization treatment. Rare Metals 2013; 32: 338-346.

[8] Koike J, Kobayashi T, Mukai T, Watanabe H, Suzuki M, Maruyama K, Higashi K. The activity of non-basal slip systems and dynamic recovery at room temperature in fine-grained AZ31B magnesium alloys. Acta Materialia 2003;51:2055-2065.

[9] http://www.aist.go.jp/aist_e/latest_research/2008/20081105/20081105.html.

[10] Park SS, Park WJ, Kim CH, You BS, Kim NJ. The twin roll casting of magnesium alloys. JOM 2009; 61:14-18.

[11] Ding PD. Twin roll strip casting of magnesium alloys in China. Transactions of Nonferrous Metals Society of China 2008; 18: 57.

[12] von Mises R, Angew Z. Mechanics of plastic deformation of crystals. Journal of Applied Mathematics and Mechanics 1928; 8:161-185.

[13] Taylor GI. Plastic strain in metals. Journal of Institute of Metals 1938; 62:307-324.

[14] Mordike BL, Ebert T. Magnesium: Properties — applications — potential. Materials Science and Engineering A 2001;302: 37-45.

[15] Lou XY, Li M, Boger RK, Agnew SR, Wagoner RH. Hardening evolution of AZ31B Mg sheet. International Journal of Plasticity 2007; 23:44-86.

[16] Jiang L, Jonas JJ, Luo AA, Sachdev AK, Godet S. Influence of {10-12} extension twinning on the flow behavior of AZ31 Mg alloy. Materials Science and Engineering A 2007;445-446: 302:309.

[17] Yoo MH. Slip, twinning, and fracture in hexagonal close-packed metals. Metallurgical and Materials Transactions A 1981;12:409.

[18] Koike J, Kobayashi T, Mukai T, Watanabe H, Suzuki M, Maruyama K, Higashi K. The activity of non-basal slip systems and dynamic recovery at room temperature in fine-grained AZ31B magnesium alloys. Acta Materialia 2003;51:2055-2065.

[19] Hao M, Zhang F, Tan C, Su T, Yu X. Effects of anisotropy on the microstructural characteristics and mechanical behavior of shock loaded AZ31 alloy. Advanced Materials Research 2011; 284-286:1537-1541.

[20] Obara T, Yoshinga H, Morozumi S. {1122}〈1123〉 Slip system in magnesium. Acta Metallurgica 1973; 21:845-853.

[21] Mukai T, Yamanoi M, Watanabe H, Ishikawa K, Higashi K. Effect of grain refinement on tensile ductility in ZK60 magnesium alloy under dynamic loading. Materials Transactions 2001; 42:1177-1181.

[22] Mayama T, Aizawa K, Tadano Y, Kuroda M. Influence of twinning deformation and lattice rotation on strength differential effect in polycrystalline pure magnesium with rolling texture. Computational Materials Science 2009; 47:448-455.

[23] Barnett MR. A Taylor model based description of the proof stress of magnesium AZ31 during hot working. Metallurgical and Materials Transactions A 2003; 34:1799–1806.

[24] Agnew SR, Duygulu O. Plastic anisotropy and the role of non-basal slip in magnesium alloy AZ31B. International Journal of Plasticity 2005; 21:1161-1193.

[25] Wonsiewicz BC, Backofen WA. Plasticity of Magnesium Crystals. Trans. Metall. Soc. AIME 1967;239:1422–1431.

[26] Buchanan ER, Reed-Hill RE. On the mechanism of rotational slip in magnesium single crystals.Trans. Metall. Soc. AIME 1960; 218:554–558.

[27] Koike J, Enhanced deformation mechanisms by anisotropic plasticity in polycrystalline Mg alloys at room temperature. Metallurgical and Materials Transactions A 2005;36:1689-1696.

[28] Conrad H, Robertson WD. JOM 1957; 9:503-512.

[29] Reed-Hill RE, Robertson WD. Additional modes of deformation twinning in magnesium. Acta Metallurgica 1957; 5:717-727.

[30] Reed-Hill RE, Robertson WD. JOM 1957; 9:496-502.

[31] Yoo MH. Slip, twinning, and fracture in hexagonal close-packed metals. Metallurgical and Materials Transactions A 1981;12:409.

[32] Wang JT, Yin DL, Liu JQ, Tao J, Su YL, Zhao X. Effect of grain size on mechanical property of Mg–3Al–1Zn alloy. Scripta Materialia 2008; 59:63–66.

[33] Barnett MR, Keshavarz Z, Beer AG, Atwell D. Influence of grain size on the compressive deformation of wrought Mg–3Al–1Zn. Acta Materialia 2004; 52: 5093-5103.

[34] Del Valle JA, Carreño F, Ruano OA. Influence of texture and grain size on work hardening and ductility in magnesium-based alloys processed by ECAP and rolling. Acta Materialia 2006;54:4247–4259.

[35] Huang S, Li M, Drews A, Hangas J, Allison J, Li D, Peng Y. Evolution of microstructure and texture during uniaxial compression of cast AZ31 Mg alloy at elevated temperatures. Metallography, Microstructure, and Analysis 2012; 1: 297-308.

[36] Stanford N, Barnett M. Effect of composition on the texture and deformation behaviour of wrought Mg alloy. Scripta Materialia 2008;58:179–182.

[37] Bohlen J, Nürnberg MR, Senn JW, Letzig D, Agnew SR. The texture and anisotropy of magnesium–zinc–rare earth alloy sheets. Acta Materialia 2007; 55: 2101-2112.

[38] Mann G, Griffiths JR, Cáceres CH. Hall-Petch parameters in tension and compression in cast Mg–2Zn alloys. Journal of Alloys and Compounds 2004; 378:188–91.

[39] Ando S, Tanaka M, Tonda H. Pyramidal Slip in Magnesium Alloy Single Crystals. Materials Science Forum 2003;419–422:87–92.

[40] Agnew SR, Senn, JW, Horton JA. Mg sheet metal forming: Lessons learned from deep drawing Li and Y solid-solution alloys. JOM 2006; 58:62–69.

[41] Ball EA, Prangnell PB. Tensile-compressive yield asymmetries in high strength wrought magnesium alloys. Scripta Metallurgica et Materialia 1994; 31:111-116.

[42] Senn JW, Agnew SR. proceedings of magnesium technology in the global age, Montreal, 2007.

[43] Yang Z, Li JP, Zhang JX, Lorimer GW, Robson J. Review on Research and Development of Magnesium Alloys. Acta Metallurgica Sinica 2008; 21:313-328.

[44] Song WQ, Beggs P, Easton M. Compressive strain-rate sensitivity of magnesium–aluminum die casting alloys. Materials & Design 2009; 30:642–648.

[45] Humphreys FJ. The nucleation of recrystallization at second phase particles in deformed aluminium. Acta Metallurgica 1977;25:1323–1344.

[46] Agnew SR, Yoo MH, Tomé CN. Application of texture simulation to understanding mechanical behavior of Mg and solid solution alloys containing Li or Y. Acta Materialia 2001;49:4277–4289.

[47] Ahmad IR, Shu DW. Dynamic response of magnesium alloy AZ31B under high strain rate compressive loading. Applied Mechanics and Materials 2011; 83:60-65.

[48] Ashby MF. The deformation of plastically non-homogeneous materials. Philosophical Magazine 1970; 21:399–424.

[49] Ion SE, Humphreys FJ, White SH. Dynamic recrystallisation and the development of microstructure during the high temperature deformation of magnesium. Acta Materialia 1982;30:1909–1919.

[50] Galiyev A, Kaibyshev R, Gottstein G. Correlation of plastic deformation and dynamic recrystallization in magnesium alloy ZK60. Acta Materialia 2001;49:1199–1207.

[51] Myshlyaev MM, McQueen HJ, Mwembela A, Konopleva E. Twinning, dynamic recovery and recrystallization in hot worked Mg–Al–Zn alloy. Materials Science and Engineering A 2002; 337:121–133.

[52] Meyers MA, Dynamic behavior of materials. Wiley-In- Interscience, New York. 1994.

[53] Beynon ND, Jones TB, Fourlaris G. Effect of high strain rate deformation on microstructure of strip steels tested under dynamic tensile conditions. Materials Science and Technology 2005; 21:103-112.

[54] Ishikawa K, Watanabe H, Mukai T. High strain rate deformation behavior of an AZ91 magnesium alloy at elevated temperatures. Materials Letters 2005;59:1511-1515.

[55] Ishikawa K, Watanabe H, Mukai T. High temperature compressive properties over a wide range of strain rates in an AZ31 magnesium alloy. Journal of Materials Science 2005; 40:1577-1582.

[56] Baghni IM, Wu Y-S, Li J-Q, Du C-W, Zhang W. Mechanical properties and potential applications of magnesium alloys. Transactions of Nonferrous Metals Society of China 2003; 13:1253-1259.

[57] Barnett MR, Keshavarz Z, Beer AG, Atwell D. Influence of grain size on the compressive deformation of wrought Mg–3Al–1Zn. Acta Materialia 2004; 52:5093-5103.

[58] Lee BH, Bang W, Ahn S, Lee CS. Effects of temperature and strain rate on the high-temperature workability of strip-cast Mg-3Al-1Zn alloy. Metallurgical and Materials Transactions 2008; 39:1426-1434.

[59] Tucker MT, Horstemeyer MF, Gullett PM, Kadiri HE, Whittington WR. Anisotropic effects on the strain rate dependence of a wrought magnesium alloy. Scripta Materialia 2009; 60:182-185.

[60] Ulacia I, Dudamell NV, Gálvez F, Yi S, Pérez-Prado MT, Hurtado I.Mechanical behavior and microstructural evolution of a Mg AZ31 sheet at dynamic strain rates. Acta Materialia 2010; 58:2988-2998.

CHAPTER 2

TEXTURE EVOLUTION AND DYNAMIC MECHANICAL BEHAVIOR OF CAST AZ MAGNESIUM ALLOYS UNDER HIGH STRAIN RATE COMPRESSIVE LOADING

2.1. Overview of Chapter 2

This chapter focuses on the effect of composition and strain rate on the dynamic deformation behavior of cast AZ alloys with different aluminum content tested at different strain rates.

This chapter is presented as manuscript # 1. The author's (H. Asgari) contributions to this manuscript were: (a) preparation and processing of the samples for the shock loading test; (b) XRD, SEM, EDS and EBSD analyses; and (c) Reviewing the relevant literature, writing and submitting the manuscript.

The manuscript was published in *Materials & Design*:

- H. Asgari, J.A. Szpunar, A.G. Odeshi. "Texture evolution and dynamic mechanical behavior of cast AZ magnesium alloys under high strain rate compressive loading", Materials & Design, 61 (2014) 26–34.

The manuscript presented here is different from the published paper in the following parts:

- In the present manuscript, Figure 2.9 and related explanation are extra to the figures of the published paper. This figure was added to show the role of second phase particles in void/crack formation. Also, some parts from 'introduction' and 'discussion' were eliminated in this chapter to avoid repetition in the content.

The copyright permission to use the manuscript in the thesis was obtained and is provided in the Appendix section.

Texture evolution and dynamic mechanical behavior of cast AZ magnesium alloys under high strain rate compressive loading

H. Asgari, J. A. Szpunar, A. G. Odeshi
Department of Mechanical Engineering, University of Saskatchewan, Saskatoon, Canada

2.2. Abstract

In this study, texture and compressive mechanical behavior of three cast magnesium alloys, including AZ31, AZ61 and AZ91D, were examined over a range of strain rates between 1000 and 1400 s^{-1} using Split Hopkinson Pressure Bar. Texture measurements showed that after shock loading, initial weak texture of the cast samples transformed to a relatively strong (00.2) basal texture that can be ascribed to deformation by twinning. Furthermore, increasing the aluminum content in the alloys resulted in an increase in the volume fraction of β-$Mg_{17}Al_{12}$ and Al_4Mn phases, strength and strain hardening but ductility decreased at all strain rates. Besides, it was found for each alloy that the tensile strength and total ductility increased with strain rate. By increasing the strain rate, the maximum value of strain hardening rate occurred at higher strains. Also, it is suggested that a combination of twinning and second phase formation would affect the hardening behavior of the cast AZ magnesium alloys studied in this research.

Keywords: Cast magnesium alloys, High strain rate, Microstructure, Texture

2.3. Introduction

The use of light structural materials to decrease the weight, improve the fuel efficiency and reduce the greenhouse gas emissions has become increasingly important in several industries particularly automotive, aerospace, defense and electronic industries [1-6]. However, it should be mentioned that magnesium alloys are commonly used as die cast products and the current application of wrought magnesium alloy products is unfortunately limited by the poor ductility of wrought magnesium products [7-9].

In general, formability of magnesium and its alloys is low at room temperature and the main deformation modes at low temperatures are basal slip and twinning [1-2,7,10-11]. The important point about twinning is that it may accommodate strain along c-axis, giving rise to higher ductility

[1-2,7,10-16]. Therefore, twinning is considered as a very effective and easy deformation mechanism for magnesium at low temperatures [1-2, 7,16-19].

Considering the fact that most of the magnesium alloys are used in the form of cast products, [9], and the request for lighter but stronger cars and planes keeps on raising, understanding the dynamic behavior of cast magnesium alloys becomes very important. To date, a limited literature is available on the mechanical response and microstructural characteristics of AZ magnesium alloys under shock loading conditions [20-23]. Also, texture evolution, twinning behavior and strain hardening behavior have so far not been addressed adequately for cast AZ alloys. Therefore, the aim of this study is to investigate the texture evolution and mechanical behavior of a series of cast magnesium alloys (i.e. AZ31, AZ61 and AZ91D that contain different concentration of aluminum) under compressive shock loading. Also, the microstructure evolution and deformation mechanism(s), particularly twinning and effect of second phase particles on the twinning of these alloys at high strain rate conditions ranging from 1000 to 1400 s^{-1} will be discussed.

2.4. Experimental procedure

The cast magnesium alloys used in this investigation are AZ31, AZ61 and AZ91D. They were provided by Prof. Li's research group (Univ. of Alberta) with their nominal chemical compositions as presented in Table 2.1.

Table 2.1. Nominal chemical composition of cast AZ alloys used in this research (wt.%).

Sample	Al	Mn	Zn	Mg
AZ31	2.5-3.5	0.1-0.5	0.3-1	Bal.
AZ61	5.5-6.5	0.1-0.5	0.3-1	Bal.
AZ91D	8.5-9.5	0.1-0.5	0.3-1	Bal.

Samples used for shock loading tests were machined from large die castings into cylindrical shaped samples and all samples had the same height of 10.5 mm and diameter of 9.5 mm. The mechanical behavior of the samples in compressive shock loading conditions was evaluated using Split Hopkinson Pressure Bar (SHPB) at strain rates of 1000, 1250 and 1400 s^{-1}.

The schematic and real images of the Split Hopkinson Pressure Bar and an example of the samples used in this research are shown in Fig. 2.1(a) and 2.1(b). A striker, fired by a gas gun, travelled through the gun barrel, impacting the incident bar and then the test sample was deformed

in between the incident and transmitter bars at a very high impact velocity. It is possible to change the velocity of the striker by changing the gas pressure in the gas (firing) chamber. An incident strain pulse was produced after impacting that travelled along the input (incident) bar and after reaching the sample, a part of this pulse was reflected back as the reflected strain (ε_R) and another part was partially transmitted to the output (transmitter) bar as transmitted (ε_T) strain. Using strain gauges on the input (incident) and output (transmitter) bars, transferring of the incident, reflected and transmitted strain waves to the oscilloscope were done. Related equations were then used to calculate the sample strain, stress and strain rate. For example, the stress (σ) and strain rate ($\dot{\varepsilon}$) are given by the following Equations [24,25]:

$$\sigma = E(A_0/A_s)\,\varepsilon_T \quad (1)$$

$$\dot{\varepsilon} = (-2C_0 / l_s)\,\varepsilon_R \quad (2)$$

where E is Young's modulus of the bars, A_0 is the cross sectional area of the bars, A_s is the initial cross sectional area of the cylindrical sample, C_0 is the sound velocity in the bars and l_s is the initial length of the test sample. More details about the Split Hopkinson Pressure bar formulae and equations can be found in the literature [24,25]. To check the reproducibility of the results, tests were repeated three times and the typical stress-strain curves for each strain rate were reported. An example of such measurements (i.e. reporting the typical curve) is shown in Fig. 2.1(c). As presented in Fig. 2.1(c), three sets of shock-loading tests were done on AE44 samples at 800 s^{-1} and it can be seen that the curves are very similar. Therefore, the typical curve, which is almost located in between the other two curves, is reported as the typical one (shown on Fig. 2.1(c)). Very similar trend was observed for other samples and the same method was used to report their typical stress-strain curves. It should be mentioned that the variation in stress was very low and was generally less than 5%. Furthermore, all shock-loading tests were performed at room temperature.

Texture of the samples, before and after shock loading tests, was measured using X-ray diffraction (XRD) method. The XRD experiments were done employing Bruker D8 discover diffractometer with Cu Kα radiation and VANTEC 500 area detector. Then, I-2Theta plots were obtained by taking 3 frames for 50 seconds with sample oscillation of 2mm along XY axis for all samples. To identify the phases which are present in the alloys, EVA software was employed while background and Kα stripping were performed. Furthermore, six incomplete pole figures (PF), namely (10.0), (00.2), (10.1), (10.2), (11.0) and (10.3) were determined. Using incomplete pole figures, orientation distribution function (ODF) was determined by ResMat software and then

recalculated (00.2) and (10.0) pole figures were derived from the ODFs. It should be mentioned that the XRD data were taken from the compression plane of the samples, i.e. the plane which is perpendicular to the compression direction.

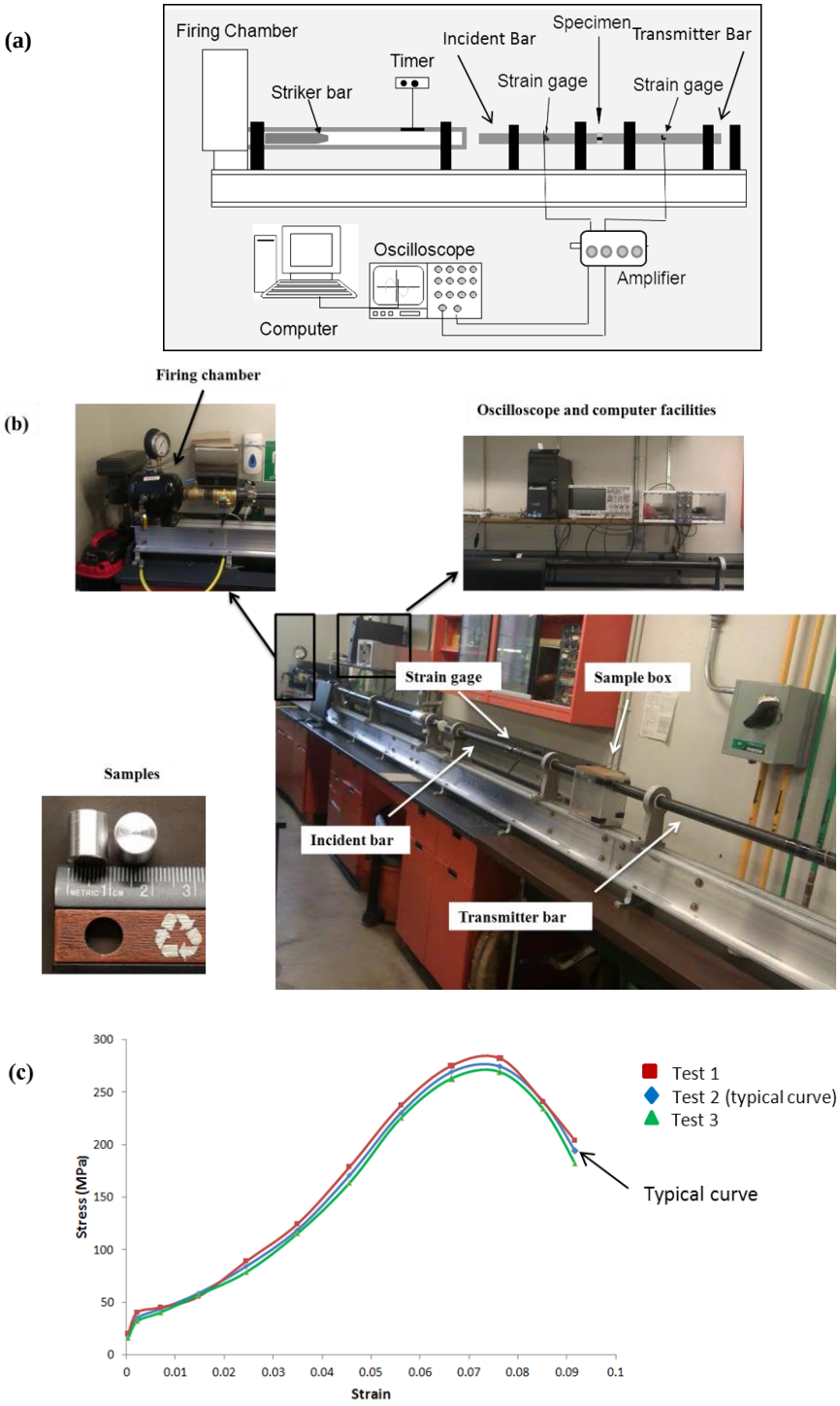

Fig. 2.1. (a) Schematic and (b) real images of Split Hopkinson Pressure Bar, (c) an example of reporting typical stress-strain curves after shock-loading tests.

For characterization of the sample microstructure and composition, a field emission scanning electron microscope Hitachi SU6600 FE-SEM equipped with an Energy Dispersive X-ray (EDX) analyzer, operating at 30 kV, was used. Orientation Imaging Microscopy (OIM) was utilized to study grain orientation, twin types and qualitative comparison of twinning fraction via electron backscattered diffraction (EBSD) by a Hitachi SU6600 FE-SEM fitted with Oxford Instruments. Data analysis was carried out using (hkl) Channel 5 data acquisition and analysis software.

To prepare the samples for SEM and OIM observation, samples were polished with 2000 and 4000 SiC papers followed by 3, 1 and 0.25 μm alcohol-based diamond suspensions. The final step of polishing was colloidal silica solution (0.04 μm) that was mixed with ethanol and ethylene glycol. It should be mentioned that in all grinding and polishing steps pure ethanol was used to wash and clean the samples. An acetic-glycol etchant (20 ml acetic acid, 1 ml nitric acid, 60 ml ethylene glycol and 20 ml water) was used to reveal the grain boundaries and second phase particles in the samples.

2.5. Results

XRD patterns of the alloy samples before shock loading tests are shown in Fig. 2.2. It is evident that the intensity of (00.2) basal texture component is weak in all samples. Another point that should be mentioned is that due to the addition of aluminum (Al) to the cast AZ magnesium alloys, brittle β-$Mg_{17}Al_{12}$ phase is formed after solidification and presence of the peaks of this phase is shown on the XRD patterns in Fig. 2.2. The peak corresponding to β-$Mg_{17}Al_{12}$ phase is like a small shoulder located in between the (00.2) and (10.1) peaks. XRD patterns of AZ91D alloy (and AZ61 alloy) show that by increasing the Al content of the alloys, the diffraction intensities of β phase relatively increase. The intensities of β-$Mg_{17}Al_{12}$ phase in the XRD patterns of AZ31 (and AZ61) alloy is weak that could be related to the low volume fraction of this phase in AZ31 and AZ61 alloys. Therefore, to confirm the formation of β-$Mg_{17}Al_{12}$ phase in the AZ alloys and evaluate the distribution and volume fraction of this phase, SEM was conducted.

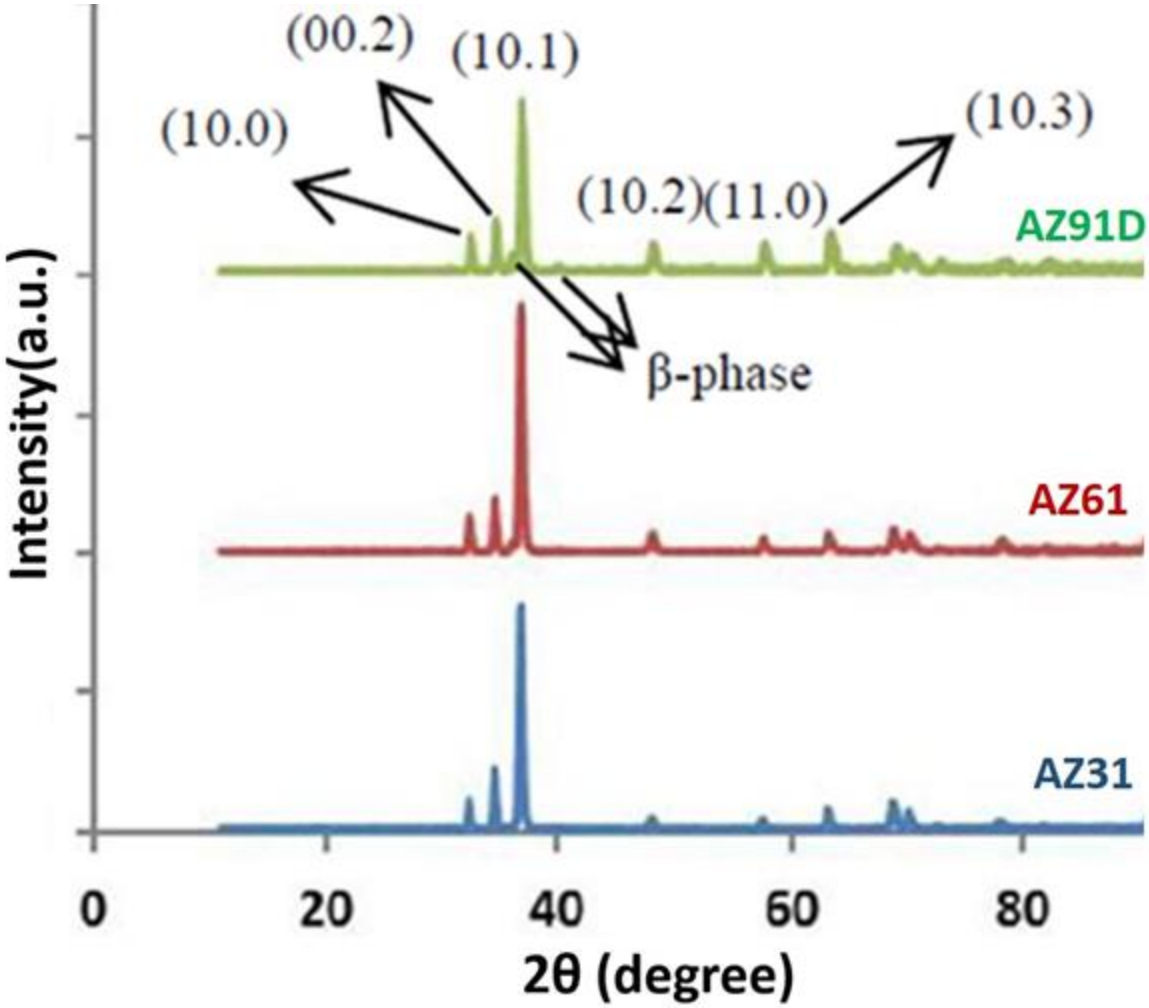

Fig. 2.2. XRD patterns of the samples before shock loading test; AZ31: blue, AZ61: red, AZ91D: green pattern (*Note*: planes inserted on the peaks belong to magnesium).

Fig. 2.3 displays the SEM images of the cast AZ31, AZ61 and AZ91D samples before shock loading. In the microstructure of these alloys, there is a network-like structure (white islands) which is almost evenly distributed in the matrix. An image of higher magnification of the white islands (β phase) in the AZ91D microstructure is shown at the top right corner of Fig. 2.3 (c). Also, there is another phase in the form of some spherical particles placed between the white islands. Increasing the Al content of the samples leads to increase in the volume fraction of both phases so that in the AZ91D sample, the number of interconnected white islands and spherical particles is very high in comparison with AZ31 and AZ61 samples (Fig. 2.3).

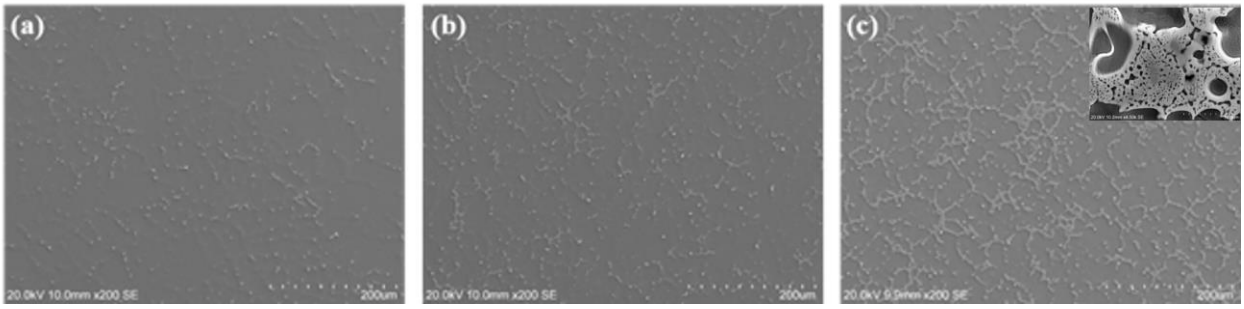

Fig. 2.3. SEM images of the as-cast samples before shock loading test; (a) AZ31, (b) AZ61, (c) AZ91D.

Examinations of the chemical composition of the alloys using the EDX spectrometer confirmed the presence of the main alloying elements as magnesium, aluminum and manganese. An example of EDX maps of the samples is shown in Fig. 2.4. Besides, considering the atomic percent of the elements obtained from EDX data, it is found that the white islands are β-$Mg_{17}Al_{12}$ phase, which is consistent with XRD results. For the spherical particles, the same calculations show that the chemical composition would be Al_4Mn. The Al_4Mn phase was not detected by XRD probably because of its low volume fraction.

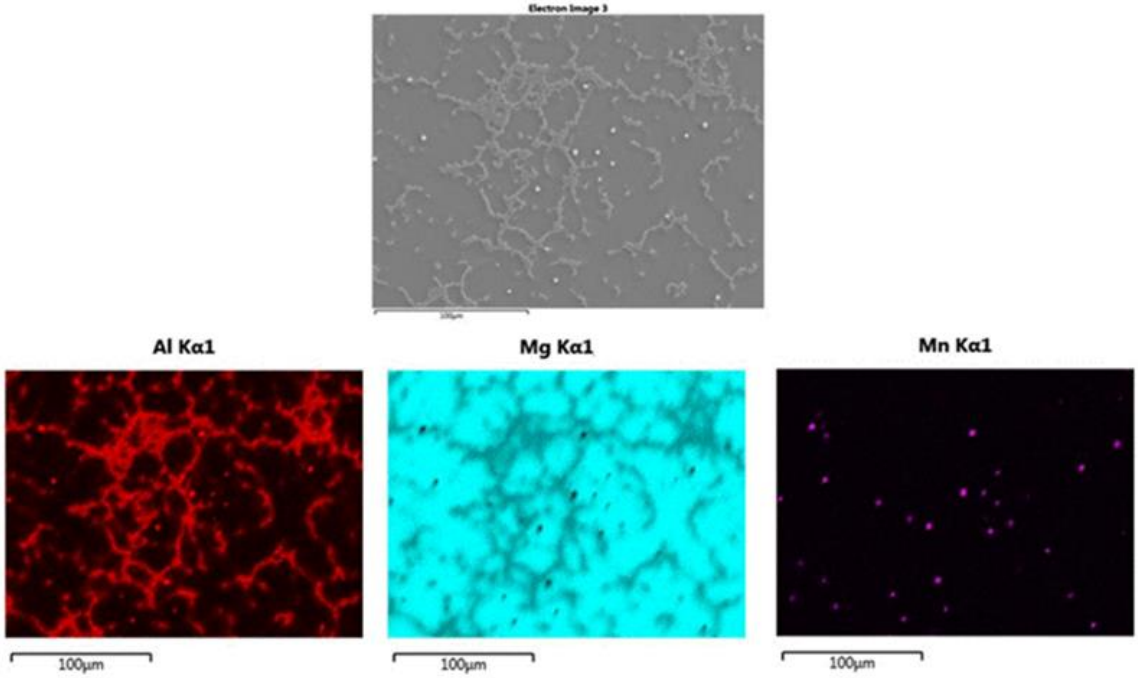

Fig. 2.4. EDX maps of AZ91D sample, showing the major alloying elements in the second phase particles.

The (00.2) and (10.0) pole figures (PFs) of the samples before shock loading tests are shown in Fig. 2.5. All samples show very weak texture intensities for (00.2) and (10.0) components. According to the pole figures of the non-shocked samples, a weak texture developed in the as-cast samples.

Fig. 2.6 presents (00.2) and (10.0) pole figures (PFs) of the samples after shock loading tests. It is clear that the texture intensities of (00.2) basal component is considerably increased, showing the change in the texture and significant strengthening of the (00.2) basal texture component. In other words, after shock loading the very weak texture of the cast samples converted to a relatively strong (00.2) basal texture in which most grains have their crystal c-axis parallel to the compression direction. Table 2.2, in which the volume fraction of (00.2) and (10.0) components are presented, confirms the strengthening of (00.2) and weakening of (10.0) texture components after shock loading test in the samples, particularly in AZ31 sample.

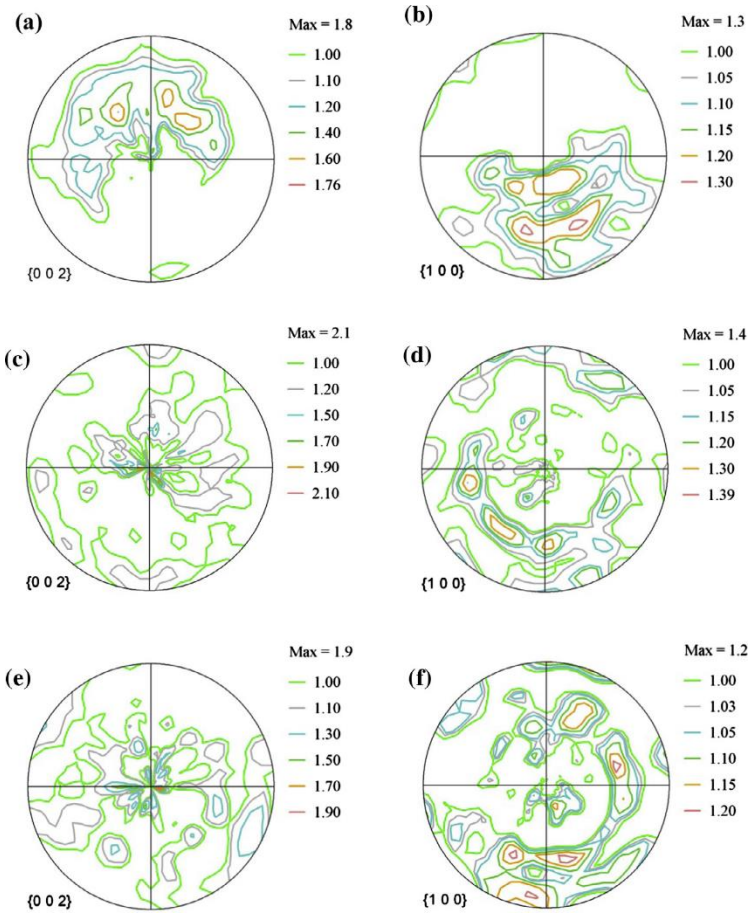

Fig. 2.5. (00.2) and (10.0) pole figures of the samples before shock loading test. (a) and (b):AZ31; (c) and (d): AZ61; (e) and (f): AZ91D.

The inverse pole figure (IPF) maps and image quality (IQ) maps of the samples after shock loading tests are shown in Fig. 2.7. It is seen that twinning occurred after shock loading in all samples and qualitative comparison between the IQ maps shows that twinning fraction decreased with increasing aluminum content in the alloys. Different types of twins that formed in the samples during shock loading test are marked in Fig. 2.7. As it is observed, the main twins are $\{10\bar{1}2\}$ extension twins. $\{10\bar{1}1\}$-$\{10\bar{1}2\}$ double twins are also present but fewer in number. Besides, very few $\{10\bar{1}1\}$ contraction twins are formed. Unlike the thick and well-developed extension twins (Fig. 2.7), contraction twins are thin and hard to detect by EBSD because they contain high levels of strain.

The dynamic true stress-strain curves and related hardening diagrams of samples at different strain rates are presented in Fig. 2.8. All the true stress-strain curves (Figs. 2.8(a), 2.8(c) and 2.8(e)), are of sigmoidal type and the stress increases to a maximum (peak stress) and then decreases because of unloading. Also, by increasing the strain rate, the peak stress and ductility increase for all samples. Besides, at each strain rate, the AZ31 and AZ91D alloys show the highest and lowest ductility, respectively. Furthermore, considering the strain hardening rate versus strain diagrams (Figs. 2.8(b), 2.8(d) and 2.8(f)), it is found that by increasing the strain rate, the maximum value of strain hardening rate takes place at higher strains. Another point is that by increasing the Al content in the samples, the rate of strain hardening increases.

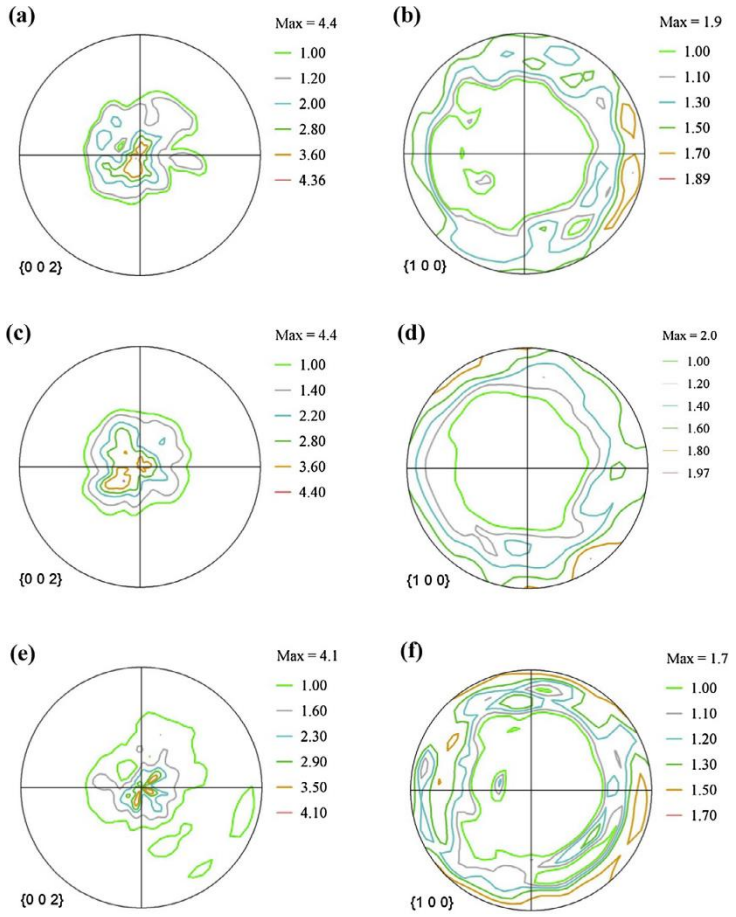

Fig. 2.6. (00.2) and (10.0) pole figures of the samples after shock loading test at strain rate of 1400 s^{-1}. [(a) and (b): AZ31; (c) and (d): AZ61; (e) and (f): AZ91D].

Table 2.2. Volume fraction percentage of (00.2) and (10.0) texture components of the samples before and after shock loading test.

Sample	(00.2) component volume fraction (%)		(10.0) component volume fraction (%)	
	before	after	before	after
AZ31	4.44	14.62	9.11	3.33
AZ61	5.15	13.65	10.24	4.97
AZ91D	5.31	11.96	10.62	5.59

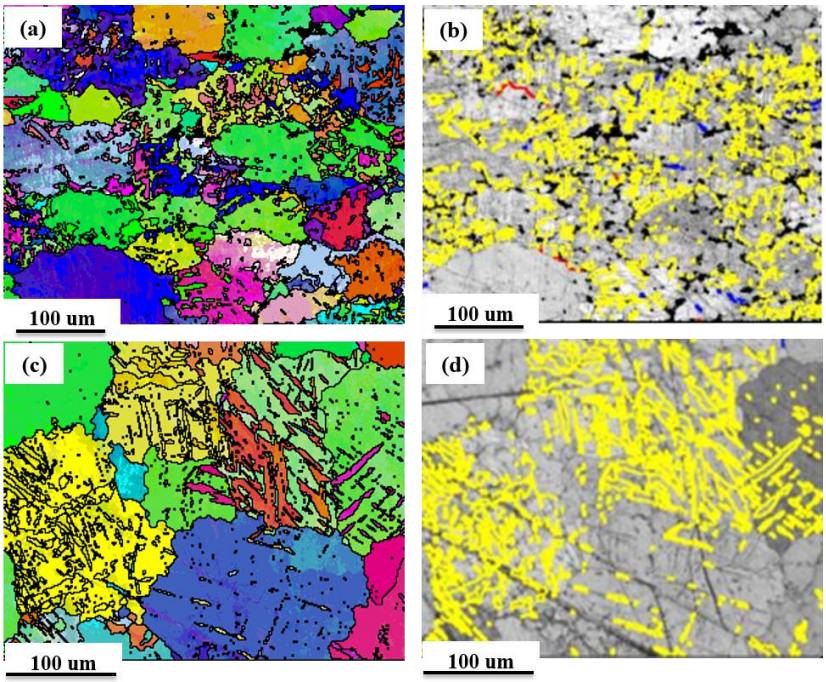

Fig. 2.7. Inverse pole figure (IPF) maps and image quality (IQ) maps of the cast samples showing the microstructure and twins type formed after shock loading test at 1400 s^{-1}. (a),(b),(c) and (d): AZ31.[*Note*: The extension twin boundaries ($86° < 11\bar{2}0 > \pm 5°$) are shown in yellow, the contraction twin boundaries ($56° < 11\bar{2}0 > \pm 5°$) are shown in red and the double twin boundaries ($38° < 11\bar{2}0 > \pm 5°$) are shown in blue]. (continued)

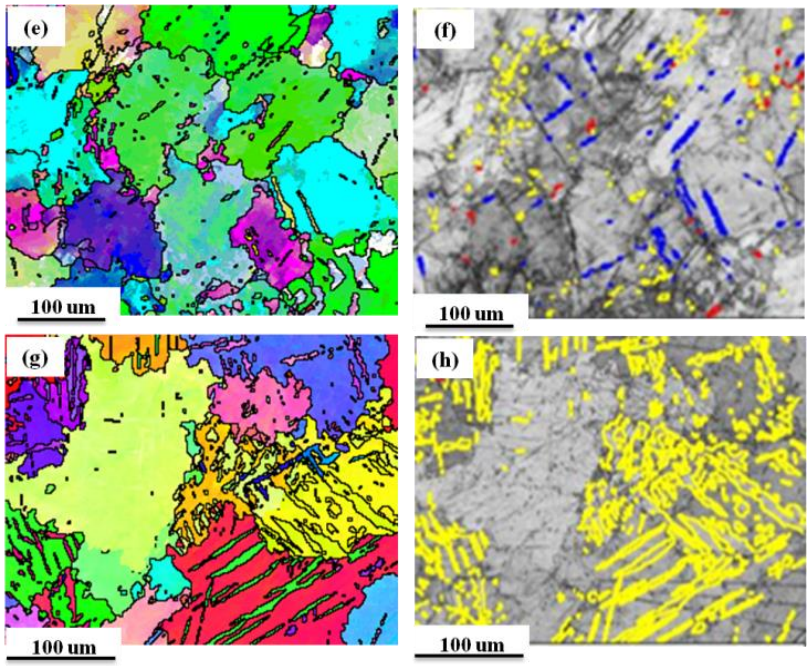

Fig. 2.7. Inverse pole figure (IPF) maps and image quality (IQ) maps of the cast samples showing the microstructure and twins type formed after shock loading test at 1400 s^{-1}. (e),(f),(g) and (h): AZ61. (continued)

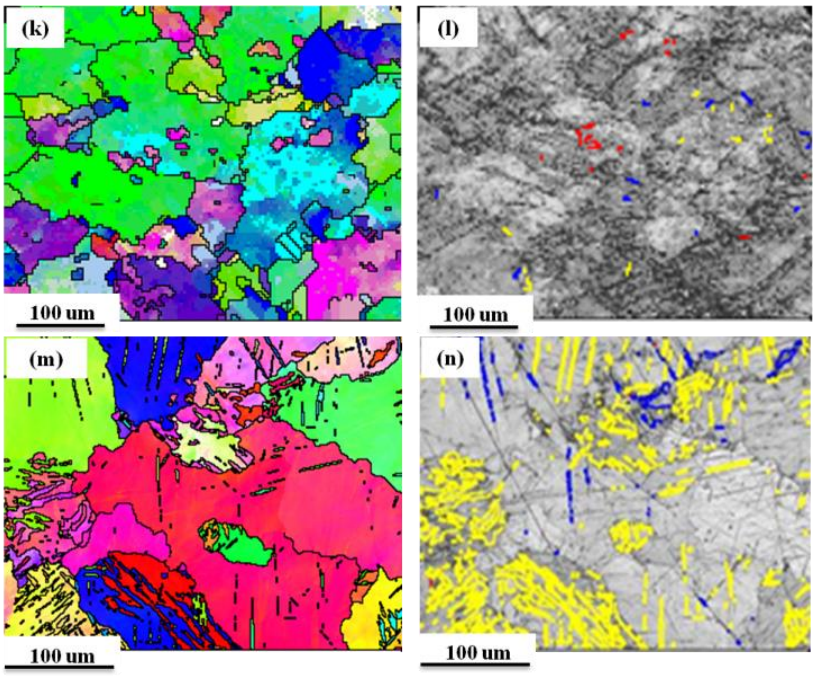

Fig. 2.7. Inverse pole figure (IPF) maps and image quality (IQ) maps of the cast samples showing the microstructure and twins type formed after shock loading test at 1400 s^{-1}. (k),(l),(m) and (n): AZ91D.

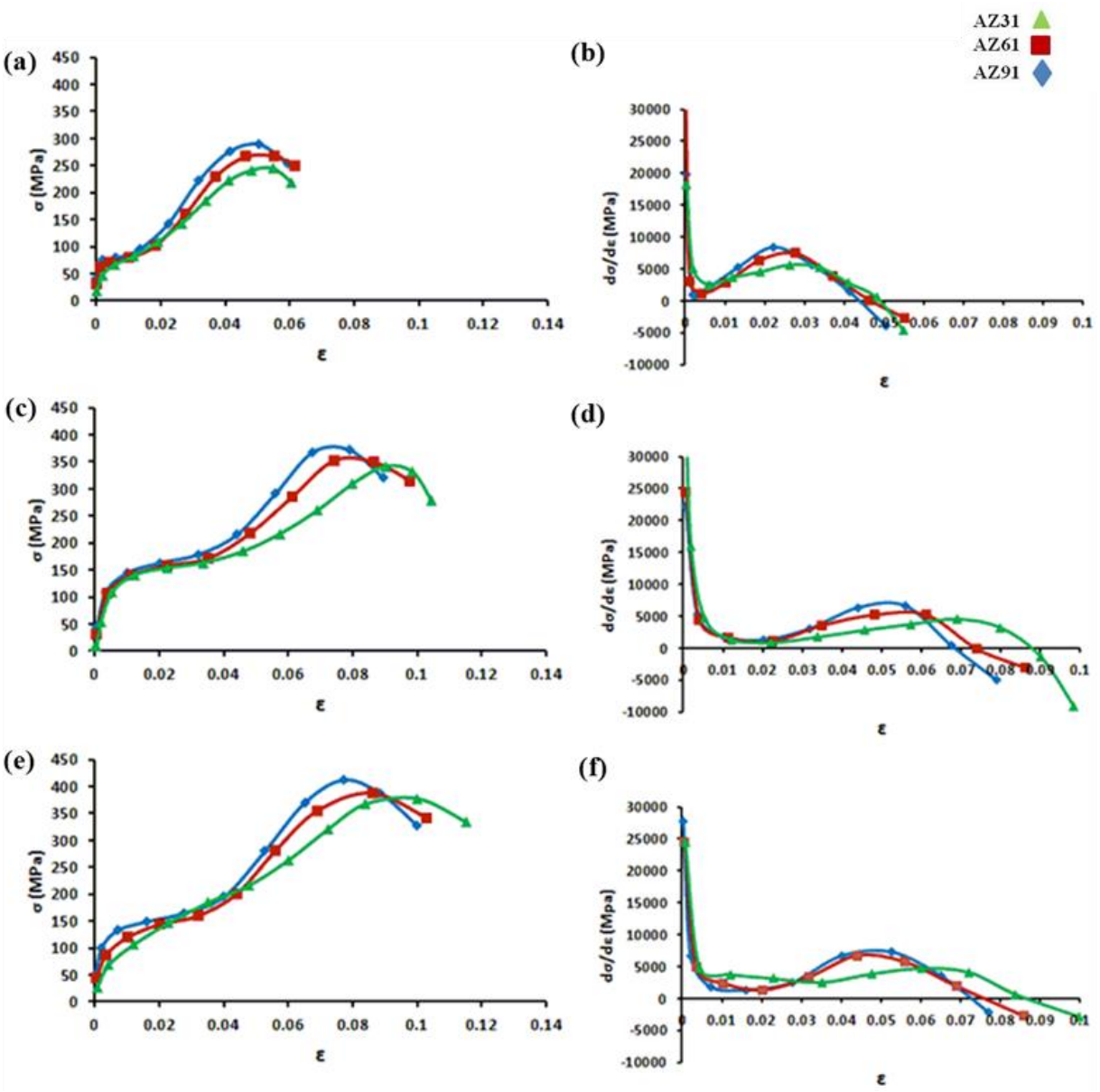

Fig. 2.8. True stress-strain curves and related hardening diagrams (strain hardening rate vs strain) for AZ31, AZ61 and AZ91D after shock loading: (a) and (b) $\dot{\varepsilon}$=1000 s^{-1}, (c) and (d) $\dot{\varepsilon}$=1250 s^{-1}, (e) and (f) $\dot{\varepsilon}$= 1400 s^{-1}.

2.6. Discussion

As can be seen from Fig. 2.2, by increasing the aluminum content of the alloys, the peak intensity of the β-$Mg_{17}Al_{12}$ phase increases. This can be related to the increase in the volume fraction of this phase due to the increased reaction of aluminum with magnesium, which is confirmed by SEM images, showing the increase in the number and fraction of β-phase islands in the matrix with increase in aluminum concentration (Fig. 2.3). Aluminum has a high affinity to

magnesium and after reaction with magnesium, brittle β-$Mg_{17}Al_{12}$ is formed and distributes almost evenly along the grain boundaries (Fig. 2.3). The presence of β- phase was confirmed by EDX analysis and also identified by other researchers [9,26-28]. Increase in volume fraction of the brittle β phase, which may play the role of a hardening phase, can increase the strength of the alloy but ductility decreases [9, 26-28]. Furthermore, although the presence of Al_4Mn phase is very likely, based on SEM images and EDX maps (Figs. 2.3 and 2.4), the corresponding diffraction peaks do not appear in the XRD patterns (Fig. 2.2) probably due to a very low fraction of this phase. Generally, a matrix of α-Mg and β-$Mg_{17}Al_{12}$ phase islands which are distributed in the matrix are observed in cast AZ alloys. Besides, cast AZ alloys contain small amount of manganese and therefore another phase that could be found in the alloy can be of the form of Al_xMn_y particles, and the values of x and y is determined by the relative amount of aluminum and manganese in the alloy. In this study, as was discussed, x and y were 4 and 1, respectively, which is consistent with the results obtained by other researchers [9, 26-28].

In Fig. 2.5, a very weak texture (or near-random texture) is seen for the cast samples which is characteristic of cast magnesium alloys [7]. However, considering the pole figures after shock loading (Fig. 2.6), a strong basal texture develops in the samples, indicating that the initial texture is significantly changed. The considerable change in the texture of the shock loaded cast samples (Fig. 2.6) could be explained by a twinning mechanism in which the crystal lattice is reoriented at some certain angles to accommodate the imposed deformation [7,12-15,28-30].

Considering the significant strengthening of basal texture component and weakening of other components (Figs. 2.1, 2.2, 2.5 and 2.6) in the samples, it is reasonable to propose that the regions with suitable and favorable orientation for twinning could have experienced several types of twinning after shock loading (Fig. 2.7). Since the texture of the cast samples before shock loading is a very weak (or near-random) texture (Fig. 2.5), it is logical to consider several regions with different orientations in the samples. Each of these regions may have had a favorable orientation for some type of twinning and therefore, during the shock loading could have experienced different types of twinning. For example, the grains (regions) in which the c-axis was perpendicular to the compression axis have experienced extension twinning and since this twinning resulted in the reorientation of basal planes at an angle of 86° (almost 90°) from their original position [1-2, 10-15], the intensity of basal planes increased after shock loading. For other regions with favorable orientations for contraction or double twins, these twins could have taken place. It should be

mentioned here that the initial texture of the cast samples was favorable for the activation of basal slip, too; however, since the basal slip mode only provides two independent slip systems, the twinning mode must have been activated to satisfy a minimum of five independent deformation modes which are required to obtain a uniform deformation [3,6, 29-30] .

In Fig. 2.7, it is shown that different fractions of twinned grains are observed in the shock loaded samples. As mentioned earlier, the fraction of twinning was lower in the samples with higher content of aluminum. This may be related to the volume fractions of β-$Mg_{17}Al_{12}$ phase (islands) in the microstructure. By increasing the aluminum content in the alloys, as shown in Fig. 2.2, the volume fraction of β-$Mg_{17}Al_{12}$ phase is increased. This increase in the volume fraction of the second phase islands may have affected the twinning nucleation and growth, resulting in less twinning in the samples with higher aluminum content.

Three types of twins can be seen in the cast samples as indicated in Fig. 2.7. It is observed that in all samples, the fraction of extension twins is larger than those of other twins (i.e. contraction and double) which can be ascribed to its lower CRSS that makes it an easy and dominant deformation mode after basal slip in magnesium alloys [10-15]. By increasing the aluminum content from AZ31 to AZ91D, the fraction of extension twinning decreased. However, a relative increase in the fraction of other twins, i.e. contraction and double, is also observed. It seems that increasing the volume fraction of β-$Mg_{17}Al_{12}$ phase could have affected the activation/deactivation of the twinning systems, leading to decrease in the fraction of extension twins. The larger fraction and presence of extension twins (Fig. 2.7) could be related to the presence of a larger number of grains, in the initial cast samples, with suitable orientations for extension twinning. Lower presence of contraction and double twins can also be explained by the high CRSS of these twins, which makes it very hard to activate this type of twinning [10-15].

Another possibility that could be considered is the activation of pyramidal <c+a> slip systems due to the increase in the temperature during the shock loading test. Due to the significant drop of the CRSS of pyramidal <c+a> slip systems at high temperatures [7, 12-15, 29-33] and considering the fact that the temperature of the samples increased during the shock loading test, particularly at higher strain rates in which all three alloys showed better ductility, <c+a> slip system could have been activated and contributed to the deformation process in the cast samples [19].

True stress-strain curves of the samples at three different strain rates, i.e. 1000, 1250 and 1400 s^{-1}, are shown in Figs. 2.8(a), 2.(8)c and 2.8(e). Samples had an upward curving flow which is a

typical feature of the stress-strain curves of the materials in which twinning is the dominant deformation mode [7,18,34]. The flow curves show yielding around 60-150 MPa which is then followed by a work hardening region. With increasing the strain, an inflection point can be seen and then, strain hardening increases with strain and again decreases after the peak stress.

Hardening diagrams (Figs. 2.8(b), 2.8(d) and 2.8(f)) first drop and then increase to a maximum before falling off again and a hump was formed on the diagrams, suggesting that twinning is the dominant deformation mechanisms in the samples [35]. The initial step of the hardening diagrams, deformation is mainly controlled by slip and {10-12} twins may also nucleate and propagate in the microstructure. The increase in the strain hardening rate, in the next step, would be ascribed to the interaction between several twinning systems and also twin-dislocation interactions. After formation and propagation of twins, particularly extension twins, the twin boundaries may block dislocation motion and this results in accumulation of dislocations [2, 7, 35]. Also, another factor that may affect the hardening behavior is the formation of twin intersections. Dislocation pile-ups and twin intersections could have been effective parameters in increasing the strain hardening rate during deformation. In the next stage of deformation, due to the coalescence of twins, they cannot possibly act as strong and effective barriers to dislocation motion, and this may result in decrease in the strain hardening rate [2, 7]. Furthermore, due to the increase in the temperature in shock loading conditions activation of non-basal slip systems could have occurred [36]. Therefore, the hardening rate decreased. The hump formation in the hardening diagrams and their broadening with increase in strain rate (Figs. 2.8(b), 2.8(d) and 2.8(f)) is related to the change of deformation mechanism and possible activation of non-basal slip systems such as pyramidal <c+a> system [35].

The second phase particles such as Al_4Mn and brittle β-$Mg_{17}Al_{12}$, particularly the brittle β phase with much larger volume fraction than Al_4Mn may also affect the strain hardening behavior of these alloys [9,37]. Aluminum, in general, is added to magnesium alloys to improve their castability; however, another effect of addition of aluminum to magnesium alloys is the formation of the brittle β-$Mg_{17}Al_{12}$ phase (Fig. 2.2) which can play the role of a hardening phase, due to the considerable interaction with dislocations and this additions may decrease the ductility [9, 37]. By increasing the Al content, a higher amount of brittle phase (and Al_4Mn) is formed in alloys having higher Al content (Fig. 2.2) and thus, the ductility decreased but the strength and strain hardening rate increased at the strain rates used in this study. Therefore, it is suggested that a combination of twinning mechanisms and formation of β-$Mg_{17}Al_{12}$ phase, with the stronger role of the latter, could

possibly affect the elongation, strength and strain hardening rate of the alloys used in the current research.

The effect of brittle β-$Mg_{17}Al_{12}$ phase on the hardening would be more significant in comparison to that of twinning because, as was shown in Fig. 2.7, the fraction of twinning in the AZ31 (that has the lowest content of aluminum among the alloys studied in this research) is larger than those of AZ61 and AZ91D and considering the fact that twin boundaries are effective barriers to the dislocation motion [7], the strength and hardening of AZ31 should be higher than those of AZ61 and AZ91D. However, referring to the stress-strain curves and hardening diagrams, it is deduced that under all strain rates, the strength and hardening rate of AZ31 is less than those of AZ61 and AZ91D. Therefore, another parameter such as the volume fraction of the brittle β-$Mg_{17}Al_{12}$ phase, may have been involved, with a considerable influence in the hardening process of the cast alloys. In other words, second phase particles could be considered as more effective barriers to dislocation motion than twin boundaries in cast AZ magnesium alloys.

One more important aspect about the second phase particles is the formation and propagation of voids and cracks around them. Due to the stress and strain incompatibilities at the interface of matrix/second phase particles (β-$Mg_{17}Al_{12}$), voids form and the interconnection of these voids results in the formation of cracks at the matrix/β phase interface, leading to lower ductility of cast AZ alloys. This effect is more significant in cast AZ alloys with higher aluminum content since more volume fractions of β-$Mg_{17}Al_{12}$ form and this increases the probability of the formation of more voids and cracks. An example of this type of void and cracks, formed at the matrix/β phase interface, is presented in Fig. 2.9.

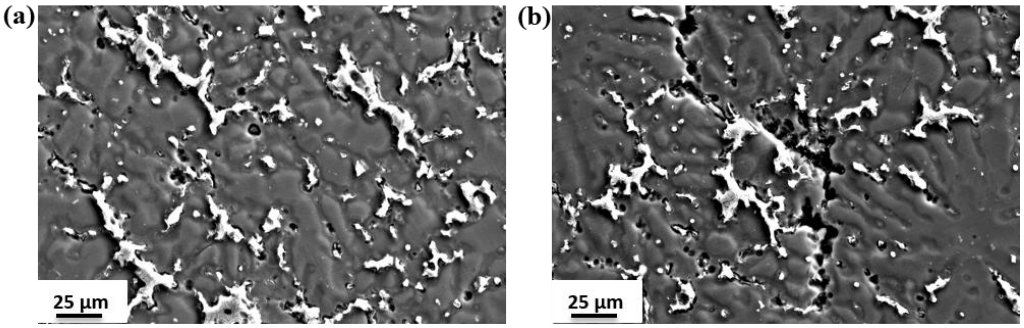

Fig. 2.9. Void and crack formation at the interface of matrix (gray region) and β-$Mg_{17}Al_{12}$ phase (white particles) in (a) AZ31 and (b) AZ91D alloy after shock loading.

2.7. Conclusions

Based on the results, it is found that by increasing the aluminum content in the cast alloys, the volume fraction of β-$Mg_{17}Al_{12}$ and Al_4Mn phases, strength and strain hardening increase but ductility decreases at all strain rates. Besides, increasing the strain rate can result in considerable increase in strength of the alloys. Moreover, the (00.2) basal texture component of the alloys is strengthened after high strain rate tests which results in change in the texture of the alloys.

Three types of twins are detected in the microstructure of the shock loaded cast samples and the extension twinning fraction is larger than those of contraction and double twins in the samples. However, by increasing the aluminum content, the fraction of twinning (particularly extension twins) is decreased. Furthermore, a combination of twinning and presence of brittle second phase particles is suggested as the effective parameters dominating the hardening behavior of the cast AZ31, AZ61 and AZ91D samples.

References

[1] Li Q. Mechanical properties and microscopic deformation mechanism of polycrystalline magnesium under high-strain-rate compressive loadings. Materials Science and Engineering A 2012; 540:130-134.

[2] Korla R., Chokshi AH. Strain-rate sensitivity and microstructural evolution in a Mg–Al–Zn alloy. Scripta Materialia 2010; 63: 913-916.

[3] Mordike BL, Ebert T. Magnesium: Properties — applications — potential. Materials Science and Engineering A 2001;302: 37-45.

[4] Gehrmann R, Frommert MM, Gottstein G. Texture effects on plastic deformation of magnesium.Materials Science and Engineering A 2005;395: 338-349.

[5] Agnew SR, Duygulu O. Plastic anisotropy and the role of non-basal slip in magnesium alloy AZ31B. International Journal of Plasticity 2005; 21:1161-1193.

[6] Lou XY, Li M, Boger RK, Agnew SR, Wagoner RH. Hardening evolution of AZ31B Mg sheet. International Journal of Plasticity 2007;23:44-86.

[7] Jiang L, Jonas JJ, Luo AA, Sachdev AK, Godet S. Influence of {10-12} extension twinning on the flow behavior of AZ31 Mg alloy. Materials Science and Engineering A 2007;445-446: 302:309.

[8] Ahmad IR, Shu DW. Dynamic response of magnesium alloy AZ31B under high strain rate compressive loading. Applied Mechanics and Materials 2011; 83:60-65.

[9] Bakke P, Pettersen K, Westengen H. Improving the Strength and Ductility of Magnesium Die-Casting Alloys via rare-earth addition. JOM 2003;46-51.

[10] Yoo MH. Slip, twinning, and fracture in hexagonal close-packed metals. Metallurgical and Materials Transactions A 1981;12:409.

[11] Wonsiewicz BC, Backofen WA. Plasticity of Magnesium Crystals. Trans TMS-AIME 1967;239:1422–31.

[12] Knezevic M, Levinson A, Harris R, Mishra RK, Doherty RD, Kalidindi SR. Deformation twinning in AZ31: Influence on strain hardening and texture evolution. Acta Materialia 2010; 58: 6230–6242.

[13] Jiang L, Jonas JJ, Luo AA, Sachdev AA, Godet S. Twinning-induced softening in polycrystalline AM30 Mg alloy at moderate temperatures. Scripta Materialia 2006; 54:771–775.

[14] Kelley EW, Hosford WF. Plane strain compression of magnesium and magnesium alloy crystals. Trans. Metall. Soc. AIME. 1968; 242:5-13.

[15] Obara T, Yoshinga H, Morozumi S. {11-22}〈1123〉 Slip system in magnesium. Acta Metalurgica 1973; 21:845.

[16] Jain A, Agnew SR. Modeling the temperature dependent effect of twinning on the behavior of magnesium alloy AZ31B sheet. Materials Science and Engineering A 2007; 462: 29-36.

[17] Barnett MR. A rationale for the strong dependence of mechanical twinning on grain size. Scripta Materialia 2008;59:696-698.

[18] Karimi E, Zarei-Hanzaki A, Pishbin MH, Abedi HR, Changizian P. Instantaneous strain rate sensitivity of wrought AZ31 magnesium alloy. Materials & Design 2013; 49:173-180

[19] Song WQ, Beggs P, Easton M. Compressive strain-rate sensitivity of magnesium–aluminum die casting alloys. Materials & Design 2009; 30:642–648.

[20] Sanjari M, Farzadfar A, Sakai T, Utsunomiya H, Essadiqi E, Jung IH, Yue S. A texture and microstructure analysis of high speed rolling of AZ31 using split Hopkinson pressure bar results. Journal of Materials Science 2013; 48:6656-6672.

[21] Xin RL, Wang BS, Chen XP, Huang G, Liu Q. Examination of dynamic recrystallization during compression of AZ31 magnesium. Science in China Series E: Technological Sciences 2009; 52:176-179.

[22] Dudamell NV, Gálvez F, Pérez-Prado MT. Dynamic deformation of high pressure die-cast magnesium alloys. Revista de Metalurgia 2012; 48:351-357.

[23] Liu Z, Dong Y, Mao PL, Yu JC. Dynamic tensile and compressive properties of vacuum and ordinary die-casting AT72 magnesium alloy at high strain rates. Journal of Magnesium and Alloys 2013; 1:150-162.

[24] Gray GT. Classic Split-Hopkinson pressure bar testing. Mechanical Testing and Evaluation. ASM Handbook, ASM International 2000; 8: 462–476.

[25] Kolsky H. An investigation of the mechanical properties of materials at very high rates of loading. Proceedings of the Physical Society. Section B 1949; 62: 676-701.

[26] Čížek L, Hanus A, Sozańska M, Tański T, Pawlica L. Structure characteristics of magnesium alloys with admixture of aluminum, silicon and zirconium. Acta Metallurgica Slovaca 2007; 13:531-538.

[27] Paramsothy M, Tan XH, Chan J, Kwok R, Gupta M. Al2O3 nanoparticle addition to concentrated magnesium alloy AZ81: Enhanced ductility. Journal of Alloys and Compounds 2012; 545:12–18.

[28] Yang Z, Li JP, Zhang JX, Lorimer GW, Robson J. Review on Research and Development of Magnesium Alloys. Acta Metallurgica Sinica 2008; 21:313-328.

[29] Beausir B, Toth LS, Qods F, Neale KW. Texture and mechanical behavior of magnesium during free end torsion. Journal of Engineering Materials and Technology 2009; 131: 1.

[30] Koike J, Kobayashi T, Mukai T, Watanabe H, Suzuki M, Maruyama K, Higashi K. The activity of non-basal slip systems and dynamic recovery at room temperature in fine-grained AZ31B magnesium alloys. Acta Materialia 2003;51:2055-2065.

[31] Barnett MR. A Taylor model based description of the proof stress of magnesium AZ31 during hot working. Metallurgical and Materials Transactions A 2003; 34:1799–1806.

[32] Agnew SR, Duygulu O. TEM investigation of dislocation mechanisms in Mg alloy AZ31B sheet. Mag. Tech. Conf. Proceedings 2004; 61-65.

[33] Keshavarz Z, Barnett MR. EBSD analysis of deformation modes in Mg–3Al–1Zn. Scripta Materialia 2006;55:915-918.

[34] Chino Y, Kimura K, Mabuchi M. Twinning behavior and deformation mechanisms of extruded AZ31 Mg alloy. Materials Science and Engineering A 2008;486:481-488.

[35] Khan AS, Pandey A, Gnäupel-Herold T, Mishra RK. Mechanical response and texture evolution of AZ31 alloy at large strains for different strain rates and temperatures. International Journal of Plasticity 2011; 27: 688–706.

[36] Chang LL, Shang EF, Wang YN, Zhao X, Qi M. Texture and microstructure evolution in cold rolled AZ31 magnesium alloy. Materials Characterization 2009; 60:487-491.

[37] Baghni IM, Wu Y-S, Li J-Q, Du C-W, Zhang W. Mechanical properties and potential applications of magnesium alloys. Transactions of Nonferrous Metals Society of China 2003; 13:1253-1259.

CHAPTER 3

EFFECT OF YTTRIUM ON THE TWINNING AND PLASTIC DEFORMATION OF AE MAGNESIUM ALLOY AT HIGH STRAIN RATES

3.1. Overview of Chapter 3

In the previous chapter, the mechanical response and deformation mechanisms of cast AZ alloys were discussed. To evaluate the dynamic mechanical properties and plastic deformation behavior of rare earth containing cast alloys, which have a different chemical composition compared to cast AZ alloys, cast AE magnesium alloys were shock loaded and using several characterization techniques, deformation behavior was analyzed and then discussed. In this chapter, the results and corresponding discussion about the effect of initial texture and strain rate on the dynamic deformation behavior of cast AE alloys are presented.

This chapter is presented as manuscript # 2. The author's (H. Asgari) contributions to this manuscript are: (a) preparation and processing of the samples for shock loading test. (b) XRD, SEM, EDS, TEM and EBSD analyses. (c) Reviewing the relevant literature, writing and submission of the manuscript. The contribution of Dr. L. J. Zeng and Prof. E. Olsson was in the area of TEM investigation and analysis and Prof. D. Y. Li reviewed the paper before submission.

The manuscript was published in *Materials Science & Engineering A*:

- H. Asgari, J.A. Szpunar, A.G. Odeshi, L.J. Zeng, E. Olsson, D.Y. Li. "Effect of yttrium on the twinning and plastic deformation of AE magnesium alloy under ballistic impact", Materials Science & Engineering A, 623 (2015) 10–21.

The manuscript presented here is different from that of published in the following parts:

- In order to avoid repetition in the content, some parts of the ‘introduction’,‘experimental procedure’, and ‘discussion’ sections were eliminated.

The copyright permission to use the manuscript in the thesis was obtained and provided in the Appendix section.

Effect of yttrium on the twinning and plastic deformation of AE magnesium alloy at high strain rates

H. Asgari[a], A. G. Odeshi[a], J. A. Szpunar[a], L. J. Zeng[b], E. Olsson[b], D. Y. Li[c]

[a] Department of Mechanical Engineering, University of Saskatchewan, Saskatoon, Canada

[b]Department of Applied Physics, Chalmers University of Technology, Göteborg, Sweden

[c] Department of Chemical and Materials Engineering, University of Alberta, Edmonton, Canada

3.2. Abstract

In this research, effect of yttrium on the texture formation, microstructural evolution and mechanical response of AE42 and AE44 cast magnesium alloys was investigated under ballistic impact. The selected strain rates were 800 and 1100 s^{-1} and the tests were conducted using Split Hopkinson Pressure Bar. It was inferred that after high velocity impact, a weaker basal texture developed in the samples with lower content of yttrium. Experimental results also showed that by increasing the concentration of yttrium in the cast AE alloys, strength, ductility and dislocation density of the impacted alloys increased but, the fraction of twinning decreased, which indicate the effective influence of yttrium on the nucleation and growth of twins.

Keywords: Magnesium alloy, Plastic deformation, Rare-earth element, Twinning

3.3. Introduction

There has been considerable interest over the past years to understand and evaluate the deformation behavior of magnesium alloys because of their potential for use in several applications and industries, especially in lightweight structural components [1-6]. However, the ductility of magnesium and its alloys is highly restricted at room temperature due to the limited active deformation modes [1-6].

Considering the wide spread application of magnesium alloys, particularly in the form of cast products in the automotive industry, the casting is the important commercial production method for these alloys [1-3]. Cast AZ and AM magnesium alloys are appropriate candidates for some automotive components such as seat frames, instrumental panel and steering wheels [7]. However, AZ and AM series do not show acceptable strength and creep resistance at high temperatures [7].

Consequently, it is required to improve the creep resistance and strength of magnesium alloys for high temperature conditions.

In general, some alloying elements such as aluminum, manganese and zinc are added to magnesium alloys for different purposes such as increasing the castability or strength [8-9]. Addition of rare-earth (RE) elements, however, would be an effective method to optimize the performance of magnesium alloys at elevated temperatures in components such as gearbox, automatic transmission housing and oil pans. Yttrium, cerium and lanthanum are often added to magnesium alloys and it has been shown that these elements can increase the ductility, creep and corrosion resistance of magnesium alloys [8-12].

Since cast magnesium alloys are used in different applications, particularly where the strain rates can be very high (e.g. crash events), improving their formability requires a better understanding of the texture transformation and mechanical property variations under shock loading conditions. Unfortunately, most of the research which has been done on dynamic behavior of magnesium alloys is about the extruded magnesium alloys and texture formation, microstructural evolution and mechanical behavior of AE cast magnesium alloys, at high strain rates have not been studied and discussed adequately in the open literature. There are only a few reports in the open literature about cast AE magnesium alloys which have mainly focused on the mechanical properties and microstructural evolution of cast AE magnesium alloys at low strain rates [4,7-9,12,13] or corrosion properties of cast AE alloys [14]. For example, Nouri *et al.* [4] have found that a small amount of yttrium may increase the homogenization of cast Mg-3%Al and increase the corrosion resistance of cast Mg-3%Al. Also, in another study, the variability in the tensile ductility of cast tensile test specimens of high-pressure die-cast AE44 Mg-alloy has been examined at low strain rates and the effects of porosities has been discussed [7]. The effect of rare-earth addition to the magnesium alloys, to produce AE cast alloys, has been studied and it has been proved that additions of rare earth elements at a given Al content may improve the ductility, and the ultimate tensile strength is slightly increased at low strain rates [8,9]. Another research that has been conducted on AE cast alloys is mainly about the characterization and microstructural evolution of cast AE alloys (AE44) and the effects of the cooling rate on the microstructure and phases formed in the alloy after solidification [12]. Creep behavior of AE cast alloys has also been investigated and the transition between the phases in the microstructure, affected by the temperature, has been addressed [13]. Another subject that has been studied by Zhang *et al.* [14] is the corrosion properties of AE

cast alloy (Mg-5Y-7Gd-1Nd-0.5Zr) and they have shown that the corrosion resistance of this alloy in 5% NaCl aqueous solution gradually deteriorates with increasing the immersion time. Therefore, as was mentioned, the reports found in the open literature are about the mechanical (at low strain rates) or chemical properties of AE cast alloys and the texture formation, microstructural evolution and deformation mechanisms at high strain rate conditions are the missing part in the literature. In other words, there is a significant lack of knowledge in the literature on the dynamic behavior and deformation mechanism of cast AE magnesium alloys and also the effect of parameters, particularly the yttrium content that can influence the dynamic properties of these alloys. Therefore, the objective of the present study is to develop the understanding of the texture formation, deformation mechanism, microstructural evolution and effect of yttrium on the mechanical properties and deformation mechanism of cast AE magnesium alloys under shock-loading conditions. In this research, a complete and comprehensive series of data, including texture measurements, microstructural evolution and mechanical properties of shock-loaded cast AE samples, and discussion about the deformation mechanisms which are involved in the deformation of cast AE alloys at high strain rates are presented. The results presented in this paper are new and can be a useful addition to the available knowledge on the dynamic mechanical behavior of cast AE magnesium alloys under shock loading condition.

3.4. Experimental procedure

Rare-earth containing cast magnesium alloys used in this study are AE42 and AE44. They were provided by Prof. Li's research group (Univ. of Alberta) with their nominal chemical compositions as presented in Table 3.1. To increase the homogeneity of the alloys, homogenization heat-treatment was performed on the AE42 and AE44 alloys at 400 ºC for 9 hours.

Table 3.1. Nominal chemical composition of investigated AE cast alloys (wt.%).

Sample	Al	Y	Mn	Zn	Mg
AE42	3.5-4.5	1.8-2	0.3-0.5	0.3-0.6	Bal.
AE44	3.5-4.5	3.7-4	0.3-0.5	0.3-0.6	Bal.

The details of shock loading test, texture measurements, SEM, EDS and EBSD are similar to the manuscript #1 (Chapter 2). It is not repeated here in order to keep the thesis concise.

Transmission electron microscopy (TEM) observations were performed using a 200 kV FEI Tecnai G^2 T20 microscope equipped with a LaB_6 filament. TEM specimens were cut from the compression plane of the samples by a precision cutter. The cut specimens were thinned further using SiC papers after which 3 mm disks were cut from the foils using a manual punch. The foils were electropolished using a twin-jet polisher in a solution of 3 vol.% perchloric acid in ethanol (13 V, -30 °C). Finally, the specimens were rinsed several times using high purity (99.5%) alcohol.

3.5. Results

XRD scans of as-cast AE42 and AE44 alloy samples are shown in Fig. 3.1. It is observed that there are some strong peaks, which belong to magnesium, and the additional weak diffraction lines correspond to Al_2Y phase in the XRD patterns of the samples, indicating the formation of an intermetallic phase.

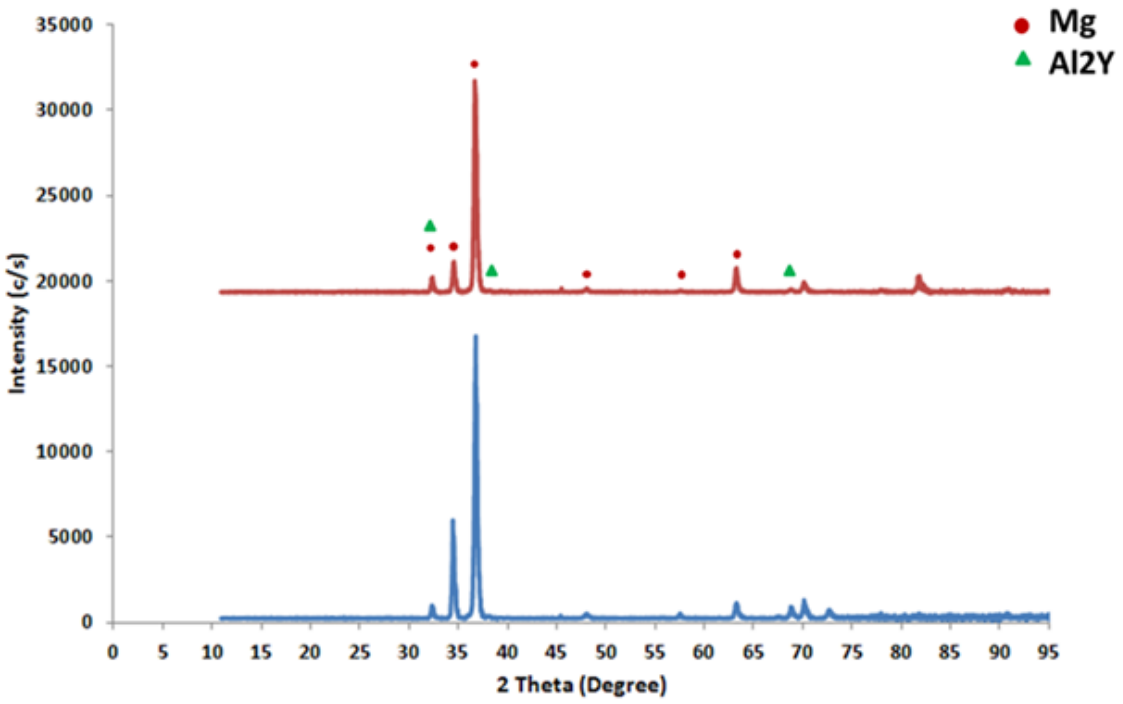

Fig. 3.1. XRD patterns of the as-cast AE42 (red) and AE44 (blue) samples.

SEM images of the cast AE42 and AE44 samples before shock loading are presented in Fig. 3.2. As can be seen the microstructure of these alloys is characterized by a magnesium matrix in which second phase particles are distributed. The structure of the second phases in the matrix can be classified as acicular, globular and plate-like (Fig. 3.2) and the acicular (or needle-like) morphology

is the dominant one. EDX analysis showed that these second phases are mainly composed of aluminum and yttrium. Considering the atomic percent of the elements obtained from EDX data, it was found that this second phase is Al_2Y, which is consistent with XRD results. By increasing the content of yttrium to 4% (AE44 sample, Fig. 3.2(b)), the Al_2Y phase appeared mainly in the form of short needles (acicular morphology) with no change in the composition, covering the whole area (Fig. 3.2(b)) of the microstructure.

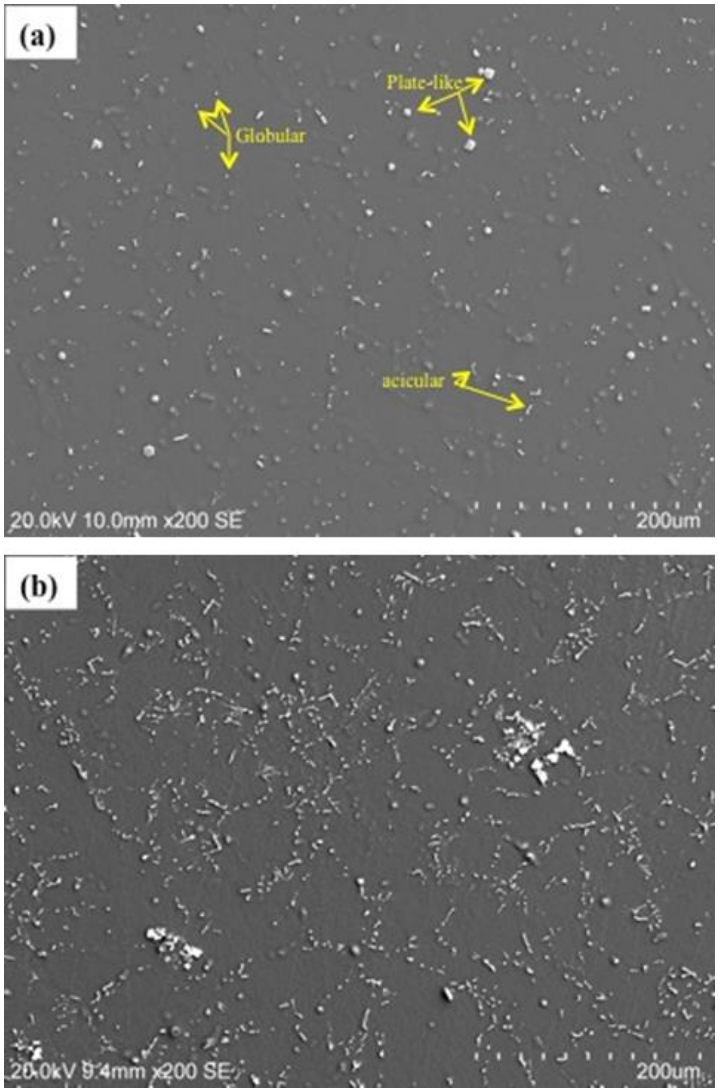

Fig. 3.2. SEM images of the as-cast samples before shock loading test; (a) AE42 and (b) AE44.

The (00.2) and (10.0) pole figures and inverse pole figures of the samples before shock loading tests are shown in Fig. 3.3. Both samples had weak texture intensities for (00.2) and (10.0) components and the maxima in the inverse pole figures were almost at the same position between

[0001] and [11-20] directions. However, in Fig. 3.4, which illustrates the (00.2) and (10.0) pole figures and inverse pole figures of the samples after shock loading tests at strain rates of 800 and 1100 s^{-1}, it is clear that texture intensities of (00.2) basal component is increased (particularly at 1100 s^{-1}) and the maxima in both inverse pole figures is shifted towards [0001] direction, showing the change in the texture and significant strengthening of the (00.2) basal texture component. In other words, after shock loading the weak initial texture of the cast samples was transformed to a strong (00.2) basal texture in which the basal planes in most grains are aligned parallel to the compression plane. The strengthening of basal texture, however, was higher in the AE42 samples compared to the AE44 samples at both strain rates (Fig. 3.4).

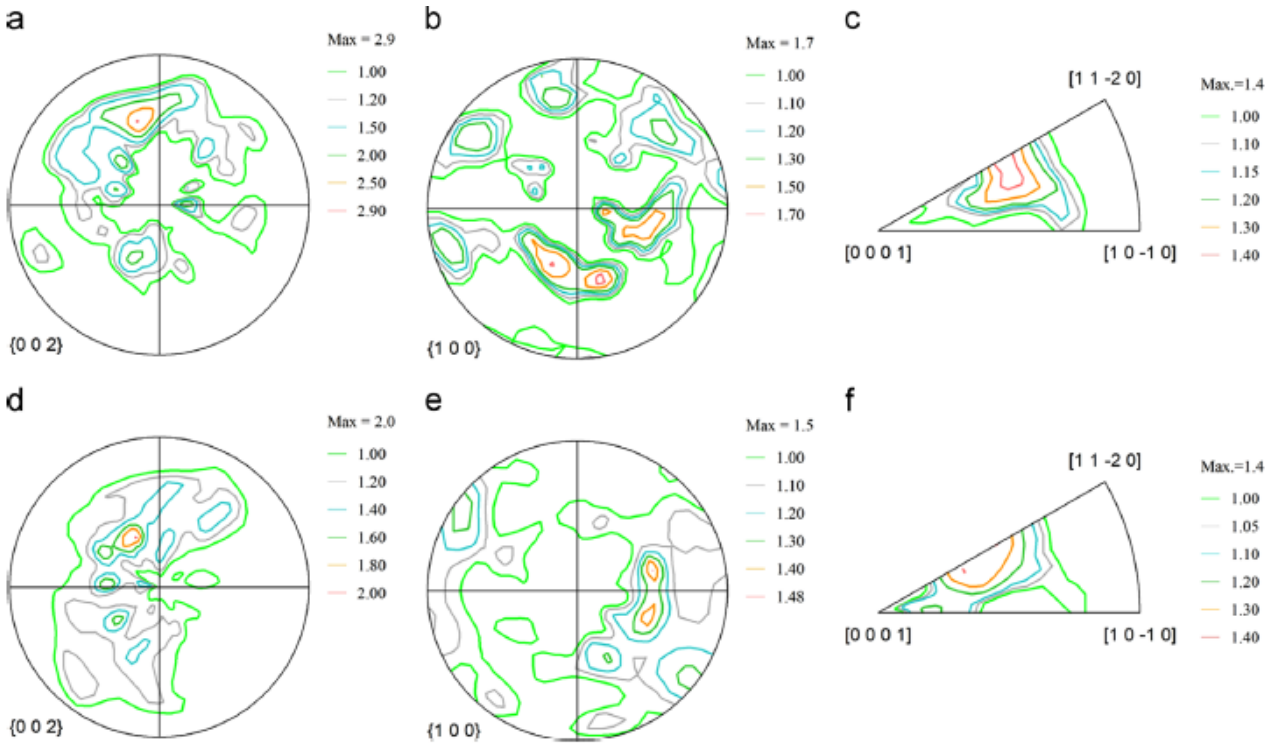

Fig. 3.3. (00.2) and (10.0) pole figures and inverse pole figures of the samples before shock loading test taken from the compression plane. [(a), (b) and (c): AE42; (d), (e) and (f): AE44].

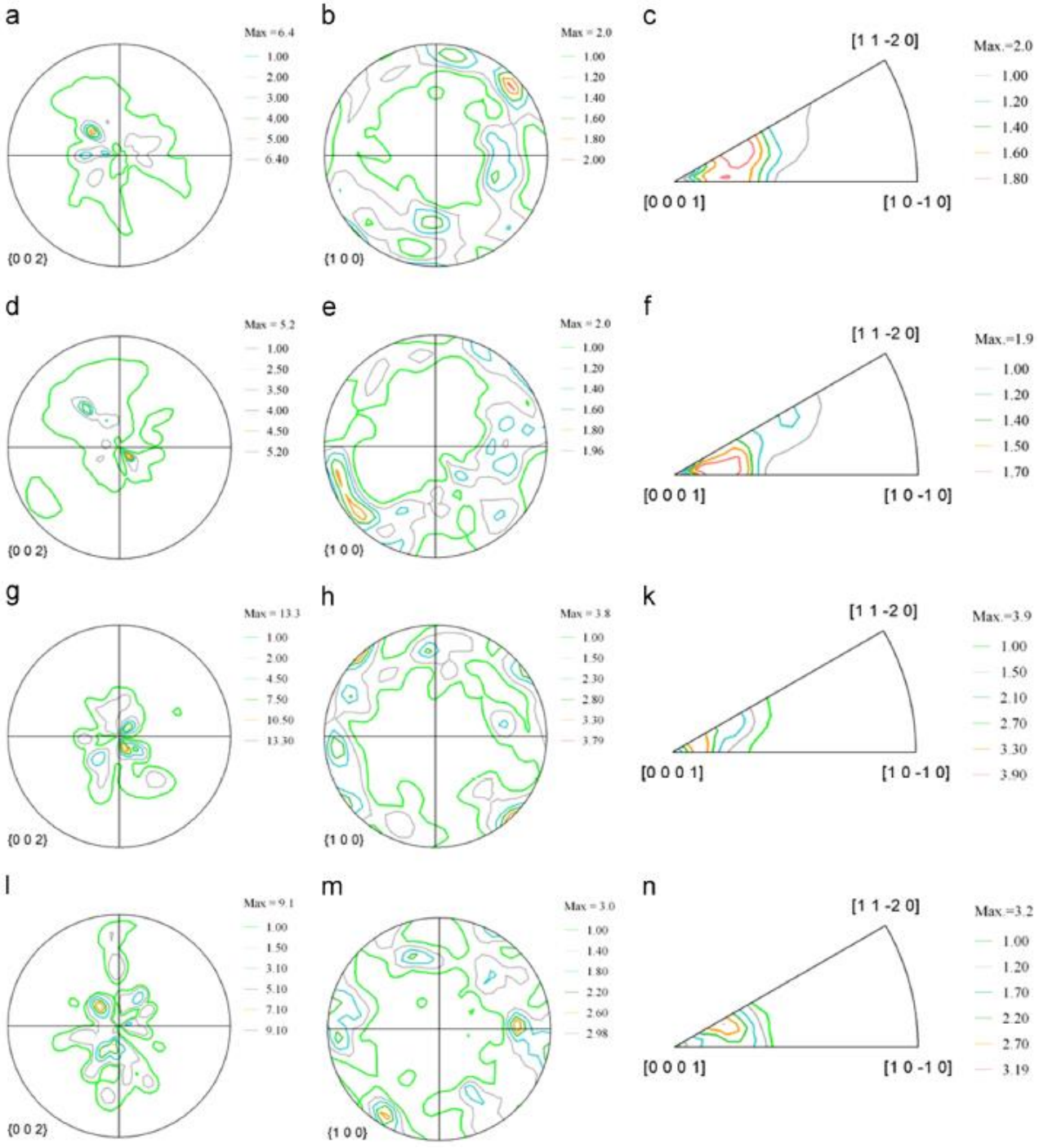

Fig. 3.4. (00.2) and (10.0) pole figures and inverse pole figures of the samples after shock loading test at strain rate of 800 and 1100 s^{-1}. [(a), (b) and (c):AE42, strain rate = 800 s^{-1}; (d), (e) and (f): AE44, strain rate = 800 s^{-1}; (g),(h) and(k): AE42, strain rate = 1100 s^{-1}; (l),(m) and (n): AE44, strain rate = 1100 s^{-1}].

Figs. 3.5 and 3.6 display the inverse pole figure and image quality maps of the samples after shock loading tests at both strain rates. It is seen that shock loading resulted in twinning in both samples and the amount that occurred was observed to decrease with increasing yttrium content of the alloys for both strain rates. Three types of twins formed in the samples during shock loading and are marked in Figs. 3.5 and 3.6. The main twins are extension twins (yellow), particularly in the AE42 sample. A smaller number of double twins (blue) and contraction twins (red) were also present. Another interesting aspect about the qualitative comparison between the IQ maps (Figs. 3.5 and 3.6) is that in both samples, by increasing the strain rate, the twinning fraction is decreased and fewer twins are observed in the maps (Fig. 3.6).

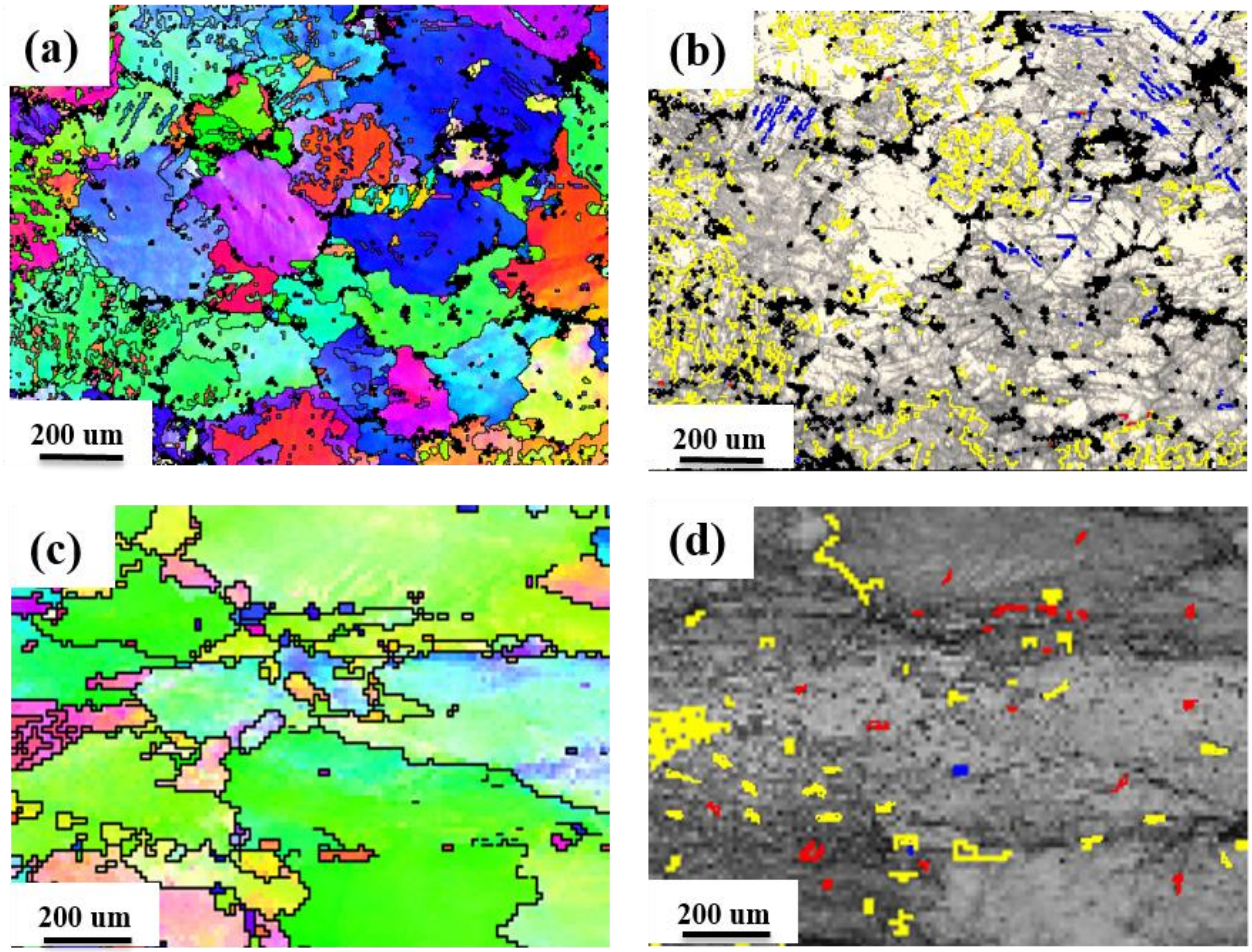

Fig. 3.5. Inverse pole figure (IPF) and image quality (IQ) maps of the samples showing the microstructure and twins type formed after shock loading test at 800 s^{-1}. (a) and (b): AE42; (c) and (d) : AE44. [*Note*: The extension twin boundaries ($86° < 11\bar{2}0 > \pm 5°$) are shown in yellow, the contraction twin boundaries ($56° < 11\bar{2}0 > \pm 5°$) are shown in red and the double twin boundaries ($38° < 11\bar{2}0 > \pm 5°$) are shown in blue].

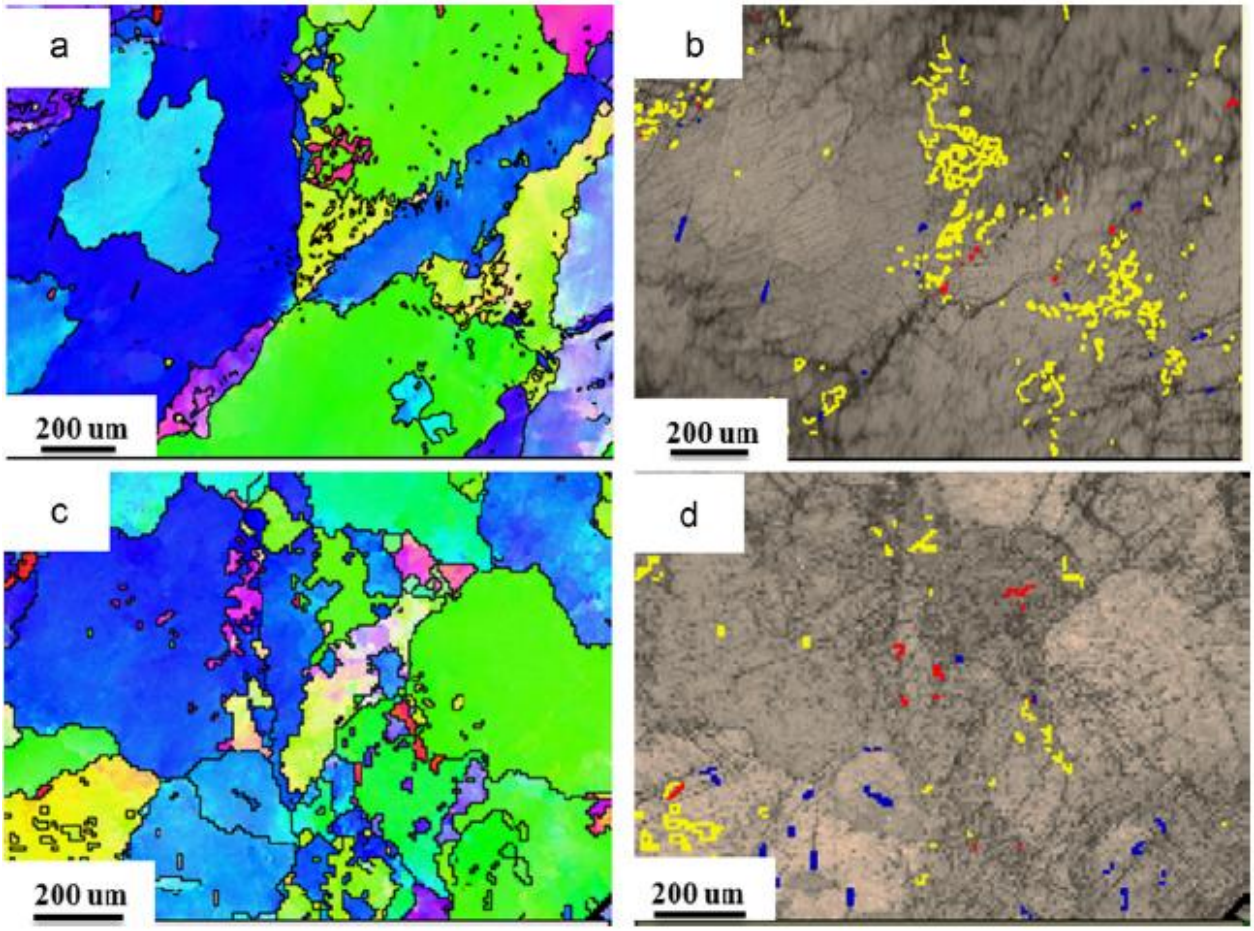

Fig. 3.6. Inverse pole figure (IPF) and image quality (IQ) maps of the samples showing the microstructure and twins type formed after shock loading test at 1100 s^{-1}. (a) and (b): AE42; (c) and (d) : AE44. [*Note*: The extension twin boundaries ($86° < 11\bar{2}0 > \pm 5°$) are shown in yellow, the contraction twin boundaries ($56° < 11\bar{2}0 > \pm 5°$) are shown in red and the double twin boundaries ($38° < 11\bar{2}0 > \pm 5°$) are shown in blue].

In Fig. 3.7, bright field TEM images of AE42 and AE44 samples after shock loading at both strain rates, i.e. 800 and 1100 s^{-1}, are shown. As is seen, in shock-loaded AE44 samples with higher concentration of yttrium, the density of dislocations is higher in comparison to AE42 at both strain rates. It seems that yttrium content in AE alloys is an effective parameter which affects the deformation mechanism by affecting the fraction of twins (Figs. 3.5 and 3.6) and density of dislocations (Fig. 3.7). Moreover, at higher strain rates in both samples (Fig. 3.7(c) and 3.7(d)), the dislocation density increases in comparison to the lower strain rates (Fig. 3.7(a) and 3.7(b)).

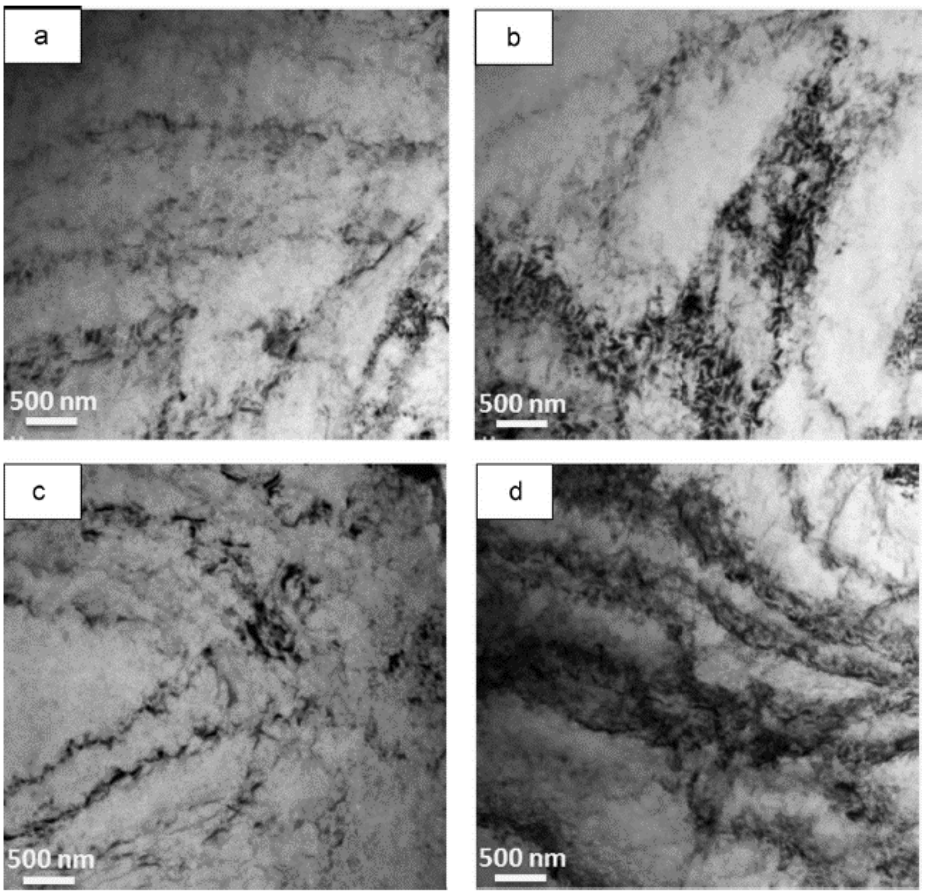

Fig. 3.7. Bright field TEM images of shock-loaded samples at 800 and 1100 s^{-1}: (a) AE42 at 800s^{-1} ;(b) AE44 at 800 s^{-1} ;(c) AE42 at 1100 s^{-1}; (d) AE44 at 1100 s^{-1}.

The true compressive stress-strain curves of the AE42 and AE44 alloys and corresponding strain hardening rate are shown in Fig. 3.8. The true stress-strain curves had a sigmoidal shape and the stress increased to a maximum and then decreased. As it is observed in Figs. 3.8(a) and 3.8(c), increasing the yttrium content led to an increase in the stress and ductility. Furthermore, considering the hardening diagrams in Figs. 3.8(b) and 3.8(d), it was found that by increasing the yttrium content, the hump on the hardening curves was attenuated and broadened.

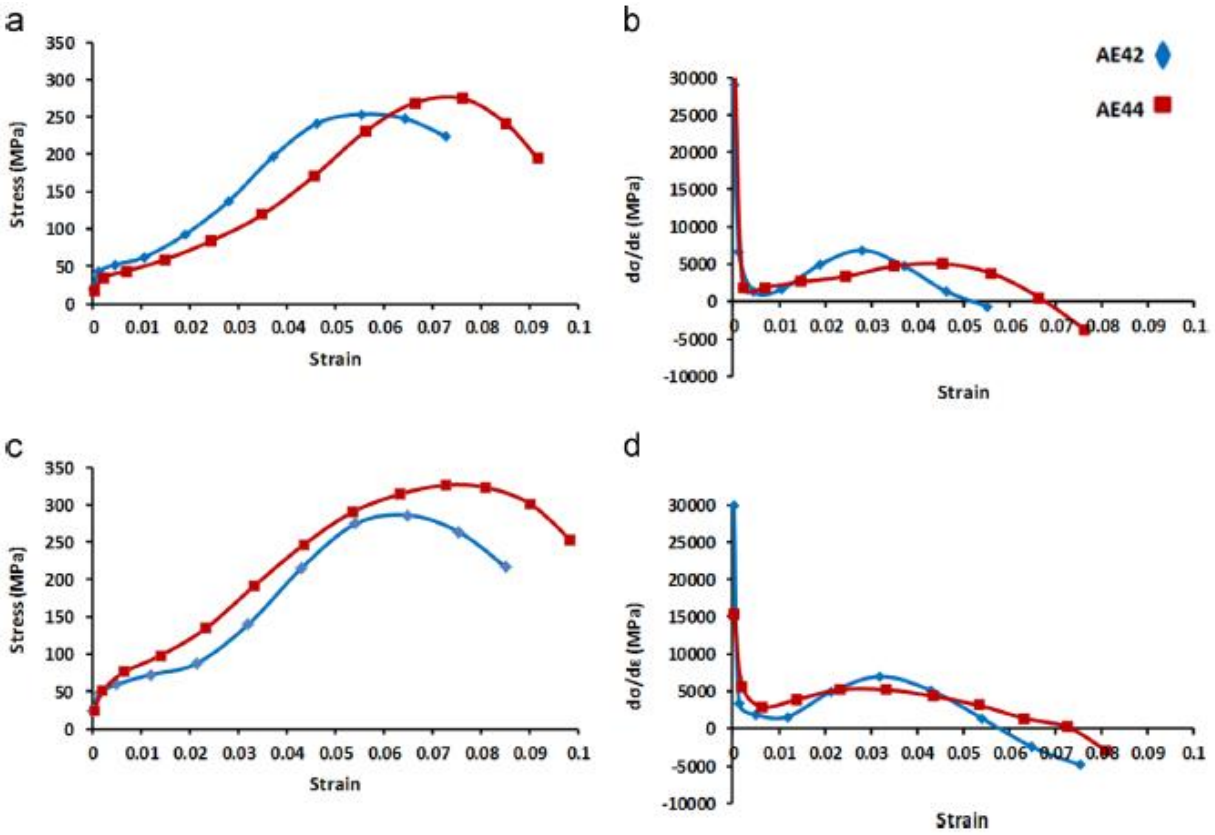

Fig. 3.8. True stress-strain curves and corresponding hardening diagrams (strain hardening rate vs strain) of AE42 and AE44 after shock loading: (a) and (b) strain rate =800 s^{-1}; (c) and (d) strain rate=1100 s^{-1}.

3.6. Discussion

It is shown in Fig. 3.1 that the yttrium in investigated magnesium alloys formed an intermetallic phase and the diffraction lines of Al_2Y phase in XRD patters confirmed the presence of this phase in the as-cast samples. SEM images show that the morphology of the second phases can be acicular (needle-like), globular and plate-like (Fig. 3.2) and the EDX technique helped to identify that these morphologies represent Al_2Y phase. Similar morphologies of precipitates and phases were observed in other research studies [4,8-9,12]. It is worth noting that other phases such as β-$Mg_{17}Al_{12}$, $Al_{11}RE_3$ and Al_2RE could have been present in the alloys, however, they did not appear in the XRD patterns probably because of their low volume fractions. Therefore, in this research study, only the effects of Al_2Y phase, having a large volume fraction, was considered on the twinning and mechanical behavior of AE alloys. Presence and volume fraction Al_2Y phase may affect the deformation behavior of AE alloys and will be discussed later.

Another feature of the SEM images is that increasing the yttrium content of the alloy led to increase in the volume fraction of the second phases, which can be ascribed to the further reaction between aluminum and rare-earth (RE) elements [12]. As was mentioned earlier, AZ and AM series do not have sufficient creep resistance for high temperature applications and RE elements are therefore added to improve the mechanical properties of magnesium alloys [4-5,10-11]. For example, in AZ or AM series, aluminum reacts with magnesium and forms the brittle β-$Mg_{17}Al_{12}$ phase, which is detrimental for formability [8-9, 15-17]. To improve the ductility of Mg-Al-based castings which contain high amounts of aluminum, the volume fraction of the brittle β-$Mg_{17}Al_{12}$ phase must be highly decreased. Yttrium, as one of the RE elements with wide application in magnesium alloys, react with aluminum to form Al_2Y phase, suppressing the formation of β-$Mg_{17}Al_{12}$. Formation of Al_2Y may increase the ductility of the rare-earth containing magnesium alloys compared to that of AZ or AM series [4-5, 12]. In the current study, as was shown by SEM images and XRD results, there was almost no brittle beta phase in the RE containing alloys.

The textures of the samples were exhibited by the pole figures and inverse pole figures before and after shock loading test in Figs. 3.3 and 3.4, respectively. According to Fig. 3.3, a weak or near-random texture developed in the samples, which is a typical texture of cast magnesium alloys [18]. However, after shock loading at both strain rates, a strong basal texture appeared in the pole figures, particularly for the samples shock-loaded at 1100 s^{-1}, and the maxima in the inverse pole figures shifted towards [0001] direction, indicating that the initial texture significantly changed (Fig. 3.4). In other words, the basal planes in the cast samples were aligned perpendicular to the direction of compressive shock loading. The change in the texture of the cast samples after shock loading, particularly AE42 sample with stronger basal component after shock loading, could be attributed to the twinning and its related effects on the grain reorientations [6,19-25].

The role of twinning becomes very important in deformation of magnesium and its alloys because the slip systems in magnesium and its alloys (except for pyramidal slip system with a high CRSS value) cannot accommodate any strain along the longitudinal axis of magnesium crystal structure. Therefore, to accommodate applied strains parallel to the c-axis, activation of twinning or pyramidal <c + a> slip is required. Activation of pyramidal <c+a> slip, unfortunately, is very difficult at low temperatures because of its high CRSS and therefore twinning becomes an important deformation mechanism particularly for straining along the c-axis [21-24, 26-29].

From the texture measurements (Fig. 3.4) a significant strengthening of basal texture component is observed which could indicate that several types of twinning were activated during shock loading. Due to the very weak initial texture of the cast samples (Fig. 3.3), grains with different orientations could have provided favorable conditions for the occurrence of different types of twins during the shock loading. Occurrence of several types of twinning systems resulted in the considerable reorientation of the grains and consequently, the texture changed after deformation at high strain rates.

As is illustrated in Figs. 3.5 and 3.6, the twinning occurred in the shock loaded samples at both strain rates. Image quality maps show that three types of twins are present in the samples of both alloys at both strain rates. Also, it is observed that in both samples at both strain rates (Figs. 3.5 and 3.6), most of the regions have experienced extension twinning which can be related to its lower CRSS that makes this twinning a very effective and active deformation mode in magnesium alloys [21-23,26,27]. Another important point about Figs. 3.5 and 3.6 is that by increasing the yttrium content of the alloys, total twinning fraction (including the extension, contraction and double twinning fraction) decreased at both strain rates and less twinning occurred in AE44 in comparison to AE42 which could have resulted in weaker basal texture component in AE44 sample after shock loading at both strain rates, as shown in the results of texture measurements (Fig. 3.4).

Although the actual reasons for a decrease in the activation of twinning mechanism with the increase of RE element content such as yttrium is still not clear [10], this suppression in twinning mechanism may be related to the presence of higher volume fractions of Al_2Y in AE alloys with higher content of yttrium. Referring to Fig. 3.2, volume fraction of the Al_2Y second phase particles increased with increase in the yttrium content of the alloy. It seems that increasing the volume fraction of second phase particles, i.e. Al_2Y, could have restricted the nucleation and growth of the twinning systems, leading to decrease in the fraction of twins particularly extension twins [20]. Decreased twinning fraction (Figs. 3.5 and 3.6) together with increased dislocation density (Fig. 3.7), which resulted from the increased yttrium content could be explained by a more important effect of second phase particles which might be the change in the deformation mechanism [20]. In other words, increasing the yttrium content in AE alloys (that increases the volume fraction of Al_2Y phase) could have activated more slip dislocations and suppressed twinning. The same authors found the similar effect in AZ cast magnesium alloys in which by increasing the volume fraction of $Mg_{17}Al_{12}$, twinning activation was decreased in AZ alloys with higher content of aluminum [21].

Weaker presence of contraction and double twins in the samples can also be explained by the high CRSS of these twins [22-24,26-31].

Figs. 3.8(a) and 3.8(c) show the true compressive stress-strain curves of the samples at strain rates of 800 and 1100 s^{-1}. Samples exhibited a S-shaped flow behavior, meaning that twinning is the dominant deformation mode [18,32,33]. Yielding is observed on the flow curves and by increasing the strain, the maximum stress is achieved followed by the decrease in the stress.

The plots of strain hardening rates against strain (Figs. 3.8(b) and 3.8(d)) exhibit three regions: in the first region, strain hardening decreases, then it increases and finally, in the third step, decreases again, resulting in the formation of a hump due to the change in the deformation mechanisms [34]. During the deformation process, twin boundaries block dislocation motion and this results in dislocation accumulation (Fig. 3.9) behind the twin boundaries [2,18,34-35]. This blocking effect against dislocation motion becomes more effective at higher strain rates (Fig. 3.9(c) and 3.9 (d)) in both alloys due to the presence of more dislocations in the microstructure. Additionally, dislocations may accumulate at twin intersections (Fig. 3.10) and this would also contribute to hardening. This effect, i.e. impeding the dislocation motion by intersecting twins, is also more remarkable at higher strain rates (Fig. 3.10(c) and 3.10(d)) because of denser pile-ups of dislocations in between the twins and behind the twin boundaries at intersections. The dislocation accumulation is known as an effective process in increasing the strain hardening rate of magnesium alloys [2, 18, 34-35].

Another parameter, which may be involved in the hardening process, is the activation of non-basal slip systems. It is worth noting here that in Figs. 3.8(b) and 3.8(d), the humps on the hardening diagrams of AE44 sample were wider than those of AE42. Widening of hardening curves could have resulted from the activation of more slip systems, particularly pyramidal <c+a> slip systems. As a result of possible activation of additional slip modes, hardening rate decreased [34]. In the present study, increase in the temperature during shock loading and presence of yttrium in the alloys, particularly in AE44 sample with about 4% of yttrium, may be considered as effective factors for higher activation of the pyramidal <c+a> slip systems [10, 30-31], which also resulted in better ductility of AE44 alloys at both strain rates (Fig. 3.8(a) and 3.8(c)).

Another aspect which is affected by the increased temperature during shock-loading could be the twinning fraction and dislocation density in shock-loaded samples. As it was seen in the results section, by increasing the strain rate in both alloys, the twinning fraction decreased (Figs. 3.5 and

3.6) and the dislocation density increased (Fig. 3.7) in the microstructure of the shock-loaded samples. This decrease in the twinning fraction and increase in the dislocation density with increased strain rate can be related to the increased CRSS of twinning and decreased CRSS of slip systems, such as pyramidal <c+a>, resulted from the further increase in temperature at higher strain rates [35]. In fact, increased strain rates will lead to further increase in the temperature during shock-loading and probability of the activation of more slip systems (i.e. more slip dislocations) is increased but the twinning contribution to the deformation process is decreased and therefore, the total fraction of twinning is decreased and the dislocation density is increased at higher strain rates [30,31,35,36].

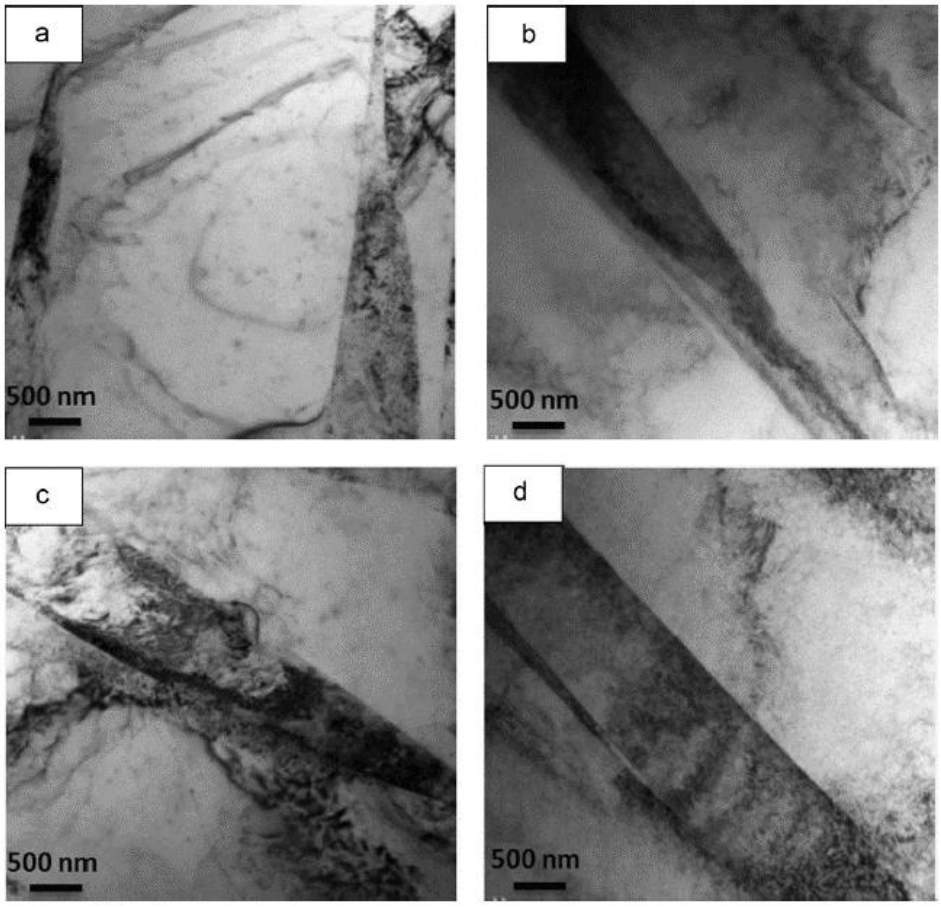

Fig. 3.9. Bright field TEM images of shock-loaded samples at 800 and 1100 s^{-1}, showing the accumulation and pile-ups of dislocations at/behind the twin boundaries: (a) AE42 at 800 s^{-1} ;(b) AE44 at 800 s^{-1} ;(c) AE42 at 1100 s^{-1}; (d) AE44 at 1100 s^{-1}.

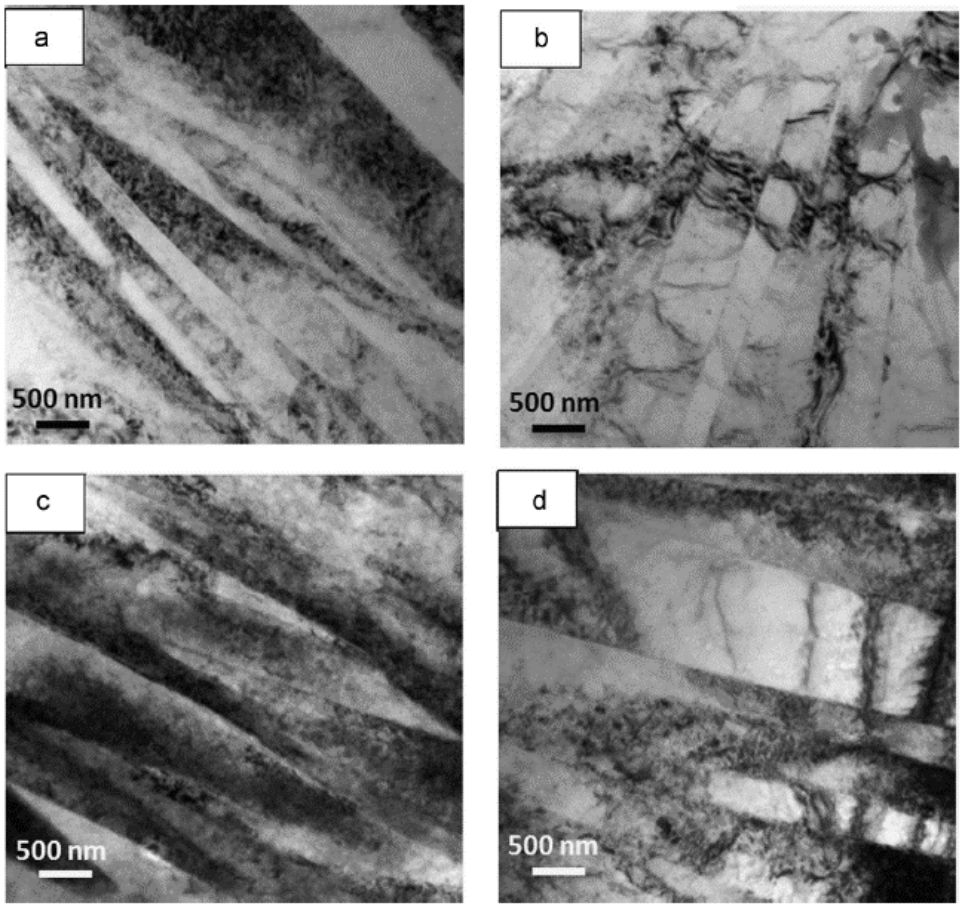

Fig. 3.10. Bright field TEM images of shock-loaded samples at 800 and 1100 s^{-1}, showing the accumulation and pile-ups of dislocations in between the twins and twin intersections: (a) AE42 at 800 s^{-1} ;(b) AE44 at 800 s^{-1} ;(c) AE42 at 1100 s^{-1}; (d) AE44 at 1100 s^{-1}.

3.7. Conclusions

This research focused on the texture formation, microstructural evolution and mechanical behavior of cast AE magnesium alloys due to the presence of a considerable lack of knowledge in the open literature about the dynamic deformation behavior of rare-earth containing cast AE magnesium alloys. Experimental results, obtained by different techniques such as XRD, SEM and TEM showed that:

1- Three types of morphology of precipitates, namely acicular (needle-like), globular and plate-like, were observed in the microstructure of the cast samples with a composition of Al_2Y. Also, after shock loading a stronger (00.2) basal texture developed in AE42 samples at both strain rates used in this research study (800 and 1100 s^{-1}).

2- Increasing the yttrium content in the cast alloys resulted in increase in the volume fraction of the second phase, i.e. Al_2Y. As a result, the tensile strength and ductility of the alloys for both strain rates increased which is an interesting result for high-strain rate applications of AE alloys.

3- It was found that by increasing the yttrium content in the alloys, the contribution of twinning in deformation process decreased but the dislocation density increased and the shape of the hardening diagrams changed at both strain rates used in this research (800 and 1100 s^{-1}). It is proposed that the decrease in twinning activity and increase in dislocation density, which resulted from increase in yttrium content, could be related to the increase in the volume fraction of second phase Al_2Y. The Al_2Y phase could have decreased the nucleation and activation of twinning systems.

References

[1] Li Q. Mechanical properties and microscopic deformation mechanism of polycrystalline magnesium under high-strain-rate compressive loadings. Materials Science and Engineering A 2012; 540:130-134.

[2] Korla R., Chokshi AH. Strain-rate sensitivity and microstructural evolution in a Mg–Al–Zn alloy. Scripta Materialia 2010; 63: 913-916.

[3] Mordike BL, Ebert T. Magnesium: Properties — applications — potential. Materials Science and Engineering A 2001;302: 37-45.

[4] Nouri M, Sun X, Li DY. Beneficial effects of yttrium on the performance of Mg–3%Al alloy during wear, corrosion and corrosive wear. Tribology International 2013;67: 154-163.

[5] Agnew SR, Duygulu O. Plastic anisotropy and the role of non-basal slip in magnesium alloy AZ31B. International Journal of Plasticity 2005; 21:1161-1193.

[6] Lou XY, Li M, Boger RK, Agnew SR, Wagoner RH. Hardening evolution of AZ31B Mg sheet. International Journal of Plasticity 2007;23:44-86.

[7] Lee SG, Patel GR, Gokhale AM, Sreeranganathan A, Horstemeyer MF. Quantitative fractographic analysis of variability in the tensile ductility of high-pressure die-cast AE44 Mg-alloy. Materials Science and Engineering A 2006;427: 255:262.

[8] Bakke P, Pettersen K, Westengen H. Enhanced ductility and strength through RE addition to magnesium die casting alloys. Magnesium Technology 2003; 171-176.

[9] Bakke P, Pettersen K, Westengen H. Improving the Strength and Ductility of Magnesium Die-Casting Alloys via rare-earth addition. JOM 2003;46-51.

[10] Sandlöbes S, Zaefferer S, Schestakow I, Yi S, Gonzalez-Martinez R. On the role of non-basal deformation mechanisms for the ductility of Mg and Mg–Y alloys. Acta Materialia 2011; 59: 429-439.

[11] Farzadfar SA, Sanjari M, Jung I-H, Essadiqi E, Yue S. Role of yttrium in the microstructure and texture evolution of Mg. Materials Science and Engineering A 2011; 528:6742-6753.

[12] Kiełbus A. Microstructure of AE44 magnesium alloy before and after hot-chamber die casting. Journal of Achievements in Materials and Manufacturing Engineering 2007;20:459-462.

[13] Rzychoń T, Kiełbus A, Cwajna J, Mizera J. Microstructural stability and creep properties of die casting Mg–4Al–4RE magnesium alloy. Materials Characterization 2009; 60:1107-1113.

[14] Zhang X, Zhang K, Li X, Wang C, Li H, Wang C, Deng X. Corrosion and electrochemical behavior of as-cast Mg-5Y-7Gd-1Nd-0.5Zr magnesium alloys in 5% NaCl aqueous solution. Progress in Natural Science: Materials International 2011;21:314-321.

[15] Paramsothy M, Tan XH, Chan J, Kwok R, Gupta M. Al2O3 nanoparticle addition to concentrated magnesium alloy AZ81: Enhanced ductility. Journal of Alloys and Compounds 2012; 545:12–18.

[16] Yang Z, Li JP, Zhang JX, Lorimer GW, J Robson. Review on Research and Development of Magnesium Alloys. Acta Metallurgica Sinica 2008; 21:313-328.

[17] Asgari H, Szpunar JA, Odeshi AG, Gurao NP. Investigation on the texture and mechanical behavior of AZ cast magnesium alloys under compressive shock loading. Proceedings of the 24th Canadian Congress of Applied Mechanics 2013; Saskatoon, Canada.68-71.

[18] Jiang L, Jonas JJ, Luo AA, Sachdev AK, Godet S. Influence of {10-12} extension twinning on the flow behavior of AZ31 Mg alloy. Materials Science and Engineering A 2007;445-446: 302:309.

[19] B. Beausir, L.S. Toth, F. Qods, K.W. Neale. Texture and mechanical behavior of magnesium during free-end torsion. Journal of Engineering Materials and Technology 2009; 131: 1.

[20] Koike J, Kobayashi T, Mukai T, Watanabe H, Suzuki M, Maruyama K, Higashi K. The activity of non-basal slip systems and dynamic recovery at room temperature in fine-grained AZ31B magnesium alloys. Acta Materialia 2003;51:2055-2065.

[21] Asgari H, Odeshi A.G, Szpunar JA. On dynamic deformation behavior of WE43 magnesium alloy sheet under shock loading conditions Materials & Design 2014; 63:552-564.

[22] Jiang L, Jonas JJ, Luo AA, Sachdev AA, Godet S. Twinning-induced softening in polycrystalline AM30 Mg alloy at moderate temperatures. Scripta Materialia 2006; 54:771–775.

[23] Kelley EW, Hosford WF. Plane strain compression of magnesium and magnesium alloy crystals. Trans. Metall. Soc. AIME. 1968; 242:5-13.

[24] Obara T, Yoshinga H, Morozumi S. {1122}〈1123〉 Slip system in magnesium. Acta Metallurgica 1973; 21:845-853.

[25] Barnett MR. A Taylor model based description of the proof stress of magnesium AZ31 during hot working. Metallurgical and Materials Transactions A 2003;34:1799–1806.

[26] Yoo MH. Slip, twinning, and fracture in hexagonal close-packed metals. Metallurgical and Materials Transactions A 1981;12:409.

[27] Wonsiewicz BC, Backofen WA. Plasticity of Magnesium Crystals. Trans TMS-AIME 1967;239:1422–1431.

[28] Agnew SR, Duygulu O. TEM investigation of dislocation mechanisms in Mg alloy AZ31B sheet. Mag. Tech. Conf. Proceedings 2004; 61-65.

[29] Keshavarz Z, Barnett MR. EBSD analysis of deformation modes in Mg–3Al–1Zn. Scripta Materialia 2006;55:915-918. [30] S. Ando, M. Tanaka, H. Tonda. Materials Science Forum 2003;419–422:87–92.

[31] Ando S, Tonda H. Non-Basal Slips in Magnesium and Magnesium-Lithium Alloy Single Crystals. Materials Science Forum 2000;350–351:43–8.

[32] Fatemi-Varzaneh SM, Zarei-Hanzaki A, Paul H. Characterization of ultrafine and nano grained magnesium alloy processed by severe plastic deformation. Materials Characterization 2014; 87:27–35.

[33] Chino Y, Kimura K, Mabuchi M. Twinning behavior and deformation mechanisms of extruded AZ31 Mg alloy. Materials Science and Engineering A 2008;486:481-488.

[34] Khan AS, Pandey A, Gnäupel-Herold T, Mishra RK. Mechanical response and texture evolution of AZ31 alloy at large strains for different strain rates and temperatures. International Journal of Plasticity 2011; 27: 688–706.

[35] Obara T, Yoshinga H, Morozumi S. {1122}〈1123〉 Slip system in magnesium. Acta Metallurgica 1973; 21:845-853. [36] H. Asgari, J. A. Szpunar, A. G. Odeshi, L. J. Zeng, E. Olsson. Materials Science and Engineering A 2014; 618:310-322.

CHAPTER 4

EXPERIMENTAL AND SIMULATION ANALYSIS OF TEXTURE FORMATION AND DEFORMATION MECHANISM OF ROLLED AZ31B MAGNESIUM ALLOY UNDER DYNAMIC LOADING

4.1. Overview of Chapter 4

In the previous chapters, the deformation behavior and related deformation mechanisms of shock loaded cast AZ and AE alloys were discussed. Hereafter, the focus is on the magnesium rolled plates and dynamic mechanical behavior of the rolled AZ31B-H24 and WE43 alloys.

In this chapter, the effect of initial texture and strain rate on the deformation behavior of rolled AZ31B-H24, with a strong initial basal texture, at high strain rates are discussed. The involved deformation mechanisms will also be explained using both experimental and simulation results.

This chapter is presented as manuscript # 3. The author's (H. Asgari) contributions to this manuscript are: (a) preparation and processing of the samples for shock loading test. (b) XRD, SEM, EDS, TEM, EBSD and simulation analyses. (c) Reviewing the relevant literature, writing and submission of the manuscript. The contribution of Dr. L. J. Zeng and Prof. E. Olsson was in the area of TEM investigation and analysis.

The manuscript was published in *Materials Science & Engineering A*:

- H. Asgari, J.A. Szpunar, A.G. Odeshi, L.J. Zeng, E. Olsson. "Experimental and simulation analysis of texture formation and deformation mechanism of rolled AZ31B magnesium alloy under dynamic loading", Materials Science & Engineering A, 618 (2014) 310–322.

The manuscript presented here is different from that of published in the following parts:

- In order to avoid repetition in content, some parts of the ‘introduction’,‘experimental procedure’ and ‘discussion’ sections were eliminated.

The copyright permission to use the manuscript in the thesis was obtained and provided in the Appendix section.

Experimental and simulation analysis of texture formation and deformation mechanism of rolled AZ31B magnesium alloy under dynamic loading

H. Asgari[1], J. A. Szpunar[1], A. G. Odeshi[1], L. J. Zeng[2], E. Olsson[2]

[1]Department of Mechanical Engineering, University of Saskatchewan, Saskatoon, Canada

[2]Department of Applied Physics, Chalmers University of Technology, Göteborg, Sweden

4.2. Abstract

Magnesium alloy components are potentially used under shock loading conditions. Considering the fact that deformation behavior is completely different under high strain rate conditions compared to that of low strain rate, evaluation of the dynamic deformation and related mechanisms in magnesium alloys are important. In this research, texture formation, microstructural changes and dynamic deformation behavior of rolled AZ31B in the tempered H24 stress-relieved conditions, shock-loaded under compressive dynamic loading, were investigated. Texture measurements showed that the as-received AZ31B alloy had a strong (00.2) basal texture. Four groups of cylindrical samples were cut in the rolling direction (RD), at 45° to the RD, in the transverse direction (TD) and in the direction perpendicular to the RD-TD plane. Dynamic shock loading of the test samples was conducted using Split Hopkinson Pressure Bar at room temperature at strain rates ranging from 600 to 1100 s^{-1}, while loading direction was parallel to the longitudinal axis of the cylindrical samples. After high strain rate deformation, although the loading direction was different, a strong (00.2) basal texture was observed in all samples. It was inferred that increasing the strain rate led to an increase in strength and ductility, but to a decrease in twinning fraction, indicating the possible activation of non-basal <c+a> slip systems. Besides, a high degree of mechanical anisotropy was found for all strain rates used such that the lowest strength was registered for the samples cut along the direction parallel to the rolling direction. Visco-plastic self-consistent simulation was used to predict the texture formation mechanisms at high strain rates.

Keywords: Rolled magnesium alloy, Mechanical anisotropy, Twinning, Deformation texture

4.3. Introduction

Magnesium alloys are increasingly used in automotive industries because of their low density which result in decreased fuel consumption and reduced CO_2 emissions [1-3]. Unfortunately, their low ductility have considerably limited the application of magnesium sheets [4-6].

Basal slip is the main deformation mode in magnesium alloys [2,4-10]. Basal slip, unfortunately, is not able to provide enough slip systems to generate uniform deformation in magnesium and its alloys. Another problem, related to basal slip is the lack of accommodation of deformation along the c-axis. However, by activation of other types of deformation modes, such as pyramidal systems, the number of active slip systems increases and von-Mises criterion can be fulfilled [11-16]. Another important deformation mode in magnesium is twinning. The activation of this mode may support the possible straining, contraction or extension, along the c-axis [17-22].

Since the deformation behavior of wrought magnesium alloys is highly dependent on the initial texture, it is very important to evaluate and understand the dynamic mechanical behavior and microstructural evolution of magnesium alloys under impact loading in different loading directions. However, the mechanical behavior and deformation mechanisms of magnesium alloys under shock loading conditions have not yet been comprehensively investigated. Particularly, the effect of initial texture on the microstructural evolution, deformation mechanisms and anisotropic mechanical properties is still not very clear. The studies that have been conducted to date have mostly focused on extruded AZ and AM alloys [23-28] and there are a few reports on the dynamic mechanical behavior and microstructural evolution of the AZ31 sheet, which are only based on experimental results [29-32]. For example, it was shown that the fracture morphology of AZ31B under high strain rates and high temperatures is mainly composed of the dimple pattern, indicating ductile fracture under these conditions [32]. In another research study, it was observed using SEM that by increasing the strain rate, the twinning fraction decreased and it was ascribed to the possible localized flow [31]. However, as mentioned previously, the information on dynamic behavior of AZ31B in the open literature is very limited and there is no comprehensive report about texture measurement, microstructural evolution, mechanical properties, simulation of texture and their correlations in the open literature. Therefore, the main aim of the current study is to investigate the effects of initial texture and high strain rate deformation on the texture evolution, microstructural change, deformation mechanisms and anisotropic mechanical behavior of rolled AZ31B alloy by both experimental and simulation analysis. The samples were tested under different high strain rate

conditions using Hopkinson bar apparatus and the correlation between the initial textures, deformation mechanisms and mechanical properties is discussed. Besides, using Visco-Plastic Self-Consistent (VPSC) model with a tangent approach, possible deformation mechanisms were evaluated. The results can be an important addition to the current knowledge available on the deformation mechanisms of AZ31B magnesium alloys at high strain rate conditions.

4.4. Experimental procedure

Hot-rolled AZ31B magnesium alloy sheet in the tempered H24 stress-relieved conditions, provided by M&B MAG Ltd Company with its nominal chemical composition as presented in Table 4.1, was used in this research.

Table 4.1. Nominal chemical composition (in wt.%) of the investigated rolled AZ31B alloy.

Mg	Al	Zn	Mn	Si	Ca
Bal.	2.5-3.5	0.7-1.3	0.2-1	0.05	0.04

Split Hopkinson Pressure Bar (SHPB) was used for conducting shock loading tests. The strain rates used in this research are 600, 800 and 1100 s^{-1}. In order to ensure different initial texture, four groups of samples (Fig. 4.1) were cut in the rolling direction (RD, denoted as IP0), at 45° to the RD (denoted as IP45), in the transverse direction (TD, hereafter denoted as IP90) and in the direction perpendicular to the RD-TD plane (denoted as OP).

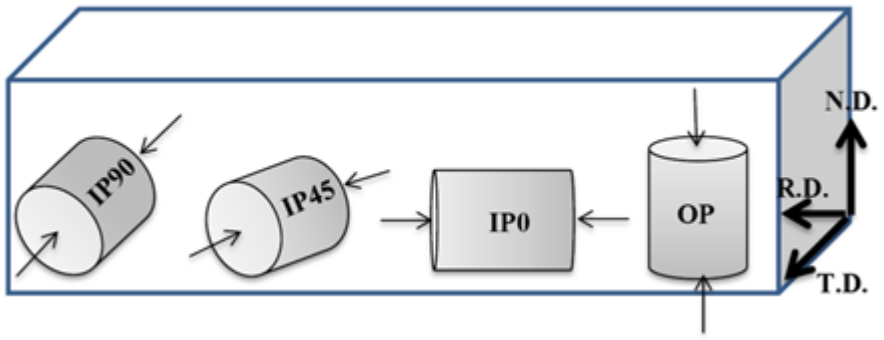

Fig. 4.1. Schematic diagram of the samples for shock loading tests and corresponding compression directions (thin arrows).

The details of shock loading tests, texture measurements, SEM, TEM and EBSD are similar to the manuscript #1 and #2 (Chapters 2 &3). It is not repeated here in order to keep the thesis concise.

Using VPSC-7 developed by Lebensohn and Tome [35], possible deformation mechanisms of the shock loaded samples were analyzed. The values of critical resolved shear stress (CRSS) used

in the VPSC simulations are listed in Tables 4.2 and 4.3 and will be discussed later. In the simulations, 2000 grains were used to represent the initial texture of the samples; the volume fraction of the grains is the same but each grain has its own orientation. Besides, a simplified linear hardening was assumed for all slip systems and extension twinning which is given as [35]:

$$\hat{\tau}^s = \tau_0^s + \theta^s \Gamma,$$

$$\Gamma = \sum_s \gamma^s \quad (1)$$

where θ^s and τ_0^s are the shear strain hardening rate and the initial threshold stress for the shear system *s*. Also, γ^s is the accumulated shear strain on the system *s*. In this research, it was assumed that the increase in critical resolved shear stresses is linear during deformation.

4.5. Results

Fig. 4.2 shows the microstructure and (00.2) pole figure of the as-rolled alloy before shock loading experiment. As is evident, the alloy has an almost twin-free microstructure (Fig. 4.2(a)) and a strong basal texture (Fig. 4.2(b)). The peak intensity is about 5.7 multiples of a random distribution (MRD) and basal poles are tilted away from ND toward RD so that spreading of the poles toward RD is larger than that of TD.

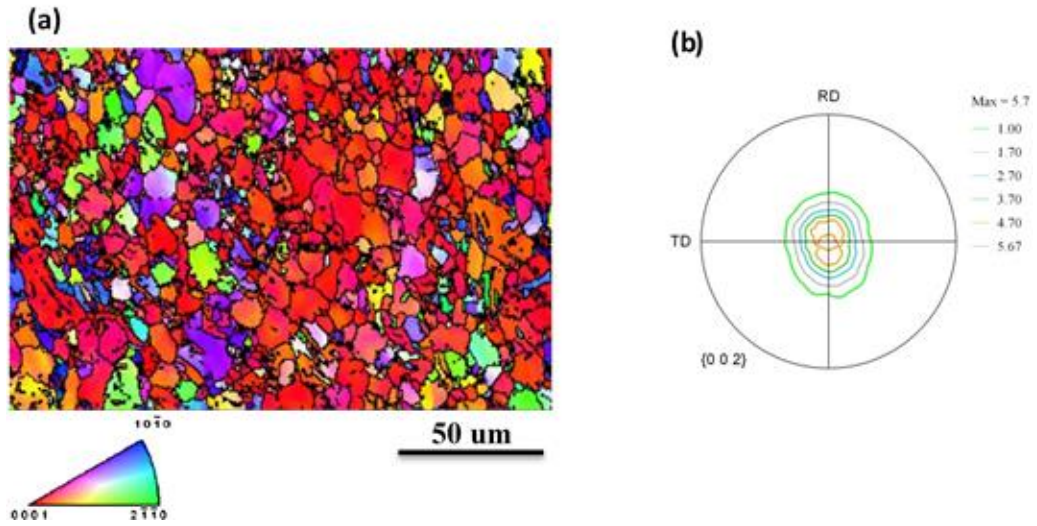

Fig. 4.2. (a) Microstructure and (b) (00.2) pole figure of the as-rolled AZ31B alloy.

In Fig. 4.3, the recalculated (00.2) and (10.0) pole figures (PF) and inverse pole figure (IPF) of the samples cut from the as-received sheet are presented. The (00.2) pole figures of OP sample show a strong basal texture (Fig. 4.3(a)). Also in the inverse pole figure of OP sample, the

maximum intensity is towards the [0001] direction, showing the development of a strong basal texture in this sample. In other samples, i.e. IP0, IP45 and IP90, the texture is totally different from that of OP sample and a prismatic texture is observed (Fig. 4.3(b) to 4.3(d)).

The textures of the shock-loaded samples (strain rate of 800 s^{-1}) are presented in Fig. 4.4, which shows that a strong basal texture has evolved for all samples. Besides, for OP samples, a c-type texture developed in which the contours of the intensity are concentrated around the center of the pole figure. For other samples, e.g. IP0, IP45 and IP90, a marked change is observed and the initial prismatic texture is transformed to a strong basal texture after shock loading (Fig. 4.4(b),(c) and (d)). Another point is the presence of peak splitting on the pole figures of IP0, IP45 and IP90 samples. Furthermore, comparing the IPFs of as-rolled and shock loaded samples, it is observed that for OP sample there is almost no change in the maxima position. However, for IP0, IP45 and IP90 samples, the maxima are shifted from <10-10> orientation toward <0001>, showing the evolution of the basal texture. In other words, the reorientation of crystallites towards the basal orientations has taken place in IP0, IP45 and IP90 samples. For other strain rates, almost the same trend was observed, i.e. a relatively strong basal texture was evolved in all samples.

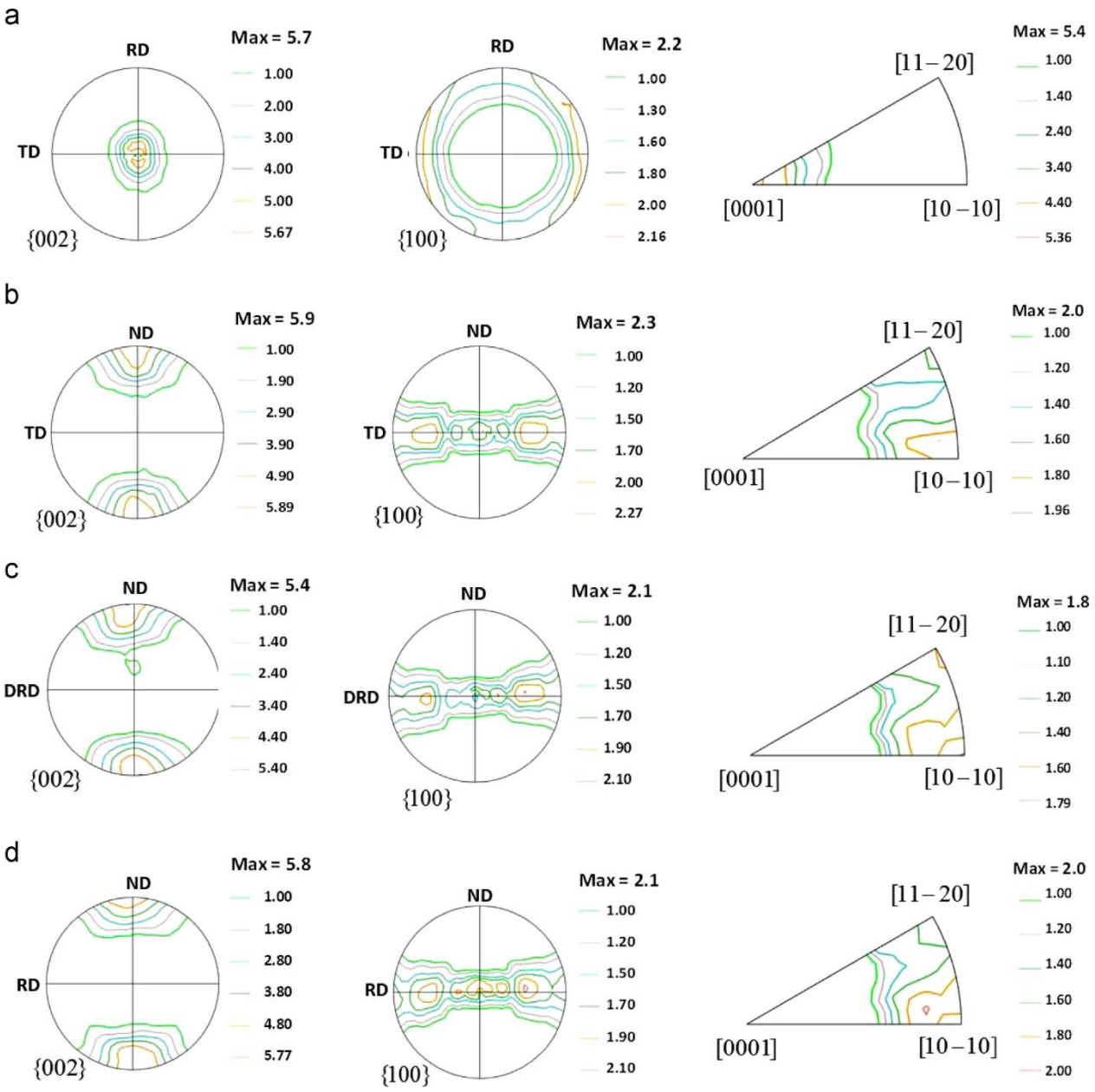

Fig. 4.3. (00.2) & (10.0) pole figures (PF) and inverse pole figures (IPF) of as-rolled samples before shock loading: a) OP, b) IP0, c) IP45 and d) IP90.

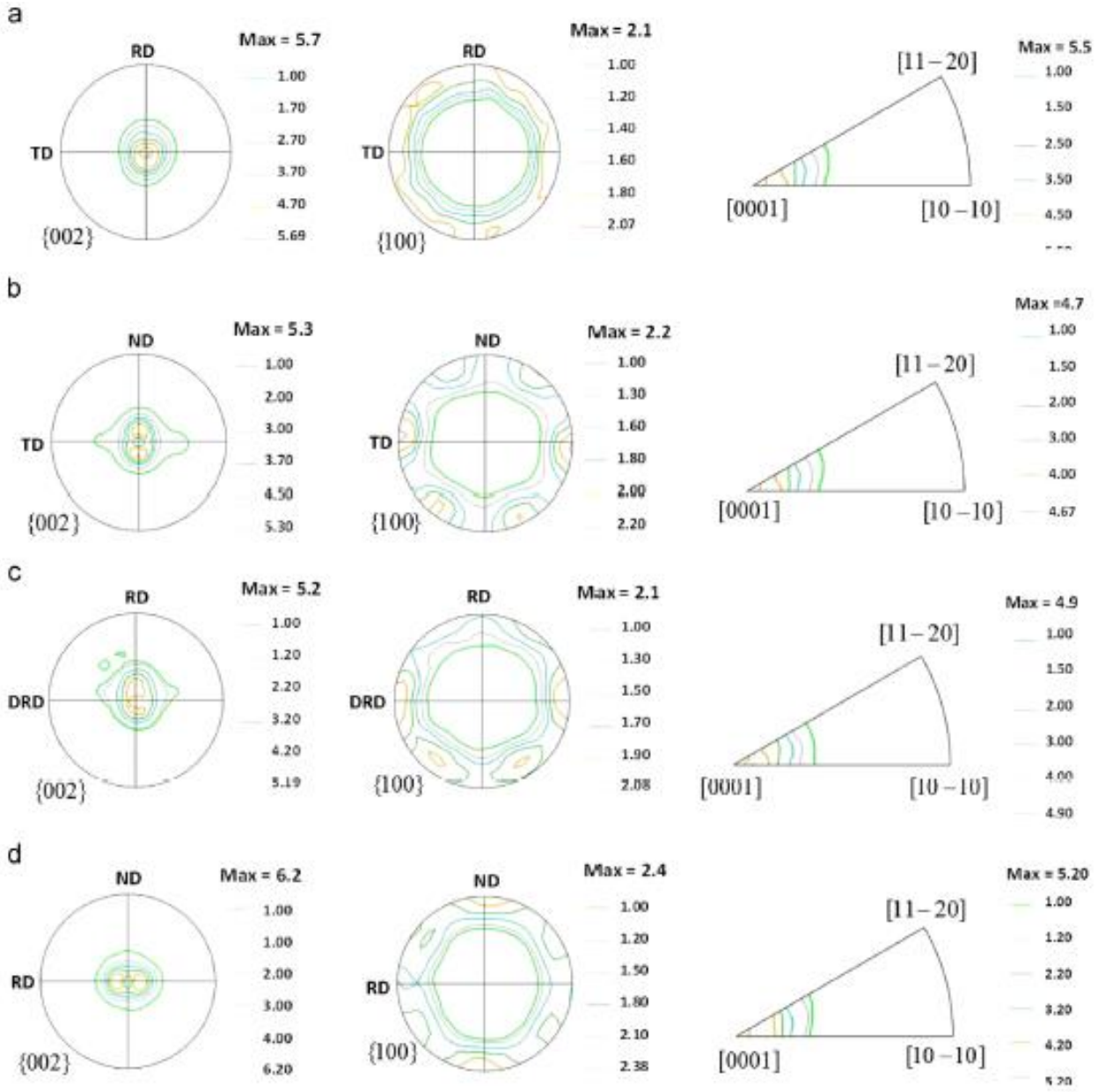

Fig. 4.4. (00.2) & (10.0) pole figures (PF) and inverse pole figures (IPF) of shock-loaded samples at $\dot{\varepsilon}$ = 800 s^{-1}: a) OP, b) IP0, c) IP45 and d) IP90.

To characterize the microstructure and identify the twin type and a qualitative comparison about the twinning volume fraction in the microstructure after shock loading, EBSD technique was used. As can be seen in the image quality (IQ) maps of the samples after shock loading at 800 s^{-1} (Fig. 4.5(a),(c),(e) and (g)), twinning with different fractions occurred in all samples. It is clear in IQ maps that the extension (tensile) twins (shown in yellow) are the major twinning mode in all

samples and a very small number of other twins, including contraction (shown in red) and double (shown in blue) twins are also formed. Moreover, by comparing the IQ maps of the samples, it is observed from qualitative analysis of the IQ maps that the twinning fraction in OP samples (Fig. 4.5(a)) is smaller than those of other samples (Fig. 4.5(c),(e) and (g)).

To determine the relationship between the strain rate and the twinning fraction, another sets of EBSD tests were conducted on some shock loaded samples deformed at 1100 s^{-1} and the IQ maps are presented in Fig. 4.5(b),(d),(f) and (h). Interestingly, as can be seen in IQ maps the twinning fraction, particularly extension twinning, in the samples shock loaded at 1100 s^{-1} is smaller than those of deformed at 800 s^{-1} (Fig. 4.5(a),(c),(e) and (g)). Decrease in twinning fraction with increase in strain rate could be related to the activation of other deformation mode(s) that will be discussed later.

In Figure 4.6, simulated (00.2) pole figures (PF) and inverse pole figures (IPF) of shock-loaded samples, obtained by VPSC simulation, are shown. In these series of simulations, basal slip, extension twinning and pyramidal <c+a> slip systems are assumed to be active deformation modes in shock loading. The maximum intensities are higher in simulated textures in comparison to experimental one; however, the key features and position of the peak intensities are well generated in the PFs and IPFs and there is a good match between the simulated (Fig. 4.6) and experimental textures (Fig. 4.4).

In Fig. 4.7, the predicted activity of various slip and twinning systems of the samples, based on the assumptions that were used to simulate their textures (Fig. 4.6) are displayed. It is clear that the basal slip is the dominant deformation mode at the onset of plastic deformation for all samples and its contribution decreases with an increase in the contribution from pyramidal <c+a> slip. Besides, the decrease in the contribution of basal slip occurs more slowly for IP0, IP45 and IP90 samples in comparison to OP sample. Additionally, it is seen that the twinning activity is lower in OP samples compared to that of other samples which is in a reasonable agreement with the results of EBSD test, showing smaller fraction of twinning in OP samples than those of IP0, IP45 and IP90 samples (Fig. 4.5). In the activity diagrams (Fig. 4.7), contribution of extension twinning is almost constant at the initial stages of plastic deformation and subsequently decreases with increase in the activity of pyramidal <c+a> slip. In the case of pyramidal <c+a> slip, the activity vs strain diagrams show a very low and constant contribution for this system at the early stage of deformation for IP0, IP45

and IP90 samples however, for OP samples, the pyramidal <c+a> slip is active from the beginning of deformation, although its contribution is very low initially.

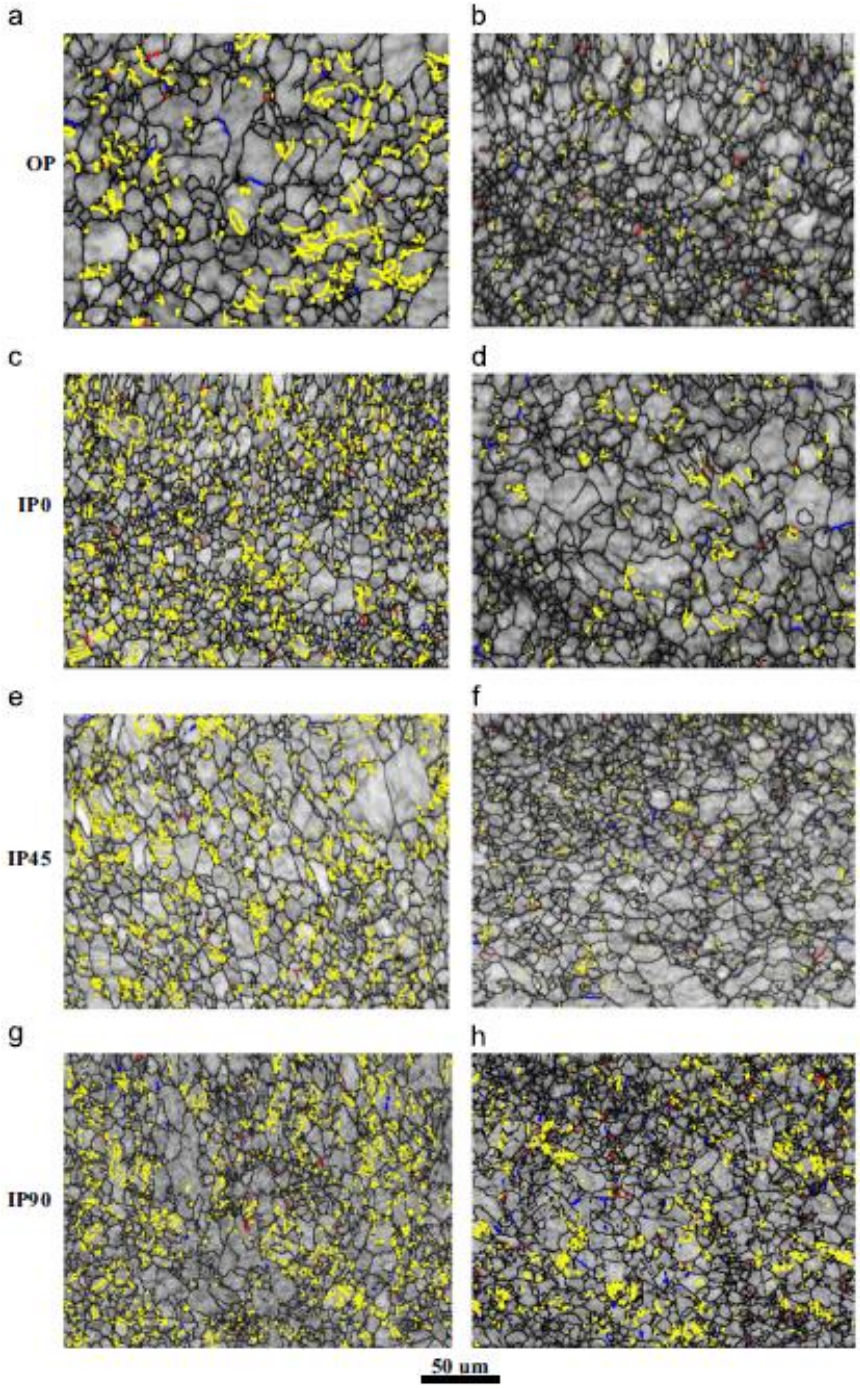

Fig. 4.5. Image quality (IQ) maps of the samples showing the microstructure and twins type after shock loading at: (a),(c),(e) and (g) $\dot{\varepsilon}$ = 800 s^{-1}; (b),(d),(f) and (h) $\dot{\varepsilon}$ = 1100 s^{-1} [*Note*: The extension twin boundaries (86°$< 11\bar{2}0 >$ ±5°) are shown in yellow, the contraction twin boundaries (56° $< 11\bar{2}0 >$ ±5°) are shown in red and the double twin boundaries (38° $< 11\bar{2}0 >$ ±5°) are shown in blue].

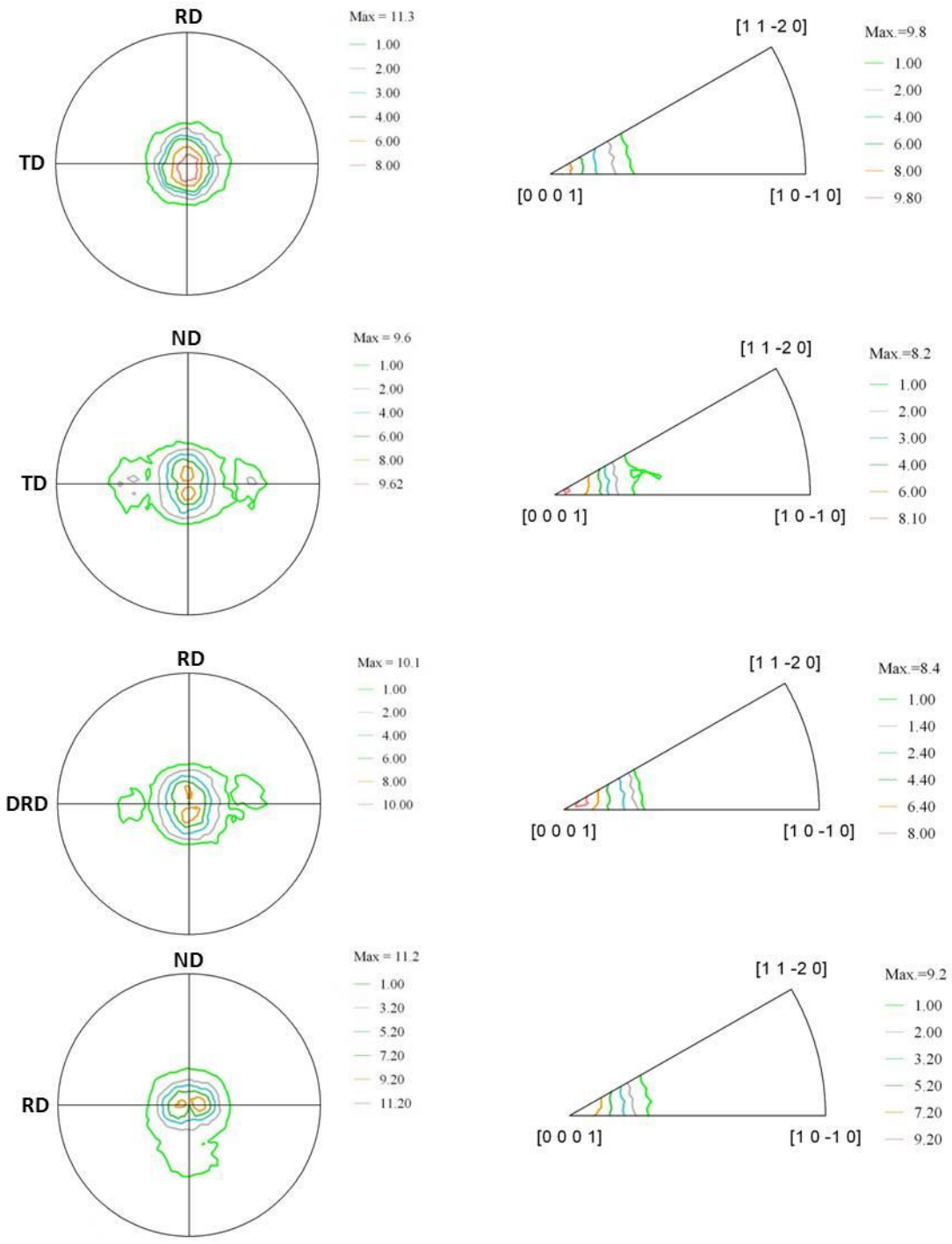

Fig. 4.6. Simulated (00.2) pole figures (PF) and inverse pole figures (IPF) of shock-loaded samples (a) and (b): OP, (c) and (d): IP0, (e) and (f): IP45, (g) and (h): IP90. (*Note*: assumed deformation systems are: basal slip, pyramidal <c+a> slip and extension twinning).

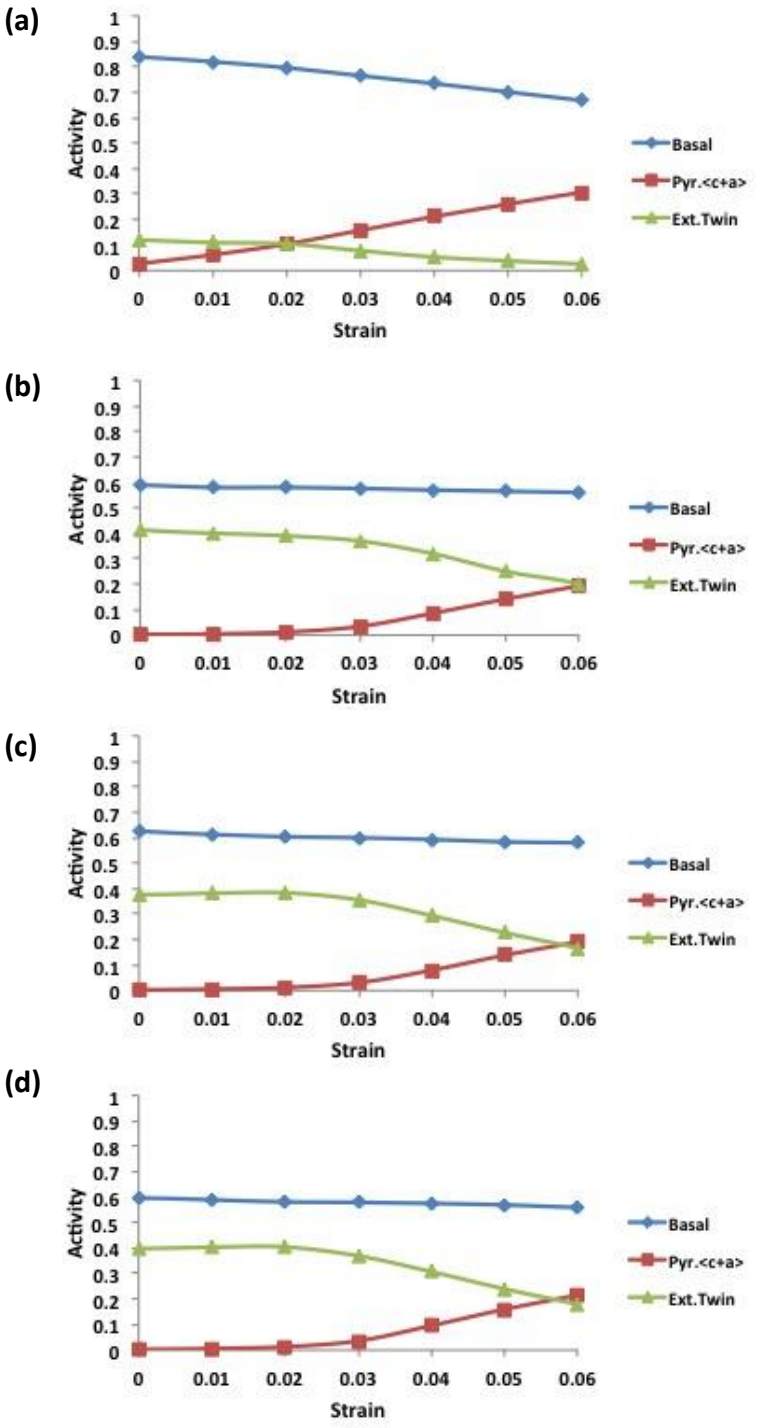

Fig. 4.7. Simulated activity of various slip and twinning systems for the shock-loaded (a) OP, (b) IP0, (c) IP45 and (d) IP90 samples.

It is worth noting that to evaluate the effect of the activation/deactivation of other deformation modes on the texture development, such as activation of prism and pyramidal <c> slip or deactivation of <c+a> slip and extension twinning, some more sets of texture simulations were conducted by VPSC simulation but the results were very qualitatively and quantitatively different from the experimental textures. For instance, splitting of basal poles along RD was eliminated and a c-type basal texture was obtained when the pyramidal <c+a> slip was not included in the simulation assumptions (or when only basal slip and extension twinning are assumed to be activated), which are totally different from the experimental ones (Fig. 4.4). Therefore, the best match between the simulated and experimental result was obtained when the activation of basal slip, extension twinning and pyramidal <c+a> slip systems in shock loading was assumed in simulations (Fig. 4.6). The values (ratios) of critical resolved shear stresses (CRSSs) used in the above-mentioned simulations are tabulated in Table 4.2.

Table 4.2. Shear systems and their corresponding properties used in the VPSC simulations. The stress values are normalized by the CRSS of basal slip.

	Basal	Pyramidal <c+a>	Extension Twinning
	$(0001) < 2\bar{1}\bar{1}0 >$	$\{11\bar{2}2\} < \bar{1}\bar{1}23 >$	$\{10\bar{1}2\} < \bar{1}011 >$
τ_0	1	12	3
θ	10	10	10

To investigate the effect of higher strain rates on the activity of the deformation modes, some other simulations were also done. To obtain logical simulated results for this part, it was assumed that increase in the strain rate could have resulted in the increase in temperature during the shock loading and therefore, the critical resolved shear stress of the pyramidal <c+a> slip could have been decreased. Also, considering the EBSD results in which the twinning fraction decreased with increase in strain rate (Fig. 4.5(b),(d),(f) and (h)), the effect of extension twinning on texture development was weakened by increasing its CRSS value in the simulations. The values of critical resolved shear stresses used in these series of simulations are tabulated in Table 4.3. The activity diagrams, simulated for shock loading of OP and IP0 samples at higher strain rates in comparison to the previous activities that were shown in Fig. 4.7, are presented in Fig. 4.8. It is seen in the activity diagrams (Fig. 4.8) that the activity of extension twinning is lower than that of at lower strain rates (Fig. 4.7). Moreover, the pyramidal <c+a> is more active at higher strain rates and the

increase in the activity of this system at higher strain rates occurs at lower strains (Fig. 4.8). The same effect was also found for other samples.

Table 4.3. Shear systems and their properties used in the VPSC simulations (higher strain rates).

	Basal	Pyramidal <c+a>	Extension Twinning
	$(0001) < 2\bar{1}\bar{1}0 >$	$\{11\bar{2}2\} < \bar{1}\bar{1}23 >$	$\{10\bar{1}2\} < \bar{1}011 >$
τ_0	1	11	4
θ	10	10	10

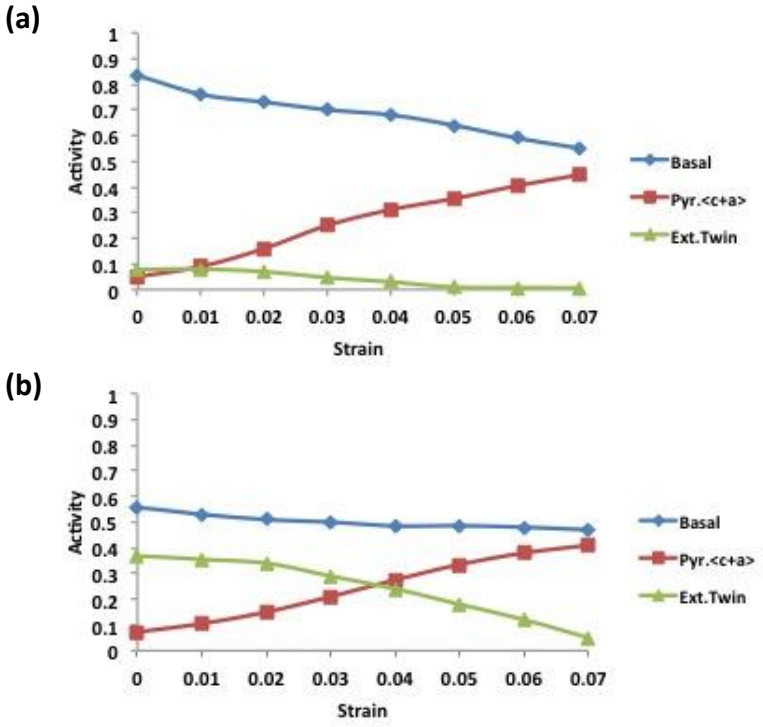

Fig. 4.8. Simulated activity of various slip and twinning systems for the shock-loaded (a) OP and (b) IP0 samples at higher strain rate (in comparison to previous activities shown in Fig. 4.7).

Fig. 4.9 shows the dynamic compressive true stress-strain curves and hardening diagrams of OP, IP0, IP45 and IP90 samples at different strain rates (i.e. 600, 800 and 1100 s^{-1}). All the stress-strain curves are sigmoidal and the stress increases to a maximum (peak stress) and then decreases possibly due to the thermal softening results from the increase in the sample's temperature (Fig. 4.9 (a), (c) and (e)). Also, by increasing the strain rate, the peak stress and ductility increase for all samples. It should be mentioned that a noticeable difference between the strength and ductility of

the samples, particularly at higher strain rates is seen in Fig.4.9, indicating a relatively high degree of mechanical anisotropy of the samples.

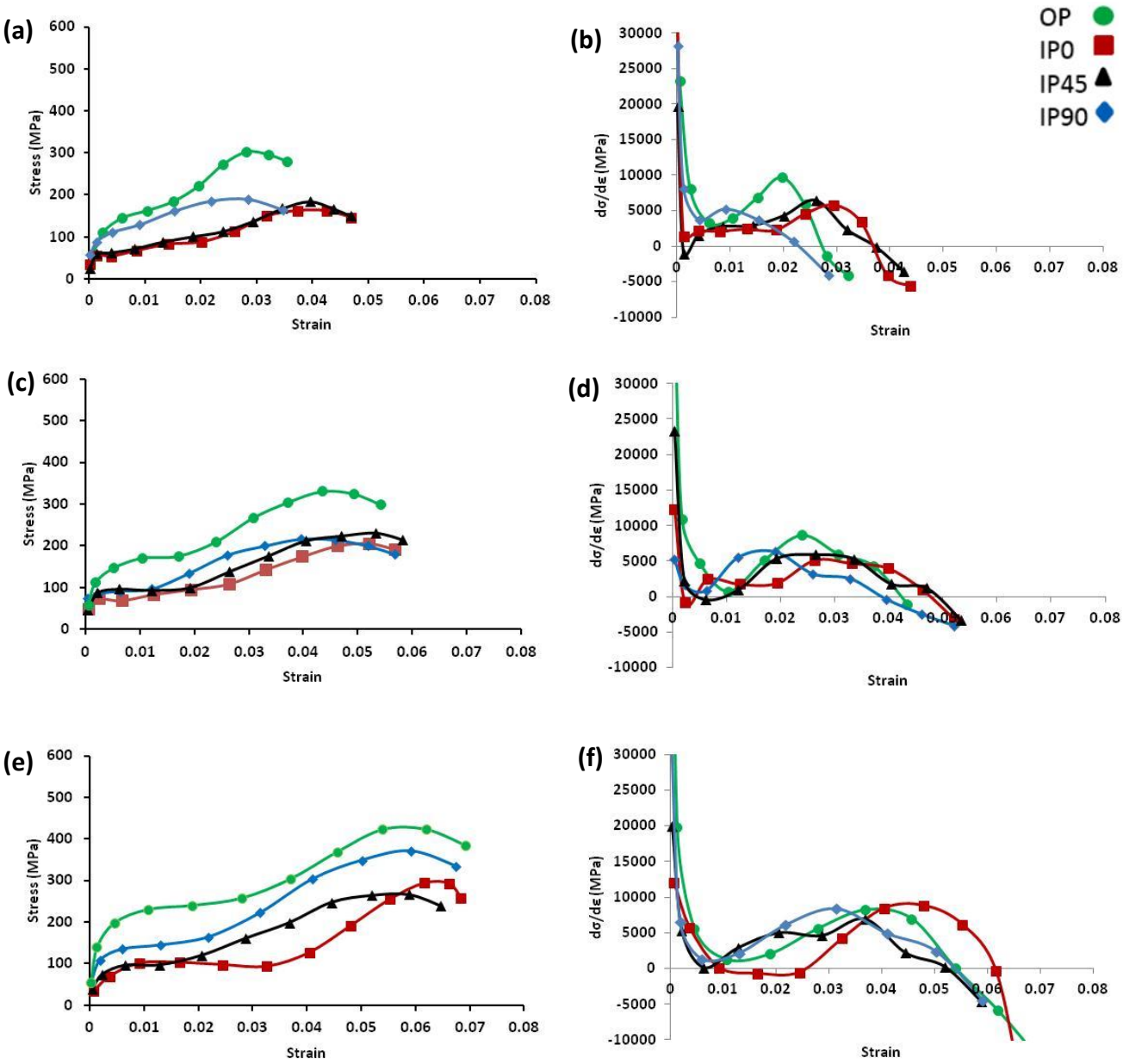

Fig. 4.9. Dynamic compressive true stress-strain curves and hardening diagrams (dσ/dε versus strain) of shock loaded samples at strain rate of a,b) 600, c,d) 800 and e,f) 1100 s^{-1}.

As an example, values of yield strengths are given in Table 4.3. As can be seen in Table 4.4, samples have different yield strengths at each strain rate and by increasing the strain rate, the yield

strength of the samples is increased. In some cases at lower strain rates, e.g. IP0 and IP45 samples at 600 s^{-1}, values seem to be close to each other which could be related to the similar initial texture of this samples or small errors in recording the data. Furthermore, it is found in hardening diagrams (Fig. 4.9 (b), (d) and (f)) that increasing the strain rate results in the shifting of maximum strain-hardening rate toward higher strains. Moreover, the width of the hump in hardening diagrams increases with increase in strain rate.

Table 4.4. Yield strength (MPa) of the AZ31B samples tested at different strain rates (extracted from Fig. 4.9 (a),(c) and (e)).

Sample	600 s^{-1}	800 s^{-1}	1100 s^{-1}
OP	123±2.5	133±2.7	173±3.4
IP0	56±1.1	72±1.5	76±1.5
IP45	59±1.2	81±1.7	88±1.8
IP90	102±2.1	77±1.9	109±2.2

4.6. Discussion

As observed in Fig. 4.3(a), the pole figure of the undeformed OP samples show a strong basal texture. This is consistent with the results reported by other researchers in which this basal texture is introduced as a typical texture of rolled AZ31B magnesium alloy sheets [36-39]. The strong basal texture develops in the rolled sheet due to the absence of sufficient active slip systems in magnesium and its alloys [14-16]. For other samples, i.e. IP0, IP45 and IP90, prismatic texture is the dominant texture (Fig. 4.3 (b-d)). After shock loading, however, a relatively strong c-type basal texture with no splitting for OP sample is seen (Fig. 4.4(a)) whereas for IP0, IP45 and IP90 samples, a strong basal texture with splitting of basal poles is observed (Fig. 4.4(b-d)) which are consistent with the results reported for high strain rate deformation of AZ31B plate [40-41]. Moreover, in all shock-loaded samples (Fig. 4.3), the maxima in the inverse pole figures have shifted toward [0001] direction, indicating the change in the texture compared to those of undeformed samples (Fig. 4.3).

The change in the texture and splitting of basal poles in the pole figures can be ascribed to the activation of twinning and pyramidal <c+a> slip systems [38,42-46]. In general, basal slip promotes the development of basal texture in magnesium sheets [47]. It has been shown that <c+a> slip can play an important role in rotating the basal poles, resulting in the splitting of basal poles and changing in the texture [38,42-46]. To justify texture evolution, microstructural development

was investigated, deformation mechanisms during shock loading of the samples were evaluated, EBSD and numerical simulation were performed and the results are discussed.

Two sets of EBSD tests were conducted on samples, which were shock-loaded at two different strain rates and the results are shown in Fig. 4.5. Based on the EBSD results obtained for shock-loaded samples at strain rate of $\dot{\varepsilon} = 800\ s^{-1}$ (Fig. 4.5(a),(c),(e) and (g)), the dominant twinning mode in the samples is the extension twinning. Moreover, by comparing the IQ maps of the shock-loaded samples (Fig. 4.5(a),(c),(e) and (g)), it is found that extension twinning fraction in OP sample is smaller than those of IP0, IP45 and IP90 samples that could be ascribed to the strong initial basal texture in OP samples, which led to restricted activity of extension twins [20]. One interesting aspect of the activity of twinning during shock loading is that the activity and twinning fraction is affected by the strain rate. In Fig. 4.5(b),(d),(f) and (h), the IQ maps of the samples shock loaded at $\dot{\varepsilon} = 1100\ s^{-1}$ are displayed. It can be observed in these EBSD maps (Fig. 4.5(b),(d),(f) and (h)) that twinning fraction is smaller in all samples in comparison to the twinning fraction in the microstructures of shock-loaded samples shown in Fig. 4.5(a),(c),(e) and (g) (lower strain rates). In other words, increasing the strain rate in shock loading results in decrease in activity and twinning fraction. The same effect has been recently reported by other researchers [31]. Considering the results of EBSD tests and the change in the twinning fraction with strain rate, it seems to be logical to suggest that non-basal deformation mode, i.e. pyramidal <c+a> slip, may have been involved in the deformation process during shock loading and the probability of the activation of <c+a> slip may increase with increase in strain rate. Since there is not enough time for heat to dissipate from the shock-loaded sample during the shock loading, the temperature of the sample highly increases which can result in a remarkable and rapid decrease in the critical resolved shear stresses of pyramidal <c+a> slip systems, leading to the activation of this deformation mode [48].

As shown in the results section (Fig. 4.6), the pole figures and inverse pole figures constructed by numerical simulations are consistent with the experimental pole figures (Fig. 4.4). Some differences between the intensities of the simulated and experimental texture could be attributed to some physical phenomena in the material, which take place during the shock loading and were not considered in the VPSC simulation [49,53]. The best agreement between the simulated and experimental textures, as was mentioned in the results section, is obtained when only a combination of extension twinning and pyramidal <c+a> slip systems together with basal slip are considered as

the active deformation modes in the simulations and other assumptions on deformation modes fail to generate an appropriate fit between simulated and experimental pole figures.

The predicted activity diagrams of the assumed deformation modes in the simulations are plotted in Fig. 4.7. According to the activity diagrams, the basal slip is the dominant deformation mode in all samples at the beginning of plastic deformation. The contribution of basal slip gradually decreases with an increase in the strain. Extension twinning also takes place at the onset of plastic deformation and decreases with increase in the strain while the activity of pyramidal <c+a> slip increases (Fig. 4.7). At the beginning of deformation process, basal slip and extension twinning system are easily activated because of their low critical resolved shear stress but, with increase in the strain and due to the decrease in the critical resolved shear stress of pyramidal <c+a> slip systems that results from considerable increase in the temperature, more strains are accommodated by the increased activation of pyramidal <c+a> systems [9,46,50]. An interesting point about the activity diagrams is that the decreased rate of basal slip with strain is higher in OP sample (Fig. 4.7(a)) than that of IP0, IP45 and IP90 samples (Fig. 4.7(b),(c) and (d)). In fact, the contribution of basal slip in OP sample decreases with a steeper slope compared to other samples, which could be attributed to its initial strong basal texture that restrict the activation of extension twinning and encourage the activation of other slip systems such as basal and pyramidal <c+a>, when the load is applied parallel to the c-axis of the samples [39, 51-52]. Also, the activity of extension twinning is smaller in OP sample compared to those of other samples (Fig. 4.7), which is in good agreement with the EBSD maps (Fig. 4.5), showing smaller activity and fraction of extension twinning in OP sample at both strain rates compared to other samples.

It is worth noting that the selection of reasonable critical resolved shear stress for different deformation modes is very important in VPSC simulations and reported ratios of critical resolved shear stress may differ [53]. Although the information about the critical resolved shear stress ratios is scattered and varies from one report to another report, the general rules that can be found in the literature about determination of critical resolved shear stress ratios are: (i) basal slip is the easiest slip system and increase in temperature has almost no marked influence on the critical stress for activation of this system [23-30, 53], (ii) extension twinning is easier than pyramidal <c+a> slip and the critical resolved shear stress values of both systems are affected by temperature [4-6, 38-39, 50-53] and (iii) pyramidal <c+a> slip can be further activated when the temperature is increased

[43,48,53]. Based on these rules, the critical resolved shear stress values (ratios) were chosen in this study (Tables 4.2 and 4.3).

To evaluate the effect of increased strain rate on the activity of deformation modes, some sets of simulations were performed and the results are shown in Fig. 4.8 for OP and IP0 samples. In these simulations, lower critical resolved shear stress is assigned for pyramidal <c+a> slip (Table 4.2) in comparison to the previous simulations that were conducted for lower strain rates and corresponding results are shown in Figs. 4.6 and 4.7. The reason why lower critical resolved shear stresses are used for pyramidal <c+a> slip in the simulation of shock loading at higher strain rates is the increase in temperature with increase in strain rate, leading to decreased critical resolved shear stress [48, 53]. For extension twinning, however, the critical resolved shear stress is slightly increased in the simulations due to the increased temperature at higher strain rates that may lead to increase in critical resolved shear stress of twinning [53,54]. The deformation modes, i.e. basal, extension twinning and pyramidal <c+a> slip, are assumed to be the possible active modes, as the previous simulations for lower strain rates (Fig. 4.7). According to the predicted activities by simulations in Fig. 4.8, increasing the strain rate results in the higher activity of pyramidal <c+a> slip in comparison to that presented in Fig. 4.7. The activity of extension twinning, however, decreases with increase in strain rate (Fig. 4.8) which is consistent with the EBSD maps obtained from the microstructures of shock-loaded samples at higher strain rates (Fig. 4.5(b),(d),(f) and (h)) that contain less fractions of extension twins compared to samples deformed at lower strain rates (Fig. 4.5(a),(c),(e) and (g)). The basal slip is still the dominant deformation mode in the samples (Fig. 4.8). An interesting aspect of Fig. 4.8 is the drop of twinning activity (and increase in pyramidal <c+a> slip) at lower strains in comparison to Fig. 4.8, showing the easier and faster activation of pyramidal <c+a> slip with increase in strain rate. In other words, increase in strain rate affects both activation/suppression and the strain at which deformation mechanisms are highly activated or suppressed. The same effect was observed for other samples (i.e. IP45 and IP90) where the simulated textures showed increased activation of pyramidal <c+a> at high strain rates.

The dynamic true stress-strain curves of the shock-loaded samples at three different strain rates, namely 600, 800 and 1100 s^{-1} are presented in Figure 4.9(a),(c) and (e). All samples exhibit an upward curving flow, which is unseen in the normal tensile or compressive curves of most metals with cubic crystal structure [55]. This concave behavior is related to the strong work hardening due to the occurrence of {10-12} twinning [4-6], which is consistent with the EBSD maps (Fig. 4.5)

and simulation results that confirm the occurrence of twinning in the samples. The same concave behavior has been also observed by other researchers in high strain rate deformation of magnesium alloys [31,39,55,56]. Generally, at the initial stage of deformation in the flow curves (Fig. 4.9), there is a region of transition from elastic to plastic and then, yielding occurs. After yielding, the work hardening region is seen and two parts can be shown on this region: the first part which shows a low rate of strain hardening and the second part in which a high strain hardening rate is observed. Finally, the peak stress appears on the diagram and then the flow stress decreases. It is seen in the stress-strain curves that there is a relatively remarkable difference in the flow curves of the samples at all strain rates. This difference in the flow curves of the shock-loaded samples can be related to the strong and different initial texture of the samples, particularly for OP samples with a strong basal texture, resulting in high mechanical anisotropy under shock loading conditions. In other words, due to the presence of a strong and different initial texture, the effect of the initial texture on the dynamic mechanical behavior is relatively high. Some other researchers have also reported similar high mechanical anisotropy of AZ31B alloys [53,57]. In contrast, in rare earth containing magnesium alloys, a very low degree of mechanical anisotropy has been reported [58,59].

Another point about the stress-strain curves (Fig. 4.9(a),(c) and (e)) is that the ductility increases with increase in strain rate. This behavior can be attributed to the higher probability of activation of pyramidal <c+a> slip systems at higher strain rates [31,60], as was shown by simulations (Fig. 4.8), which results in higher ductility of the samples.

It is worth noting here that the sigmoidal shaped flow curves observed for shock-loaded OP samples at all strain rates in this research are not usual due to the strong initial basal texture of these samples. In fact, c-axes of most grains of the initial OP samples are almost tilted away about ±10° from compression direction, which do not activate much extension twinning, but significantly support the operation of contraction and double twinning [52,61]. However, the extension twins are observed in the EBSD maps of OP samples (Fig. 4.5(a) and (b)) and the activation of extension twinning is also predicted by simulations (Figs. 4.7(a) and 4.8(a)). Moreover, very few contraction and double twins are formed in shock-loaded OP samples (Fig. 4.5(a) and (b)). The reason for this surprising phenomenon that has been also reported by some other researchers [39], is not entirely clear but, it is probably related to: (1) generation of extension twinning during unloading or (2) activation of extension twinning in response to some local stress created by the neighboring grains during deformation process or (3) presence of previous twins in the microstructure [39,42].

The hardening behaviors of the samples (Fig. 4.9(b), (d) and (f)) is related to the activation of different deformation modes during the deformation. For instance, at the initial stage, basal and tensile twinning are operative modes and the material deform easily at low strain values, resulting in the decreased hardening rate [62-64]. However, due to the formation, growth and intersection of more twins, more barriers (twin boundaries) are produced to impede dislocation motions, giving rise to pile-ups of dislocation at twin boundaries (Fig. 4.10) and increased hardening rate [62-65]. As can be seen, by increasing the strain rate, the density of dislocations increases and more dislocations contribute to pile-ups at twin boundaries (Fig. 4.10). These pile-ups at twin boundaries will increase the rate of hardening [62-63,31,55,64-65].

At the final stage of hardening process, non-basal slip systems such as pyramidal <c+a> slip system could have been activated (as shown in the simulation results in Figs. 4.7 and 4.8), resulting in the decrease in the hardening rate after the ultimate compressive stress. Further investigation is in progress to confirm the presence and activation of <c+a> dislocations in shock-loaded samples by TEM.

In Figs. 4.9(b), (d) and (f), by increasing the strain rate, the humps on the hardening diagrams are broadened which is related to the possible activation of pyramidal <c+a> slip systems [64]. In the current research, the decreased twinning fraction was shown by EBSD maps (Fig. 4.5(b),(d),(f) and (h)) and the increased activity of pyramidal <c+a> slip with increase in strain rate was confirmed by numerical simulations (Fig. 4.8) and may support the possible activation of pyramidal slip system and its effect on the hardening of the samples during shock loading.

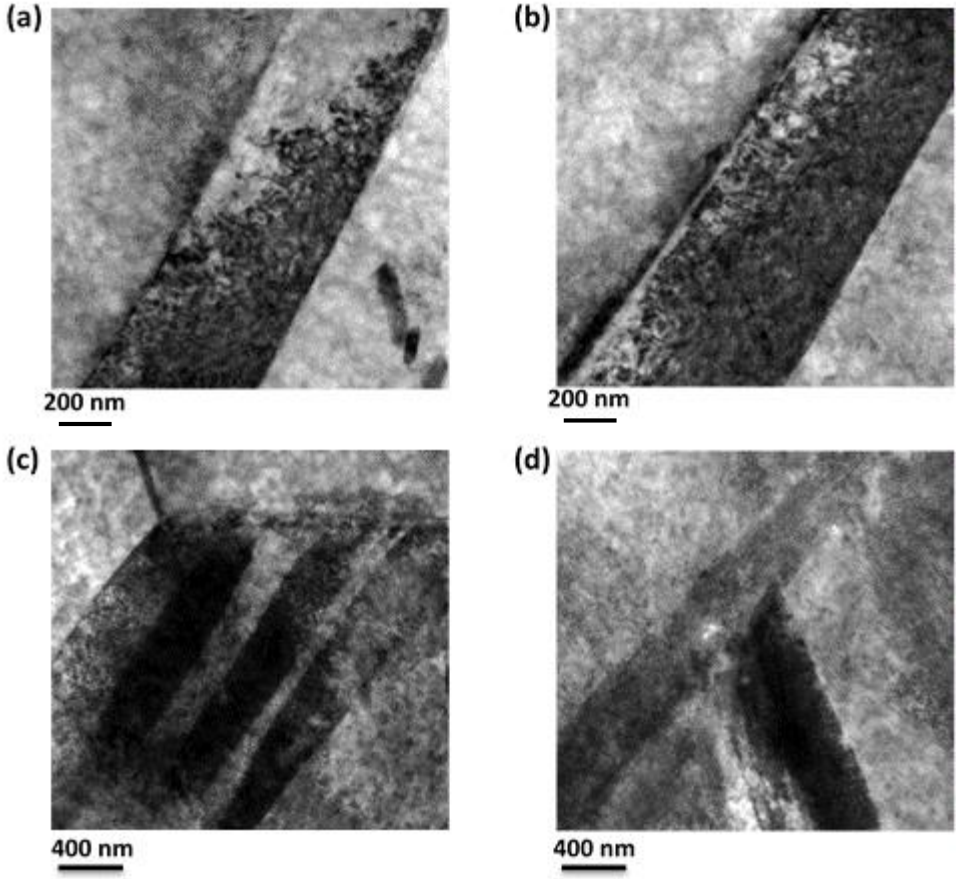

Fig. 4.10. Bright field TEM images of (a) pile-up and accumulation of dislocations in a twin and behind twin boundaries in OP sample at strain rate of 800/s, (b) pile-up and accumulation of dislocations in a twin in OP sample at strain rate of 1100/s,(c) pile-ups of dislocations at twin boundaries, grian boundaries and grain interior in OP sample shock loaded at 800/s,(d) dislocation pile-up at twin intersection in OP sample shock loaded at 800/s.

4.7. Conclusions

Based on the experimental results and simulation of texture formation and activity of deformation modes during shock loading, the following conclusions can be drawn:

(1) After shock loading, initial texture of all samples transforms to a strong (00.2) basal texture in which the splitting of basal poles indicates a high probability of pyramidal <c+a> activation at high strain rates.

(2) Increasing the strain rate results in the increased strength and ductility and decreased contribution of twinning to deformation, indicating the strain rate dependence of twinning.

(3) The most active deformation modes are basal slip, pyramidal <c+a> slip and extension twinning. Basal slip is the dominant mode of deformation at the onset of deformation, and increasing the strain leads to a gradual decrease in the activity of this system. In OP samples, the activation of <c+a> slip is higher which is related to its strong initial basal texture.

(4) Simulations show that activity of pyramidal <c+a> slip system increases and activity of extension twinning decreases with increase in strain rate. Confirming the high probability of activation of <c+a> slip systems, which is related to the increased strain, rate, by both experiment and simulation analysis, is an important finding of this research.

(5) The degree of stress and strain anisotropy is high which is a remarkable consequence of the strong initial basal texture.

References

[1] Mordike BL, Ebert T. Magnesium: Properties — applications — potential. Materials Science and Engineering A 2001;302: 37-45.

[2] Agnew SR, Duygulu O. A mechanistic understanding of the formability of magnesium: Examining the role of temperature on the deformation mechanisms. Materials Science Forum 2003; 419-422:177-188.

[3] Hakamada M, Furuta T, Chino Y, Chen Y, Kusuda H, Mabuchi M. Life cycle inventory study on magnesium alloy substitution in vehicles. Energy 2007;32:1352.

[4] Meyers MA. Dynamic behavior of materials. Wiley-In- Interscience, New York. 1994.

[5] Meyers M, Andrade U, Chokshi A. The effect of grain size on the high-strain, high-strain-rate behavior of copper. Metallurgical and Materials Transactions A 1995; 26:2881-2893.

[6] McCauley JW, Strassburger E, Patel P, Paliwal B, Ramesh KT. Experimental observations on dynamic response of selected transparent armor materials. Experimental Mechanics 2013; 53: 3-29.

[7] Roberts CS. Magnesium and its alloys. New York/London: Wiley,1960.

[8] Kelley EW, Hosford WF. Plane strain compression of magnesium and magnesium alloy crystals. Trans. Metall. Soc. AIME. 1968; 242:5-13.

[9] Obara T, Yoshinga H, Morozumi S. {1122}〈1123〉 Slip system in magnesium. Acta Metallurgica 1973; 21:845-853.

[10] Lou XY, Li M, Boger RK, Agnew SR, Wagoner RH. Hardening evolution of AZ31B Mg sheet. *International Journal of Plasticity* 2007; 23:44-86.

[11] Stohr JF, Poirier JP. Electron microscope study of {1122}<1123> pyramidal slip in magnesium Philosophical Magazine 1972; 25:1313-1329.

[12] Yoshinaga H, Obara T, Morozumi S. Twinning deformation in magnesium compressed along the C-axis Materials Science and Engineering A 1973; 12:255-264.

[13] Agnew SR, Tome´ CN, Brown DW, Holden TM, Vogel SC. Study of slip mechanisms in a magnesium alloy by neutron diffraction and modeling. Scripta Materialia 2003; 48:1003-1008.

[14] Agnew SR, Duygulu O, Alan A. TEM investigation of dislocation mechanisms in Mg alloy AZ31B sheet. Magnesium Technology 2004. Warrendale, PA: TMS 2004;61-65.

[15] Keshavarz Z, Barnett MR. EBSD analysis of deformation modes in Mg–3Al–1Zn. Scripta Materialia 2006; 55:915-918.

[16] Muránsky O, Carr DG, Barnett MR, Oliver EC, Šittner P. Investigation of deformation mechanisms involved in the plasticity of AZ31 Mg alloy: In situ neutron diffraction and EPSC modelling. Materials Science and Engineering A 2008; 496:14-24.

[17] Yoo MH. Slip, twinning, and fracture in hexagonal close-packed metals. Metallurgical and Materials Transactions A 1981; 12:409-418.

[18] Hosford WF. The mechanics of crystals and textured polycrystals. New York: Oxford University Press; 1993.

[19] Barnett MR. Twinning and the ductility of magnesium alloys: Part I: "Tension" twins. Materials Science and Engineering A 2007; 464:1-7.

[20] Beausir B, Toth LS, Qods F, Neale KW. Texture and mechanical behavior of magnesium during free end torsion. *Journal of Engineering Materials and Technology 2009*; 131: 1.

[21] Buchanan ER, Reed-Hill RE. On the mechanism of rotational slip in magnesium single crystals.*Trans. Metall. Soc. AIME* 1960; 218:554–558. [22] B.C. Wonsiewicz, W.A. Backofen. Trans Metall Soc AIME 1967; 1422-1431.

[23] Mukai T, Mohri T, Mabuchi M, Nakamura M, Ishikawa K, Higashi K. Experimental study of a structural magnesium alloy with high absorption energy under dynamic loading. Scripta Materialia 1998; 39:1249-1253.

[24] Mukai T, Yamanoi M, Higashi K. Ductility enhancement in magnesium alloys under dynamic loading. Materials Science Forum 2000; 350–351:97-102.

[25] Yokohama T. Strain 2003; 39:167.

[26] El-Magd E, Abouridouane M. Journal De Physique. IV 2003; 110:15-20.

[27] Shu DW, Zhou W, Ma GW. Tensile Mechanical Properties of AM50A Alloy by Hopkinson Bar. Key Engineering Materials 2007; 340–341:247-254.

[28] Ishikawa K, Watanabe H, Mukai T. High strain rate deformation behavior of an AZ91 magnesium alloy at elevated temperatures. Materials Letters 2005; 59:1511-1515.

[29] Tucker MT, Horstemeyer MF, Gullett PM, El Kadiri H, Whittington WR. Anisotropic effects on the strain rate dependence of a wrought magnesium alloy. Scripta Materialia 2009; 60:182-185.

[30] Sanjari M, Farzadfar A, Sakai T, Utsunomiya H, Essadiqi E, Jung IH, Yue S. A texture and microstructure analysis of high speed rolling of AZ31 using split Hopkinson pressure bar results. Journal of Materials Science 2013; 48: 6656-6672.

[31] Ahmad IR, Shu DW. Compressive and constitutive analysis of AZ31B magnesium alloy over a wide range of strain rates. Materials Science and Engineering A 2014; 592:40-49.

[32] Feng F, Huang S, Meng Z, Hu J, Lei Y, Zhou M, Wu D, Yang Z. Experimental study on tensile property of AZ31B magnesium alloy at different high strain rates and temperatures. Materials and Design 2014; 57:10-20.

[33] Kolsky H. An investigation of the mechanical properties of material at a very high rate of loading Proceedings of the Phys. Soc. B 62 (1949); 676-701.

[34] Gray GT. Classic Split-Hopkinson Pressure Bar Testing. Mechanical Testing and Evaluation .Mech. Test. Eval. ASM Int. 8 (2000); 462-476.

[35] Lebensohn RA, Tomé CN. A self-consistent anisotropic approach for the simulation of plastic deformation and texture development of polycrystals: Application to zirconium alloys. Acta Metallurgica et Materialia 1993; 41: 2611-2624.

[36] Wang BS, Xin RL, Huang GJ, Liu Q. Strain rate and texture effects on microstructural characteristics of Mg-3Al-1Zn alloy during compression. Scripta Materialia 2012; 66:239-242.

[37] Fatemi SM, Zarei A, Haghshenas M. The room temperature mechanical properties of hot-rolled AZ31 magnesium alloy. Journal of Alloys and Compounds 2009; 475:126-130.

[38] Chang LL, Shang EF, Wang YN, Zhao X, Qi M. Texture and microstructure evolution in cold rolled AZ31 magnesium alloy. Materials Characterization 2009; 60:487-491.

[39] Dudamell NV, Ulacia I, Gálvez F, Yi S, Bohlen J, Letzig D, Hurtado I, Pérez-Prado MT. Twinning and grain subdivision during dynamic deformation of a Mg AZ31 sheet alloy at room temperature. Acta Materialia 2011; 59:6949-6962.

[40] Hamada G, Sakai T, Utsunomiya H. Effect of rolling speed on deformability and microstructure in rolling of AZ31B magnesium alloy. Advanced Materials Research 2010; 89-91:227-231.

[41] Chun YB, Davies CHJ. Texture effects on development of shear bands in rolled AZ31 alloy. Materials Science and Engineering A (2012); 556:253-259.

[42] Agnew SR, Yoo MH, Tomé CN. Application of texture simulation to understanding mechanical behavior of Mg and solid solution alloys containing Li or Y. Acta Materialia 2001; 49:4277-4289.

[43] Khosravani A, Scott J, Miles MP, Fullwood D, Adams BL, Mishra RK. Twinning in magnesium alloy AZ31B under different strain paths at moderately elevated temperatures. International Journal of Plasticity 2013; 45: 160-173.

[44] Chino , Kimura K, Mubachi M. Twinning behavior and deformation mechanisms of extruded AZ31 Mg alloy. Materials Science and Engineering A (2008); 486:481-488.

[45] Sanjari M, Farzadfar SA, Utsunomiya H, Sakai T, Essadiqi E, Yue S. High speed rolling of Mg-3Al-1Zn alloy: Texture and microstructure analysis. Materails Science and Technology 2012; 28: 928-933.

[46] Li X, Jiao F, Al-Samman T, Ghosh Chowdhury S. Influence of second-phase precipitates on the texture evolution of Mg–Al–Zn alloys during hot deformation. Scripta Materialia 2012; 66:159-162.

[47] Bohlen J, Nürnberg MR, Senn JW, Letzig D, Agnew SR. The texture and anisotropy of magnesium–zinc–rare earth alloy sheets. Acta Materialia 2007; 55: 2101-2112.

[48] Obara T, Yoshinga H, Morozumi S. $\{11\bar{2}2\}\langle 1123\rangle$ Slip system in magnesium. Acta Metallurgica 1973; 21:845-853.

[49] Gurao NP, Kapoor R, Suwas S. Deformation behaviour of commercially pure titanium at extreme strain rates. Acta Materialia 2011; 59: 3431-3446.

[50] Sandlöbes S, Zaefferer S, Schestakow I, Yi S, Gonzalez-Martinez R. On the role of non-basal deformation mechanisms for the ductility of Mg and Mg–Y alloys. Acta Materialia 2011; 59: 429-439.

[51] Sanjari M, Farzadfar SA, Jung IH, Essadiqi E, Yue S. Influence of strain rate on hot deformation behaviour and texture evolution of AZ31B. Materails Science and Technology 2012; 28: 437-447.

[52] Yi S, Schestakow I, Zaeffere S. Twinning-related microstructural evolution during hot rolling and subsequent annealing of pure magnesium. Materials Science and Engineering A (2009); 516:58-64.

[53] Jain A, Agnew SR. Modeling the temperature dependent effect of twinning on the behavior of magnesium alloy AZ31B sheet. Materials Science and Engineering A (2007); 462:29-36.

[54] Tomé CN, Lebensohn RA, Kocks UF. A model for texture development dominated by deformation twinning: Application to zirconium alloys. Acta Metallurgica et Materialia 1991; 39: 2667-2680.

[55] Sarker D, Chen DL. Detwinning and strain hardening of an extruded magnesium alloy during compression. Scripta Materialia 2012; 67:165-168.

[56] Wang B, Xin R, Huang G, Liu Q. Effect of crystal orientation on the mechanical properties and strain hardening behavior of magnesium alloy AZ31 during uniaxial compression. Materials Science and Engineering A (2012); 534:588-593.

[57] Hao M, Zhang F, Tan C, Su T, Yu X. Effects of anisotropy on the microstructural characteristics and mechanical behavior of shock-loaded of AZ31 alloy. Advanced Materials Research 2011; 284-286:1537-1541.

[58] Asgari H, Szpunar JA, Odeshi AG. Texture evolution and dynamic mechanical behavior of cast AZ magnesium alloys under high strain rate compressive loading. Materials and Design 2014; 61:26-34.

[59] Agnew S, Whittington W, Oppedal A, El-Kadiri H, Shaeffer M, Ramesh KT, Bhattacharyya J, Delorme R, Davis B. Dynamic behavior of a rare-earth-containing Mg alloy, WE43B-T5, plate with comparison to conventional alloy, AM30-F. JOM 2014; 66: 277-290.

[60] Song WQ, Beggs P, Easton M. Compressive strain-rate sensitivity of magnesium–aluminum die casting alloys. Materials & Design 2009; 30:642–648.

[61] Jiang L, Jonas JJ, Luo AA, Sachdev AK, Godet S. Twinning-induced softening in polycrystalline AM30 Mg alloy at moderate temperatures. Scripta Materialia 2006; 54:771-775.

[62] Korla R, Chokshi AH. Strain-rate sensitivity and microstructural evolution in a Mg–Al–Zn alloy. Scripta Materialia 2010; 63:913-916.

[63] Jiang L, Jonas JJ, Luo AA, Sachdev AK, Godet S. Influence of {10-12} extension twinning on the flow behavior of AZ31 Mg alloy. Materials Science and Engineering A 2007; 445-446:302-309.

[64] Khan AS, Pandey A, Gnäupel-Herold T, Mishra RK. Mechanical response and texture evolution of AZ31 alloy at large strains for different strain rates and temperatures. International Journal of Plasticity 2011; 27: 688–706.

[65] Wang X, Jiang L, Luo A, Song J, Liu Z, Yin F, Han Q, Yue S, Jonas JJ. Deformation of twins in a magnesium alloy under tension at room temperature. Journal of Alloys and Compounds 2014; 594:44-47.

CHAPTER 5

ON DYNAMIC DEFORMATION BEHAVIOR OF WE43 MAGNESIUM ALLOY SHEET UNDER SHOCK LOADING CONDITIONS

5.1. Overview of Chapter 5

In Chapter 4, the deformation behavior and involved deformation mechanisms of shock loaded rolled AZ31B sheet were discussed. Considering the fact that rare earth elements have a significant effect on the texture and mechanical properties of magnesium alloys, the dynamic deformation behavior of a rare earth containing magnesium alloy with considerable application in automotive and aerospace industries, i.e. WE43, is also studied. This chapter will focus on the effect of initial texture and strain rate on the high strain rate deformation behavior of rolled WE43 alloy, with a weak initial texture. The involved deformation mechanisms will also be explained by experimental and simulation results.

This chapter is presented as manuscript # 4. The author's (H. Asgari) contributions to this manuscript are: (a) preparation and processing of the samples for shock loading test. (b) XRD, SEM, EDS, EBSD and simulation analyses. (c) Reviewing the relevant literature, writing and submission of the manuscript.

The manuscript was published in *Materials & Design*:

- H. Asgari, A.G. Odeshi, J.A. Szpunar. "On dynamic deformation behavior of WE43 magnesium alloy sheet under shock loading conditions", Materials & Design, 63 (2014) 552-564.

The manuscript presented here is different from the published paper in the following parts:

- In order to avoid repetition in the content, some parts of the ‘introduction’,‘experimental procedure’, and ‘discussion’ sections were eliminated.

The copyright permission to use the manuscript in the thesis was obtained and provided in the Appendix section.

On dynamic deformation behavior of WE43 magnesium alloy sheet under shock loading conditions

H. Asgari, A. G. Odeshi, J. A. Szpunar

Department of Mechanical Engineering, University of Saskatchewan, Saskatoon, Canada

5.2. Abstract

In the present study, the texture evolution, microstructure and mechanical behavior of WE43 magnesium sheet at high strain rates was investigated. Samples cut along the rolling direction (RD), 45° from the RD, transverse direction (TD) and perpendicular to the RD-TD plane were shock loaded by Split Hopkinson Pressure Bar at strain rates of 800, 1200 and 1400 s^{-1}. It is observed that after shock loading, the initial weak texture converts to a weak (00.2) basal texture in all samples. Besides, it is found that the strength and ductility increase and twinning fraction decreases with increase in strain rate. Moreover, another effect of increase in strain rate is found to be the higher activation of pyramidal <c+a> slip systems. In addition, degree of stress and strain anisotropy is low particularly at higher strain rates, which is mainly related to the weak initial texture of the samples. Using viscoplastic self-consistent simulation, probability of the activation of deformation modes at shock loading conditions was evaluated.

Keywords: Magnesium alloy sheet, Anisotropy, Twinning, Texture evolution

5.3. Introduction

Magnesium alloys are excellent candidates for several structural applications in the automotive and aerospace industries however, wide industrial applications of magnesium are limited because of poor ductility at room temperature and a strong basal texture of magnesium sheets [1-3].The common method to improve the formability of magnesium alloys is to form the alloy at elevated temperature. However, this consumes a lot of energy which leads to a significant increase in production cost [1-3].

A suitable way to increase the ductility of magnesium wrought products would be the development of a more random grain orientation or weaker texture. It has been shown in a number of studies that the addition of rare earth (RE) elements such as yttrium and neodymium can significantly improve the ductility due to texture modification [4-6]. Also, the addition of RE

elements increase the probability of the activation of <c+a> pyramidal slip at room temperature that may modify the ductility [4-5,7].

In some industrial products, such as automotive components, there is a high probability of the exposure of these components to high strain rate situations. Therefore, enough knowledge about the mechanical behavior of magnesium products at high strain rates may help to optimize their properties for more application in the above-mentioned industries [8].

To date, unfortunately, a limited literature is available on the texture evolution, microstructural development, deformation mechanisms and dynamic mechanical behavior of rare-earth (RE) containing wrought magnesium alloys sheet, such as WE43, at high strain rate compressive loading. For instance, in research work conducted by Hamilton et al., only the microstructure of cast WE43 alloy was investigated at high strain rate compressive loadings to check the shear localization and the texture evolution, mechanical properties and also simulation of results was not performed to establish a strong relationship between the texture, microstructure, deformation mechanisms and mechanical properties [9]. Furthermore, in other research work, tensile shock loading tests were conducted on extruded WE43 to investigate the texture evolution and mechanical properties without enough focusing on the microstructural changes after shock loading [10]. Therefore, the main objective of the present study is to investigate the texture evolution, microstructural development, deformation mechanisms and anisotropy of mechanical behavior of WE43 magnesium alloy sheet under dynamic compressive shock loading conditions. A complete, comprehensive and related series of information including texture evolution, microstructural development and mechanical properties at compressive shock loading will be presented in this paper. Besides, deformation mechanisms involved in shock loading deformation will be discussed using both experimental and simulated results.

5.4. Experimental procedure

The hot-rolled WE43 magnesium alloy sheet, provided by Magnesium Elektron Company with its nominal chemical composition as presented in Table 5.1, was used in this study. The dynamic mechanical behavior of the samples in compression was evaluated using Split Hopkinson Pressure Bar at strain rates of 800, 1200 and 1400 s^{-1}. Shock loading tests were conducted on several number of samples which were cut in the rolling direction (IP0 samples), at 45° to the RD (IP45 samples),

in the transverse direction (IP90 samples) and in the direction perpendicular to the RD-TD plane (OP samples).

The details of shock loading tests, texture measurements, SEM, EBSD and VPSC simulation are similar to those described in Chapters 3 and 4. They are not repeated here in order to keep the thesis concise. However, the ratio of critical resolved shear stress (CRSS) used in VPSC simulations are listed in Tables 5.2 and 5.3.

Table 5.1. Nominal chemical composition (in wt.%) of the rolled WE43 alloy.

Mg	Li	Mn	Nd	Y	Zn	Zr	RE*
Bal.	0.05	0.03	2-2.5	3.7-4.3	0.06	0.2-1	0.3-1

*Other rare earth (RE) elements including Gd, Dy, Er, Sm and Yb.

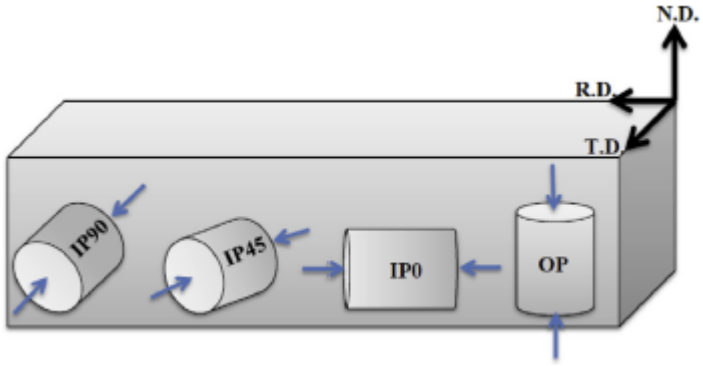

Fig. 5.1. Schematic diagram of the samples and compression directions (thin blue arrows).

Table 5.2. Deformation modes and their properties used in the VPSC simulations of WE43 samples.

	Basal	Pyramidal <c+a>	Extension Twinning
	$(0001) < 2\bar{1}\bar{1}0 >$	$\{11\bar{2}2\} < \bar{1}\bar{1}23 >$	$\{10\bar{1}2\} < \bar{1}011 >$
τ_0	1	8	2
θ	10	10	10

Table 5.3. Deformation modes and their properties used in the VPSC simulations of WE43 samples. (higher strain rates).

	Basal	Pyramidal <c+a>	Extension Twinning
	$(0001) < 2\bar{1}\bar{1}0 >$	$\{11\bar{2}2\} < \bar{1}\bar{1}23 >$	$\{10\bar{1}2\} < \bar{1}011 >$
τ_0	1	7	2
θ	10	10	10

5.5. Results

Microstructure and (00.2) pole figure of the alloy before deformation at high strain rates is illustrated in Fig. 5.2 ((a) and (b)). Also, some ideal pole figures of some important texture components for Mg are presented in Fig. 5.2 ((c) and (d)). For more information, the reader is referred to Wang and Huang's paper on texture analysis in HCP metals [12]. As can be seen in Fig. 5.2 (a), the equiaxed grains are clearly visible and according to the (00.2) basal pole figure (Fig. 5.2 (b)), a weak texture with a peak intensity of about 2.5 multiples of a random distribution developed in the undeformed alloy. It should be noted that due to the presence of several types of RE elements such as yttrium and neodymium in the WE43 alloy, some Mg-Nd-Y or Mg-Y phases may be present in the microstructure of the samples, however, their effects on the microstructural evolution or mechanical properties have not been considered in this research.

In Fig. 5.3, the inverse pole figure (IPF) and image quality (IQ) maps of the as-rolled alloy taken from two different planes, i.e. RD-TD (Fig. 3a and 3b) and ND-TD planes (Fig. 5.3(c) and 5.3(d)), before shock loading are presented. Very few twins are observed in the microstructure of both planes and number of grains with non-basal orientation is relatively larger in ND-TD plane (Fig. 5.3(c)).

Fig. 5.4 shows the recalculated (00.2) and (10.0) pole figures (PF) and inverse pole figures (IPF) of the samples before shock loading, projected on the compression plane of the samples. Generally, it shows that the samples had a very weak texture. In OP samples, there was a weak pole intensity which was tilted away from the ND toward the RD (Fig. 4a). In other samples, i.e. IP0, IP45 and IP90, a very weak prismatic texture was observed (Fig. 5.4(d) to 5.4(l)).

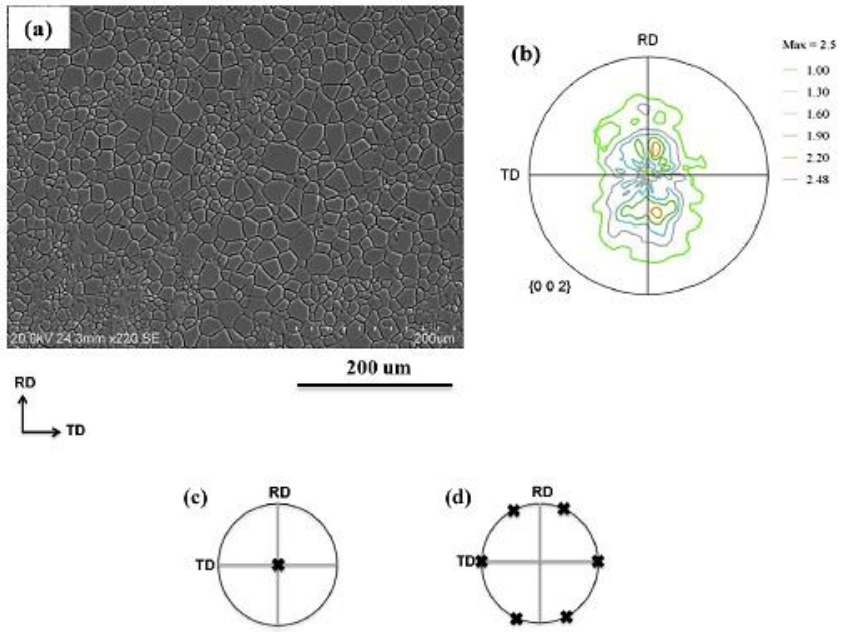

Fig. 5.2. (a) Microstructure, (b) (00.2) pole figure of the as-rolled WE43 sample, (c) ideal pole figure of important texture component (00.2) and (d) ideal pole figure of important texture component (10-10).

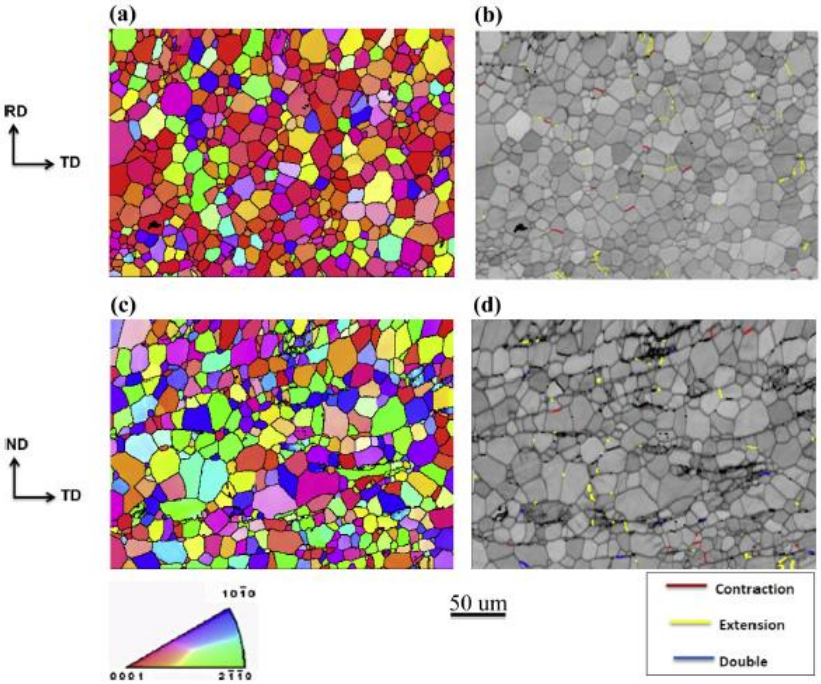

Fig. 5.3. Inverse pole figure (IPF) maps and image quality (IQ) maps of the as-rolled samples showing the microstructure and twins type. (a) and (b): RD-TD plane, (c) and (d): ND-TD plane. [*Note*: The extension twin boundaries ($86° < 11\bar{2}0 > \pm 5°$) are shown in yellow, the contraction twin boundaries ($56° < 11\bar{2}0 > \pm 5°$) are shown in red and the double twin boundaries ($38° < 11\bar{2}0 > \pm 5°$) are shown in blue].

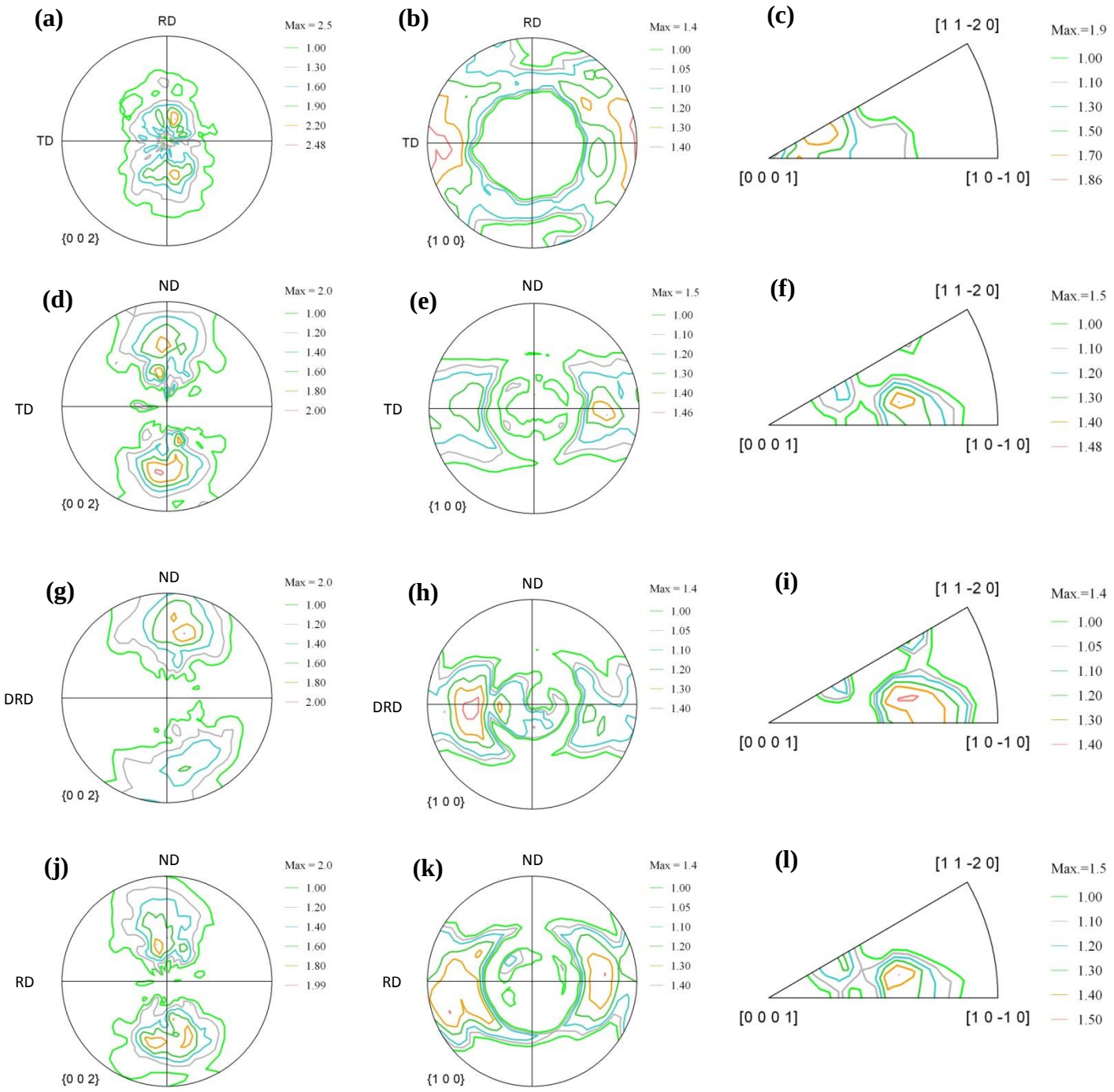

Fig. 5.4. (00.2) & (10.0) pole figures (PF) and inverse pole figures (IPF) of as-rolled samples: (a-c) OP, d-f) IP0, (g-i) IP45 and (j-l) IP90.

The recalculated (00.2) and (10.0) pole figures (PF) and inverse pole figures (IPF) of shock loaded samples at a strain rate of $1200s^{-1}$ (shown in Fig. 5.5) indicate that a basal texture with low intensity evolved in all samples. For instance, in OP samples a weak basal texture was observed (Fig. 5.5(a)) in which there is a splitting of the basal poles almost by ± 20° from the ND toward RD. The intensity of basal poles in OP sample, however, was slightly stronger than that of the initial texture of this sample before shock loading (Fig. 5.4(a)). For the other samples, i.e. IP0, IP45 and IP90, a more marked change was observed and the weak (10.0) prismatic texture was replaced by a weak (00.2) basal texture after shock loading (Fig. 5.5(d), (g) and (j)). Furthermore, comparing the IPFs of the samples before (Fig. 5.4(c),(f), (i) and (l)) and after shock loading (Fig. 5.5(c),(f),(i) and (l)), it is found that there is a shift in maximum intensity and in the IPF of shock loaded samples, the maximum intensity is placed around <0001>. In other words, basal texture formed in the samples during high strain rate deformation, particularly in IP0, IP45 and IP90 samples. For other strain rates, i.e. 800 or 1400 s^{-1}, a weak basal texture also developed and the maximum intensity of the basal poles increased with increase in strain rate. For instance, in OP and IP0 samples the intensity of the basal poles increased slightly with increase in the strain rate (Figs. 5.6 and 5.7). The important feature is that in all cases, the splitting of the basal poles after shock loading was observed.

In Fig. 5.8, typical examples of the microstructure of the alloy before and after the shock loading experiment are presented. One point about Fig. 5.8(a) is that no second phase particle can be observed in this SEM image. It could be related to the fact that the second phase particles are very fine (nano-sized) and in this magnification, it is really difficult to observe them. Moreover, in these SEM images, it is observed that the fractions of twins formed in both samples are different. Considering the morphology of the twins in Fig. 5.8, it seems that most of them are thick and well-grown twins and their fraction in the IP0 sample is larger than that of OP sample. To determine the type and volume fraction of the twins in the samples, EBSD was performed on the shock loaded samples and the results are presented in Fig. 5.9.

The inverse pole figure (IPF) maps and image quality (IQ) maps of the samples after shock loading at 1200 s^{-1} are shown in Fig. 5.9. It is seen that a few twins, including extension (shown in yellow), contraction (shown in red) and double twins (shown in blue), formed in OP samples and the fraction of extension twins is larger than those of contraction and double twins. However, in all other samples, the qualitative comparison of IQ maps shows that the fraction of twinning is larger

compared to that of OP sample. Moreover, as it is observed in Fig. 5.9, the main twins which formed in the shock loaded OP, IP0, IP45 and IP90 samples are {10-12} extension twins.

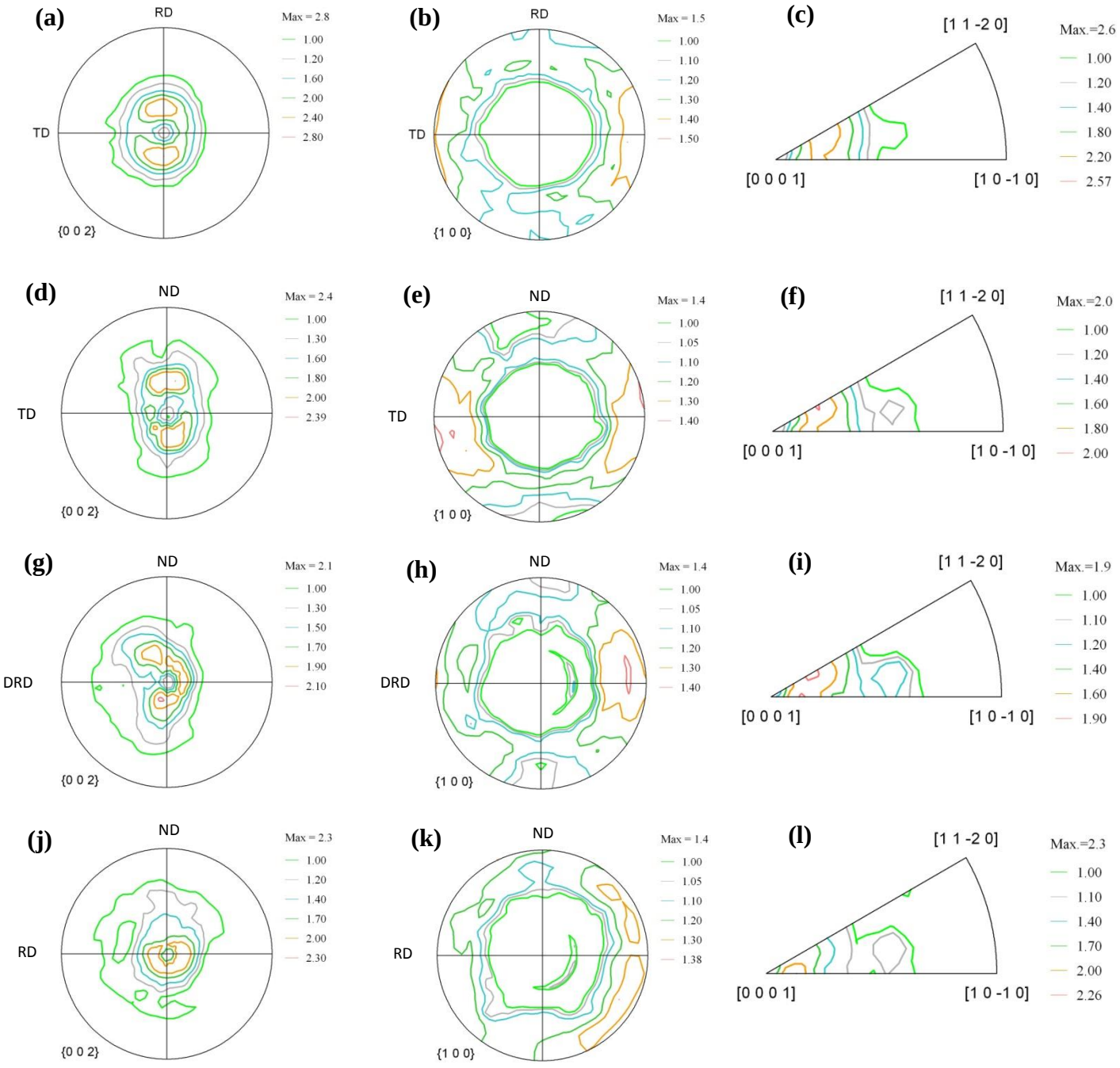

Fig. 5.5. (00.2) and (10.0) pole figures (PF) and inverse pole figures (IPF) of shock-loaded samples at $\dot{\varepsilon} = 1200\ s^{-1}$. (a-c) OP, (d-f) IP0, (g-i) IP45 and j-l) IP90.

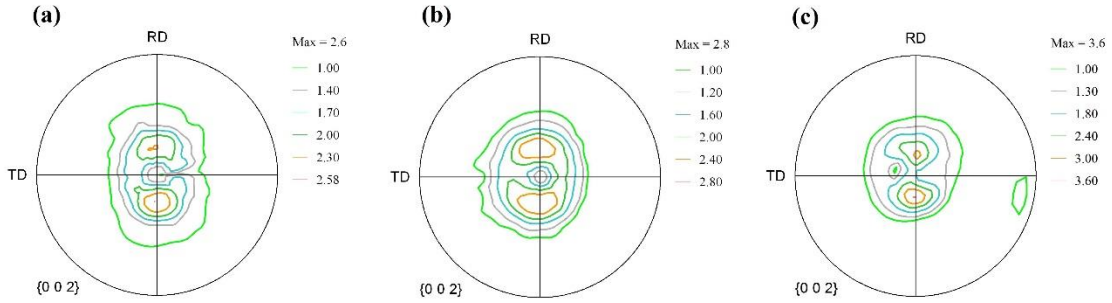

Fig. 5.6. (00.2) pole figures of shock-loaded OP samples at: (a) $\dot{\varepsilon}$ = 800 s^{-1},(b) $\dot{\varepsilon}$ = 1200 s^{-1} and (c) $\dot{\varepsilon}$ = 1400 s^{-1} .

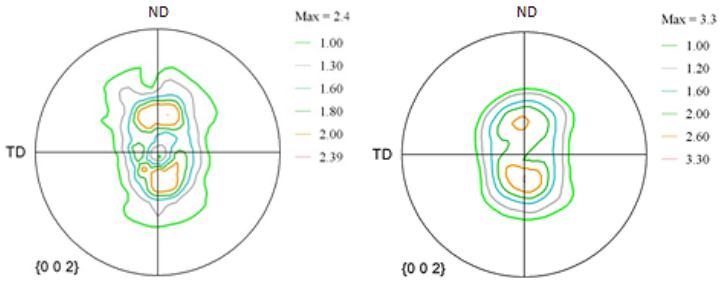

Fig. 5.7. (00.2) pole figures of shock-loaded IP0 samples at: (a) $\dot{\varepsilon}$ = 1200 s^{-1},(b) $\dot{\varepsilon}$ = 1400 s^{-1} .

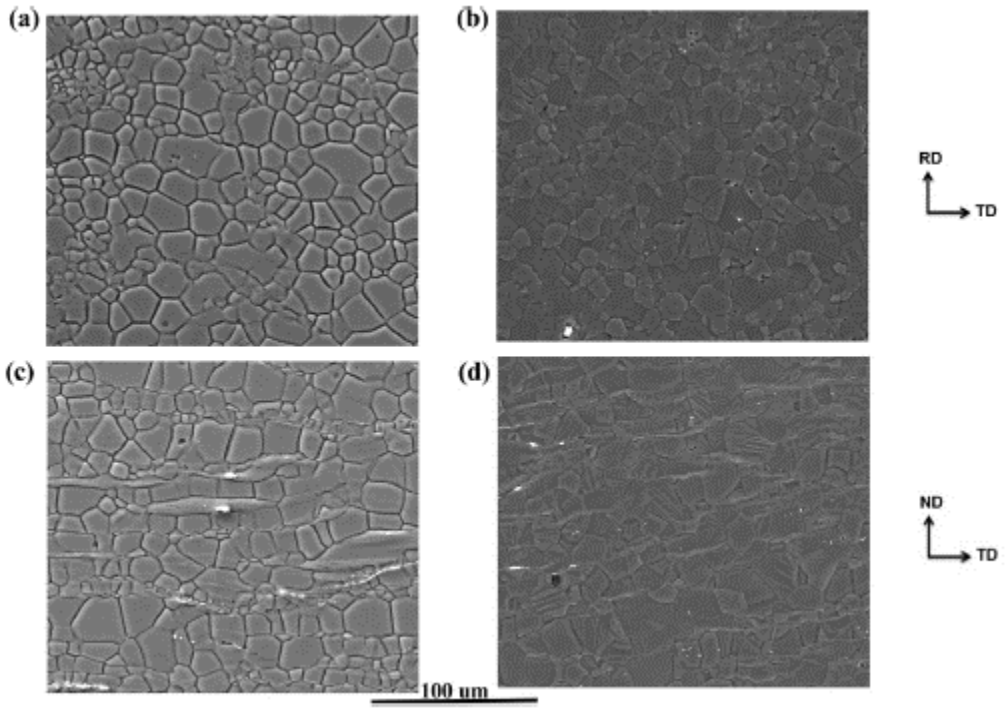

Fig. 5.8. SEM images of the samples before and after shock loading at $\dot{\varepsilon}$ = 1200 s^{-1}; (a) OP sample before shock loading, (b) OP sample after shock loading, (c) IP0 before shock loading, (d) IP0 after shock loading.

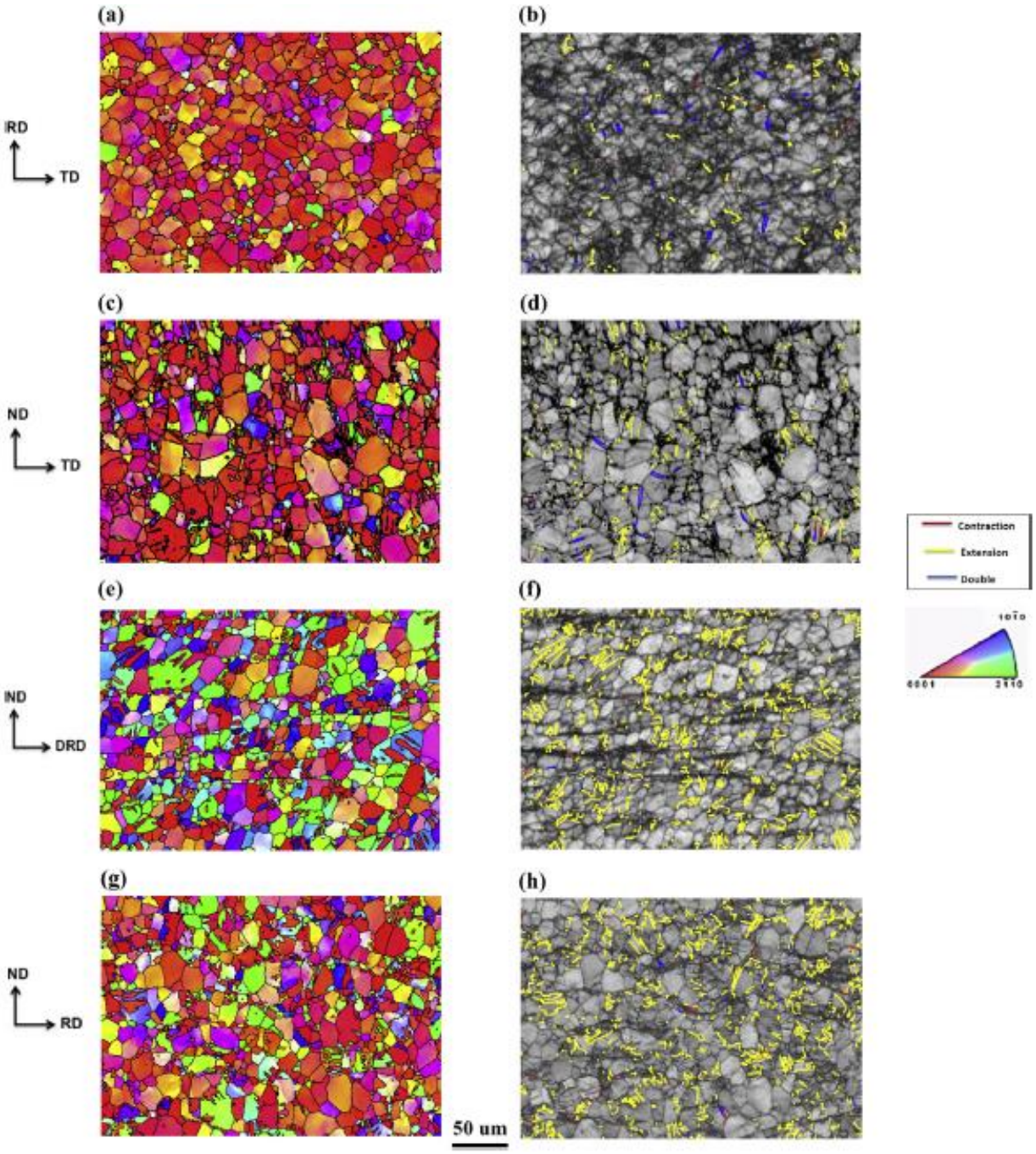

Fig. 5.9. Inverse pole figure (IPF) maps and image quality (IQ) maps of the samples showing the microstructure and twins type after shock loading at $\dot{\varepsilon}$ = 1200 s^{-1}. (a) and (b): OP, (c) and (d): IP0, (e) and (f): IP45, (g) and (h): IP90 sample. [*Note*: The extension twin boundaries (86°< $11\bar{2}0$ > ±5°) are shown in yellow, the contraction twin boundaries (56° < $11\bar{2}0$ > ±5°) are shown in red and the double twin boundaries (38° < $11\bar{2}0$ > ±5°) are shown in blue].

To evaluate the effect of strain rate on the twinning, the inverse pole figure (IPF) maps and image quality (IQ) maps of the OP and IP0 samples after shock loading at 800 s^{-1} are presented in Fig. 5.10. It is evident that that the fraction of twinning, particularly extension twinning, in the samples deformed at lower strain rates (i.e. 800 s^{-1}) is larger than those of deformed at higher strain rates (i.e. 1200 s^{-1}) shown in Fig. 5.9. The same trend was also observed for IP45 and IP90 samples in which the fraction of twinning was larger at 800s^{-1}. It seems that by increasing the strain rate, the twinning mechanism is suppressed and replaced by some other deformation mechanism(s) that will be discussed later.

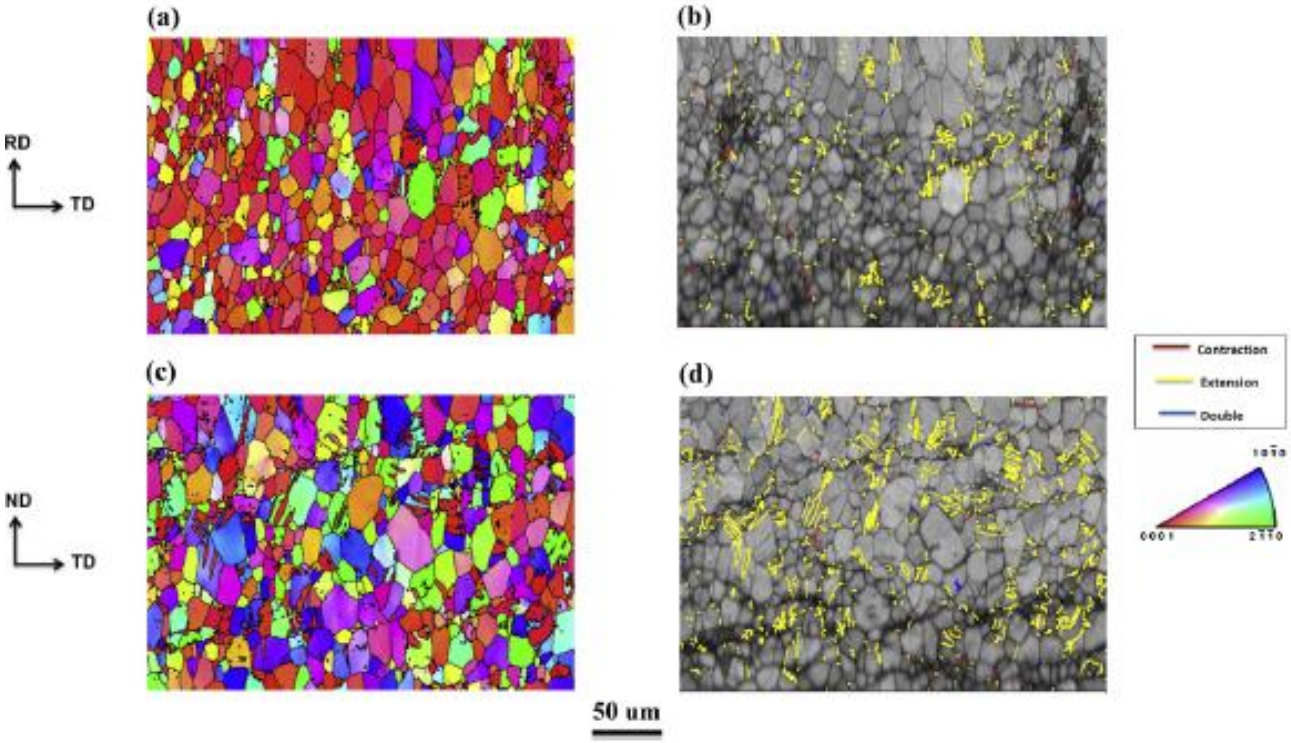

Fig. 5.10. Inverse pole figure (IPF) maps and image quality (IQ) maps of the samples showing the microstructure and twins type after shock loading at $\dot{\varepsilon}$ = 800 s^{-1}. (a) and (b): OP, (c) and (d): IP0 [*Note*: The extension twin boundaries ($86° < 11\bar{2}0 > \pm 5°$) are shown in yellow, the contraction twin boundaries ($56° < 11\bar{2}0 > \pm 5°$) are shown in red and the double twin boundaries ($38° < 11\bar{2}0 > \pm 5°$) are shown in blue].

The (00.2) pole figures (PF) and inverse pole figures (IPF) of shock-loaded samples as obtained by VPSC simulations, based on the assumption that basal slip, extension twinning and pyramidal <c+a> slip systems are activated in shock loading, are shown in Fig. 5.11. Although the maximum

intensities are higher in simulated textures, a reasonable match exists between the simulated (Fig. 5.11) and experimental textures (Fig. 5.5).

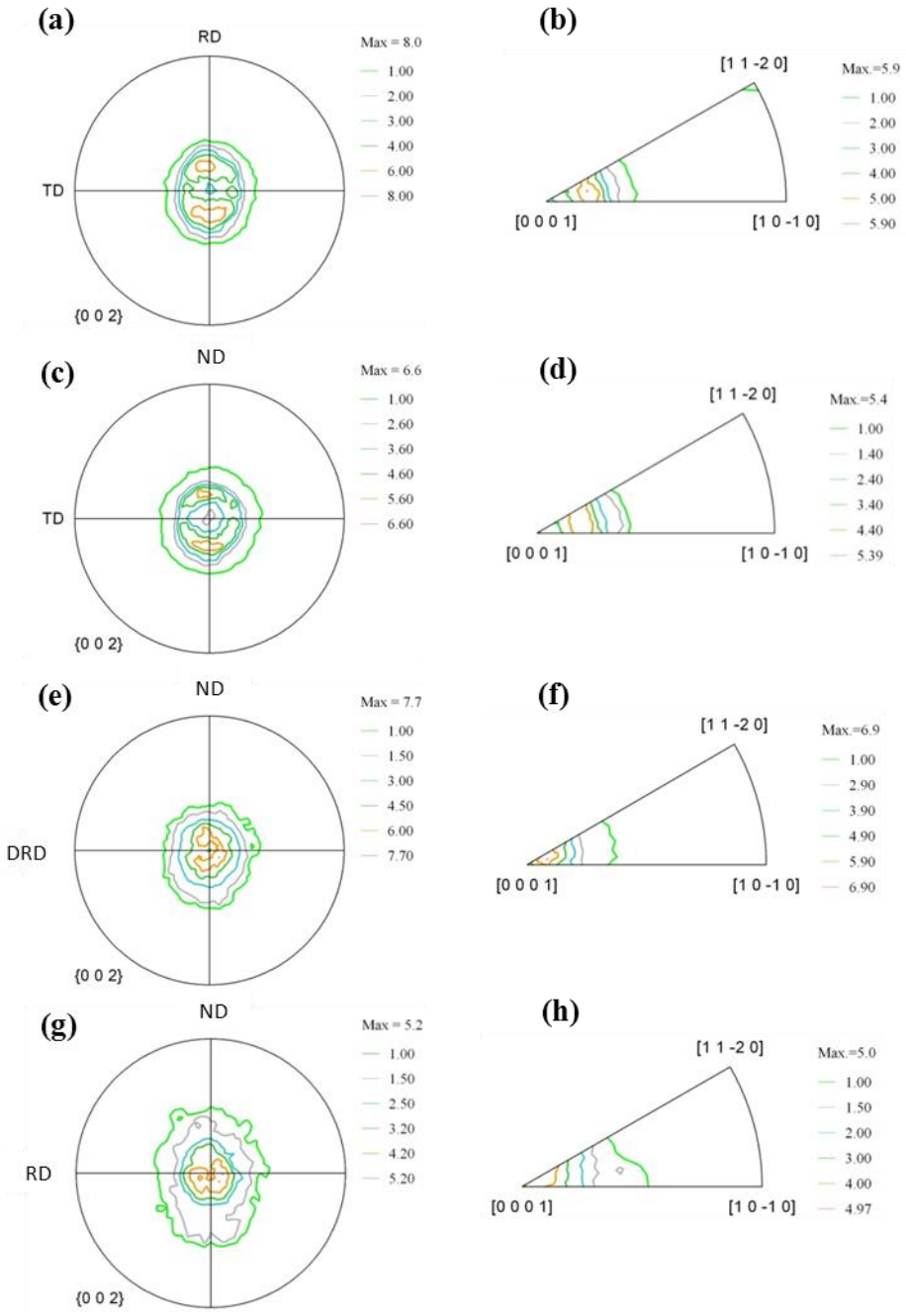

Fig. 5.11. Simulated (00.2) pole figures (PF) and inverse pole figures (IPF) of shock-loaded samples (a) and (b): OP, (c) and (d): IP0, (e) and (f): IP45, (g) and (h): IP90. (*Note*: assumed deformation systems are: basal slip, pyramidal <c+a> slip and extension twinning).

To evaluate the effect of neglecting the operation of one of the possible and important deformation modes, i.e. pyramidal <c+a> slip system, on the texture development during dynamic loading, another set of pole figures were reproduced by VPSC simulations for shock-loaded OP and IP0 samples (Fig. 5.12). As can be seen in Fig. 5.12, in which the simulated textures show a very strong basal plane orientation, when the pyramidal <c+a> slip is not included in the simulation (or when only basal slip and extension twinning are assumed to be activated), the resulting textures (Fig. 5.12) are very different from the experimental ones (Fig. 5.5). Therefore, assuming the activation of basal slip, extension twinning and pyramidal <c+a> slip will give the best fit between the simulated and experimental result (Fig. 5.11), suggesting that these modes are the most probable active modes during dynamic impact loading. The values (ratios) of CRSSs used in the above-mentioned simulations are tabulated in Table 5.2.

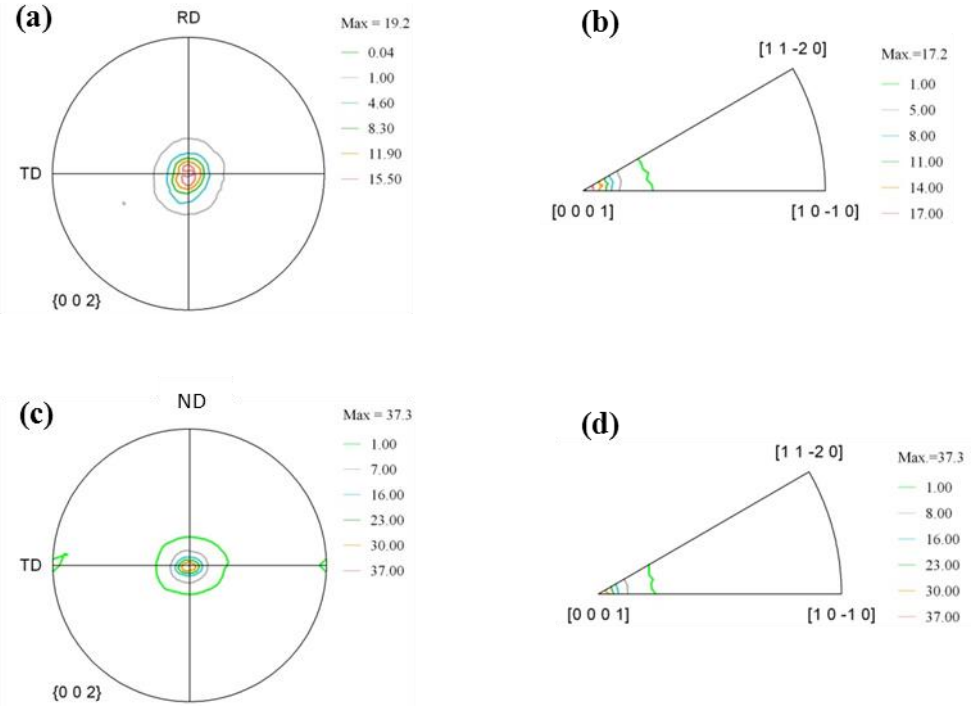

Fig. 5.12. Simulated (00.2) pole figures (PF) and inverse pole figures (IPF) of shock-loaded samples (a) and (b): OP, (c) and (d): IP0. (*Note*: assumed deformation systems are: basal slip and extension twinning).

In Fig. 5.13, the activity of various slip and twinning systems of OP and IP0 samples, based on the assumptions that were used to simulate the textures, presented in Fig. 5.11, are shown. Results

clearly indicate that basal slip was dominant in the samples at the onset of plastic deformation and its contribution gradually decreased with an increase in the contribution from pyramidal<c+a> slip. Besides, it is evident that the contribution of extension twinning was almost constant at the beginning stages of plastic deformation and decreased with increase in the activity of pyramidal<c+a> slip. The fraction of extension twinning in the IPO sample is slightly larger than that of OP sample which is in good agreement with the EBSD results (Fig. 5.9).

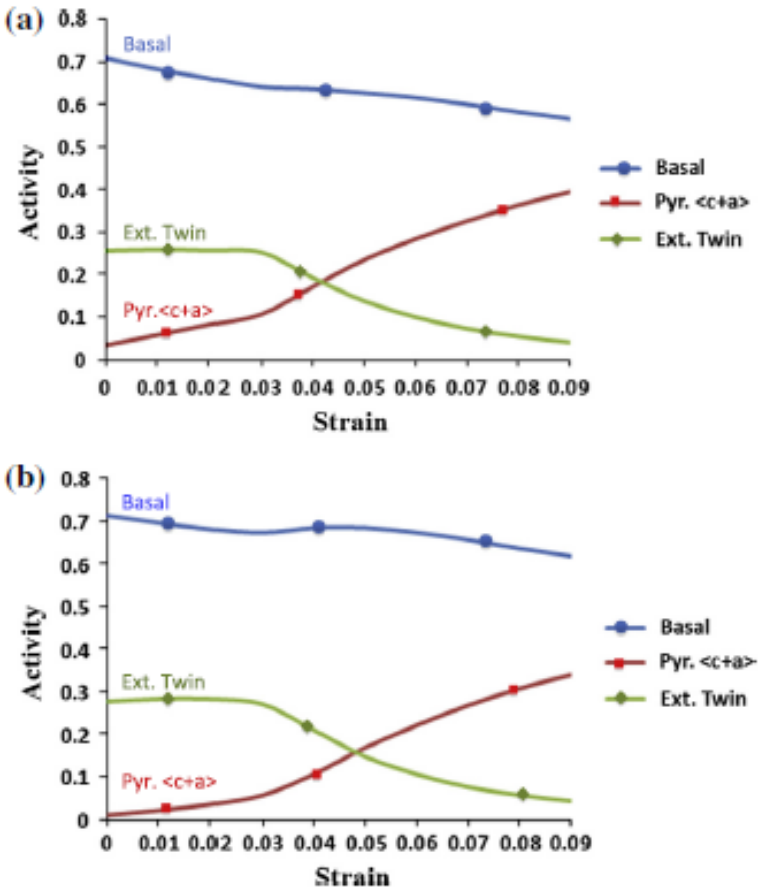

Fig. 5.13. Simulated activity of various slip and twinning systems for the (a) OP and (b) IP0 samples.

Other sets of simulations were done to evaluate the texture evolution when the strain rate increased. Experimental results in Figs. 5.6 and 5.7 showed that by increasing the strain rate, the intensities on the pole figures slightly increased but the position of the peaks were kept the same as for the lower strain rates (Fig. 5.5). In Fig. 5.14, some examples of simulated textures for OP and IP0 samples are presented assuming that the strain rate increased. The results of simulation are

in good agreement with the experimental results (Figs. 5.6 and 5.7), showing the increase in the intensities with increase in strain rate. To conduct logical simulations for this part, it was assumed that due to the increase in the strain rate, the temperature during the shock loading was also increased and therefore, the CRSS of the pyramidal <c+a> slip decreased; furthermore, considering the results of the EBSD test, in which the twinning fraction decreased with an increase in the strain rate (Figs. 5.9 and 5.10), the CRSS value for twinning was increased in the simulations to attenuate its contribution in deformation process. The values of CRSS used in these simulations are tabulated in Table 5.3. The interesting aspect about the simulated textures at higher strain rates, is the decreased activity of extension twinning and increased activity of pyramidal <c+a> slip systems compared to that presented in Fig. 5.13. As an example, the activity vs strain diagram of OP sample is shown in Fig. 5.15. It is seen that the activity of extension twinning is less than that of at lower strain rates (Fig. 5.13(a)). Also, the pyramidal <c+a> is more active at higher strain rates in OP sample.

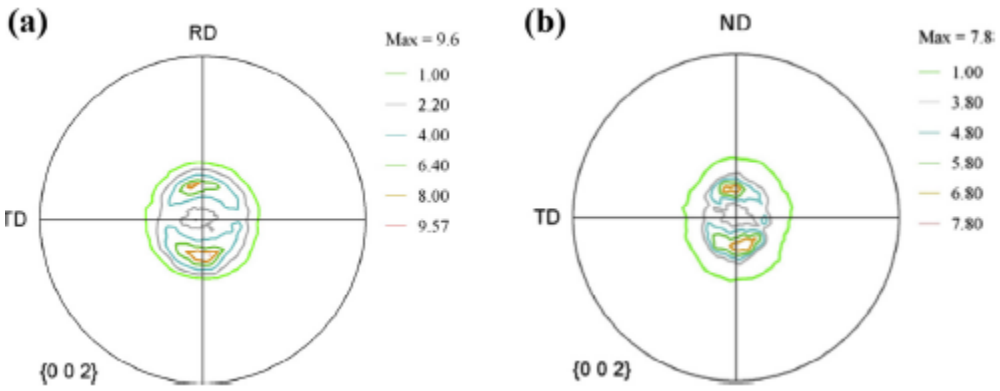

Fig. 5.14. Simulated (00.2) pole figures (PF) and inverse pole figures (IPF) of shock-loaded (a): OP sample and (b): IP0 sample at higher strain rates with respect to the Fig 5.11.

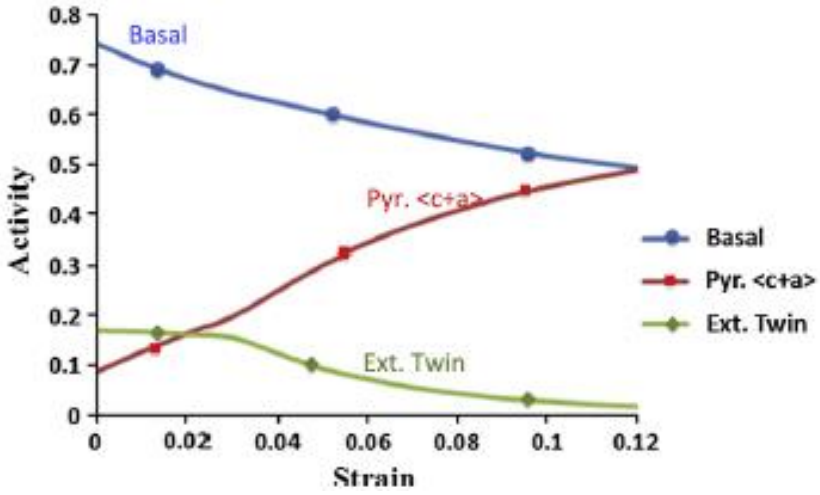

Fig. 5.15. Simulated activity of various slip and twinning systems for the OP samples. (Strain rate is higher compared to those of Fig. 5.13).

The dynamic compressive true stress-strain curves and hardening diagrams of the samples deformed at high strain rates, i.e. 800, 1200 and 1400 s^{-1}, are presented in Fig. 5.16. All the curves are S-shaped and the stress increased to a maximum and then decreased. It is worth noting that a small difference between the dynamic behavior of the samples is observed particularly at higher strain rates, that is, the difference between the strength or ductility of samples is not significant at different strain rates used in the current study (Fig. 5.16). In other words, the degree of mechanical anisotropy of samples as represented by shock loading results is low. Furthermore, considering the hardening diagrams (Fig. 5.16(b),(d) and (f)), it was found that the humps were narrower at lower strain rates and broadened at higher strain rates.

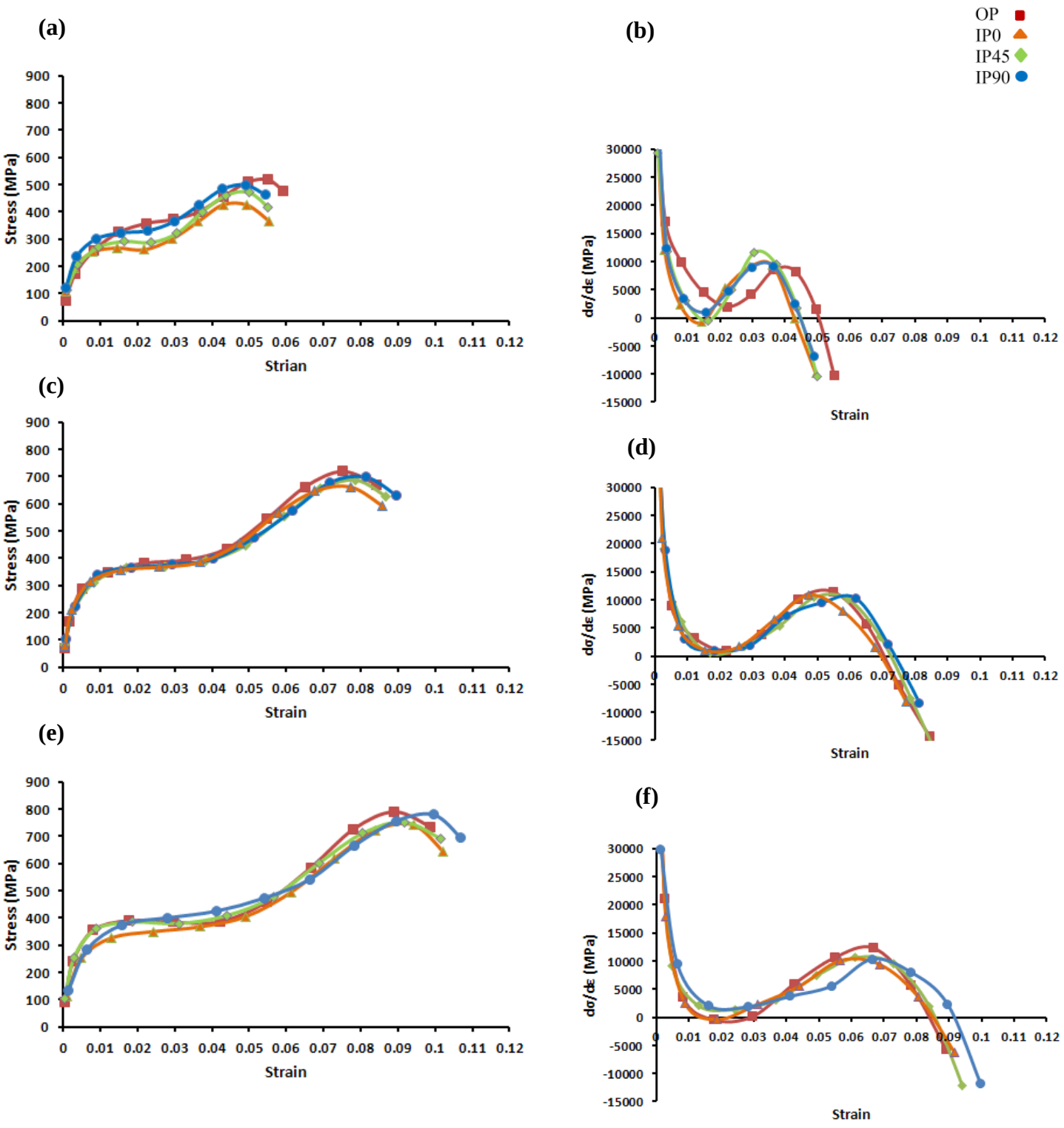

Fig. 5.16. Stress-Strain curves and hardening diagrams (dσ/dε versus strain) of shock loaded samples at strain rate of a,b) 800, c,d) 1200 and e,f) 1400 s^{-1}.

5.6. Discussion

It is shown in Fig. 5.4(a),(b) and (c) that the OP sample before shock loading exhibited a weak (00.2) basal texture, having a low intensity, which is much less than the maximum intensity commonly reported in rolled AZ31 sheet [13-14]. In other samples, i.e. IP0, IP45 and IP90, a very weak prismatic texture developed (Fig. 5.4(d) and Fig. 5.4(l)). The very weak texture developed in the samples is typical of RE containing rolled magnesium alloy sheets [4,5,7,15]. Also, spreading and splitting of the basal poles toward RD means that the c-axis of the HCP unit cells in most of the grains is tilted away from the normal direction toward the rolling direction of the sheet. Consequently, the corresponding (10.0) prismatic planes are not oriented parallel to the compression plane and therefore, a weak prismatic texture was recorded for other samples (IP0, IP45 and IP90). The weak basal texture developed in the as-rolled WE43 sheets has been related to the texture-randomizing or texture-optimizing effect of RE elements, which could be associated with particle-stimulated nucleation (PSN) of recrystallization [5,7,16]. Generally, modification and randomization of texture, due to the addition of RE elements takes place during recrystallization process in rare earth containing magnesium alloys. In fact, because of the formation of stable second phase particles which usually contain Zn, Nd, Y and Mg, suitable nucleation sites for DRX are produced during hot rolling, resulting in the recrystallization and growth of a wide variety of grains of different crystallographic orientations [4,5,7]. As a result, the texture is modified, giving rise better formability at low temperatures [4,5,7].

After shock loading, as shown in Fig. 5.5, a weak (00.2) basal texture was observed in all samples. Also, by changing the strain rate, similar textures were obtained and the difference between the intensities was small (Figs. 5.6 and 5.7). Considering the splitting of basal poles in the pole figures, it is reasonable to suggest that both twinning and pyramidal <c+a> slip could have been responsible for development of such textures after shock loading [17-19].

According to the EBSD results (Fig. 5.9), extension twinning is the dominant twinning mode in the samples and the fraction of extension twinning in IP0, IP45 and IP90 samples is larger than that of OP sample. It may be related to the formation of a weak basal texture in OP samples. As a result, the activation and development of extension twins were limited in comparison to other samples [20]. Besides, comparing the EBSD results (Figs. 5.9 and 5.10) shows that increasing the strain rate resulted in the decreased fraction of extension twinning and it seems that another deformation mode, i.e. pyramidal <c+a> slip, is involved in the deformation process. The reasons by which the

activation of pyramidal <c+a> slip can be considered during the shock loading are:

(i) Increase in temperature during the shock loading test which can result in a decreased CRSS of pyramidal <c+a> slip systems [21].

(ii) The presence of RE elements, particularly yttrium and neodymium in the investigated WE43 magnesium alloy, which affects the stacking fault energy (SFE) of <c+a> dislocations and results in a decreased CRSS of pyramidal <c+a> slip system and increased stability of glissile <c+a> dislocations [7]. This increase the probability of the activation of pyramidal <c+a> slip systems [7].

As mentioned previously, the best match between the simulated and experimental textures was only obtained by considering the combination of extension twinning and pyramidal <c+a> slip systems (together with basal slip) and any other assumptions on deformation modes failed to establish a reasonable match between simulated and experimental textures (for instance, Fig. 5.12). Besides, activity vs strain diagrams (Fig. 5.13) revealed that basal slip was dominant deformation mode in the samples at the onset of plastic deformation. However, basal slip contribution gradually decreased with an increase in the contribution from pyramidal<c+a> slip. Extension twinning occurred at the beginning of plastic deformation and decreased with increase in the activity of pyramidal <c+a> slip. Basal slip and extension twinning system are easily activated at the beginning of deformation process because of their low CRSS [7, 16, 21-23]. However, with increasing the strain, the activity of pyramidal slip increase considerably due to the decreased CRSS of this system with increasing the temperature during shock loading. Besides, the increased temperature with increasing the strain rate resulted in higher probability of activation of pyramidal slip systems at higher strain rates in OP samples (Fig. 5.15). It could be related to the further decrease in CRSS of pyramidal <c+a> systems at higher strain rates.

In Fig. 5.16, it was seen that there is a small difference in the flow curves of the samples especially at higher strain rates. This similarity in the mechanical behavior is attributed to the very weak initial (random-like) texture of the samples. In other magnesium alloys, for example AZ31B sheet, a high anisotropy was observed in the mechanical behavior of the samples after shock loading at different directions, resulting from the initial strong basal texture of the sheet [14, 24]. Therefore, an important role of rare-earth elements is their ability to minimize mechanical anisotropy at high strain rates by lowering the strength of texture.

5.7. Conclusions

Based on the experimental results and simulation of texture transformation during high impact deformation, the following conclusions are made:

(1) After shock loading, the weak but different initial textures are transformed to a weak basal texture in all samples in which splitting of basal poles is observed, indicating the high probability of pyramidal <c+a> activation under shock loading.

(2) By increasing the strain rate, the strength and ductility increase, contribution of twinning to deformation decreases and the maximum strain hardening rate takes place at the highest strain.

(3) Increasing the strain rate results in an increase in the intensity of basal poles in the pole figures of OP and IP0 samples which is correlated with higher probability of activation of pyramidal <c+a> slip systems.

(4) The most active deformation modes were basal slip, pyramidal <c+a> slip and extension twinning. However, at the onset of deformation, basal slip is the dominant mode of deformation and by increasing the strain, the activity of this system gradually decreases. Under the same condition the decrease of activity of extension twinning is more rapid.

(5) Activity of pyramidal <c+a> slip system increases and activity of extension twinning decreases with increase in strain rate.

(6) The degree of stress and strain anisotropy is low which is related to the weak initial texture due to the presence of rare-earth (RE) elements in the alloy.

References

[1] Li Q. Mechanical properties and microscopic deformation mechanism of polycrystalline magnesium under high-strain-rate compressive loadings. Materials Science and Engineering A 2012; 540:130-134.

[2] Korla R, Chokshi AH. Strain-rate sensitivity and microstructural evolution in a Mg–Al–Zn alloy. Scripta Materialia 2010; 63: 913-916.

[3] Jiang L, Jonas JJ, Luo AA, Sachdev AK, Godet S. Influence of {10-12} extension twinning on the flow behavior of AZ31 Mg alloy. Materials Science and Engineering A 2007;445-446: 302:309.

[4] Hirsch J, Al-Samman T. Superior light metals by texture engineering: Optimized aluminum and magnesium alloys for automotive applications. Acta Materialia 2013; 61:818-843.

[5] Bohlen J, Nürnberg MR, Senn JW, Letzig D, Agnew SR. The texture and anisotropy of magnesium–zinc–rare earth alloy sheets. Acta Materialia 2007; 55: 2101-2112.

[6] Farzadfar SA, Sanjari M, Jung I-H, Essadiqi E, Yue S. Role of yttrium in the microstructure and texture evolution of Mg. Materials Science and Engineering A 2011; 528:6742-6753.

[7] Sandlöbes S, Zaefferer S, Schestakow I, Yi S, Gonzalez-Martinez R. On the role of non-basal deformation mechanisms for the ductility of Mg and Mg–Y alloys. Acta Materialia 2011; 59: 429-439.

[8] Ping-li M, Jin-cheng Y, Zheng L, Yang D. Microstructure evolution of extruded Mg-Gd-Y magnesium alloy under dynamic compression. Journal of Magnesium and Alloys 2013; 1:64-75.

[9] Hamilton J, Brennan S.T., Sohn Y, Davis B, DeLorme R, Cho K. Microstructural characteristics of high rate plastic deformation in Elektron WE43 magnesium alloy. TMS 2012, Magnesium Technology Symposium, Edited by Suveen N. Mathaudhu, Wim H. Sillekens, Neale R. Neelameggham and Norbert Hort; 433-438.

[10] Agnew S. Whittington W, Oppedal A, El-Kadiri H, Shaeffer M, Ramesh KT, Bhattacharyya J, Delorme R, Davis B. Dynamic behavior of a rare-earth-containing Mg alloy, WE43B-T5, plate with comparison to conventional alloy, AM30-F. JOM 2014; 66: 277-290.

[11] Lebensohn RA, Tomé CN. A self-consistent anisotropic approach for the simulation of plastic deformation and texture development of polycrystals: Application to zirconium alloys. Acta Metallurgica et Materialia 1993; 41: 2611-2624.

[12] Wang YN, Huang JC. Texture analysis in hexagonal materials. Materials Chemistry and Physics 2003; 81: 11-26.

[13] Jeong HT, Ha TK. Texture development in a warm rolled AZ31 magnesium alloy. Journal of Materials Processing Technology 2007; 187–188: 559-561.

[14] Asgari H, Szpunar JA, Odeshi AG, Gurao NP. Investigation on the texture and mechanical behavior of AZ cast magnesium alloys under compressive shock loading. Proceedings of the 24th Canadian Congress of Applied Mechanics 2013; Canada. 68-71.

[15] Ball EA, Prangnell PB. Tensile-compressive yield asymmetries in high strength wrought magnesium alloys. Scripta Metallurgica et Materialia 1994; 31:111-116.

[16] Li X, Jiao F, Al-Samman T, Chowdhury SG. Influence of second-phase precipitates on the texture evolution of Mg–Al–Zn alloys during hot deformation. Scripta Materialia 2012; 66:159-162.

[17] Chang LL, Shang EF, Wang YN, Zhao X, Qi M. Texture and microstructure evolution in cold rolled AZ31 magnesium alloy. Materials Characterization 2009; 60:487-491.

[18] Agnew SR, Yoo MH, Tomé CN. Application of texture simulation to understanding mechanical behavior of Mg and solid solution alloys containing Li or Y. Acta Materialia 2001; 49:4277-4289.

[19] Barnett MR. A Taylor model based description of the proof stress of magnesium AZ31 during hot working. Metallurgical and Materials Transactions A 2003;34:1799–806.

[20] Yi S, Schestakow I, Zaefferer S. Twinning-related microstructural evolution during hot rolling and subsequent annealing of pure magnesium. Materials Science and Engineering A 2009; 516: 58-64.

[21] Obara T, Yoshinga H, Morozumi S. {1122}〈1123〉 Slip system in magnesium. Acta Metallurgica 1973; 21:845-853.

[22] Gurao NP, Kapoor R, Suwas S. Deformation behaviour of commercially pure titanium at extreme strain rates. Acta Materialia 2011; 59: 3431-3446.

[23] Tomé CN, Lebensohn RA, Kocks UF. A model for texture development dominated by deformation twinning: Application to zirconium alloys. Acta Metallurgica et Materialia 1991; 39: 2667-2680.

[24] Hao M, Zhang F, Tan C, Su T, Yu X. Effects of anisotropy on the microstructural characteristics and mechanical behavior of shock loaded AZ31 alloy. Advanced Materials Research 2011; 284-286:1537-1541.

CHAPTER 6

GRAIN SIZE DEPENDENCE OF DYNAMIC MECHANICAL BEHAVIOR OF AZ31B MAGNESIUM SHEET UNDER SHOCK LOADING

6.1. Overview of Chapter 6

In Chapters 4 and 5, the effects of strain rate and initial texture on the microstructural evolution, deformation behavior and deformation mechanisms which are involved during the shock loading of AZ31B and WE43 rolled sheets were discussed. In this chapter the effect of another key parameter, i.e. grain size, on the dynamic mechanical behavior of rolled AZ31B-H24 is explained. Besides, the effect of grain size on the deformation mechanisms of fine-grained and coarse-grained AZ31B alloy will also be discussed.

This chapter is presented as manuscript # 5. The author's (H. Asgari) contributions to this manuscript are: (a) preparation and processing of the samples for shock loading test. (b) XRD, SEM, EDS, EBSD and TEM analyses. (c) Reviewing the relevant literature, writing and submission of the manuscript. The contribution of Dr. L. J. Zeng and Prof. E. Olsson was in the area of TEM investigation and analysis.

The manuscript was submitted to *Materials Characterization*. It is currently under review.

- H. Asgari, A.G. Odeshi, J.A. Szpunar, L.J. Zeng, E. Olsson. "Grain size dependence of dynamic mechanical behavior of AZ31B magnesium sheet at compressive shock loading".

The manuscript presented here is different from the published paper in the following parts:

- In order to avoid repetition in the content, some parts of the 'introduction','experimental procedure', and 'discussion' sections were eliminated.

The copyright permission to use the manuscript in the thesis was obtained and provided in the Appendix section.

Grain size dependence of dynamic mechanical behavior of AZ31B magnesium alloy sheet under shock loading

H. Asgari[1], A. G. Odeshi[1], J. A. Szpunar[1], L. J. Zeng[2], E. Olsson[2]

[1]Department of Mechanical Engineering, University of Saskatchewan, Saskatoon, Canada

[2]Department of Applied Physics, Chalmers University of Technology, Göteborg, Sweden

6.2. Abstract

The effects of grain size on the dynamic deformation behavior of rolled AZ31B alloy at high strain rates were investigated. Rolled AZ31B alloy samples with grain sizes of 6, 18 and 37 μm, were subjected to shock loading tests using Split Hopkinson Pressure Bar at room temperature and at a strain rate of 1100 s^{-1}. It was found that a double-peak basal texture formed in the shock loaded samples. The strength and ductility of the alloy under the high strain-rate compressive loading increased with decreasing grain size. However, twinning fraction and strain hardening rate were found to decrease with decreasing grain size. In addition, orientation imaging microscopy showed a higher contribution of double and contraction twins in the deformation process of the coarse-grained samples. Using transmission electron microscopy, different type of dislocations, including <c+a> dislocations were detected in the shock loaded sample, proving the activation of pyramidal <c+a> slip system under dynamic impact loading.

Keywords: AZ31B magnesium alloy, Dynamic deformation mechanism, Twinning, Mechanical properties.

6.3. Introduction

Magnesium alloys, as the lightest structural materials, are promising materials for various applications in the transportation industry [1-3] however, wrought magnesium alloys normally form a strong basal which results in low room temperature ductility and therefore, their structural application are limited [4-10].

Grain size is one of the key parameters that significantly affects the dynamic mechanical response of magnesium alloys which are exposed to high strain rate situations. For this reason, understanding and determining the role of grain size in changing the deformation behavior of wrought magnesium alloys under shock loading conditions if an important issue. To date, there is

almost no information in the available literature about the effects of grain size on the texture formation and dynamic behavior of AZ31B magnesium alloy during high velocity impact. It should be mentioned that so far, the studies that have been conducted on the effect of grain size on the mechanical behavior of AZ31B magnesium alloys have been done in the low strain rate conditions [11-22]. Besides, in the available reports in the literature about the high strain rate deformation of AZ31B alloys [23-30], the effect of grain size is not investigated and there is a considerable lack of information in the correlation between the grain size and dynamic impact response of AZ31B magnesium alloys.

In the current study, the effect of grain size on the texture formation, microstructural evolution and dynamic mechanical response of rolled AZ31B alloy with different grain sizes under shock loading conditions is investigated. The effect of grain size on the deformation behavior is also explained.

6.4. Experimental procedure

Hot-rolled AZ31B magnesium alloy sheet in the tempered H24 stress-relieved conditions provided by M&B MAG Ltd Company, with an initial grain size of 6μm, was used in this research. The nominal chemical composition of the AZ31B alloy sheet is presented in Table 4.1 (Chapter 4). To investigate the dynamic deformation behavior of the alloy, Split Hopkinson Pressure Bar (SHPB) was used. The shock loading tests were conducted at room temperature at a strain rate of 1100 s^{-1}. Three groups of samples, with different grain sizes of 6 μm (as received), 18 μm and 37 μm, were prepared for shock loading tests. To produce the samples with coarser grain size (18 and 37 μm), heat-treatment in box furnace at temperatures ranging between 350 and 450 °C for about 12 hours was done. Shock loading test samples were placed in small ceramic containers and then the container was filled with fine-grained alumina powder and then covered with aluminum foil to reduce the oxidation of the samples during the heat-treatment.

The samples were machined into cylindrical test sample, 9.5 mm in diameter and 10.5 mm long. The test samples were cut in two different directions with respect to the rolled as-received sheet: (i) in the rolling direction (RD), hereafter denoted as IP0 and (ii) in the direction perpendicular to the RD-TD (transverse direction) plane, hereafter denoted as OP.

The cylindrical samples were impacted in a direction parallel to their longitudinal axis. Therefore, in the IP0 samples, the impact direction is parallel to the RD of the sheet and in the OP

samples, the impact direction is parallel to the ND (normal direction) of the sheet. The sample ends were lubricated to eliminate the friction effect on the surfaces of the samples during shock loading.

The 'g.b = 0' invisibility criterion, where *g* is diffraction vector and *b* is Burgers vector of the dislocation, was used to confirm the presence of <c+a> dislocations in the shock-loaded samples. In Table 6.1, the values of 'g.b' for the dislocations in hcp crystals for low-index reflections near the zone axis $[1\bar{2}10]$ used in this research are tabulated. Basically, when the value of 'g.b' is zero, the dislocation is not visible or the dislocation contrast is very weak. The g=[0002] and g=$[10\bar{1}0]$ diffraction vectors were used to find dislocations with a 'c+a' component because only <c+a> dislocations which are visible under both g=[0002] and g=$[10\bar{1}0]$ diffraction conditions [32-33]. Due to the similarity in the pole figures of the shock-loaded samples, i.e. double peak basal pole figures, two shock-loaded samples, namely one OP and one IP0 sample were selected for 'g.b' analysis.

Table 6.1. The *g.b* values for dislocations in the HCP crystals close to $[1\bar{2}10]$ zone axis [33].

Mode	Burgers vector (*b*)	*g* = [0002]	*g* = $[10\bar{1}0]$
		g.b	g.b
<a>	1/3$[11\bar{2}0]$	0	1
	1/3$[1\bar{2}10]$	0	0
	1/3$[\bar{2}110]$	0	-1
<c+a>	1/3$[11\bar{2}3]$	2	1
	1/3$[1\bar{2}13]$	2	0
	1/3$[\bar{2}113]$	2	-1
	1/3$[11\bar{2}\bar{3}]$	-2	1
	1/3$[1\bar{2}1\bar{3}]$	-2	0
	1/3$[\bar{2}11\bar{3}]$	-2	-1
<c>	[0001]	2	0

The details of shock loading test, texture measurements, SEM, EBSD and TEM analysis are similar to those described in Chapter 5. It is not repeated here in order to keep the thesis concise.

6.5. Results

Figs. 6.1 and 6.2 show the initial texture of the OP and IP0 samples, respectively. As can be seen, the initial texture of the OP samples is a strong (00.2) basal texture in which most of the basal planes are aligned parallel to the sheet surface and the maximum intensity increase with increasing grain size (Fig. 6.1). However, in IP0 samples, the basal planes are perpendicular to the ND-TD plane and in the samples with coarser grains, the maximum intensity is larger (Fig. 6.2).

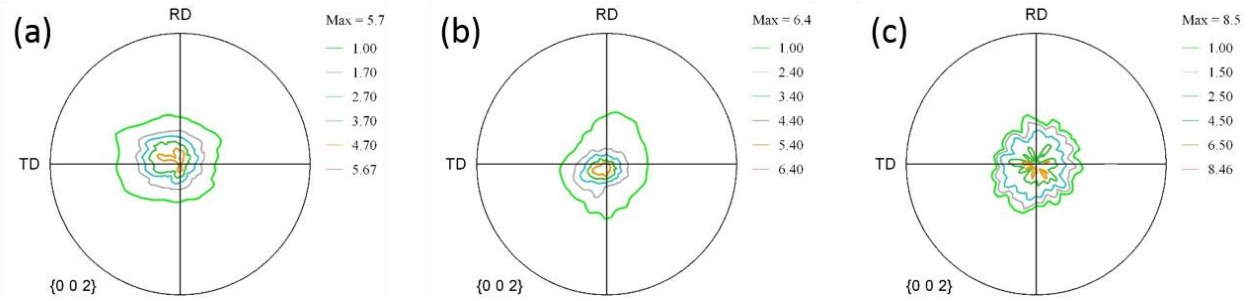

Fig. 6.1. (00.2) pole figures (PF) of the OP samples with different grain sizes before shock-loading: (a) 6 µm, (b) 18 µm, (c) 37 µm.

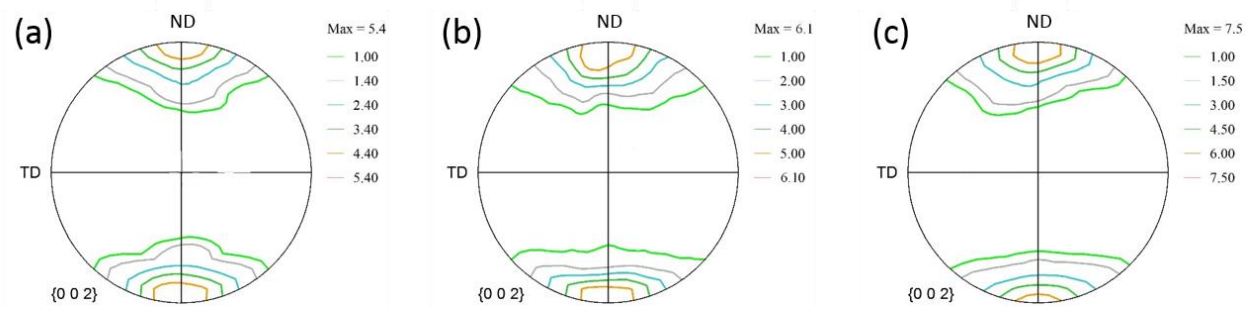

Fig. 6.2. (00.2) pole figures (PF) of the IP0 samples with different grain sizes before shock-loading: (a) 6 µm, (b) 18 µm, (c) 37 µm.

Texture of the shock loaded samples is demonstrated in Figs. 6.3 and 6.4. Interestingly, in all samples, including OP and IP0 samples with different grain sizes, a double peak (00.2) basal texture can be seen and the maximum intensity is higher for samples with coarser grains.

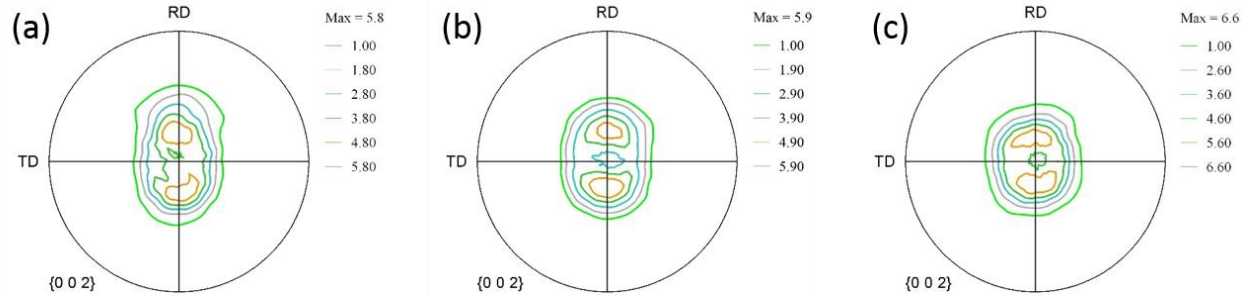

Fig. 6.3. (00.2) pole figures (PF) of the OP samples with different grain sizes after shock-loading at 1100/s: (a) 6 µm grain size, (b) 18 µm grain size, (c) 37 µm grain size.

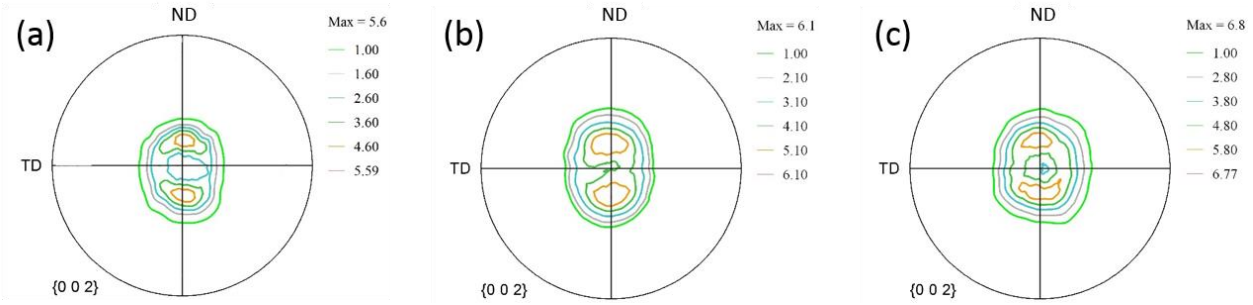

Fig. 6.4. (00.2) pole figures (PF) of the IP0 samples with different grain sizes after shock-loading at 1100/s: (a) 6 µm grain size, (b) 18 µm grain size, (c) 37 µm grain size.

EBSD maps of the shock loaded samples are presented in Figs. 6.5 and 6.6. As can be seen, there is a variation in the total twinning fraction in the samples which is proportional to the grain size of the samples. In both OP (Fig. 6.5) and IP0 (Fig. 6.6) samples, increasing the grain size resulted in larger total twinning fraction. However, the increase in the twinning fraction of double twinning is greater than other twins.

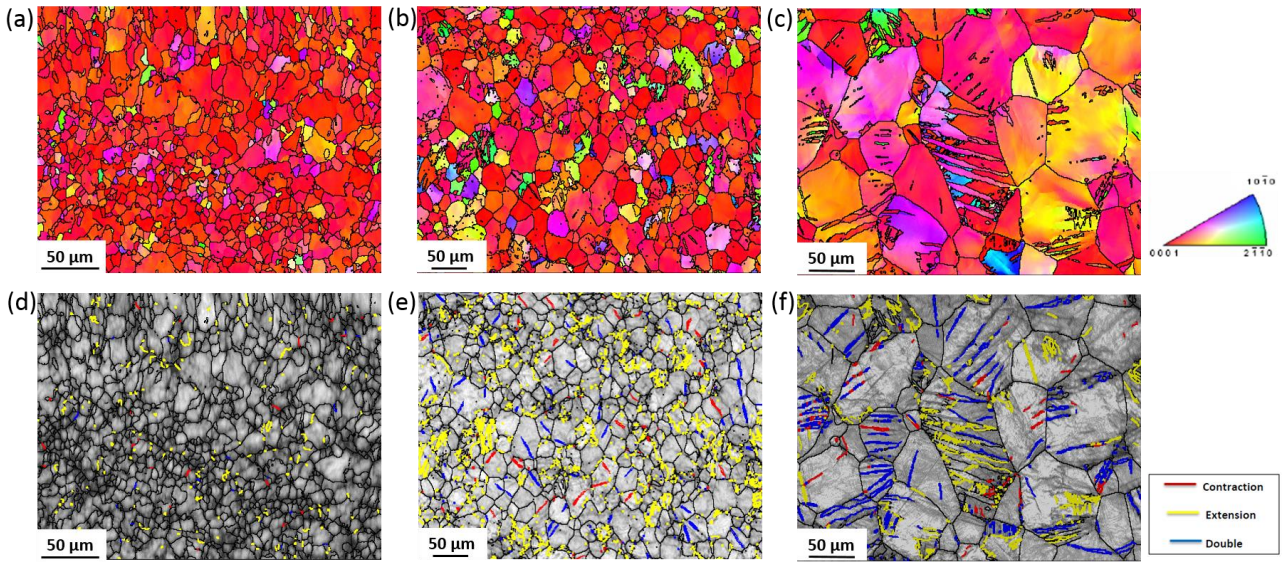

Fig. 6.5. Inverse pole figure (IPF) maps and image quality (IQ) maps of the OP samples showing the twins type and distribution after shock loading of the OP samples, with different grain size at 1100/s: (a) 6 µm grain size, (b) 18 µm grain size, (c) 37 µm grain size [*Note*: The extension twin boundaries (86°< $11\bar{2}0$ > ±5°) are shown in yellow, the contraction twin boundaries (56° < $11\bar{2}0$ > ±5°) are shown in red and the double twin boundaries (38° < $11\bar{2}0$ > ±5°) are shown in blue].

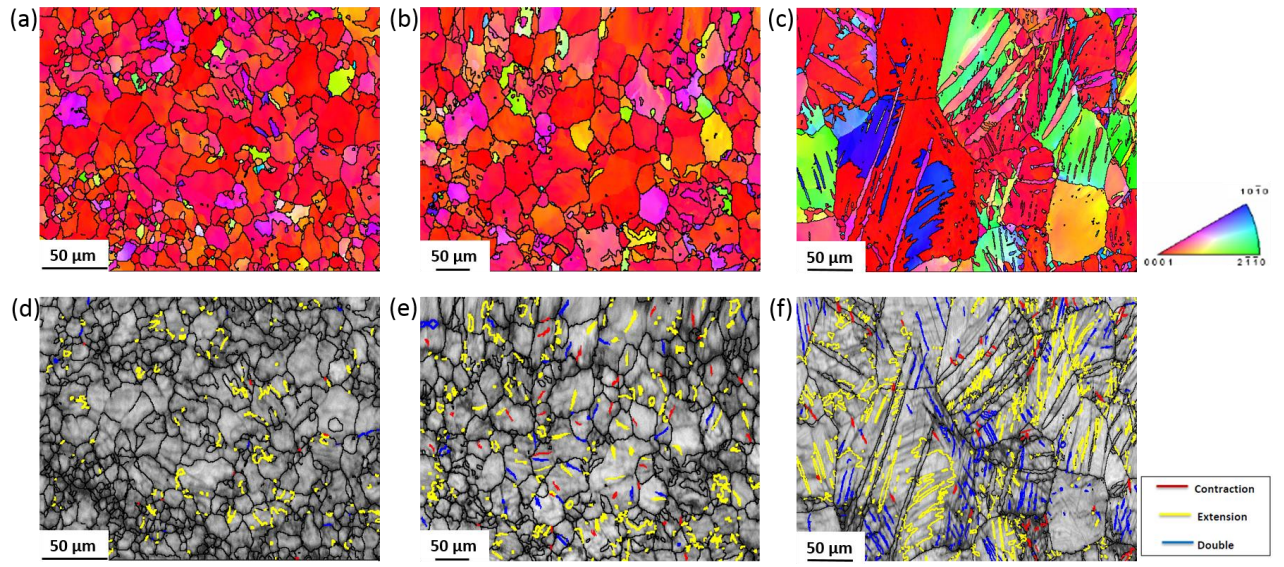

Fig. 6.6. Inverse pole figure (IPF) maps and image quality (IQ) maps of the IP0 samples showing the twins type and distribution after shock loading of the IP0 samples, with different grain size at 1100/s: (a) 6 µm grain size, (b) 18 µm grain size, (c) 37 µm grain size.

To investigate the dislocation interactions with twins, TEM tests were done and corresponding images are shown in Figs. 6.7 and 6.8. As is seen, there is a dense pile-up of dislocations behind the twin boundaries, indicating the effective role of twins as a strong barrier against dislocation motion. In coarse-grained samples, this effect can be stronger due to the presence of larger fraction of twins and twin intersections. The mechanical properties of the alloys change because of these interactions and will be discussed later.

It is seen in the stress-strain curves of the shock loaded samples (Fig. 6.9) that stress level increases with increasing the strain rate and the curves are sigmoidal for all samples and the values of the yield stress, maximum stress and also ductility decrease with increasing the grain size. Moreover, from the hardening diagrams ($d\sigma/d\varepsilon$ vs strain), it is clear that increasing the grain size leads to the increase in the maximum strain hardening rate.

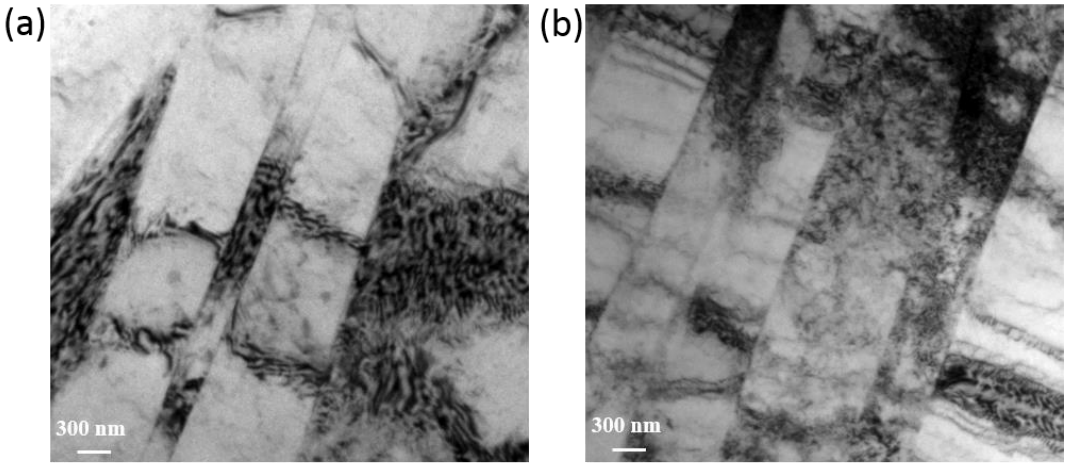

Fig. 6.7. Bright field TEM images of shock-loaded OP samples at strain rate of 1100 s^{-1} with different grain sizes showing the accumulation and pile-ups of dislocations inside and behind the twin boundaries and twin intersections: (a) 6 μm grain size, (b) 37 μm grain size.

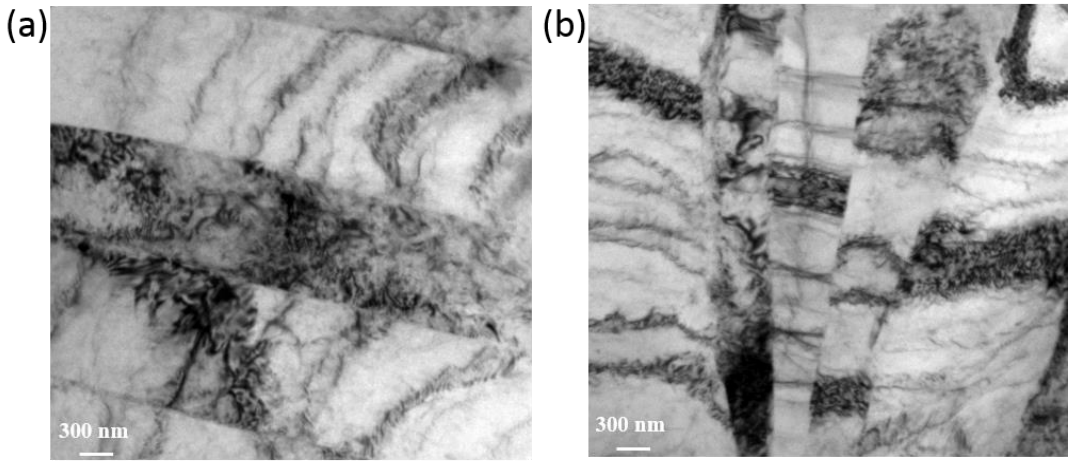

Fig. 6.8. Bright field TEM images of shock-loaded IP0 samples at strain rate of 1100 s^{-1} with different grain sizes showing the accumulation and pile-ups of dislocations inside and behind the twin boundaries and twin intersections: (a) 6 µm grain size, (b) 37 µm grain size.

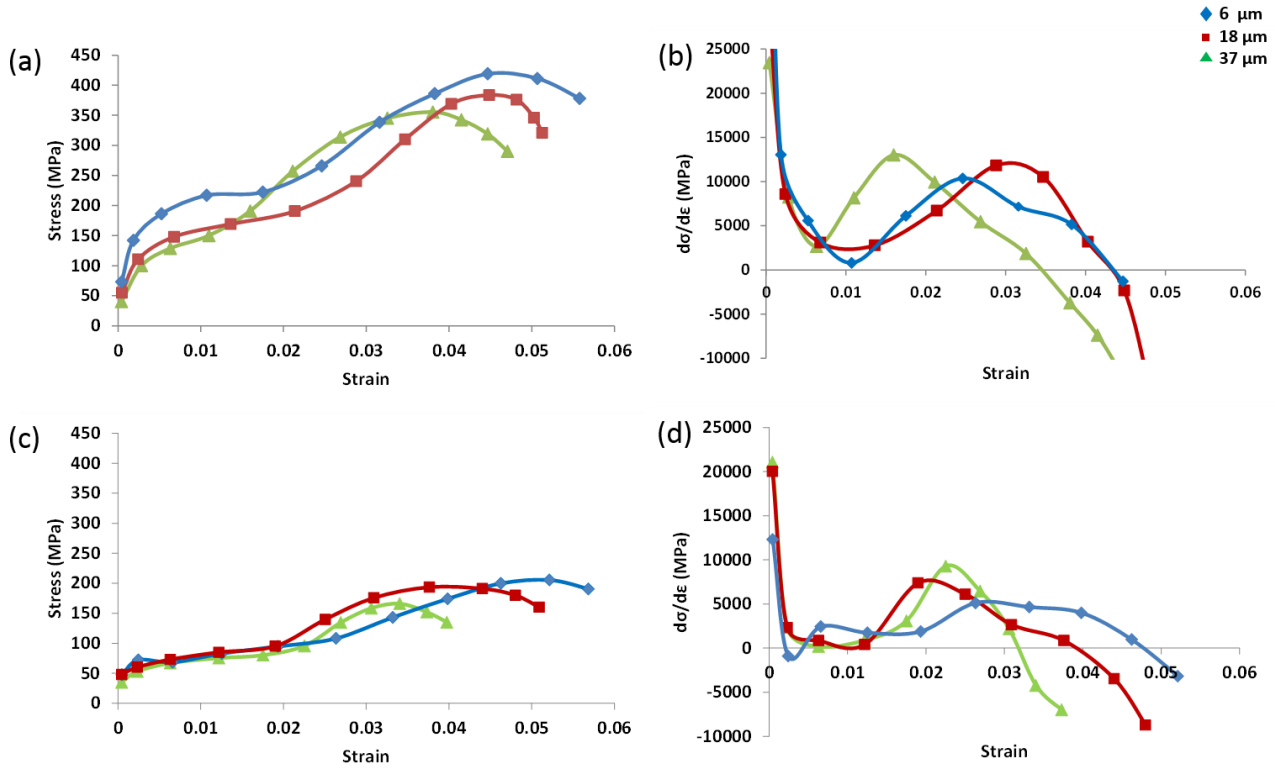

Fig. 6.9. Dynamic true stress-strain curves and hardening diagrams (dσ/dε versus strain) of shock loaded samples, having different grain sizes, at strain rate of 1100 s^{-1} : (a,b) OP ; (c,d) IP0.

To determine the consistency of the results with Hall-Petch relationship, in which the yield stress is inversely proportional to the square root of the grain size, the yield stress versus grain size plot is shown in Fig. 6.10 for OP and IP0 samples. The plots confirm that the results are consistent with Hall-Petch relationship and increase in the yield stress is a direct consequence of fine grains.

In Fig. 6.11, the plastic strain against grain size diagrams are presented. It is obvious that with increasing the grain size, the plastic strain decreases in the samples. In other words, fine-grained samples exhibit better ductility during shock loading in comparison to the coarse-grained samples. Therefore, from Figs. 6.10 and 6.11, contrary to the behavior of many strain-hardened materials, fine-grained AZ31B magnesium samples exhibit better ductility and strength during shock loading compared to coarse-grained samples, suggesting the application of fine-grained AZ31B alloys for high strain rate situations.

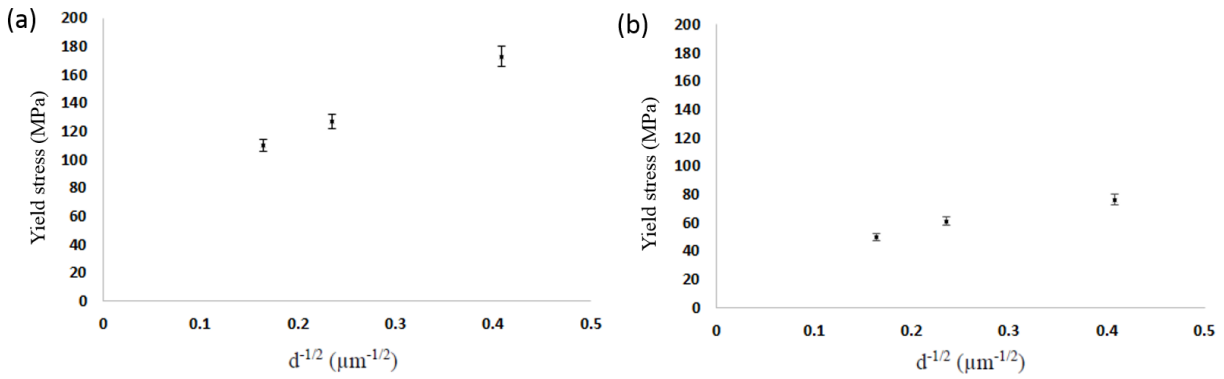

Fig. 6.10. Values of the yield strength versus the reciprocal of the square of the grain size for (a) OP and (b) IP0 samples after shock loading.

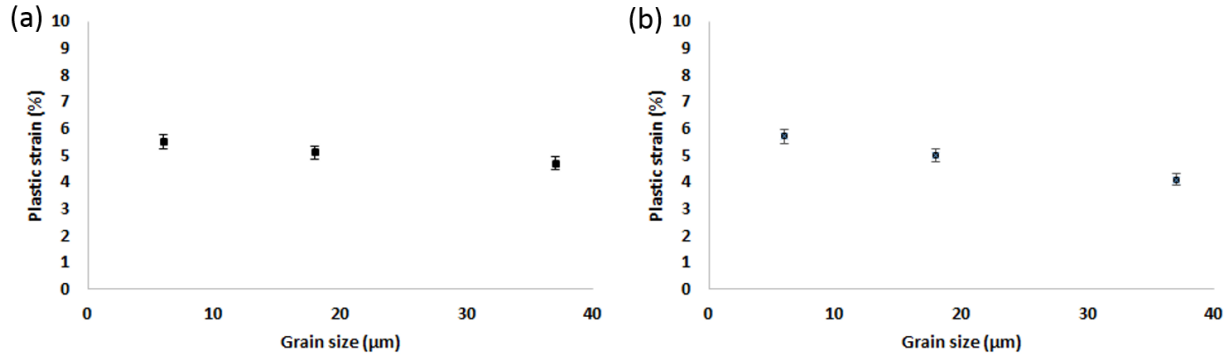

Fig. 6.11. Plastic strain to failure versus grain size for (OP) and (b) IP0 samples after shock loading.

6.6. Discussion

As shown in Figs. 6.3 and 6.4, a double-peak basal texture developed in all the samples during shock loading. It can be related to the activation of twinning and <c+a> slip systems, resulting in the splitting of basal poles [34-38]. In addition, it is observed in the pole figures of the shock loaded samples that the intensity of the basal texture increases with increasing grain size. This increase in intensity could be related to the more effective role and larger fraction of the twinning in coarse-grained samples. Larger fraction of twinning was confirmed in Figs. 6.5 and 6.6 by EBSD technique and it is seen in the EBSD maps that in coarse-grained samples, particularly with grain size of 37 μm, most of the grains are twinned during shock loading.

From the EBSD maps, Figs. 6.5 and 6.6, it is seen that the total twinning fraction is different and increases with increasing grain size. Moreover, the increase in the twinning fraction of double and contraction twins, particularly double twin, with grain size is higher than that of extension twins. In other words, in OP and IP0 samples with a grain size of 6 μm, the governing twinning system is extension twining, with much higher fraction in comparison to those of contraction and double twins (Figs. 6.5 (a) and 6.6(a)). However, with increasing the grain size, it seems that the contribution of the contraction and double twinning in the deformation process increases significantly in comparison to that of extension twinning.

Another important feature of the EBSD maps is that although the initial textures of the OP and IP0 samples are different, the qualitative comparison of IQ maps shows the same trend for twinning fraction in which the total twinning fraction increases with increasing the grain size and double and contraction twins, particularly double twins, play a stronger role during the deformation of coarse-grained samples. This point may indicate the more important role of grain size on the twinning mode in comparison to that of the initial texture.

The change in the total twinning fraction with grain size is ascribed to the variation in twinning interface energy [39] and change in the critical resolved shear stress (CRSS) for twinning [40]. In magnesium and its alloys, the energy of twin interfaces is very large ranging from 84 to 122 mJ/m^2 for contraction and extension twins [41]. This will result in a decreased twin nucleation with decreasing grain size [39,41]. Therefore, in fine-grained alloys, the twinning fraction decreases, as observed in the present study. Additionally, the twinning stress, which is required to activate a twinning system, increases with decreasing grain size, and consequently, the twinning activity and fraction decrease in deformed fine-grained alloys [40]. In fact, increased twinning stress may lead

to the decreased contribution of twinning systems in fine-grained alloys. In contrast, the slip stress decreases with decreasing grain size, resulting in higher activation of slip systems and larger contribution of slip modes in fine-grained alloys [13,40].

The reason for the increase in twinning fraction and activity of double twins in samples with larger grain sizes is still not clear. It could, however, be related to the low elastic strain energy which is associated with the generation of double twins in coarse-grained samples [42,43]. In coarse-grained samples, there is enough space for the double twins to nucleate and propagate and therefore, under these conditions, longer double twins could be formed while in fine-grained samples, due to the lack of enough area for the growth of double twins, small number of double twins with short lengths may form [42,43].

The dynamic true stress-strain curves of the shock-loaded samples at 1100 s^{-1} (Fig. 6.9) showed an upward curving flow, which is related to the strong work hardening due to the occurrence of twinning [8-10, 44-46], which was confirmed by EBSD maps (Figs. 6.5 and 6.6). Considering the stress-strain curves of the shock-loaded samples (Fig. 6.9), it is evident that both strength and ductility decrease with increasing grain size for all the samples. The relationship between the grain size (d) and strength (σ) can be expressed by the Hall-Petch equation:

$$\sigma = \sigma_0 + kd^{-1/2} \quad (6.1)$$

where σ_0 is the friction stress and k is a constant indicating the efficacy of grain boundaries in enhancing strength. It is then concluded that decreasing the grain size results in the formation and presence of more grain boundaries. Therefore, larger numbers of barriers to dislocation motions are acting in the fine-grained samples [14,47]. These barriers (grain boundaries) will result in the discontinuity in the slip system at grain boundaries. Therefore, dislocations are stuck at grain boundaries and to free the dislocations from these barriers, more stress is needed [14,47]. This is the reason why with increasing the grain size of the alloy, the strength decreases (Fig. 6.9).

Low ductility of the coarse-grained samples in shock loading (Fig. 6.9) could be related to the large numbers of twins (Figs. 6.5 and 6.6). Accumulation of dislocations at twins and twin intersections, may produce high values of stress concentrations around the twins and twin intersections, resulting in void and crack formation (twinning-induced fracture) [2,17,48-53].

In the hardening diagrams shown in Fig. 6.9, the strain hardening rate decreases initially, then increases and again decreases for all samples. In general, the hardening behavior of magnesium alloys is mainly governed by the activation or suppression of deformation mechanisms [47,54,55].

In hardening diagrams shown in Fig. 6.9, with increasing the grain size, the maximum hardening rate increases and the maximum hardening rates are observed in samples with 37 μm grain size. The variation of hardening rate could be related to the different capacity of dislocation storage in fine-grained and coarse-grained materials [56]. Strain hardening behavior of the materials is significantly affected by the dislocations and their strain fields. Increased dislocation density during deformation process may decrease the distance between dislocations, giving rise to difficult movement of dislocations and decreased hardening rate [57]. A coarse-grained alloy, may provide more space or area for dislocations, leading to stronger hardening ability in the coarse-grained samples [56]. Some examples of the increased density of dislocations (in the shock loaded microstructure of the samples) with increase in grain size are demonstrated in Figs. 6.12 and 6.13 for shock loaded OP and IP0 samples having different grain sizes.

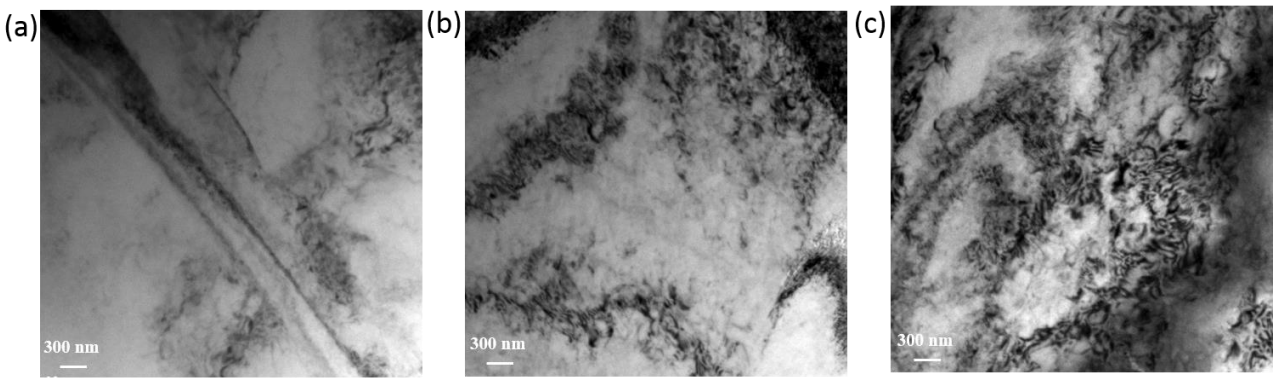

Fig. 6.12. Bright field TEM images of shock-loaded OP samples, with different grain size at 1100 s^{-1}: (a) 6 μm grain size, (b) 18 μm grain size, (c) 37 μm grain size.

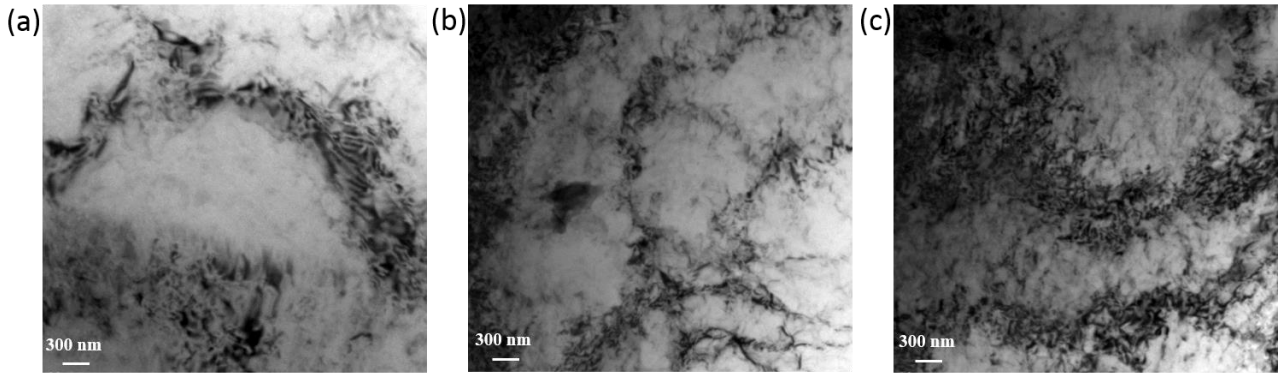

Fig. 6.13. Bright field TEM images of shock-loaded IP0 samples, with different grain size at 1100 s^{-1}: (a) 6 μm grain size, (b) 18 μm grain size, (c) 37 μm grain size.

To investigate the presence of <c+a> dislocations, which, in fact, confirms the activation of pyramidal <c+a> slip system, *g.b = 0* invisibility criterion was used. Due to the similarity in the pole figures of shock-loaded samples (Figs. 6.3 and 6.4), one sample, i.e. IP0 with 18 μm grain size, was analyzed using *g.b* analysis. In this research, two diffraction conditions, namely g=[0002] and g=$[10\bar{1}0]$, for a certain area on the sample were used. The only visible dislocations at both g=[0002] and g=$[10\bar{1}0]$ diffraction conditions are <c+a> dislocations. In Fig. 6.14 (a), only <c> and <c+a> dislocations can be seen for g=[0002] and <a> dislocations are invisible since the *g.b* value is zero (Table 1). After changing the diffraction condition from [0002] to $[10\bar{1}0]$, <c+a> and <a> dislocations are visible for the new diffraction condition with relatively strong contrasts. The visibility factor of <c> dislocations is zero for g=$[10\bar{1}0]$ therefore, these dislocations do not appear in the contrast of g=$[10\bar{1}0]$, as shown in Fig. 6.14(b). The <c+a> dislocations, however, are still visible in the contrast of g=$[10\bar{1}0]$. By comparison between the images taken at [0002] and $[10\bar{1}0]$ diffraction conditions (Fig. 6.14), it is seen that some dislocations are present and visible in the contrasts of both diffraction conditions. These dislocations, shown by solid arrows, are <c+a> dislocations which have been activated in the shock-loaded samples. This clearly confirms the activation of pyramidal <c+a> slip systems during the shock-loading process of AZ31B magnesium alloys. Increase in temperature during the shock loading encourages the activation of pyramidal <c+a> slip in AZ31B magnesium alloy. As a result of the activation of this system at high strain rates, higher ductility is obtained in AZ31B magnesium alloys under shock loading conditions [34].

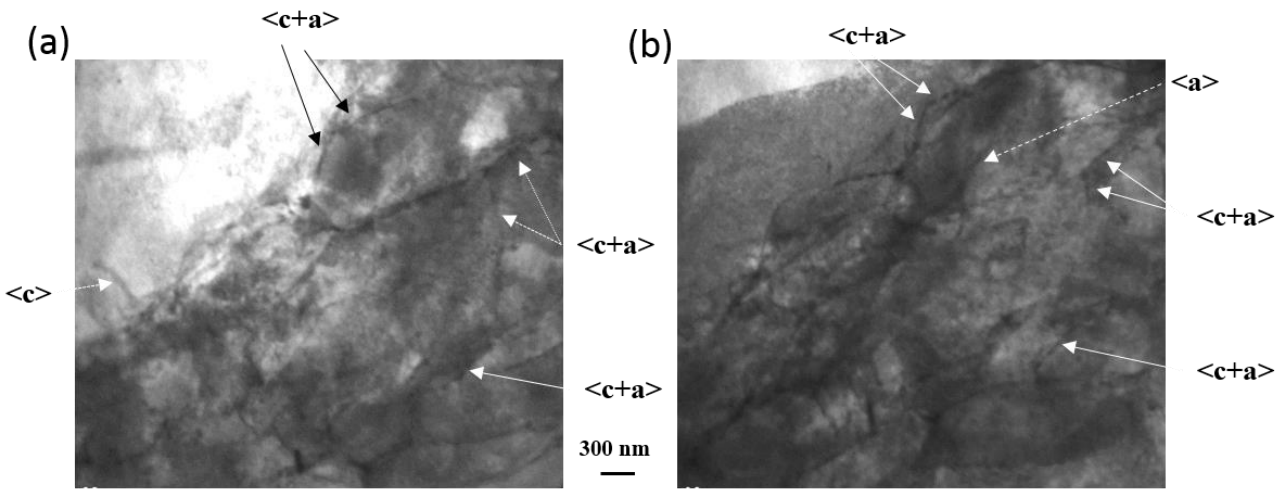

Fig. 6.14. Bright field TEM images under different diffraction conditions emphasizing the presence of <c+a> dislocations in shock-loaded IP0, with grain size 18μm (strain rate: 1100 s^{-1}): (a) g=[0002], (b) g=[$10\bar{1}0$].

6.7. Conclusions

The effect of grain size on the texture formation, microstructural evolution and deformation behavior of rolled AZ31B alloy was investigated under shock loading conditions and several characterization techniques such as XRD, SEM and TEM were used. The following conclusions can be reached:

(1) The initial basal texture of the samples converts to a double-peak basal texture in all shock loaded samples. The splitting of basal poles in the double-peak texture of the samples is an indication of the activation of <c+a> pyramidal slip systems. Using 'g.b' analysis, the <c+a> dislocations were found and the activation of the pyramidal system was confirmed at high strain rate deformation of AZ31B alloy.

(2) Increasing the grain size results in larger twinning fraction and higher strain hardening rates in AZ31B alloy during shock loading.

(3) Fine-grained samples showed better strength and ductility under shock loading conditions. Therefore, it is recommended to use fine-grained AZ31B alloy for high-strain rate applications and situations.

(4) Increasing the grain size encourages the formation and activation of double (and contraction) twins. Therefore, it is logical to consider more contribution of double (and contraction) twinning in deformation process of coarse-grained samples at high strain rate conditions.

References

[1] Cheng YQ, Chen ZH. Anisotropy of deformation behavior of AZ31 magnesium alloy sheets. Advanced Materials Research 2011; 314-316: 1121-1125.

[2] Mabuchi M, Chino Y, Iwasaki H. Influence of grain size on elongation at elevated temperatures in AZ31 Mg alloy. Materials Transactions 2003; 44:490-495.

[3] Ahmad IR, Shu DW. Compressive and constitutive analysis of AZ31B magnesium alloy over a wide range of strain rates. Materials Science and Engineering A 2014; 592:40-49.

[4] Mordike BL, Ebert T. Magnesium: Properties — applications — potential. Materials Science and Engineering A 2001; 302:37-45.

[5] Agnew SR, Duygulu O. A mechanistic understanding of the formability of magnesium: Examining the role of temperature on the deformation mechanisms. Materials Science Forum 2003; 419-422:177-188.

[6] Hakamada M, Furuta T, Chino Y, Chen Y, Kusuda H, Mabuchi M. Life cycle inventory study on magnesium alloy substitution in vehicles. Energy 2007;32:1352.

[7] Sarker D, Friedman J, Chen DL. Influence of pre-deformation and subsequent annealing on strain hardening and anisotropy of AM30 magnesium alloy. Journal of Alloys and Compounds 2014; 611:341-350.

[8] Meyers MA. Dynamic behavior of materials. Wiley-In- Interscience, New York. 1994.

[9] Meyers M, Andrade U, Chokshi A. The effect of grain size on the high-strain, high-strain-rate behavior of copper. Metallurgical and Materials Transactions A 1995; 26:2881-2893.

[10] McCauley JW, Strassburger E, Patel P, Paliwal B, Ramesh KT. Experimental observations on dynamic response of selected transparent armor materials. Experimental Mechanics 2013; 53: 3-29.

[11] Wang XL, Yu Y, Wang ED. The effects of grain size on ductility of AZ31 magnesium alloy. Materials Science Forum 2005; 488-489:535-538.

[12] Chino Y, Kimura K, Mabuchi M. Twinning behavior and deformation mechanisms of extruded AZ31 Mg alloy. Materials Science and Engineering A 2008;486:481-488.

[13] Barnett MR, Keshavarz Z, Beer AG, Atwell D. Influence of grain size on the compressive deformation of wrought Mg–3Al–1Zn. Acta Materialia 2004; 52: 5093-5103.

[14] Barnett MR, Atwell DL, Beer AG. Grain size in Mg alloys: Recrystallization and mechanical consequences. Materials Science Forum 2007; 558-559:433-440.

[15] Al-Samman T. Comparative study of the deformation behavior of hexagonal magnesium–lithium alloys and a conventional magnesium AZ31 alloy. Acta Materialia 2004; 57:2229-2242.

[16] Jain A, Duygulu O, Brown DW, Tome CN, Agnew SR. Grain size effects on the tensile properties and deformation mechanisms of a magnesium alloy, AZ31B, sheet. Materials Science and Engineering A 2008; 486:545-555.

[17] Barnett MR. A rationale for the strong dependence of mechanical twinning on grain size. Scripta Materialia 2008;59:696-698.

[18] Chino Y, Kimura K, Hakamada M, Mabuchi M. Mechanical anisotropy due to twinning in an extruded AZ31 Mg alloy. Materials Science and Engineering A 2008; 485:311-317.

[19] Yin DL, Wang JT, Liu JQ, Zhao X. On tension–compression yield asymmetry in an extruded Mg–3Al–1Zn alloy. Journal of Alloys and Compounds 2009; 478:789-795.

[20] Wang JT, Yin DL, Liu JQ, Tao J, Su YL, Zhao X. Effect of grain size on mechanical property of Mg–3Al–1Zn alloy. Scripta Materialia 2008; 59:63-66.

[21] Yin SM, Wang CH, Diao YD, Wu SD, Li SX. Influence of grain size and texture on the yield asymmetry of Mg-3Al-1Zn alloy. Journal of Materials Science and Technology 2011; 27:29-34.

[22] Yuan W, Mishra RS. Grain size and texture effects on deformation behavior of AZ31 magnesium alloy. Materials Science and Engineering A 2012; 558:716-724.

[23] Wang BS, Xin RL, Huang GJ, Liu Q. Strain rate and texture effects on microstructural characteristics of Mg-3Al-1Zn alloy during compression. Scripta Materialia 2012; 66:239-242.

[24] Wan G, Wu BL, Zhao YH, Zhang YD, Esling C. Strain-rate sensitivity of textured Mg–3.0Al–1.0Zn alloy (AZ31) under impact deformation. Scripta Materialia 2011; 65:461-464.

[25] Tucker MT, Horstemeyer MF, Gullett PM, Kadiri HE, Whittington WR. Anisotropic effects on the strain rate dependence of a wrought magnesium alloy. Scripta Materialia 2009; 60:182-185.

[26] Sanjari M, Farzadfar A, Sakai T, Utsunomiya H, Essadiqi E, Jung IH, Yue S. A texture and microstructure analysis of high speed rolling of AZ31 using split Hopkinson pressure bar results. Journal of Materials Science 2013; 48:6656-6672.

[27] Feng F, Huang S, Meng Z, Hu J, Lei Y, Zhou M, Wu D, Yang Z. Experimental study on tensile property of AZ31B magnesium alloy at different high strain rates and temperatures. Materials and Design 2014; 57:10-20.

[28] Dudamell NV, Ulacia I, Gálvez F, Yi S, Bohlen J, Letzig D, Hurtado I, Pérez-Prado MT. Influence of texture on the recrystallization mechanisms in an AZ31 Mg sheet alloy at dynamic rates. Materials Science and Engineering A 2012; 532: 528-535.

[29] Ulacia I, Salisbury CP, Hurtado I, Worswick MJ. Tensile characterization and constitutive modeling of AZ31B magnesium alloy sheet over wide range of strain rates and temperatures. Journal of Materials Processing Technology 2011; 211: 830-839.

[30] Ulacia I, Dudamell NV, Gálvez F, Yi S, Pérez-Prado MT, Hurtado I. Mechanical behavior and microstructural evolution of a Mg AZ31 sheet at dynamic strain rates. Acta Materialia 2010; 58:2988-2998.

[31] Asgari H, Szpunar JA, Odeshi AG, Zeng LJ, Olsson E, Li DY. Effect of yttrium on the twinning and plastic deformation of AE magnesium alloy under ballistic impact. Materials Science and Engineering A 2015; 623:10-21.

[32] Sandlöbes S, Friák M, Zaefferer S, Dick A, Yi S, Letzig D, Pei Z, Zhu LF, Neugebauer J, Raabe D. The relation between ductility and stacking fault energies in Mg and Mg–Y alloy. Acta Materialia 2012; 60:3011-3021.

[33] Okamoto PR, Thomas G. On the four-axis hexagonal reciprocal lattice and its use in the indexing of transmission electron diffraction patterns. Physica Status Solidi 1968; 25:81-91.

[34] Asgari H, Odeshi AG, Szpunar JA. On dynamic deformation behavior of WE43 magnesium alloy sheet under shock loading conditions. Materials & Design 2014; 63: 552-564.

[35] Chang LL, Shang EF, Wang YN, Zhao X, Qi M. Texture and microstructure evolution in cold rolled AZ31 magnesium alloy. Materials Characterization 2009; 60:487-491.

[36] Agnew SR, Yoo MH, Tomé CN. Application of texture simulation to understanding mechanical behavior of Mg and solid solution alloys containing Li or Y. Acta Materialia 2001;49:4277–4289.

[37] Basu I, Al-Samman T, Gottstein G. Shear band-related recrystallization and grain growth in two rolled magnesium-rare earth alloys. Materials Science and Engineering A 2013; 579:50-56.

[38] Yi S, Bohlen J, Sandlobes S, Zaefferer S, Letzig D, Kainer KU. Microstructural evolution during recrystallization of magnesium alloys. Materials Science Forum 2012;706-709:1291-1296.

[39] Koike J, Kobayashi T, Mukai T, Watanabe H, Suzuki M, Maruyama K, Higashi K. The activity of non-basal slip systems and dynamic recovery at room temperature in fine-grained AZ31B magnesium alloys. Acta Materialia 2003;51:2055-2065.

[40] Meyers MA, Vöhringer O, Lubarda VA. The onset of twinning in metals: a constitutive description. Acta Materialia 2001; 49:4025-4039.

[41] Wang Y, Chen LQ, Liu ZK, Mathaudhu SN. First-principles calculations of twin-boundary and stacking-fault energies in magnesium. Scripta Materialia 2010; 62: 646-649.

[42] Wan G, Wu BL, Zhang YD, Sha GY, Esling C. Anisotropy of dynamic behavior of extruded AZ31 magnesium alloy. Materials Science and Engineering A 2010; 527:2915-2924.

[43] Bhadeshia HKDH, Worked examples in the geometry of crystals, second edition, (2001, updated 2006), The institute of metals, London.

[44] Dudamell NV, Ulacia I, Gálvez F, Yi S, Bohlen J, Letzig D, Hurtado I, Pérez-Prado MT. Twinning and grain subdivision during dynamic deformation of a Mg AZ31 sheet alloy at room temperature. Acta Materialia 2011; 59:6949-6962.

[45] Sarker D, Chen DL. Detwinning and strain hardening of an extruded magnesium alloy during compression. Scripta Materialia 2012; 67:165-168.

[46] Wang B, Xin R, Huang G, Liu Q. Effect of crystal orientation on the mechanical properties and strain hardening behavior of magnesium alloy AZ31 during uniaxial compression. Materials Science and Engineering A (2012); 534:588-593.

[47] Korla R, Chokshi AH. Strain-rate sensitivity and microstructural evolution in a Mg–Al–Zn alloy. Scripta Materialia 2010; 63: 913-916.

[48] Mukai T, Mohri T, Mabuchi M, Nakamura M, Ishikawa K, Higashi K. Experimental study of a structural magnesium alloy with high absorption energy under dynamic loading. Scripta Materialia 1998; 39:1249-1253.

[49] Barnett MR. Twinning and the ductility of magnesium alloys: Part II. “Contraction” twins. Materials Science and Engineering A 2007; 464:8-16.

[50] Christian JW, Mahajan S. Deformation twinning. Progress in Materials Science 1995; 39:1-157.

[51] Mukai T, Yamanoi M, Watanabe H, Ishikawa K, Higashi K. Effect of grain refinement on tensile ductility in ZK60 magnesium alloy under dynamic loading. Materials Transactions 2001; 42:1177-1181.

[52] Yi S, Schestakow I, Zaefferer S. Twinning-related microstructural evolution during hot rolling and subsequent annealing of pure magnesium. Materials Science and Engineering A 2009; 516: 58-64.

[53] Jiang L, Jonas JJ, Luo AA, Sachdev AA, Godet S. Twinning-induced softening in polycrystalline AM30 Mg alloy at moderate temperatures. Scripta Materialia 2006; 54:771–775.

[54] Jiang L, Jonas JJ, Luo AA, Sachdev AK, Godet S. Influence of {10-12} extension twinning on the flow behavior of AZ31 Mg alloy. Materials Science and Engineering A 2007;445-446: 302:309.

[55] Khan AS, Pandey A, Gnäupel-Herold T, Mishra RK. Mechanical response and texture evolution of AZ31 alloy at large strains for different strain rates and temperatures. International Journal of Plasticity 2011; 27: 688–706.

[56] Afrin N, Chen DL, Cao X, Jahazi M. Strain hardening behavior of a friction stir welded magnesium alloy. Scripta Materialia 2007; 57:1004-1007.

[57] Callister WD. Jr. Materials Science and Engineering-An Introduction, seventh edition, John Wiley & Sons, New York, 2007.

CHAPTER 7

EFFECT OF GRAIN SIZE ON HIGH STRAIN RATE DEFORMATION OF ROLLED Mg-4Y-3RE ALLOY IN COMPRESSION

7.1. Overview of Chapter 7

In the previous chapter, the effect of grain size on the microstructural development and dynamic deformation behavior of rolled AZ31B alloy was discussed. In this chapter, the same effect but on the high strain rate deformation of rolled WE43 magnesium alloy, which contains rare earth elements will be discussed.

This chapter is presented as manuscript # 6. The author's (H. Asgari) contributions to this manuscript are: (a) preparation and processing of the samples for shock loading test. (b) XRD, SEM, EDS, EBSD and TEM analyses. (c) Reviewing the relevant literature, writing and submission of the manuscript. The contribution of Dr. L. J. Zeng and Prof. E. Olsson was in the area of TEM investigation and analysis.

The manuscript was published in *Materials Science & Engineering A*:

- H. Asgari, J.A. Szpunar, A.G. Odeshi, L.J. Zeng, E. Olsson. "Effect of grain size on high strain rate deformation of rolled Mg-4Y-3RE alloy in compression", Materials Science & Engineering A, 633 (2015) 92–102.

The manuscript presented here is different from the published paper in the following parts:

- In order to avoid repetition in the content, some parts of the 'introduction','experimental procedure', and 'discussion' sections were eliminated.

The copyright permission to use the manuscript in the thesis was obtained and provided in the Appendix section.

Effect of grain size on high strain rate deformation of rolled Mg-4Y-3RE alloy in compression

H. Asgari[1], J. A. Szpunar[1], A. G. Odeshi[1], L. J. Zeng[2], E. Olsson[2]

[1]Department of Mechanical Engineering, University of Saskatchewan, Saskatoon, Canada

[2]Department of Applied Physics, Chalmers University of Technology, Göteborg, Sweden

7.2. Abstract

Grain size is an important factor that can affect the mechanical behavior of magnesium alloys at high strain rates. Therefore, it is very important to evaluate the effects of grain size on the dynamic mechanical response of magnesium alloys under shock-loading conditions. In this research, texture evolution, microstructural changes and dynamic mechanical behavior of rolled Mg-4Y-3RE alloy samples, with grain sizes of 8, 25 and 46 μm, deformed under compressive shock-loading were investigated. Dynamic shock loading tests were conducted using Split Hopkinson Pressure Bar at room temperature at a strain rate of 1200 s^{-1}. Texture measurements indicate development of a double-peak (00.2) basal texture in all the samples during shock loading. However, slightly higher intensities were observed for coarse-grained samples. Both strength and ductility were found to decrease with increasing grain size, while twinning fraction and strain hardening rate increase with increasing grain size. The activity of double and contraction twins increased with increase in grain size. Furthermore, activation of pyramidal <c+a> slip system during the shock loading of the Mg-4Y-3RE alloy was confirmed using 'g.b' analysis method.

Keywords: Rolled Mg-4Y-3RE sheet, Grain size, Dynamic mechanical behavior, Twinning.

7.3. Introduction

Magnesium alloys, as the lightest structural alloys, have attracted significant interest of designers and manufacturers in the automotive and aerospace industries due to their high specific strengths [1-5]. In fact, application of light magnesium alloys in automobile and airplane parts to reduce their weight will consequently result in significant reduction of fuel consumption and greenhouse gas emission [6-8]. However, structural applications of wrought magnesium alloys

such as rolled plates are limited due to their low room temperature ductility and strong basal texture [9-11].

An appropriate way to increase the ductility of magnesium alloys is addition of rare earth elements to randomize their texture. Therefore, the increased ductility of wrought magnesium alloys, obtained by texture randomization, may facilitate their applications under different loading conditions [12-16].

Grain size is one of the important parameters having considerable influence on the mechanical properties of magnesium alloys. Thus, it is very important to evaluate and understand the effects of grain size on the dynamic mechanical behavior and deformation mechanisms in wrought magnesium alloys at high strain rates. Unfortunately, the dynamic mechanical response and deformation mechanisms of magnesium alloys under shock loading conditions, particularly rare-earth containing magnesium alloys, have not yet been extensively investigated. Moreover, there is almost no information in the open literature on the effects of grain size on the microstructural evolution, deformation mechanisms and mechanical properties during high strain rate deformation of rare-earth containing magnesium alloys, such as Mg-3Y-4RE (WE43) and this issue is yet to be understood. To date, the studies that have been conducted on the effect of grain size on the mechanical behavior of magnesium alloys have mostly focused on AZ31 alloy at low strain rates [17-24] and there is a considerable knowledge gap about the relationship between the grain size and dynamic impact response of rolled magnesium alloys at high strain rates or shock-loading conditions.

The main aim of the current study is to investigate the effects of grain size on the microstructural change, deformation mechanisms and dynamic mechanical behavior of rolled Mg-3Y-4RE alloy under shock loading conditions. The samples with different grain sizes were subjected to high strain-rate deformation using Split Hopkinson Pressure Bar and the correlation between the grain size, deformation mechanisms and mechanical properties is discussed.

7.4. Experimental procedure

The as-received alloy used in this study is hot-rolled Mg-3Y-4RE (hereafter referred to as WE43) magnesium alloy, provided by Magnesium Elektron Company, which had a grain size of 8μm. Its nominal chemical composition is presented in Table 7.1. The samples were shock loaded by Split Hopkinson Pressure Bar at a strain rate of 1200 s^{-1}. Three groups of cylindrical samples,

with different grain sizes of 8 (as received), 25 and 46 μm (produced by heat-treating at 350 and 450 °C for 10 hours, respectively) were used for shock loading experiments. It should be mentioned that due to the heat-treatment of the WE43 alloy to obtain different grain size, some RE containing phases (particles) could have formed, e.g. Mg-Y-Nd or Mg-Y phases, however, in this research their possible effect on the mechanical properties has not been considered and only the effect of grain size on the dynamic mechanical behavior of WE43 alloy was investigated. The diameter and height of the samples were 9.5 mm and 10.5 mm, respectively. The test samples were cut in the rolling direction, in the transverse direction and in the direction perpendicular to the RD-TD plane, as shown and labeled in Fig. 7.1. More details about the shock-loading tests and measurements have been discussed elsewhere [25].

The details of shock loading test, texture measurements, SEM, EBSD, TEM and 'g.b' analysis are similar to those described in Chapter 6. It is not repeated here in order to keep the thesis concise.

Table 7.1. Nominal chemical composition (in wt.%) of the rolled WE43 alloy.

Mg	Li	Mn	Nd	Y	Zn	Zr	RE*
Bal.	0.05	0.03	2-2.5	3.7-4.3	0.06	0.2-1	0.3-1

*Other rare earth (RE) elements including Gd, Dy, Er, Sm and Yb.

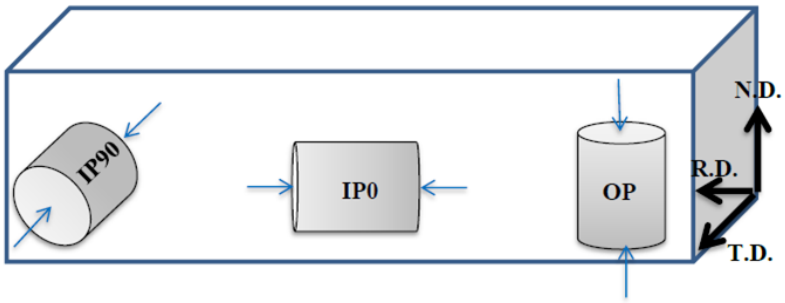

Fig. 7.1. Schematic diagram of the samples and compression directions.

7.5. Results

In Fig. 7.2, (00.2) pole figures (PF) of the undeformed samples with different grain sizes are shown. A weak basal texture can be observed in all the samples. However, there are some small variations in the intensity of the basal textures and the position of the highest intensity within the basal pole figures also differs slightly from one sample to another. In all samples, except for OP samples which have 25 and 46 μm grain size (Fig. 7.2. (d) and 7.2(g)), the peak intensity is tilted

away from ND resulting in a weak texture with basal split. For OP samples of 25 and 46 μm grain size, a weak C-type basal texture is observed in the pole figures (Fig. 7.2(d) and 7.2(g)) in which the highest intensity is located at the center of the pole figures.

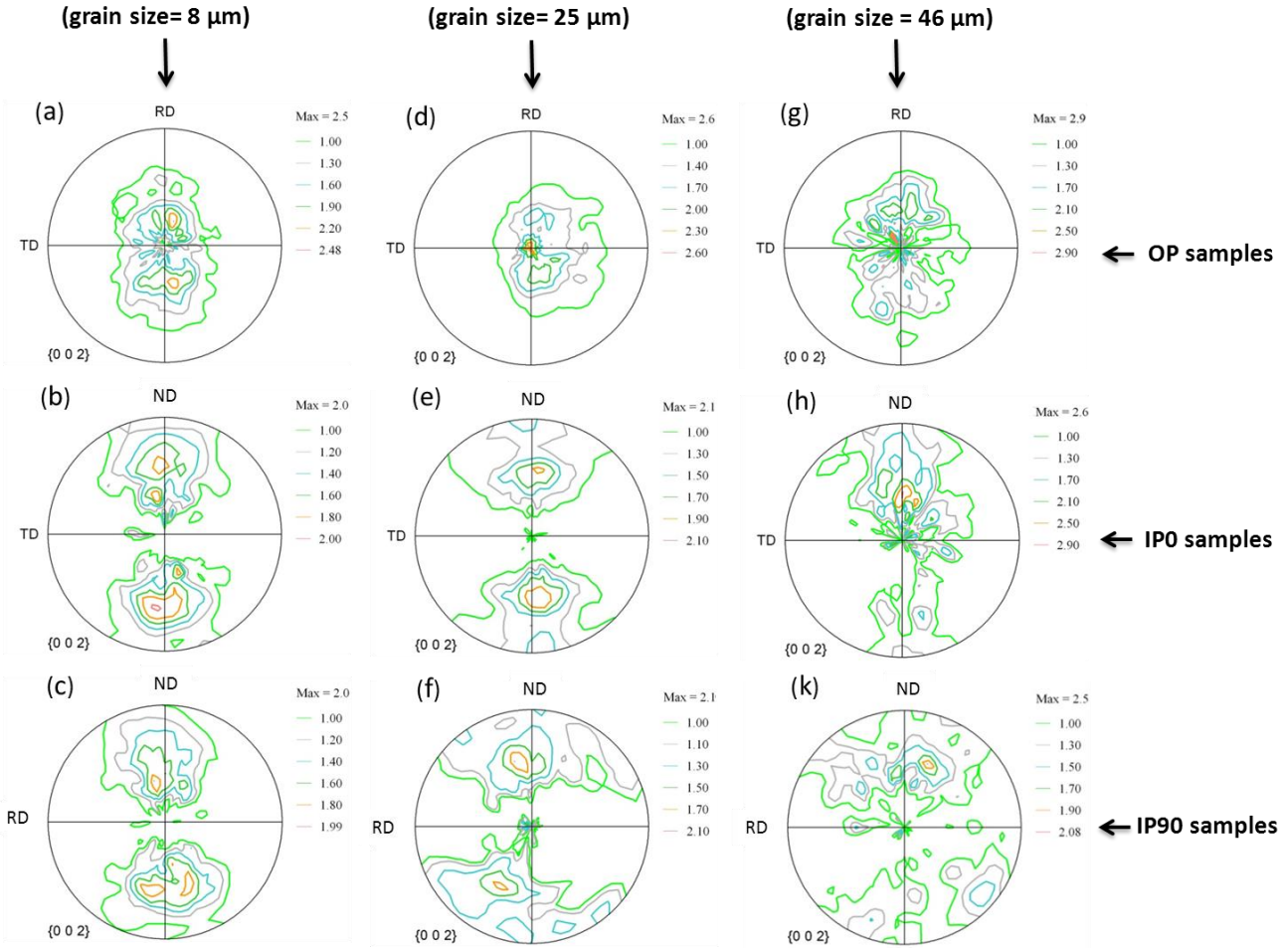

Fig. 7.2. (00.2) pole figures (PF) of the samples with different grain sizes before shock-loading: (a),(d) and (g) OP; (b),(e) and (h) IP0; (c),(f) and (k) IP90.

Fig. 7.3 indicates the (00.2) pole figures of the samples after shock-loading at strain rate of 1200 s^{-1}. From these pole figures, a double-peak basal texture forms in the samples after shock-loading which are stronger than those of the samples before shock-loading (Fig. 7.2). In all OP samples, with different grain sizes, a relatively symmetrical double-peak basal texture forms after shock-loading in which the basal poles are tilted toward RD (Fig. 7.3(a),(d) and (g)). A change in the texture in terms of both intensity and shape of the pole figures is observed after shock-loading for

all samples. This change in the texture is more remarkable for OP samples, having 25 and 46 μm grain sizes, in which the initial C-type texture converts to a double-peak basal texture with higher intensity.

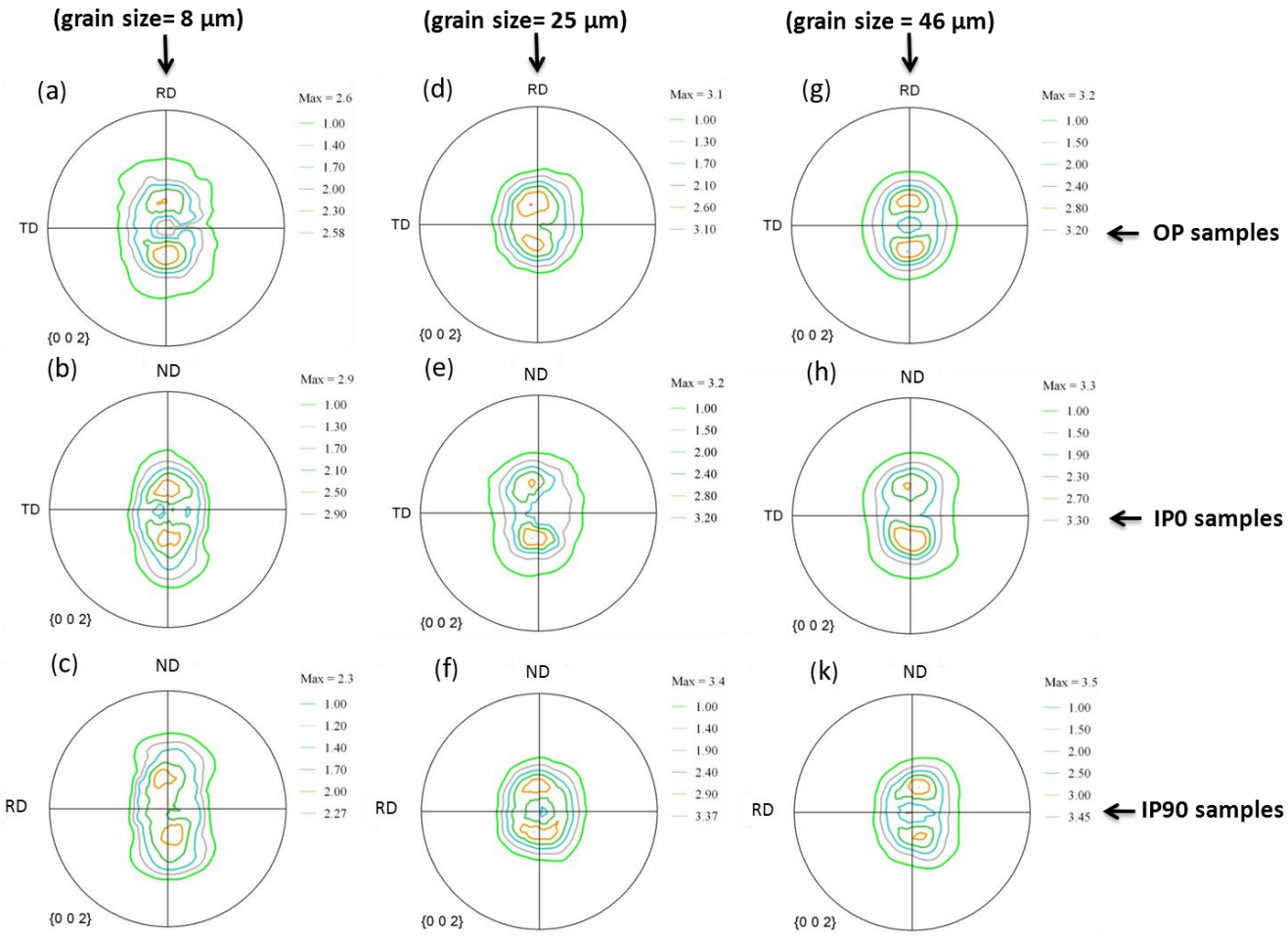

Fig. 7.3. (00.2) pole figures (PF) of the samples with different grain sizes after shock-loading at 1200/s: (a),(d) and (g) OP; (b),(e) and (h) IP0; (c),(f) and (k) IP90.

Another important feature about the basal pole figures of the samples is that the tilting of the basal poles decreases after shock-loading, i.e. the position of the maximum intensity is closer to the center of the pole figures after deformation.

To identify the type and distribution of the twins in the microstructure of the samples after shock loading, EBSD technique was used. It is evident in the inverse pole figure (IPF) and image quality (IQ) maps of the samples after shock loading (Figs. 7.4 to 7.6) twinning, with different fractions, has occurred in all samples. In all samples, the total twinning fraction (including extension,

contraction and double twinning) increases with increase in grain size. The minimum and maximum twinning fractions (qualitatively) are observed for samples having 8 and 46 μm grain size, respectively.

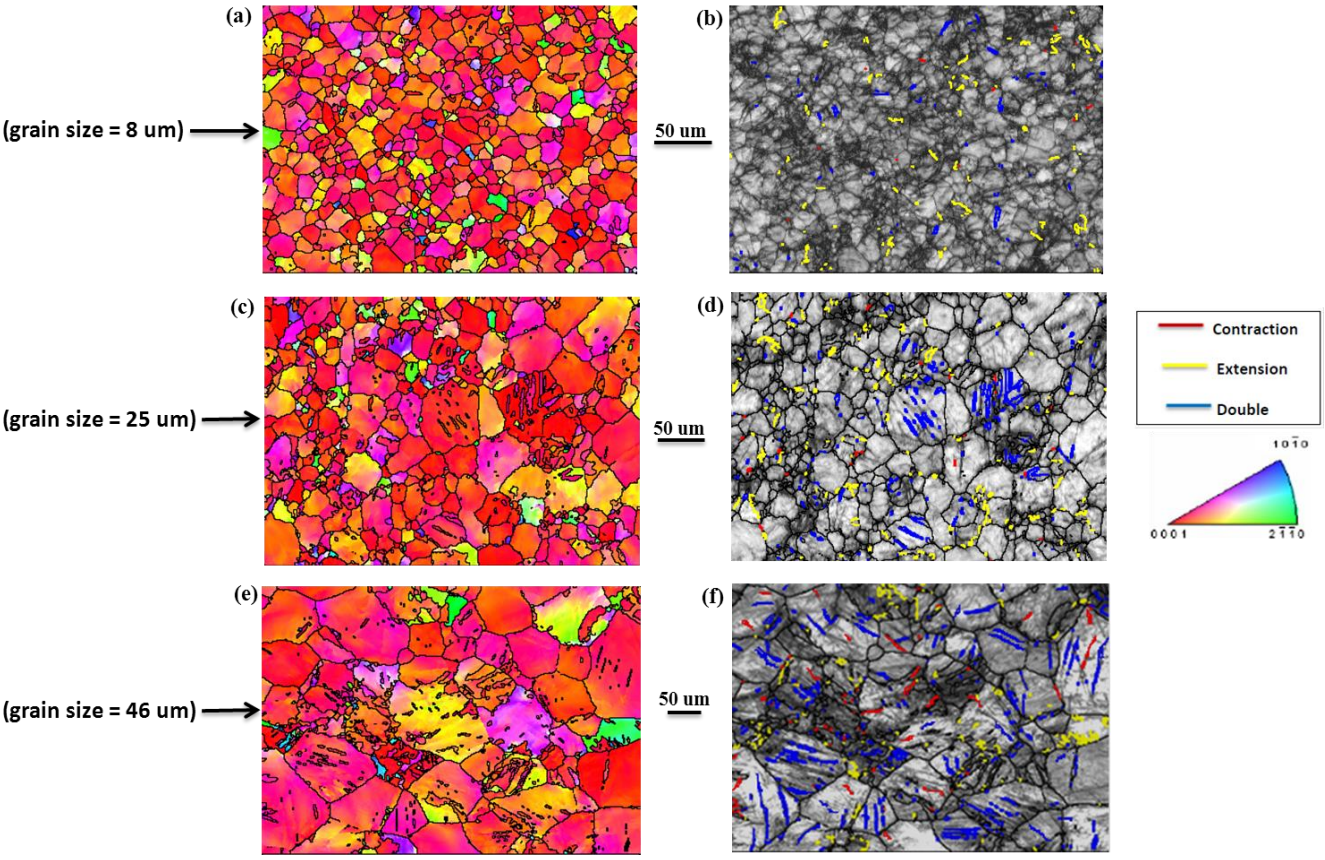

Fig. 7.4. Inverse pole figure (IPF) maps and image quality (IQ) maps of the samples showing the twins type and distribution after shock loading of OP samples at 1200/s. (a) and (b): grain size = 8 μm; (c) and (d): grain size = 25 μm; (e) and (f): grain size = 46 μm [*Note*: The extension twin boundaries ($86° < 11\bar{2}0 > \pm 5°$) are shown in yellow, the contraction twin boundaries ($56° < 11\bar{2}0 > \pm 5°$) are shown in red and the double twin boundaries ($38° < 11\bar{2}0 > \pm 5°$) are shown in blue].

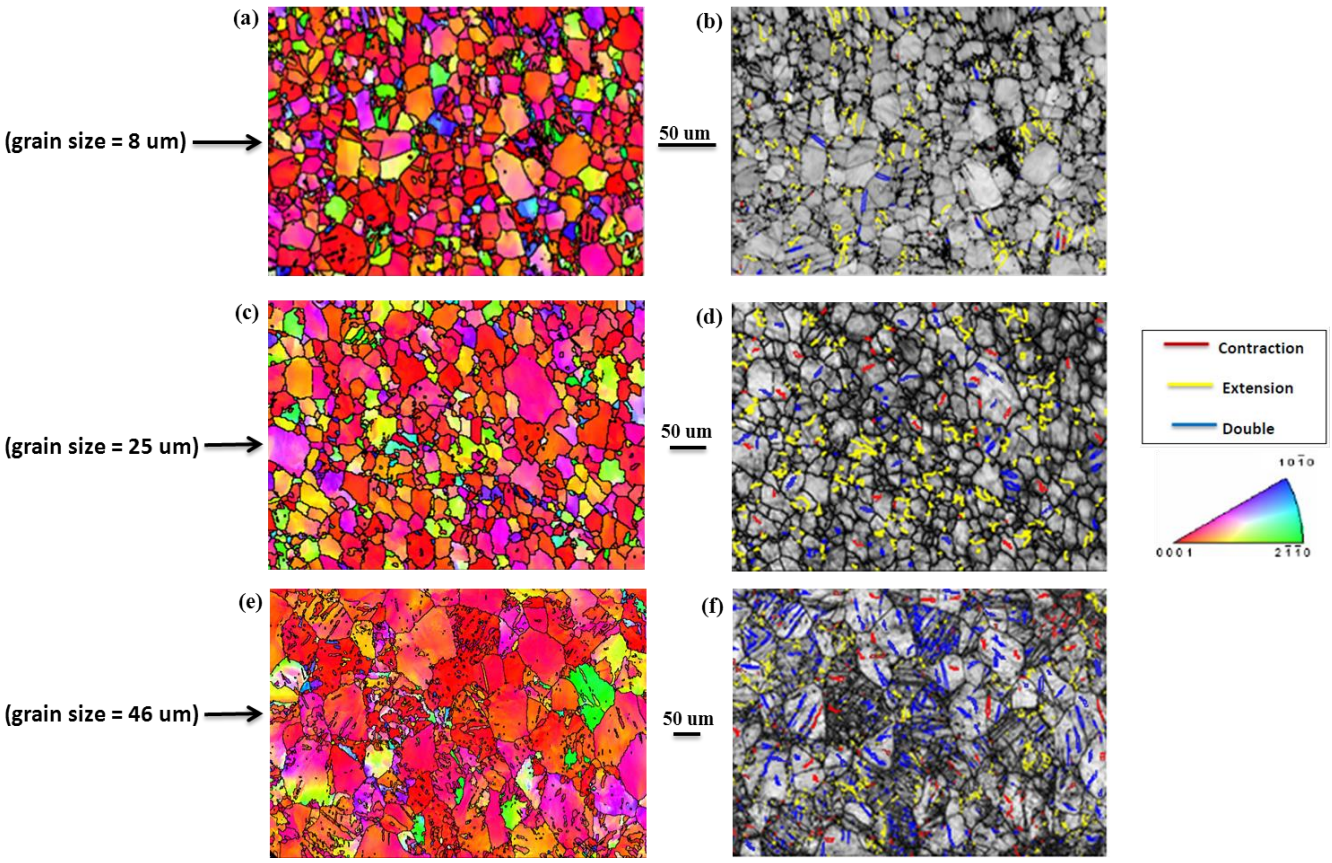

Fig. 7.5. Inverse pole figure (IPF) maps and image quality (IQ) maps of the samples showing the twins type and distribution after shock loading of IP0 samples at 1200/s. (a) and (b): grain size = 8 μm; (c) and (d): grain size = 25 μm; (e) and (f): grain size = 46 μm [*Note*: The extension twin boundaries ($86° < 11\bar{2}0 > \pm 5°$) are shown in yellow, the contraction twin boundaries ($56° < 11\bar{2}0 > \pm 5°$) are shown in red and the double twin boundaries ($38° < 11\bar{2}0 > \pm 5°$) are shown in blue].

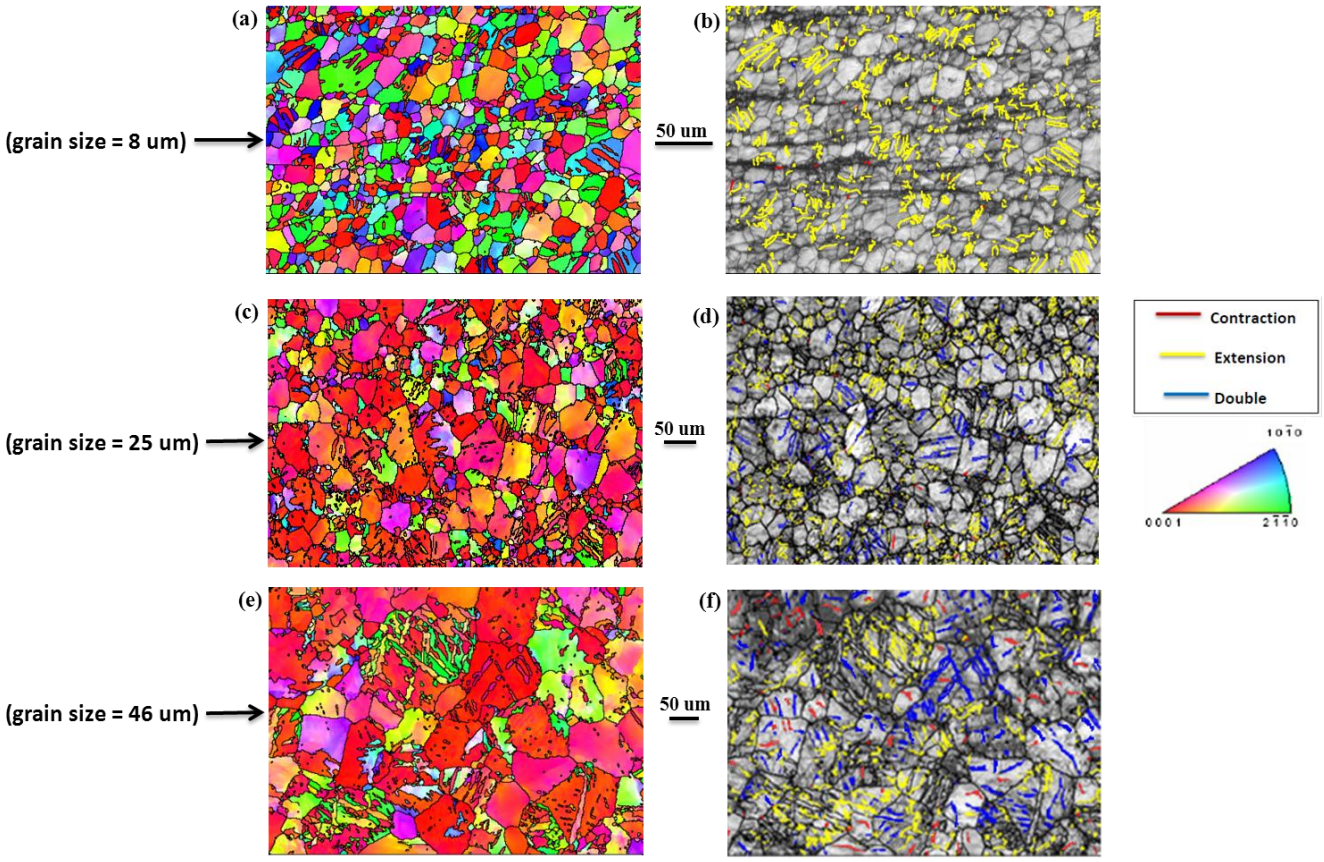

Fig. 7.6. Inverse pole figure (IPF) maps and image quality (IQ) maps of the samples showing the twins type and distribution after shock loading of IP90 samples at 1200/s. (a) and (b): grain size = 8 μm; (c) and (d): grain size = 25 μm; (e) and (f): grain size = 46 μm[*Note*: The extension twin boundaries ($86° < 11\bar{2}0 > \pm 5°$) are shown in yellow, the contraction twin boundaries ($56° < 11\bar{2}0 > \pm 5°$) are shown in red and the double twin boundaries ($38° < 11\bar{2}0 > \pm 5°$) are shown in blue].

Besides, an interesting feature of the EBSD maps is that double twinning fraction (shown in blue), increases with increase in the grain size in all samples. It seems that increasing the grain size results in the further activation of double twins but suppresses the contribution and activation of extension twins (shown in yellow) in the deformation process.

Transmission electron microscopy (TEM) was conducted on the shock-loaded samples to observe the dislocations and their interaction with twins. This process affects the mechanical behavior and hardening of magnesium alloys at high strain. Some examples of such interactions for shock-loaded IP0 samples are represented in Figs. 7.7 and 7.8. High density pile-ups and accumulations of dislocations are seen behind the twin boundaries, in between the twins and at twin intersections (Figs. 7.7 and 7.8), confirming that twin boundaries impede the motions of

dislocations. Moreover, it seems that by increasing the grain size, denser pile-ups of dislocations form around the twins and behind the twin boundaries.

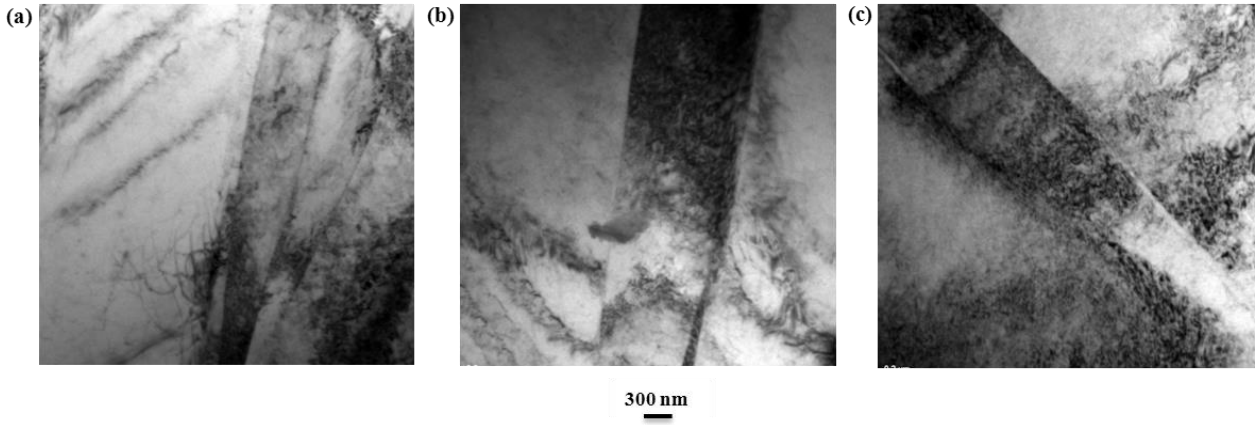

Fig. 7.7. Bright field TEM images of shock-loaded IP0 samples at strain rate of 1200 s^{-1} with different grain sizes showing the accumulation of dislocations inside and behind the twin boundaries: (a) 8 μm grain size (b) 25 μm grain size, (c) 46 μm grain size.

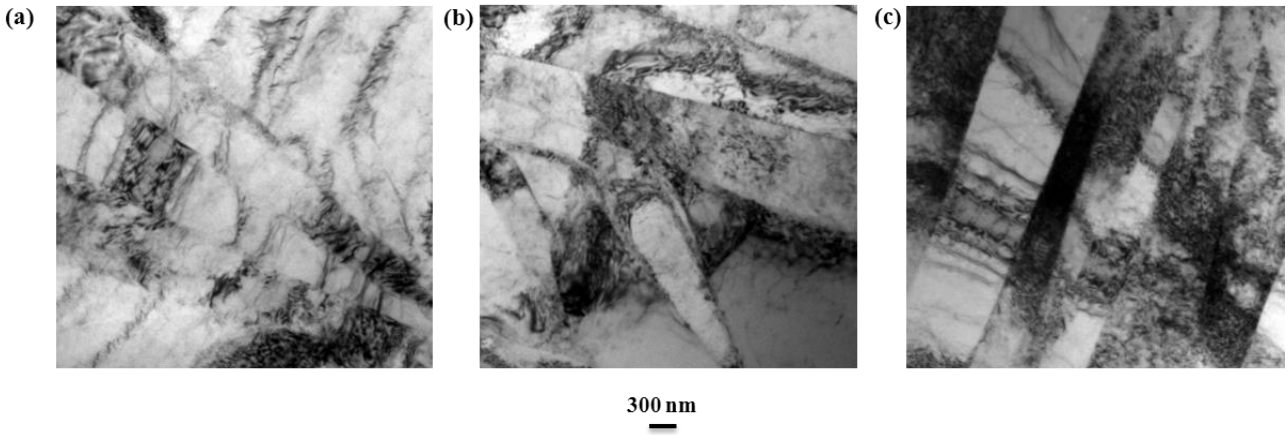

Fig. 7.8. Bright field TEM images of shock-loaded IP0 samples at strain rate of 1200 s^{-1} showing the pile-ups of dislocations at twin boundaries and intersections: (a) 8 μm grain size (b) 25 μm grain size, (c) 46 μm grain size.

Fig. 7.9 illustrates the formation of voids and cracks around the twins and at twin intersections in IP90 sample. This suggests that twins and twin intersections are suitable sites for the void formation and crack initiation. With increasing twin fraction, more voids and larger cracks are observed (Fig. 7.9(b)). The EBSD maps confirmed the presence of twins around the cracks. An example of the EBSD maps taken from a crack and surrounding area is shown in Fig. 7.10. As can be seen, there are several twins around the crack (black region) which are mainly extension twins.

Twins, as mentioned earlier, can impede the dislocation motion and increase the stress concentration which cause the crack to form and propagate.

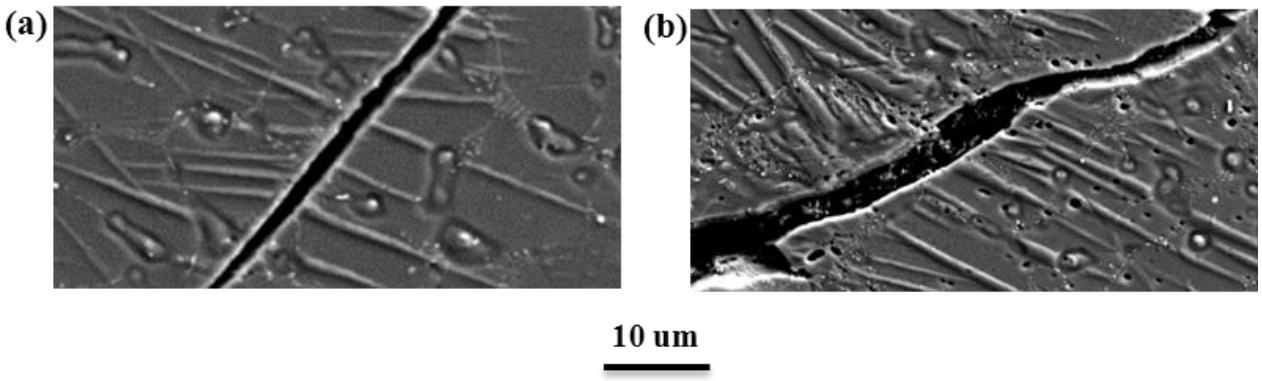

Fig. 7.9. SEM images of shock-loaded (a) IP90 (25 μm) and (b) IP90 (46 μm) samples, showing the formation of voids and cracks around the twins and at twin intersections.

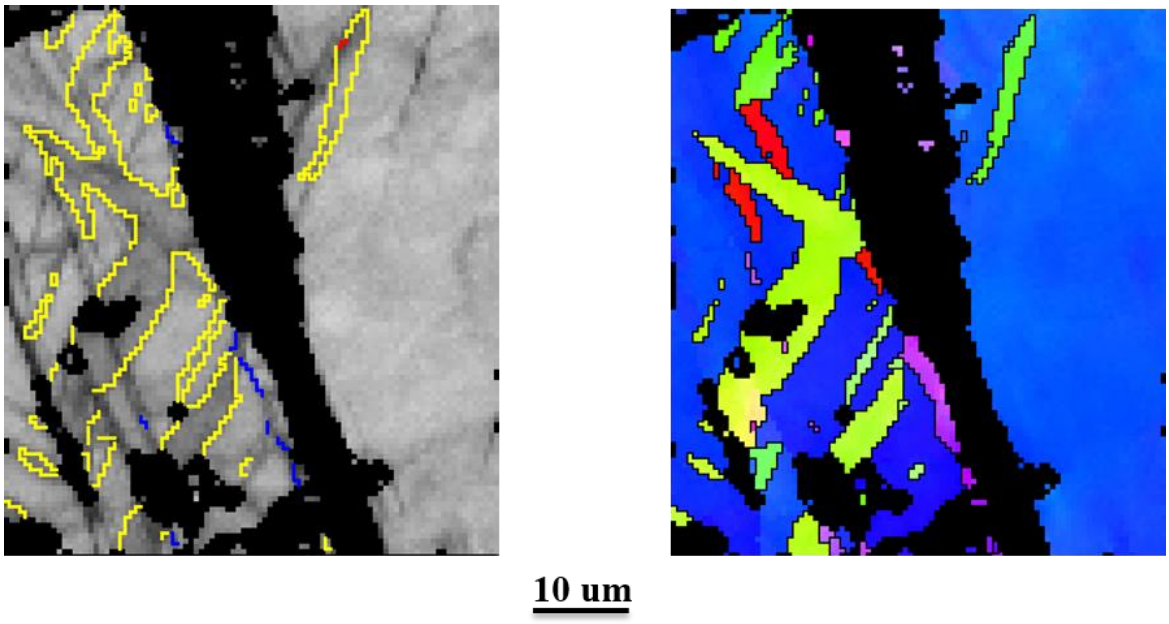

Fig. 7.10. Inverse pole figure (IPF) maps and image quality (IQ) maps of the shock loaded IP0 sample (grain size: 25μm) showing the presence of twins around a crack (black area) after shock loading test at 1100 s^{-1}. [*Note*: The extension twin boundaries ($86° < 11\bar{2}0 > \pm 5°$) are shown in yellow, the contraction twin boundaries ($56° < 11\bar{2}0 > \pm 5°$) are shown in red and the double twin boundaries ($38° < 11\bar{2}0 > \pm 5°$) are shown in blue].

In Fig. 7.11, the dynamic compressive true stress-strain curves and related hardening diagrams of the samples after shock-loading at strain rate of 1200 s^{-1}, are presented. All the stress-strain

graphs at both strain rates are of sigmoidal type and strength and ductility decrease with increasing grain size for all samples. In Table 7.2, mechanical properties of the samples, extracted from the stress-strain diagrams, are tabulated.

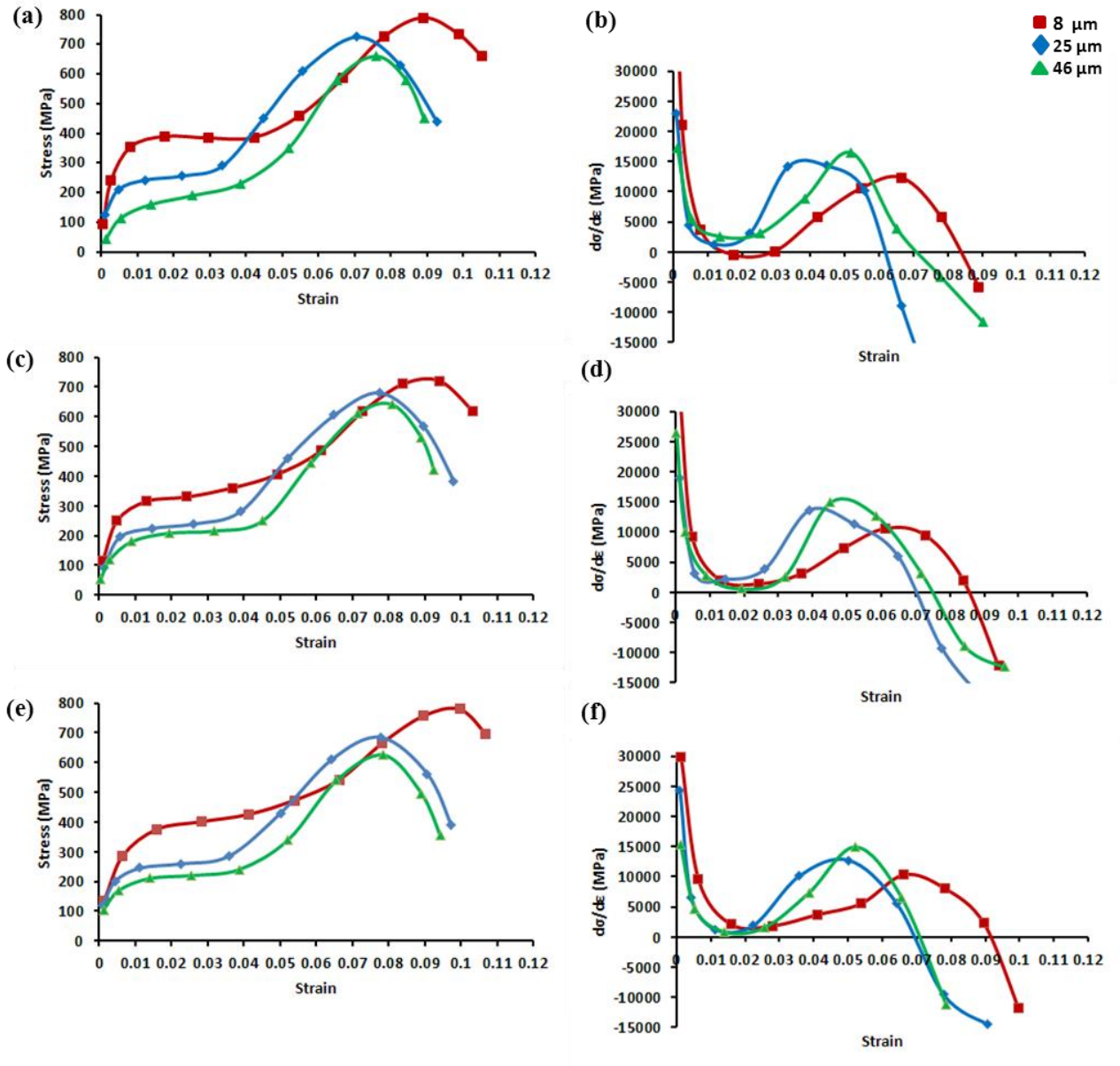

Fig. 7.11. True stress-strain curves and hardening diagrams (dσ/dε versus strain) of shock loaded samples, having different grain sizes, at strain rate of 1200 s^{-1} : (a,b) OP ; (c,d) IP0 and (e,f) IP90.

Table 7.2. Mechanical properties of the samples after compressive shock loading.

Sample	Grain size (μm)	YS (MPa)	UTS (MPa)	Strain before failure (%)
OP	8	236±4.5	790±8.2	10.5±0.17
	25	155±3.1	725±7.6	9.2±0.15
	46	109±2.1	660±6.9	8.8±0.14
IP0	8	215±4.2	720±7.5	10.3±0.16
	25	147±2.9	680±7.1	9.8±0.15
	46	119±2.3	640±6.7	9.2±0.13
IP90	8	208±2.4	779±8.1	10.6±0.18
	25	132±2.6	685±7.1	9.7±0.15
	46	115±2.3	625±6.5	9.4±0.16

The effect of grain size is also obvious in hardening diagrams (Fig. 7.11) indicating that the maximum hardening rate increases with increase in grain size for all samples.

7.6. Discussion

It is observed in Fig. 7.3 that after shock-loading, the weak initial basal texture of all samples which is typical of RE containing rolled magnesium alloy sheets [9,10,15,28], converts to a relatively stronger (00.2) basal texture with basal pole split. It should be mentioned that the weak initial texture in the samples (before shock-loading) has been related to the texture-randomizing effect of RE elements in magnesium alloys with rare-earth (RE) elements [10,15,29]. The important point, however, is the conversion of the initial weak texture to the double-peak basal texture after shock-loading in all samples (Fig.7.3) which can be resulted from twinning and pyramidal <c+a> slip [16,30-33]. Another feature about the pole figures of the shock-loaded samples is that the intensity of the basal textures is slightly higher for the samples with coarser grains compared to those with finer grains. (Fig. 7.3), indicating the strong effect of twinning and <c+a> slip on the texture transformation in coarse-grained samples after shock-loading. One more point to note is that the splitting of basal texture has taken place along RD in the initial rolled samples (e.g. Fig. 7.2(a)) and after shock loading (e.g. 7.3(a), (d)and (g)). This behavior is related to the deformation mechanisms of magnesium alloys during the deformation process and the crystal structure of the magnesium alloys. In magnesium and its alloys, several deformation mechanisms are involved during the deformation process, such as basal, twinning and <c+a> pyramidal, and these mechanisms affect the splitting of the basal poles. Also, ‘c/a’ ratio is another parameter that affect

the basal texture splitting behavior of hcp alloys [34,35]. When the deviation of c/a ratio from the ideal value (1.63) is large, such as zirconium and its alloys, the splitting occurs along the TD direction. However, in magnesium alloys, with a c/a ratio of about 1.624, the deviation from ideal c/a ratio is very small and therefore, the splitting of basal poles is observed along the RD direction. This c/a ratio, in fact, affects the involving mechanisms during the deformation and results in the splitting along different directions (RD or TD) [34,35].

It is observed from the EBSD maps that the dominant twinning in the samples having 8μm grain size is extension twinning; however, with increasing grain size, double twinning becomes the dominant twinning mode and the fraction of double twins increases (Figs. 7.4 to 7.6). As mentioned previously, another interesting feature of the EBSD maps in Figs. 7.4 to 7.6 is that the total twinning fraction increases with increasing grain size and the maximum twinning fractions is observed for the samples with 46 μm grain size (Figs. 7.4(f), 7.5(f) and 7.6(f)). It is worth noting that for OP samples, although the initial texture of the sample having 8 μm grain size is a double-peak basal texture (Fig. 7.2(a)) and is slightly different from those of OP samples with 25 and 46 μm, which is a C-type basal texture (Fig. 7.2(d) and 7.2(g)), the same trend for twinning fraction is seen in which the total twinning fraction increases with increasing the grain size and double twins are the dominant twins for coarse-grained samples (Fig. 7.4). This indicates the stronger influence of grain size on the twinning in comparison to that of the initial texture. Another effect of this increased twinning fraction could be the relatively higher intensity of the double-peak basal textures obtained for shock-loaded samples having coarser grains (Fig. 7.3). In other words, it seems that with increasing the grain size of the alloy, the contribution of the twinning, particularly double and contraction twinning, increases in the deformation process during the shock loading and this deformation mode will play a more important role during the deformation process of coarse-grained alloys. It is worth noting that other deformation modes (mechanisms), such as basal slip and <c+a> pyramidal slip, are involved in the deformation process together with twinning; however, their contribution decreases with increase in grain size which will be discussed in the next sections.

The variation of twinning fraction with grain size (Figs. 7.4 to 7.6) can be related to the twinning interface energy [36] and critical resolved shear stress for twinning [37]. The energy of twin interfaces is considerably large in magnesium and its alloys and decreasing grain size gives rise to decreased twinning nucleation [36]. Besides, the twinning stress, which is required to activate

twinning systems, increases with decreasing grain size, leading to decreased twinning activity and twinning fraction for deformed fine-grained alloys [37]. The reason for decreased twinning fraction and activity of double twins in samples with smaller grain sizes, particularly samples having 8μm grain size, is still not clear but may be related to the high elastic strain energy which is associated with the generation of double twins in fine-grained samples [38,39]. In fine-grained samples, there is not enough space for the double twins to grow and propagate and therefore, under these conditions, short double twins could be formed. However, according to the relation: $E= (c/r)\ \mu s^2$ [39], where E is elastic energy, c is the twin thickness and r is the length of the twin, μ is the shear modulus and s is the twinning shear, formation of possible short double twins needs a high elastic energy due to small r values and even if the short twin is formed, the generation of high elastic energy due to the formation of the short twin in the grain may inhibit the formation of new double twins [38,39].

Considering the stress-strain curves of the shock-loaded samples (Fig. 7.11), it is clear that the strength and ductility decrease with increasing grain size for all the samples (i.e. OP, IP0 and IP90). The influence of grain size (d) on the strength (σ) is generally characterized by the Hall-Petch equation:

$$\sigma = \sigma_0 + kd^{-1/2} \quad (1)$$

where σ_0 is the friction stress and k is a constant indicating the effectiveness of grain boundaries in strengthening process. Therefore, for the samples having smaller grain sizes, the number of grain boundaries, (or surface area of the grain boundaries) is larger than that of the samples with larger grain sizes and it means that there are much more obstacles against the dislocation motions [20,43]. Due to the discontinuity in the slip system at grain boundaries, dislocations are impeded and blocked at grain boundaries and more stress is required to move them to pass the grain boundaries [20,43]. For this reason, with increasing the grain size, the strength decreases in the stress-strain curves (Fig. 11).

The decreased ductility of the shock-loaded samples with increasing grain size (Fig. 7.11) could be related to the larger twinning fraction in coarse-grained samples. As shown in the EBSD maps (Figs. 7.4 to 7.6), increasing the grain size leads to increase in the total twinning fraction in the microstructure of the samples after shock-loading so that the largest twinning fraction is observed for the samples having 46μm grain size. Besides, dislocation pile-ups and accumulation at twins and twin intersections are clearly shown in Figs. 7.7 and 7.8. Twins serve as effective barriers to

dislocation movement and the number of dislocations accumulated behind the twin boundaries during the deformation increases with strain. This accumulation of dislocations at twins, which increases with strain, may cause high values of stress concentrations around the twins and twin intersections, resulting in void and crack formation (Fig. 9), which eventually causes premature fracture [2,17,44-47]. In other words, increasing the grain size will encourage high stress localization and twinning-induced fracture [45,47]. Another reason could be the difference between the deformation level of double twins and that of the parent material [19]. It is believed that double twins may accommodate more strain compared to the matrix. This may cause generation of large incompatibilities at the interface of parent-twin which consequently cause fracture [19,48-52]. Therefore, the larger double twinning fraction is likely to be responsible for the lower ductility of the samples having coarser grain sizes.

As shown in hardening diagrams (Fig. 7.11), the maximum hardening rate increases with increasing the grain size, and the maximum hardening rates are registered for samples having 46 μm grain size. This increase in hardening rate with increased grain size may be related to enhanced dislocation storage capacity in coarse-grained samples [53]. The increased density of dislocations with increase in grain size is demonstrated in Figs. 7.7 and 7.8. In general, the strain hardening behavior of a material strongly depends on the dislocation density and interactions between dislocation strain fields. Increasing the dislocation density during deformation can decrease the distance between dislocations and further increase in dislocation density results in the increased resistance to dislocation motion [54]. In larger (coarser) grains, more space may be provided to accommodate dislocations, leading to stronger hardening ability in the coarse-grained samples [53].

As the final step of this research, $g.b = 0$ invisibility criterion analysis was done to assess the presence of <c+a> dislocations which in fact indicates the activation of pyramidal <c+a> slip system. Considering the similarity in the pole figures of shock-loaded samples (Fig. 7.3), in which a double-peak basal texture is seen for all samples, only one of the shock-loaded samples, i.e. IP90 with 25 μm grain size, was selected for this analysis. To prove the presence of <c+a> dislocations, two diffraction conditions (vectors) for a certain area on the sample were used, i.e. [0002] and $[10\bar{1}0]$. The only dislocations which are visible in these diffraction conditions are <c+a> dislocations. In Fig. 7.12 (a), only <c> and <c+a> dislocations appear in contrast for g=[0002] because according to the Table 7.3, <a> dislocations are invisible in this contrast (g.b

value is zero). However, by tilting the sample to obtain g= $[10\bar{1}0]$, <c+a> and <a> dislocations are visible for this diffraction condition and exhibit strong contrast whereas <c> dislocations are not visible under this diffraction condition because the visibility factor for <c> dislocations is zero for g= $[10\bar{1}0]$, as tabulated in Table 7.3. Considering both diffraction conditions in Fig. 7.12, it is evident that some dislocations are present in the contrasts of both g= [0002] and g=$[10\bar{1}0]$, which are shown by solid arrows in Fig. 7.12. These dislocations, visible at both diffraction conditions, are <c+a> dislocations which have been activated in the shock-loaded samples. This proves the activation of pyramidal <c+a> slip systems during the shock-loading process. Activation and presence of pyramidal <c+a> dislocations, using *g.b* analysis, have been reported by some researchers for cold-deformed Mg-Y [26] and cold-worked Mg-Li [55], but, this is the first time that the activation of pyramidal <c+a> slip dislocation has been reported for shock-loaded WE43 magnesium sheet using *g.b* analysis.

Activation of pyramidal <c+a> slip during the shock loading of WE43 magnesium alloy can be traced to: (1) considerable increase in temperature during the shock loading test [56] and (2) presence of RE elements in the investigated WE43 magnesium alloy that increases the density of sources which may generate <c+a> dislocations [16].

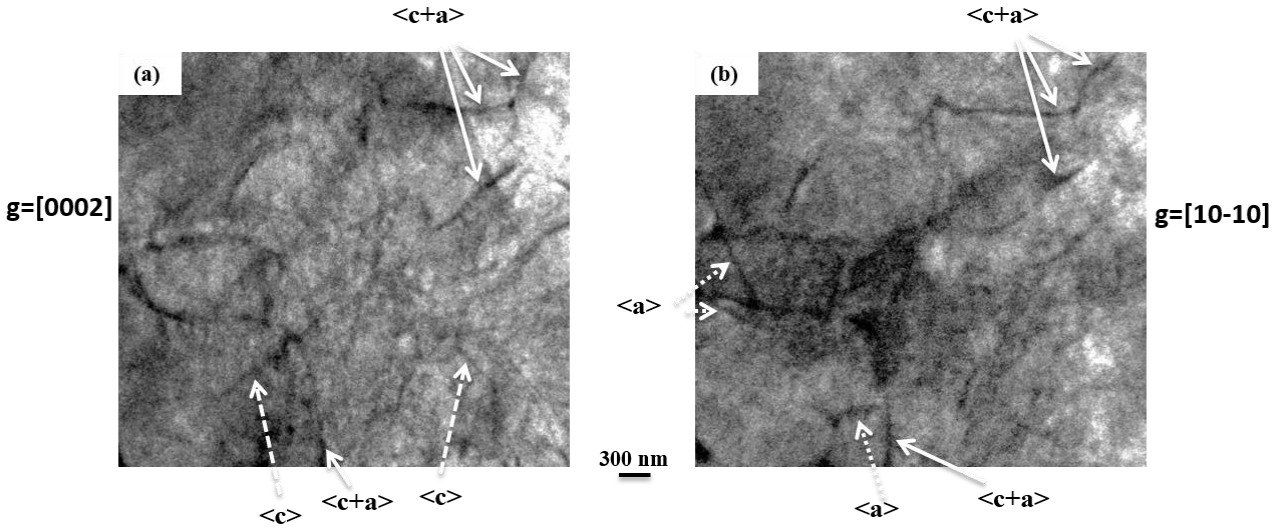

Fig. 7.12. Bright field TEM images under different diffraction conditions emphasizing the presence of <c+a> dislocations in shock-loaded IP (strain rate: 1200 s^{-1}): (a) g=[0002], (b) g=$[10\bar{1}0]$.

Table 7.3. The *g.b* values for dislocations in the HCP crystals close to $[1\bar{2}10]$ zone axis [27].

Mode	Burgers vector (*b*)	$g = [0002]$	$g = [10\bar{1}0]$
		g.b	g.b
<a>	$1/3[11\bar{2}0]$	0	1
	$1/3[1\bar{2}10]$	0	0
	$1/3[\bar{2}110]$	0	-1
<c+a>	$1/3[11\bar{2}3]$	2	1
	$1/3[1\bar{2}13]$	2	0
	$1/3[\bar{2}113]$	2	-1
	$1/3[11\bar{2}\bar{3}]$	-2	1
	$1/3[1\bar{2}1\bar{3}]$	-2	0
	$1/3[\bar{2}11\bar{3}]$	-2	-1
<c>	[0001]	2	0

7.7. Conclusions

Based on the experimental results obtained using several techniques such as XRD, SEM and TEM, the following conclusions can be drawn for the shock-loaded Mg-4Y-3RE alloy:

(1) The initial weak (00.2) basal texture of all samples transforms to a stronger double-peak (00.2) basal texture after shock-loading in which the splitting of basal poles indicates the activation of pyramidal <c+a> slip under shock-loading conditions. The *g.b* analysis method confirmed the activation and presence of <c+a> dislocations after shock-loading of Mg-4Y-3RE magnesium alloy.

(2) Increasing the grain size results in decreased strength and ductility which are detrimental properties for Mg-4Y-3RE magnesium alloys particularly under high strain rate conditions. Therefore, fine-grained Mg-4Y-3RE magnesium alloy is suggested for use in high strain rate

situations.

(3) Total twinning fraction and strain hardening rate increases with increasing grain size of Mg-4Y-3RE alloy at high strain rates.

(4) After shock-loading, the activity of double and contraction twins, particularly double twins, increase with increase in grain size of the Mg-4Y-3RE alloy.

(5) In comparison to AZ31B sheet, the mechanical anisotropy is still very low even in coarse-grained WE43 alloy.

References

[1] Cheng YQ, Chen ZH. Anisotropy of deformation behavior of AZ31 magnesium alloy sheets. Advanced Materials Research 2011; 314-316: 1121-1125.

[2] Mabuchi M, Chino Y, Iwasaki H. Influence of grain size on elongation at elevated temperatures in AZ31 Mg alloy. Materials Transactions 2003; 44:490-495.

[3] Ahmad IR, Shu DW. Compressive and constitutive analysis of AZ31B magnesium alloy over a wide range of strain rates. Materials Science and Engineering A 2014; 592:40-49.

[4] Del Valle JA, Carreño F, Ruano OA. Influence of texture and grain size on work hardening and ductility in magnesium-based alloys processed by ECAP and rolling. Acta Materialia 2006;54:4247–4259.

[5] Guo L, Chen Z, Gao L. Effects of grain size, texture and twinning on mechanical properties and work-hardening behavior of AZ31 magnesium alloys. Materials Science and Engineering A 2011; 528:8537-8545.

[6] Mordike BL, Ebert T. Magnesium: Properties — applications — potential. Materials Science and Engineering A 2001;302: 37-45.

[7] Agnew SR, Duygulu O. A mechanistic understanding of the formability of magnesium: Examining the role of temperature on the deformation mechanisms. Materials Science Forum 2003; 419-422:177-188.

[8] Hakamada M, Furuta T, Chino Y, Chen Y, Kusuda H, Mabuchi M. Life cycle inventory study on magnesium alloy substitution in vehicles. Energy 2007;32:1352.

[9] Meyers MA, Dynamic behavior of materials. Wiley-In- Interscience, New York. 1994.

[10] Meyers M, Andrade U, Chokshi A. The effect of grain size on the high-strain, high-strain-rate behavior of copper. Metallurgical and Materials Transactions A 1995; 26:2881-2893.

[11] McCauley JW, Strassburger E, Patel P, Paliwal B, Ramesh KT. Experimental observations on dynamic response of selected transparent armor materials. Experimental Mechanics 2013; 53: 3-29.

[12] Hirsch J, Al-Samman T. Superior light metals by texture engineering: Optimized aluminum and magnesium alloys for automotive applications. Acta Materialia 2013; 61:818-843.

[13] Bohlen J, Nürnberg MR, Senn JW, Letzig D, Agnew SR. The texture and anisotropy of magnesium–zinc–rare earth alloy sheets. Acta Materialia 2007; 55: 2101-2112.

[14] Farzadfar SA, Sanjari M, Jung I-H, Essadiqi E, Yue S. Role of yttrium in the microstructure and texture evolution of Mg. Materials Science and Engineering A 2011; 528:6742-6753.

[15] Sandlöbes S, Zaefferer S, Schestakow I, Yi S, Gonzalez-Martinez R. On the role of non-basal deformation mechanisms for the ductility of Mg and Mg–Y alloys. Acta Materialia 2011; 59: 429-439.

[16] Asgari H, Odeshi A.G, Szpunar JA. On dynamic deformation behavior of WE43 magnesium alloy sheet under shock loading conditions Materials & Design 2014; 63:552-564.

[17] Wang XL, Yu Y, Wang ED. The effects of grain size on ductility of AZ31 magnesium alloy. Materials Science Forum 2005; 488-489:535-538.

[18] Chino Y, Kimura K, Mabuchi M. Twinning behavior and deformation mechanisms of extruded AZ31 Mg alloy. Materials Science and Engineering A 2008;486:481-488.

[19] Barnett MR, Keshavarz Z, Beer AG, Atwell D. Influence of grain size on the compressive deformation of wrought Mg–3Al–1Zn. Acta Materialia 2004; 52: 5093-5103.

[20] Barnett MR, Atwell DL, Beer AG. Grain size in Mg alloys: Recrystallization and mechanical consequences. Materials Science Forum 2007; 558-559:433-440.

[21] Al-Samman T. Comparative study of the deformation behavior of hexagonal magnesium–lithium alloys and a conventional magnesium AZ31 alloy. Acta Materialia 2004; 57:2229-2242.

[22] Jain A, Duygulu O, Brown DW, Tome CN, Agnew SR. Grain size effects on the tensile properties and deformation mechanisms of a magnesium alloy, AZ31B, sheet. Materials Science and Engineering A 2008; 486:545-555.

[23] Barnett MR. A rationale for the strong dependence of mechanical twinning on grain size. Scripta Materialia 2008;59:696-698.

[24] Chino Y, Kimura K, Hakamada M, Mabuchi M. Mechanical anisotropy due to twinning in an extruded AZ31 Mg alloy. Materials Science and Engineering A 2008; 485:311-317.

[25] Asgari H, Szpunar JA, Odeshi AG, Zeng LJ, Olsson E, Li DY. Effect of yttrium on the twinning and plastic deformation of AE magnesium alloy under ballistic impact. Materials Science and Engineering A 2015; 623:10-21.

[26] Sandlöbes S, Friák M, Zaefferer S, Dick A, Yi S, Letzig D, Pei Z, Zhu LF, Neugebauer J, Raabe D. The relation between ductility and stacking fault energies in Mg and Mg–Y alloy. Acta Materialia 2012; 60:3011-3021.

[27] Okamoto PR, Thomas G. On the four-axis hexagonal reciprocal lattice and its use in the indexing of transmission electron diffraction patterns. Physica Status Solidi 1968; 25:81-91.

[28] Ball EA, Prangnell PB. Tensile-compressive yield asymmetries in high strength wrought magnesium alloys. Scripta Metallurgica et Materialia 1994; 31:111-116.

[29] Li X, Jiao F, Al-Samman T, Ghosh Chowdhury S. Influence of second-phase precipitates on the texture evolution of Mg–Al–Zn alloys during hot deformation. Scripta Materialia 2012; 66:159-162.

[30] Chang LL, Shang EF, Wang YN, Zhao X, Qi M. Texture and microstructure evolution in cold rolled AZ31 magnesium alloy. Materials Characterization 2009; 60:487-491.

[31] Agnew SR, Yoo MH, Tomé CN. Application of texture simulation to understanding mechanical behavior of Mg and solid solution alloys containing Li or Y. Acta Materialia 2001;49:4277–4289.

[32] Basu I, Al-Samman T, Gottstein G. Shear band-related recrystallization and grain growth in two rolled magnesium-rare earth alloys. Materials Science and Engineering A 2013; 579:50-56.

[33] Yi S, Bohlen J, Sandlobes S, Zaefferer S, Letzig D, Kainer KU. Microstructural evolution during recrystallization of magnesium alloys. Materials Science Forum 2012;706-709:1291-1296.

[34] E. Tenckhoff. Review of deformation mechanisms, texture, and mechanical anisotropy in Zirconium and Zirconium base alloys. ASTM Special Technical Publication 2005; 1467:25-50.

[35] Y.N. Wang, J.C. Huang. Texture analysis in hexagonal materials. Materials Chemistry and Physics 2003; 81:11-26.

[36] Koike J, Kobayashi T, Mukai T, Watanabe H, Suzuki M, Maruyama K, Higashi K. The activity of non-basal slip systems and dynamic recovery at room temperature in fine-grained AZ31B magnesium alloys. Acta Materialia 2003;51:2055-2065.

[37] Meyers MA, Vöhringer O, Lubarda VA. The onset of twinning in metals: a constitutive description. Acta Materialia 2001; 49:4025-4039.

[38] Wan G, Wu BL, Zhang YD, Sha GY, Esling C. Anisotropy of dynamic behavior of extruded AZ31 magnesium alloy. Materials Science and Engineering A 2010; 527:2915-2924.

[39] Bhadeshia HKDH, Worked examples in the geometry of crystals, second edition, (2001, updated 2006), The institute of metals, London.

[40] Dudamell NV, Ulacia I, Gálvez F, Yi S, Bohlen J, Letzig D, Hurtado I, Pérez-Prado MT. Twinning and grain subdivision during dynamic deformation of a Mg AZ31 sheet alloy at room temperature. Acta Materialia 2011; 59:6949-6962.

[41] Sarker D, Chen DL. Detwinning and strain hardening of an extruded magnesium alloy during compression. Scripta Materialia 2012; 67:165-168.

[42] B. Wang, R. Xin, G. Huang, Q. Liu. Materials Science and Engineering A 2012; 534:588-593.

[43] R. Korla, A.H. Chokshi. Scripta Materialia 2010; 63: 913-916.

[44] Mukai T, Mohri T, Mabuchi M, Nakamura M, Ishikawa K, Higashi K. Experimental study of a structural magnesium alloy with high absorption energy under dynamic loading. Scripta Materialia 1998; 39:1249-1253.

[45] Barnett MR. Twinning and the ductility of magnesium alloys: Part II. "Contraction" twins. Materials Science and Engineering A 2007; 464:8-16.

[46] Christian JW, Mahajan S. Deformation twinning. Progress in Materials Science 1995; 39:1-1577.

[47] Mukai T, Yamanoi M, Watanabe H, Ishikawa K, Higashi K. Effect of grain refinement on tensile ductility in ZK60 magnesium alloy under dynamic loading. Materials Transactions 2001; 42:1177-1181.

[48] Hartt WH, Reed-Hill RE, Trans. TMS-AIME 1968; 242:1127–1133.

[49] Buchanan ER, Reed-Hill RE. On the mechanism of rotational slip in magnesium single crystals.Trans. Metall. Soc. AIME 1960; 218:554–558.

[50] Jiang L, Jonas JJ, Mishra RK, Luo AA, Sachdev AK, Godet S. Twinning and texture development in two Mg alloys subjected to loading along three different strain paths. Acta Materialia 2007; 55:3899-3910.

[51] Jiang L, Jonas JJ, Luo AA, Sachdev AK, Godet S. Influence of {10-12} extension twinning on the flow behavior of AZ31 Mg alloy. Materials Science and Engineering A 2007;445-446: 302:309.

[52] Khan AS, Pandey A, Gnäupel-Herold T, Mishra RK. Mechanical response and texture evolution of AZ31 alloy at large strains for different strain rates and temperatures. International Journal of Plasticity 2011; 27: 688–706.

[53] Afrin N, Chen DL, Cao X, Jahazi M. Strain hardening behavior of a friction stir welded magnesium alloy. Scripta Materialia 2007; 57:1004-1007.

[54] W.D. Callister Jr. Materials Science and Engineering-An Introduction, seventh edition, John Wiley & Sons, New York, 2007.

[55] S.R. Agnew, J.A. Horton, M.H. Yoo. Transmission electron microscopy investigation of 〈c + a〉 dislocations in Mg and α-solid solution Mg-Li alloys. Metallurgical and Materials Transactions A 2002; 33:851-858.

CHAPTER 8

SUMMARY, CONCLUSIONS AND RECOMMENDATIONS FOR FUTURE WORK

8.1. Summary

In this research study, the dynamic deformation behavior of several cast and rolled magnesium alloys including AZ, AE and WE series with high potential for application in automotive and aerospace industries was investigated under compressive shock loading condition. Moreover, the effect of parameters such as composition, initial texture, grain size and strain rate on the possible deformation mechanisms was evaluated. Furthermore, several methods, e.g. XRD, SEM, OIM, TEM and VPSC simulation, were used to determine the effects of above-mentioned parameters on the dynamic deformation behavior of the tested alloys. The conclusions are presented in the next section.

8.2. Conclusions

Based on the results obtained in various aspects of this project, the following conclusions can be drawn:

1. Increasing the aluminum content in cast AZ magnesium alloys results in an increase in the volume fraction of second phase particles, strength and strain hardening, but to a decrease in the ductility. Twinning fraction, particularly extension twinning, decreases considerably with increasing aluminum content.
2. Increasing the yttrium content of cast AE alloys leads to an increase in both the strength and the ductility of the alloys. Furthermore, twinning fraction decreases while the dislocation density increases with increase in yttrium content. The presence of yttrium decreases the nucleation and activation of twinning systems.

3. Increasing the aluminum and yttrium content in cast magnesium alloys results in a decreased basal texture intensity which could be related to the decreased contribution of twinning in deformation process. This effect is more significant for alloys with higher content of rare earth elements.
4. Increasing the strain rate leads to higher strength and ductility in cast magnesium alloys. However, higher ductility is obtained in the presence of rare earth elements.
5. In rolled alloys, including WE43 and AZ31B, initial texture of all samples transforms to a double-peak (00.2) basal texture. This double peak basal texture has a low intensity in rare earth containing WE43 alloys but high intensity in AZ31B alloy. Increasing the strain rate results in increased strength and ductility and decreased contribution of twinning to deformation. Moreover, it was inferred that the most active deformation modes are basal slip, pyramidal <c+a> slip and extension twinning. Increasing the strain rate results in higher activity of pyramidal <c+a> slip system and lower activity of extension twinning under shock loading conditions.
6. The strong initial basal texture results in a high degree of mechanical anisotropy in AZ31B alloy. However, the degree of mechanical anisotropy is low in rolled WE43 alloy which is an important consequence of the weak initial texture due to the presence of rare-earth elements, mainly yttrium and neodymium, in the alloy.
7. The activation of <c+a> pyramidal slip system is confirmed in shock loaded rolled alloys using "g.b" analysis. However, simulation results show that in rare earth containing alloys, the activity of <c+a> slip system is higher during shock loading.
8. Increasing the grain size results in decreased ductility and strength in rolled alloys. Therefore, it is recommended to use fine-grained rolled alloys for high-strain rate applications. Moreover, increasing the grain size encourages the formation and activation of double (and contraction) twins. It is then logical to conclude that double (and contraction) twinning contribute more to the deformation process in coarse-grained samples at high strain rates, in comparison to other twinning modes.

8.3. Recommendations for future work

The effect of several parameters, such as composition, initial texture, strain rate and grain size on the dynamic deformation behavior of magnesium alloys was investigated in this research study. However, there are still some areas which need further exploration and can be listed as follows:

1. Another important parameter, which significantly affect the mechanical properties and deformation mechanisms of magnesium alloys at high strain rates is temperature. It would be of interest to determine the effect of temperature on dynamic mechanical response of cast AZ and AE alloys and rolled AZ31B and WE43 alloys at high strain rates.
2. All the shock loading tests in this study were conducted under compressive mode. The high strain rate tests can be done under torsional mode to evaluate the effect of loading mode on the texture formation, microstructural evolution and dynamic deformation behavior of the cast and rolled alloys investigated in this research.
3. In-situ SEM and EBSD tests can be done on the rolled AZ31B and WE43 alloys to investigate the twin and crack formation and growth mechanisms at low strain rates.
4. Production of new alloys, using calcium with similar characteristics to RE elements but at a much cheaper price, and subjecting them to impact loading to evaluate the dynamic mechanical behavior and deformation mechanisms in the presence of new alloying elements can also be of interest.

Appendix A

VPSC Simulation

In this research, as explained in Chapters 4 and 5, commercial VPSC (visco-plastic self-consistent) software was used for simulation. The main idea of the simulations is to reproduce the experimental textures using VPSC software for some shock-loaded samples. In fact, these simulations may explain the texture formation mechanisms which consequently helped in the discussion of the probable deformation mechanisms involved in the high strain rate deformation of the investigated alloys.

The initial assumptions (inputs) of VPSC simulations are listed as follows:

(1) Deformation modes, i.e. slip/twin systems: Based on experimental data, such as experimental textures and EBSD maps, it is possible to assume that some of the deformation modes are activated during shock-loading (and in simulations). For example, the double-peak basal textures obtained from texture measurement on impacted samples using XRD (e.g. Fig. 4.4) can be considered as a good indication of activation of <c+a> slip systems [41-43] and IQ maps confirm the presence and activation of extension twinning (e.g. Fig. 4.5). Additionally, basal slip system, with a very low critical resolved shear stress (CRSS), is usually activated even at very low strain rates and loading conditions. Therefore, these modes were considered (assumed) as the active deformation modes in the VPSC simulation software (input data) and were labelled as active modes in the corresponding input file.

(2) Critical resolved shear stress (CRSS) for each deformation mode: another important input (assumption) in the VPSC simulation is the ratio of critical resolved shear stresses (CRSS) of the deformation modes (slip/twin). It is worth noting that reported values of the ratios of CRSS for non-basal to basal slip and also the ratio of CRSS of the extension twinning to the basal slip are different from each other. However, there are some general rules that can be followed: (i) basal slip system has the lowest CRSS and therefore, it is the easiest deformation mode, (ii) The activation of extension twinning, with the lowest CRSS after basal slip is much easier than pyramidal <c+a> slip system and (iii) the probability for the activation of pyramidal <c+a> slip system increases with increasing temperature. Based on these rules, the CRSS ratios are chosen in our simulations which are listed in Table 4.1, for AZ31B alloy. Basal slip is considered as the base due to its lowest CRSS.

(3) The initial texture: This is another input in the VPSC simulations. The initial crystallographic orientation of the grains is extracted from the experimental textures obtained from the XRD measurements in the form of orientation distribution factor (ODF). However, instead of using the measured textures directly as VPSC input, this data (orientation distribution function or ODF) is subjected to some processing using 'ResMat' software.

(4) Strain history: This is defined using the experimental data on the straining of the samples after shock loading.

A number of models and theories which were used in the VPSC simulation are briefly discussed in this appendix. Generally, using crystal plasticity models, it is possible to establish a relationship between the single crystal behavior (micro-properties) and polycrystal behavior (macro-properties). In fact, these models enable us to evaluate the effect of CRSS and preferred crystallographic orientation on the mechanical response of a polycrystal. Finite element (FE) based methods and mean field models are the main models by which it is possible to explain the operation of slip systems in a crystal. Finite element models are useful to study the interactions between the grains during deformation but in the case of mean field models, it is possible to find the properties of the polycrystal based on the volumetric averages of the properties of each crystal. For example, the value of stress in the polycrystal is the volumetric averages of the related grain magnitudes. To satisfy this averaging condition, models such as Taylor, Sachs and self-consistency is required. In Sachs model, a stress equilibrium across the grains is assumed, meaning that the magnitude of stress in each grain is equal to the magnitude of stress in the polycrystal. In Taylor model, however, strain in each grain is assumed to be equal to the strain in the polycrystal. In self-consistent (SC) models, each grain is assumed as an inclusion embedded in a homogeneous matrix with the properties of the polycrystal. For the simulation work in this study, as mentioned in Chapters 4 and 5, a model based on the self-consistent scheme was used and some details are given in the following.

In most polycrystal models, a constitutive equation is used which is formulated at the level of the grain. The strain rate in this equation can be related to the stress:

$$\dot{\varepsilon}_g = \dot{\gamma}_0 \sum_s m_s \left(\left|m_s\, \sigma_g\right|/\tau_s^c\right)^n sgn\,(m_s\, \sigma_g) \qquad \text{(A.1)}$$

$\dot{\gamma}_0$ is the effective shear step size, m_s are the Schmid tensors, σ_g is grain level stress, *s* is the slip system and *sgn* denotes the direction of the resolved stress on the slip system. n is the strain rate sensitivity exponent. The threshold stresses τ_s^c is the required stress to activate the *sth* slip (or

twin) system. The values of threshold stresses τ_s^c can be constant during plastic deformation, or may follow an the Voce hardening rule as a function of accumulated shear strain Γ_g :

$$\tau_s^c(\Gamma_g) = \tau_s^0 + (\tau_s^1 + \theta_s^1 \Gamma_g) \{1 - exp(-\Gamma_g \theta_s^0 / \tau_s^1)\} \quad \text{(A.2)}$$

τ_s^0 and τ_s^1 are the initial and back-extrapolated increase in the threshold stress, and θ_s^0 and θ_s^1 are the initial and final slope of the hardening curve, respectively. In our simulations, the linear mode of Voce law was assumed in which the increase in critical resolved shear stresses is linear during deformation.

To calculate the averaged magnitudes of stress and strain rate in the polycrystal during deformation, the self-consistent model based on the Eshelby inclusion problem is used. In this model, the stress and strain rates magnitudes of the grain are obtained during each deformation increment so that both Eq. (A.2) and the self-consistency criteria are satisfied. To satisfy the self-consistency criteria, the volumetric averages of the grain stress and strain rate magnitudes must be consistent with the boundary conditions imposed on the polycrystal.

In between each straining step, the orientation and magnitude of stress of the grain are updated. The method, which was briefly explained, is the visco-plastic self-consistent (VPSC) model. The details of this visco-plastic self-consistent polycrystal model can be found in Lebensohn and Tomé [1] and Tomé and Lebensohn [2].

In Eshelby inclusion problem, each grain is considered as an inclusion embedded in a homogenous matrix (polycrystal) [3]. This ellipsoidal inclusion which is supposed to deform, is removed from the matrix. Under these conditions, the matrix stress and strain are zero but the inclusion is able to deform with no constraint. The strain in the inclusion under aforementioned situation is referred to as eigenstrain. The next step is to apply a force on the inclusion to return it to the original form. At the final stage, the inclusion is put back inside the matrix and the applied force on the inclusion (the force that applied in the previous step) is removed. After removal of the force, the inclusion can obtain the state which corresponds to the proposed problem. The solution of the Eshelby problem, which is the stress state of the matrix and inclusion, can be now obtained. Due to the iterative nature of the method, obtaining the solution for Eshelby inclusion problem may be a lengthy process and take a relatively long time.

The results of the simulations performed in this study, which are in facts some of the outputs of VPSC simulations such as simulated textures and activity diagrams, are presented and discussed in details in Chapters 4 and 5 for shock loaded AZ31B and WE43 alloys, respectively.

References

[1] Lebensohn RA, Tomé CN. A self-consistent anisotropic approach for the simulation of plastic deformation and texture development of polycrystals: application to zirconium alloys. Acta Metallurgica et Materialia 1993; 41: 2611–2624.

[2] Tomé CN, Lebensohn RA. Manual for Code Visco-Plastic Self-Consistent (VPSC) (Version 7c). Los Alamos National Laboratory 2009; USA.

[3] Eshelby JD. The determination of the elastic field of an ellipsoidal inclusion, and related problems. Proceedings of the Royal Society 1957; 241 A: 376–396.

Appendix B

COPY RIGHT PERMISSION

For previously published manuscripts that form a part of a thesis, written permission from the publisher (copyright holder) is required by the College of Graduate Studies and Research (CGSR). All of the manuscripts used in this thesis were published or are under review in the Elsevier's journals. Therefore, this appendix includes the copyright permissions from the Elsevier for each of the papers in this thesis. Also, the below quotation, which is copied from the Elsevier website in February 2014, is applicable for all enclosed manuscripts in the thesis.
(https://help.elsevier.com/app/answers/detail/a_id/565/session/L3RpbWUv/p/8045)

"*As an author, you retain rights for a large number of author uses, including use by your employing institute or company. These rights are retained and permitted without the need to obtain specific permission from Elsevier. These include:*

- *The right to make copies of the article for your own personal use, including for your own classroom teaching use.*
- *The right to make copies and distribute copies (including through e-mail) of the article to research colleagues, for the personal use by such colleagues (but not commercially or systematically, e.g. via an e-mail list or list serve).*
- *The right to post a pre-print version of the article on Internet web sites including electronic pre-print servers, and to retain indefinitely such version on such servers or sites (see also our information on electronic preprints for a more detailed discussion on these points.).*
- *The right to post a revised personal version of the text of the final article (to reflect changes made in the peer review process) on the author's personal or institutional web site or server, with a link to the journal home page (on elsevier.com).*
- *The right to present the article at a meeting or conference and to distribute copies of such paper or article to the delegates attending the meeting.*
- *For the author's employer, if the article is a 'work for hire', made within the scope of the author's employment, the right to use all or part of the information in (any version of) the article for other intra-company use (e.g. training).*
- *Patent and trademark rights and rights to any process or procedure described in the article.*

- *The right to include the article in full or in part in a thesis or dissertation (provided that this is not to be published commercially).*
- *The right to use the article or any part thereof in a printed compilation of works of the author, such as collected writings or lecture notes (subsequent to publication of the article in the journal).*
- *The right to prepare other derivative works, to extend the article into book-length form, or to otherwise re-use portions or excerpts in other works, with full acknowledgement of its original publication in the journal."*

Copyright Permission for Fig. 1.1 (Chapter 1)

AIST

Public Relations Department
National Institute of Advanced
Industrial Science and Technology
AIST Central-2, Umezono 1-1-1
Tsukuba, Japan 305-8563

Request to Reprint Copyrighted Material

Please complete this form and return to AIST by e-mail.

Name: Hamed_____Title: Asgari Moslehabadi_____
Organization: University of Saskatchewan
Department of Mechanical Engineering
Address: Department of Mechanical Engineering, University of Saskatchewan, 57 Campus Drive
City: Saskatoon_____State: SK_____
Zip: S7N5A9_____
Country: Canada_____
Phone: 3063614637_____Fax:____E-mail: hamed.asgari@usask.ca_____

Please check all intended uses.

__Personal
__Commercial
*__Educational
__News Reporting
__Comment/criticism
__Scholarship/Research

Description of item to be copied:

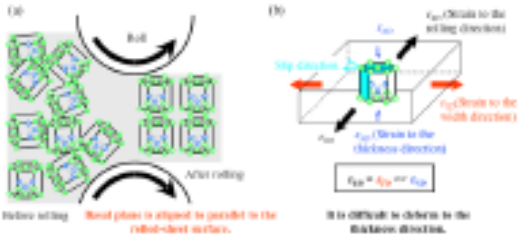

Title: Figure 3
Publication:
http://www.aist.go.jp/aist_e/latest_research/2008/20081105/20081105.html
Volume & number:_____
Copyright date:_____Page number(s):_____Number of copies: _____
Describe in detail how the copies will be used and distributed, and media to be used: I need to use this Figure (Fig.3(a)) in the "introduction" chapter of my PhD thesis, in both print and electronic versions. After, defense, the electronic version will be available on the website of the university and some printed copied may be distributed among the reviewers of my PhD thesis._____
Name of author: Hamed Asgari Moslehabadi_____
Estimated publication date: September 2015_____
Price/value of publication (in yen): no fee_____
Signature: Hamed Asgari Moslehabadi_____Date: Feb 16th, 2015_____
Please grant permission by (specify date needed): February 25th, 2015._____
Please check your desired delivery method and data format as shown below.

__CD-R __FD __MO __*E-mail attachment
__EPS __jpg __pdf __*tiff

Reprint Permission Approval of Copyrighted Material

__X__AIST, the copyright owner, grants permission for the item(s) described above to be reprinted, subject to the above listed conditions (i.e. number of copies, specific usage, etc.). The user must give credit to AIST by using either "courtesy of AIST" or "cAIST" and include our web site, http://www.aist.go.jp No modifications to the graphic images (photograph and drawings) are allowed except enlargement and reduction. Trimming and further modification is prohibited. For printed materials, please send us one copy or photocopy of the pages with the above requested items. At the time of the application if there is additional reprints or conditions change, the user must make another application.

__AIST, the copyright owner of the item(s) described above hereby denies the request to reprint such items.

Name: Masahiro Seto Title: Director-General, Public Relations Department

Signature: omitted Date: February 18, 2015

Copyright Permission for Fig. 1.2 (Chapter 1)

ELSEVIER LICENSE
TERMS AND CONDITIONS

Feb 09, 2015

This is a License Agreement between Hamed Asgari Moslehabadi ("You") and Elsevier ("Elsevier") provided by Copyright Clearance Center ("CCC"). The license consists of your order details, the terms and conditions provided by Elsevier, and the payment terms and conditions.

All payments must be made in full to CCC. For payment instructions, please see information listed at the bottom of this form.

Supplier	Elsevier Limited The Boulevard,Langford Lane Kidlington,Oxford,OX5 1GB,UK
Registered Company Number	1982084
Customer name	Hamed Asgari Moslehabadi
Customer address	Department of Mechanical Engineering, Saskatoon, SK S7N 5A9
License number	3564881325937
License date	Feb 09, 2015
Licensed content publisher	Elsevier
Licensed content publication	Computational Materials Science
Licensed content title	Influence of twinning deformation and lattice rotation on strength differential effect in polycrystalline pure magnesium with rolling texture
Licensed content author	Tsuyoshi Mayama,Kazuya Aizawa,Yuichi Tadano,Mitsutoshi Kuroda
Licensed content date	December 2009
Licensed content volume number	47
Licensed content issue number	2
Number of pages	8
Start Page	448
End Page	455
Type of Use	reuse in a thesis/dissertation
Portion	figures/tables/illustrations
Number of figures/tables/illustrations	1
Format	both print and electronic

Are you the author of this Elsevier article?	No
Will you be translating?	No
Original figure numbers	Fig. 1
Title of your thesis/dissertation	DYNAMIC MECHANICAL BEHAVIOR OF MAGNESIUM ALLOYS UNDER SHOCK LOADING CONDITIONS
Expected completion date	Jun 2015
Estimated size (number of pages)	200
Elsevier VAT number	GB 494 6272 12
Permissions price	0.00 USD
VAT/Local Sales Tax	0.00 USD / 0.00 GBP
Total	0.00 USD
Terms and Conditions	

INTRODUCTION

1. The publisher for this copyrighted material is Elsevier. By clicking "accept" in connection with completing this licensing transaction, you agree that the following terms and conditions apply to this transaction (along with the Billing and Payment terms and conditions established by Copyright Clearance Center, Inc. ("CCC"), at the time that you opened your Rightslink account and that are available at any time at http://myaccount.copyright.com).

GENERAL TERMS

2. Elsevier hereby grants you permission to reproduce the aforementioned material subject to the terms and conditions indicated.

3. Acknowledgement: If any part of the material to be used (for example, figures) has appeared in our publication with credit or acknowledgement to another source, permission must also be sought from that source. If such permission is not obtained then that material may not be included in your publication/copies. Suitable acknowledgement to the source must be made, either as a footnote or in a reference list at the end of your publication, as follows:

"Reprinted from Publication title, Vol /edition number, Author(s), Title of article / title of chapter, Pages No., Copyright (Year), with permission from Elsevier [OR APPLICABLE SOCIETY COPYRIGHT OWNER]." Also Lancet special credit - "Reprinted from The Lancet, Vol. number, Author(s), Title of article, Pages No., Copyright (Year), with permission from Elsevier."

4. Reproduction of this material is confined to the purpose and/or media for which permission is hereby given.

5. Altering/Modifying Material: Not Permitted. However figures and illustrations may be altered/adapted minimally to serve your work. Any other abbreviations, additions, deletions and/or any other alterations shall be made only with prior written authorization of Elsevier Ltd. (Please contact Elsevier at permissions@elsevier.com)

6. If the permission fee for the requested use of our material is waived in this instance, please be advised that your future requests for Elsevier materials may attract a fee.

7. Reservation of Rights: Publisher reserves all rights not specifically granted in the combination of (i) the license details provided by you and accepted in the course of this licensing transaction, (ii) these terms and conditions and (iii) CCC's Billing and Payment terms and conditions.

8. License Contingent Upon Payment: While you may exercise the rights licensed immediately upon issuance of the license at the end of the licensing process for the transaction, provided that you have disclosed complete and accurate details of your proposed use, no license is finally effective unless and until full payment is received from you (either by publisher or by CCC) as provided in CCC's Billing and Payment terms and conditions. If full payment is not received on a timely basis, then any license preliminarily granted shall be deemed automatically revoked and shall be void as if never granted. Further, in the event that you breach any of these terms and conditions or any of CCC's Billing and Payment terms and conditions, the license is automatically revoked and shall be void as if never granted. Use of materials as described in a revoked license, as well as any use of the materials beyond the scope of an unrevoked license, may constitute copyright infringement and publisher reserves the right to take any and all action to protect its copyright in the materials.

9. Warranties: Publisher makes no representations or warranties with respect to the licensed material.

10. Indemnity: You hereby indemnify and agree to hold harmless publisher and CCC, and their respective officers, directors, employees and agents, from and against any and all claims arising out of your use of the licensed material other than as specifically authorized pursuant to this license.

11. No Transfer of License: This license is personal to you and may not be sublicensed, assigned, or transferred by you to any other person without publisher's written permission.

12. No Amendment Except in Writing: This license may not be amended except in a writing signed by both parties (or, in the case of publisher, by CCC on publisher's behalf).

13. Objection to Contrary Terms: Publisher hereby objects to any terms contained in any purchase order, acknowledgment, check endorsement or other writing prepared by you, which terms are inconsistent with these terms and conditions or CCC's Billing and Payment terms and conditions. These terms and conditions, together with CCC's Billing and Payment terms and conditions (which are incorporated herein), comprise the entire

agreement between you and publisher (and CCC) concerning this licensing transaction. In the event of any conflict between your obligations established by these terms and conditions and those established by CCC's Billing and Payment terms and conditions, these terms and conditions shall control.

14. Revocation: Elsevier or Copyright Clearance Center may deny the permissions described in this License at their sole discretion, for any reason or no reason, with a full refund payable to you. Notice of such denial will be made using the contact information provided by you. Failure to receive such notice will not alter or invalidate the denial. In no event will Elsevier or Copyright Clearance Center be responsible or liable for any costs, expenses or damage incurred by you as a result of a denial of your permission request, other than a refund of the amount(s) paid by you to Elsevier and/or Copyright Clearance Center for denied permissions.

LIMITED LICENSE

The following terms and conditions apply only to specific license types:

15. **Translation**: This permission is granted for non-exclusive world **English** rights only unless your license was granted for translation rights. If you licensed translation rights you may only translate this content into the languages you requested. A professional translator must perform all translations and reproduce the content word for word preserving the integrity of the article. If this license is to re-use 1 or 2 figures then permission is granted for non-exclusive world rights in all languages.

16. **Posting licensed content on any Website**: The following terms and conditions apply as follows: Licensing material from an Elsevier journal: All content posted to the web site must maintain the copyright information line on the bottom of each image; A hyper-text must be included to the Homepage of the journal from which you are licensing at http://www.sciencedirect.com/science/journal/xxxxx or the Elsevier homepage for books at http://www.elsevier.com; Central Storage: This license does not include permission for a scanned version of the material to be stored in a central repository such as that provided by Heron/XanEdu.

Licensing material from an Elsevier book: A hyper-text link must be included to the Elsevier homepage at http://www.elsevier.com . All content posted to the web site must maintain the copyright information line on the bottom of each image.

Posting licensed content on Electronic reserve: In addition to the above the following clauses are applicable: The web site must be password-protected and made available only to bona fide students registered on a relevant course. This permission is granted for 1 year only. You may obtain a new license for future website posting.

17.**For journal authors:** the following clauses are applicable in addition to the above: Permission granted is limited to the author accepted manuscript version* of your paper.

***Accepted Author Manuscript (AAM) Definition:** An accepted author manuscript (AAM) is the author's version of the manuscript of an article that has been accepted for publication and which may include any author-incorporated changes suggested through the processes of submission processing, peer review, and editor-author communications. AAMs do not include other publisher value-added contributions such as copy-editing, formatting, technical enhancements and (if relevant) pagination.

You are not allowed to download and post the published journal article (whether PDF or HTML, proof or final version), nor may you scan the printed edition to create an electronic version. A hyper-text must be included to the Homepage of the journal from which you are licensing at http://www.sciencedirect.com/science/journal/xxxxx. As part of our normal production process, you will receive an e-mail notice when your article appears on Elsevier's online service ScienceDirect (www.sciencedirect.com). That e-mail will include the article's Digital Object Identifier (DOI). This number provides the electronic link to the published article and should be included in the posting of your personal version. We ask that you wait until you receive this e-mail and have the DOI to do any posting.

18.**Posting to a repository:** Authors may post their AAM immediately to their employer's institutional repository for internal use only and may make their manuscript publically available after the journal-specific embargo period has ended.

Please also refer to Elsevier's Article Posting Policy for further information.

19. **For book authors** the following clauses are applicable in addition to the above: Authors are permitted to place a brief summary of their work online only.. You are not allowed to download and post the published electronic version of your chapter, nor may you scan the printed edition to create an electronic version. **Posting to a repository:** Authors are permitted to post a summary of their chapter only in their institution's repository.

20. **Thesis/Dissertation**: If your license is for use in a thesis/dissertation your thesis may be submitted to your institution in either print or electronic form. Should your thesis be published commercially, please reapply for permission. These requirements include permission for the Library and Archives of Canada to supply single copies, on demand, of the complete thesis and include permission for Proquest/UMI to supply single copies, on demand, of the complete thesis. Should your thesis be published commercially, please reapply for permission.

- Promotional purposes (advertising or marketing)
- Commercial exploitation (e.g. a product for sale or loan)
- Systematic distribution (for a fee or free of charge)

Please refer to Elsevier's Open Access Policy for further information.

21. **Other Conditions**:

v1.7

Questions? customercare@copyright.com or +1-855-239-3415 (toll free in the US) or +1-978-646-2777.

Gratis licenses (referencing $0 in the Total field) are free. Please retain this printable license for your reference. No payment is required.

Copyright Permission for Fig. 1.3 (Chapter 1)

SPRINGER LICENSE
TERMS AND CONDITIONS

Feb 09, 2015

This is a License Agreement between Hamed Asgari Moslehabadi ("You") and Springer ("Springer") provided by Copyright Clearance Center ("CCC"). The license consists of your order details, the terms and conditions provided by Springer, and the payment terms and conditions.

All payments must be made in full to CCC. For payment instructions, please see information listed at the bottom of this form.

License Number	3564890814169
License date	Feb 09, 2015
Licensed content publisher	Springer
Licensed content publication	Metallurgical and Materials Transactions A
Licensed content title	A taylor model based description of the proof stress of magnesium AZ31 during hot working
Licensed content author	M. R. Barnett
Licensed content date	Jan 1, 2003
Volume number	34
Issue number	9
Type of Use	Thesis/Dissertation
Portion	Figures
Author of this Springer article	No
Order reference number	None
Original figure numbers	Fig. 1
Title of your thesis / dissertation	DYNAMIC MECHANICAL BEHAVIOR OF MAGNESIUM ALLOYS UNDER SHOCK LOADING CONDITIONS
Expected completion date	Jun 2015
Estimated size(pages)	200
Total	0.00 USD
Terms and Conditions	

Introduction

The publisher for this copyrighted material is Springer Science + Business Media. By clicking "accept" in connection with completing this licensing transaction, you agree that the following terms and conditions apply to this transaction (along with the Billing and

Payment terms and conditions established by Copyright Clearance Center, Inc. ("CCC"), at the time that you opened your Rightslink account and that are available at any time at http://myaccount.copyright.com).

Limited License
With reference to your request to reprint in your thesis material on which Springer Science and Business Media control the copyright, permission is granted, free of charge, for the use indicated in your enquiry.

Licenses are for one-time use only with a maximum distribution equal to the number that you identified in the licensing process.

This License includes use in an electronic form, provided its password protected or on the university's intranet or repository, including UMI (according to the definition at the Sherpa website: http://www.sherpa.ac.uk/romeo/). For any other electronic use, please contact Springer at (permissions.dordrecht@springer.com or permissions.heidelberg@springer.com).

The material can only be used for the purpose of defending your thesis limited to university-use only. If the thesis is going to be published, permission needs to be re-obtained (selecting "book/textbook" as the type of use).

Although Springer holds copyright to the material and is entitled to negotiate on rights, this license is only valid, subject to a courtesy information to the author (address is given with the article/chapter) and provided it concerns original material which does not carry references to other sources (if material in question appears with credit to another source, authorization from that source is required as well).

Permission free of charge on this occasion does not prejudice any rights we might have to charge for reproduction of our copyrighted material in the future.

Altering/Modifying Material: Not Permitted
You may not alter or modify the material in any manner. Abbreviations, additions, deletions and/or any other alterations shall be made only with prior written authorization of the author(s) and/or Springer Science + Business Media. (Please contact Springer at (permissions.dordrecht@springer.com or permissions.heidelberg@springer.com)

Reservation of Rights
Springer Science + Business Media reserves all rights not specifically granted in the combination of (i) the license details provided by you and accepted in the course of this licensing transaction, (ii) these terms and conditions and (iii) CCC's Billing and Payment terms and conditions.

Copyright Notice:Disclaimer
You must include the following copyright and permission notice in connection with any reproduction of the licensed material: "Springer and the original publisher /journal title,

volume, year of publication, page, chapter/article title, name(s) of author(s), figure number(s), original copyright notice) is given to the publication in which the material was originally published, by adding; with kind permission from Springer Science and Business Media"

Warranties: None

Example 1: Springer Science + Business Media makes no representations or warranties with respect to the licensed material.

Example 2: Springer Science + Business Media makes no representations or warranties with respect to the licensed material and adopts on its own behalf the limitations and disclaimers established by CCC on its behalf in its Billing and Payment terms and conditions for this licensing transaction.

Indemnity
You hereby indemnify and agree to hold harmless Springer Science + Business Media and CCC, and their respective officers, directors, employees and agents, from and against any and all claims arising out of your use of the licensed material other than as specifically authorized pursuant to this license.

No Transfer of License
This license is personal to you and may not be sublicensed, assigned, or transferred by you to any other person without Springer Science + Business Media's written permission.

No Amendment Except in Writing
This license may not be amended except in a writing signed by both parties (or, in the case of Springer Science + Business Media, by CCC on Springer Science + Business Media's behalf).

Objection to Contrary Terms
Springer Science + Business Media hereby objects to any terms contained in any purchase order, acknowledgment, check endorsement or other writing prepared by you, which terms are inconsistent with these terms and conditions or CCC's Billing and Payment terms and conditions. These terms and conditions, together with CCC's Billing and Payment terms and conditions (which are incorporated herein), comprise the entire agreement between you and Springer Science + Business Media (and CCC) concerning this licensing transaction. In the event of any conflict between your obligations established by these terms and conditions and those established by CCC's Billing and Payment terms and conditions, these terms and conditions shall control.

Jurisdiction
All disputes that may arise in connection with this present License, or the breach thereof, shall be settled exclusively by arbitration, to be held in The Netherlands, in accordance with

Dutch law, and to be conducted under the Rules of the 'Netherlands Arbitrage Instituut' (Netherlands Institute of Arbitration).***OR:***

All disputes that may arise in connection with this present License, or the breach thereof, shall be settled exclusively by arbitration, to be held in the Federal Republic of Germany, in accordance with German law.

Other terms and conditions:

v1.3

Questions? customercare@copyright.com or +1-855-239-3415 (toll free in the US) or +1-978-646-2777.

Gratis licenses (referencing $0 in the Total field) are free. Please retain this printable license for your reference. No payment is required.

Copyright Permission for Fig. 1.5 (Chapter 1)

ELSEVIER LICENSE
TERMS AND CONDITIONS

Feb 09, 2015

This is a License Agreement between Hamed Asgari Moslehabadi ("You") and Elsevier ("Elsevier") provided by Copyright Clearance Center ("CCC"). The license consists of your order details, the terms and conditions provided by Elsevier, and the payment terms and conditions.

All payments must be made in full to CCC. For payment instructions, please see information listed at the bottom of this form.

Supplier	Elsevier Limited The Boulevard,Langford Lane Kidlington,Oxford,OX5 1GB,UK
Registered Company Number	1982084
Customer name	Hamed Asgari Moslehabadi
Customer address	Department of Mechanical Engineering, Saskatoon, SK S7N 5A9
License number	3564891019052
License date	Feb 09, 2015
Licensed content publisher	Elsevier
Licensed content publication	Scripta Materialia
Licensed content title	Anisotropic effects on the strain rate dependence of a wrought magnesium alloy
Licensed content author	None
Licensed content date	February 2009
Licensed content volume number	60
Licensed content issue number	3
Number of pages	4
Start Page	182
End Page	185
Type of Use	reuse in a thesis/dissertation
Intended publisher of new work	other
Portion	figures/tables/illustrations
Number of figures/tables/illustrations	1
Format	both print and electronic

Are you the author of this Elsevier article?	No
Will you be translating?	No
Original figure numbers	Fig.2
Title of your thesis/dissertation	DYNAMIC MECHANICAL BEHAVIOR OF MAGNESIUM ALLOYS UNDER SHOCK LOADING CONDITIONS
Expected completion date	Jun 2015
Estimated size (number of pages)	200
Elsevier VAT number	GB 494 6272 12
Permissions price	0.00 USD
VAT/Local Sales Tax	0.00 USD / 0.00 GBP
Total	0.00 USD
Terms and Conditions	

INTRODUCTION

1. The publisher for this copyrighted material is Elsevier. By clicking "accept" in connection with completing this licensing transaction, you agree that the following terms and conditions apply to this transaction (along with the Billing and Payment terms and conditions established by Copyright Clearance Center, Inc. ("CCC"), at the time that you opened your Rightslink account and that are available at any time at http://myaccount.copyright.com).

GENERAL TERMS

2. Elsevier hereby grants you permission to reproduce the aforementioned material subject to the terms and conditions indicated.

3. Acknowledgement: If any part of the material to be used (for example, figures) has appeared in our publication with credit or acknowledgement to another source, permission must also be sought from that source. If such permission is not obtained then that material may not be included in your publication/copies. Suitable acknowledgement to the source must be made, either as a footnote or in a reference list at the end of your publication, as follows:

"Reprinted from Publication title, Vol /edition number, Author(s), Title of article / title of chapter, Pages No., Copyright (Year), with permission from Elsevier [OR APPLICABLE SOCIETY COPYRIGHT OWNER]." Also Lancet special credit - "Reprinted from The Lancet, Vol. number, Author(s), Title of article, Pages No., Copyright (Year), with permission from Elsevier."

4. Reproduction of this material is confined to the purpose and/or media for which permission is hereby given.

5. Altering/Modifying Material: Not Permitted. However figures and illustrations may be altered/adapted minimally to serve your work. Any other abbreviations, additions, deletions and/or any other alterations shall be made only with prior written authorization of Elsevier Ltd. (Please contact Elsevier at permissions@elsevier.com)

6. If the permission fee for the requested use of our material is waived in this instance, please be advised that your future requests for Elsevier materials may attract a fee.

7. Reservation of Rights: Publisher reserves all rights not specifically granted in the combination of (i) the license details provided by you and accepted in the course of this licensing transaction, (ii) these terms and conditions and (iii) CCC's Billing and Payment terms and conditions.

8. License Contingent Upon Payment: While you may exercise the rights licensed immediately upon issuance of the license at the end of the licensing process for the transaction, provided that you have disclosed complete and accurate details of your proposed use, no license is finally effective unless and until full payment is received from you (either by publisher or by CCC) as provided in CCC's Billing and Payment terms and conditions. If full payment is not received on a timely basis, then any license preliminarily granted shall be deemed automatically revoked and shall be void as if never granted. Further, in the event that you breach any of these terms and conditions or any of CCC's Billing and Payment terms and conditions, the license is automatically revoked and shall be void as if never granted. Use of materials as described in a revoked license, as well as any use of the materials beyond the scope of an unrevoked license, may constitute copyright infringement and publisher reserves the right to take any and all action to protect its copyright in the materials.

9. Warranties: Publisher makes no representations or warranties with respect to the licensed material.

10. Indemnity: You hereby indemnify and agree to hold harmless publisher and CCC, and their respective officers, directors, employees and agents, from and against any and all claims arising out of your use of the licensed material other than as specifically authorized pursuant to this license.

11. No Transfer of License: This license is personal to you and may not be sublicensed, assigned, or transferred by you to any other person without publisher's written permission.

12. No Amendment Except in Writing: This license may not be amended except in a writing signed by both parties (or, in the case of publisher, by CCC on publisher's behalf).

13. Objection to Contrary Terms: Publisher hereby objects to any terms contained in any purchase order, acknowledgment, check endorsement or other writing prepared by you, which terms are inconsistent with these terms and conditions or CCC's Billing and Payment terms and conditions. These terms and conditions, together with CCC's Billing and Payment terms and conditions (which are incorporated herein), comprise the entire

agreement between you and publisher (and CCC) concerning this licensing transaction. In the event of any conflict between your obligations established by these terms and conditions and those established by CCC's Billing and Payment terms and conditions, these terms and conditions shall control.

14. Revocation: Elsevier or Copyright Clearance Center may deny the permissions described in this License at their sole discretion, for any reason or no reason, with a full refund payable to you. Notice of such denial will be made using the contact information provided by you. Failure to receive such notice will not alter or invalidate the denial. In no event will Elsevier or Copyright Clearance Center be responsible or liable for any costs, expenses or damage incurred by you as a result of a denial of your permission request, other than a refund of the amount(s) paid by you to Elsevier and/or Copyright Clearance Center for denied permissions.

LIMITED LICENSE

The following terms and conditions apply only to specific license types:

15. **Translation**: This permission is granted for non-exclusive world **English** rights only unless your license was granted for translation rights. If you licensed translation rights you may only translate this content into the languages you requested. A professional translator must perform all translations and reproduce the content word for word preserving the integrity of the article. If this license is to re-use 1 or 2 figures then permission is granted for non-exclusive world rights in all languages.

16. **Posting licensed content on any Website**: The following terms and conditions apply as follows: Licensing material from an Elsevier journal: All content posted to the web site must maintain the copyright information line on the bottom of each image; A hyper-text must be included to the Homepage of the journal from which you are licensing at http://www.sciencedirect.com/science/journal/xxxxx or the Elsevier homepage for books at http://www.elsevier.com; Central Storage: This license does not include permission for a scanned version of the material to be stored in a central repository such as that provided by Heron/XanEdu.

Licensing material from an Elsevier book: A hyper-text link must be included to the Elsevier homepage at http://www.elsevier.com . All content posted to the web site must maintain the copyright information line on the bottom of each image.

Posting licensed content on Electronic reserve: In addition to the above the following clauses are applicable: The web site must be password-protected and made available only to bona fide students registered on a relevant course. This permission is granted for 1 year only. You may obtain a new license for future website posting.

17.**For journal authors:** the following clauses are applicable in addition to the above: Permission granted is limited to the author accepted manuscript version* of your paper.

***Accepted Author Manuscript (AAM) Definition:** An accepted author manuscript (AAM) is the author's version of the manuscript of an article that has been accepted for publication and which may include any author-incorporated changes suggested through the processes of submission processing, peer review, and editor-author communications. AAMs do not include other publisher value-added contributions such as copy-editing, formatting, technical enhancements and (if relevant) pagination.

You are not allowed to download and post the published journal article (whether PDF or HTML, proof or final version), nor may you scan the printed edition to create an electronic version. A hyper-text must be included to the Homepage of the journal from which you are licensing at http://www.sciencedirect.com/science/journal/xxxxx. As part of our normal production process, you will receive an e-mail notice when your article appears on Elsevier's online service ScienceDirect (www.sciencedirect.com). That e-mail will include the article's Digital Object Identifier (DOI). This number provides the electronic link to the published article and should be included in the posting of your personal version. We ask that you wait until you receive this e-mail and have the DOI to do any posting.

18.**Posting to a repository:** Authors may post their AAM immediately to their employer's institutional repository for internal use only and may make their manuscript publically available after the journal-specific embargo period has ended.

Please also refer to Elsevier's Article Posting Policy for further information.

19. **For book authors** the following clauses are applicable in addition to the above: Authors are permitted to place a brief summary of their work online only.. You are not allowed to download and post the published electronic version of your chapter, nor may you scan the printed edition to create an electronic version. **Posting to a repository:** Authors are permitted to post a summary of their chapter only in their institution's repository.

20. **Thesis/Dissertation**: If your license is for use in a thesis/dissertation your thesis may be submitted to your institution in either print or electronic form. Should your thesis be published commercially, please reapply for permission. These requirements include permission for the Library and Archives of Canada to supply single copies, on demand, of the complete thesis and include permission for Proquest/UMI to supply single copies, on demand, of the complete thesis. Should your thesis be published commercially, please reapply for permission.

Elsevier Open Access Terms and Conditions

Elsevier publishes Open Access articles in both its Open Access journals and via its Open Access articles option in subscription journals.

Authors publishing in an Open Access journal or who choose to make their article Open Access in an Elsevier subscription journal select one of the following Creative Commons user licenses, which define how a reader may reuse their work: Creative Commons Attribution License (CC BY), Creative Commons Attribution – Non Commercial - ShareAlike (CC BY NC SA) and Creative Commons Attribution – Non Commercial – No Derivatives (CC BY NC ND)

Terms & Conditions applicable to all Elsevier Open Access articles:

Any reuse of the article must not represent the author as endorsing the adaptation of the article nor should the article be modified in such a way as to damage the author's honour or reputation.

The author(s) must be appropriately credited.

If any part of the material to be used (for example, figures) has appeared in our publication with credit or acknowledgement to another source it is the responsibility of the user to ensure their reuse complies with the terms and conditions determined by the rights holder.

Additional Terms & Conditions applicable to each Creative Commons user license:

CC BY: You may distribute and copy the article, create extracts, abstracts, and other revised versions, adaptations or derivative works of or from an article (such as a translation), to include in a collective work (such as an anthology), to text or data mine the article, including for commercial purposes without permission from Elsevier

CC BY NC SA: For non-commercial purposes you may distribute and copy the article, create extracts, abstracts and other revised versions, adaptations or derivative works of or from an article (such as a translation), to include in a collective work (such as an anthology), to text and data mine the article and license new adaptations or creations under identical terms without permission from Elsevier

CC BY NC ND: For non-commercial purposes you may distribute and copy the article and include it in a collective work (such as an anthology), provided you do not alter or modify the article, without permission from Elsevier

Any commercial reuse of Open Access articles published with a CC BY NC SA or CC BY NC ND license requires permission from Elsevier and will be subject to a fee.

Commercial reuse includes:

- Promotional purposes (advertising or marketing)
- Commercial exploitation (e.g. a product for sale or loan)
- Systematic distribution (for a fee or free of charge)

Please refer to Elsevier's Open Access Policy for further information.

21. **Other Conditions**:

v1.7

Questions? customercare@copyright.com or +1-855-239-3415 (toll free in the US) or +1-978-646-2777.

Gratis licenses (referencing $0 in the Total field) are free. Please retain this printable license for your reference. No payment is required.

Copyright Permission for Fig. 1.6 (Chapter 1)

ELSEVIER LICENSE
TERMS AND CONDITIONS

Feb 09, 2015

This is a License Agreement between Hamed Asgari Moslehabadi ("You") and Elsevier ("Elsevier") provided by Copyright Clearance Center ("CCC"). The license consists of your order details, the terms and conditions provided by Elsevier, and the payment terms and conditions.

All payments must be made in full to CCC. For payment instructions, please see information listed at the bottom of this form.

Supplier	Elsevier Limited The Boulevard,Langford Lane Kidlington,Oxford,OX5 1GB,UK
Registered Company Number	1982084
Customer name	Hamed Asgari Moslehabadi
Customer address	Department of Mechanical Engineering, Saskatoon, SK S7N 5A9
License number	3564891240777
License date	Feb 09, 2015
Licensed content publisher	Elsevier
Licensed content publication	Acta Materialia
Licensed content title	Mechanical behavior and microstructural evolution of a Mg AZ31 sheet at dynamic strain rates
Licensed content author	I. Ulacia,N.V. Dudamell,F. Gálvez,S. Yi,M.T. Pérez-Prado,I. Hurtado
Licensed content date	May 2010
Licensed content volume number	58
Licensed content issue number	8
Number of pages	11
Start Page	2988
End Page	2998
Type of Use	reuse in a thesis/dissertation
Intended publisher of new work	other
Portion	figures/tables/illustrations
Number of figures/tables/illustrations	1
Format	both print and electronic

Are you the author of this Elsevier article?	No
Will you be translating?	No
Original figure numbers	Fig.3
Title of your thesis/dissertation	DYNAMIC MECHANICAL BEHAVIOR OF MAGNESIUM ALLOYS UNDER SHOCK LOADING CONDITIONS
Expected completion date	Jun 2015
Estimated size (number of pages)	200
Elsevier VAT number	GB 494 6272 12
Permissions price	0.00 USD
VAT/Local Sales Tax	0.00 USD / 0.00 GBP
Total	0.00 USD
Terms and Conditions	

INTRODUCTION

1. The publisher for this copyrighted material is Elsevier. By clicking "accept" in connection with completing this licensing transaction, you agree that the following terms and conditions apply to this transaction (along with the Billing and Payment terms and conditions established by Copyright Clearance Center, Inc. ("CCC"), at the time that you opened your Rightslink account and that are available at any time at http://myaccount.copyright.com).

GENERAL TERMS

2. Elsevier hereby grants you permission to reproduce the aforementioned material subject to the terms and conditions indicated.

3. Acknowledgement: If any part of the material to be used (for example, figures) has appeared in our publication with credit or acknowledgement to another source, permission must also be sought from that source. If such permission is not obtained then that material may not be included in your publication/copies. Suitable acknowledgement to the source must be made, either as a footnote or in a reference list at the end of your publication, as follows:

"Reprinted from Publication title, Vol /edition number, Author(s), Title of article / title of chapter, Pages No., Copyright (Year), with permission from Elsevier [OR APPLICABLE SOCIETY COPYRIGHT OWNER]." Also Lancet special credit - "Reprinted from The Lancet, Vol. number, Author(s), Title of article, Pages No., Copyright (Year), with permission from Elsevier."

4. Reproduction of this material is confined to the purpose and/or media for which permission is hereby given.

5. Altering/Modifying Material: Not Permitted. However figures and illustrations may be altered/adapted minimally to serve your work. Any other abbreviations, additions, deletions and/or any other alterations shall be made only with prior written authorization of Elsevier Ltd. (Please contact Elsevier at permissions@elsevier.com)

6. If the permission fee for the requested use of our material is waived in this instance, please be advised that your future requests for Elsevier materials may attract a fee.

7. Reservation of Rights: Publisher reserves all rights not specifically granted in the combination of (i) the license details provided by you and accepted in the course of this licensing transaction, (ii) these terms and conditions and (iii) CCC's Billing and Payment terms and conditions.

8. License Contingent Upon Payment: While you may exercise the rights licensed immediately upon issuance of the license at the end of the licensing process for the transaction, provided that you have disclosed complete and accurate details of your proposed use, no license is finally effective unless and until full payment is received from you (either by publisher or by CCC) as provided in CCC's Billing and Payment terms and conditions. If full payment is not received on a timely basis, then any license preliminarily granted shall be deemed automatically revoked and shall be void as if never granted. Further, in the event that you breach any of these terms and conditions or any of CCC's Billing and Payment terms and conditions, the license is automatically revoked and shall be void as if never granted. Use of materials as described in a revoked license, as well as any use of the materials beyond the scope of an unrevoked license, may constitute copyright infringement and publisher reserves the right to take any and all action to protect its copyright in the materials.

9. Warranties: Publisher makes no representations or warranties with respect to the licensed material.

10. Indemnity: You hereby indemnify and agree to hold harmless publisher and CCC, and their respective officers, directors, employees and agents, from and against any and all claims arising out of your use of the licensed material other than as specifically authorized pursuant to this license.

11. No Transfer of License: This license is personal to you and may not be sublicensed, assigned, or transferred by you to any other person without publisher's written permission.

12. No Amendment Except in Writing: This license may not be amended except in a writing signed by both parties (or, in the case of publisher, by CCC on publisher's behalf).

13. Objection to Contrary Terms: Publisher hereby objects to any terms contained in any purchase order, acknowledgment, check endorsement or other writing prepared by you, which terms are inconsistent with these terms and conditions or CCC's Billing and Payment terms and conditions. These terms and conditions, together with CCC's Billing and Payment terms and conditions (which are incorporated herein), comprise the entire

agreement between you and publisher (and CCC) concerning this licensing transaction. In the event of any conflict between your obligations established by these terms and conditions and those established by CCC's Billing and Payment terms and conditions, these terms and conditions shall control.

14. Revocation: Elsevier or Copyright Clearance Center may deny the permissions described in this License at their sole discretion, for any reason or no reason, with a full refund payable to you. Notice of such denial will be made using the contact information provided by you. Failure to receive such notice will not alter or invalidate the denial. In no event will Elsevier or Copyright Clearance Center be responsible or liable for any costs, expenses or damage incurred by you as a result of a denial of your permission request, other than a refund of the amount(s) paid by you to Elsevier and/or Copyright Clearance Center for denied permissions.

LIMITED LICENSE

The following terms and conditions apply only to specific license types:

15. **Translation**: This permission is granted for non-exclusive world **English** rights only unless your license was granted for translation rights. If you licensed translation rights you may only translate this content into the languages you requested. A professional translator must perform all translations and reproduce the content word for word preserving the integrity of the article. If this license is to re-use 1 or 2 figures then permission is granted for non-exclusive world rights in all languages.

16. **Posting licensed content on any Website**: The following terms and conditions apply as follows: Licensing material from an Elsevier journal: All content posted to the web site must maintain the copyright information line on the bottom of each image; A hyper-text must be included to the Homepage of the journal from which you are licensing at http://www.sciencedirect.com/science/journal/xxxxx or the Elsevier homepage for books at http://www.elsevier.com; Central Storage: This license does not include permission for a scanned version of the material to be stored in a central repository such as that provided by Heron/XanEdu.

Licensing material from an Elsevier book: A hyper-text link must be included to the Elsevier homepage at http://www.elsevier.com . All content posted to the web site must maintain the copyright information line on the bottom of each image.

Posting licensed content on Electronic reserve: In addition to the above the following clauses are applicable: The web site must be password-protected and made available only to bona fide students registered on a relevant course. This permission is granted for 1 year only. You may obtain a new license for future website posting.

17.**For journal authors:** the following clauses are applicable in addition to the above: Permission granted is limited to the author accepted manuscript version* of your paper.

***Accepted Author Manuscript (AAM) Definition:** An accepted author manuscript (AAM) is the author's version of the manuscript of an article that has been accepted for publication and which may include any author-incorporated changes suggested through the processes of submission processing, peer review, and editor-author communications. AAMs do not include other publisher value-added contributions such as copy-editing, formatting, technical enhancements and (if relevant) pagination.

You are not allowed to download and post the published journal article (whether PDF or HTML, proof or final version), nor may you scan the printed edition to create an electronic version. A hyper-text must be included to the Homepage of the journal from which you are licensing at http://www.sciencedirect.com/science/journal/xxxxx. As part of our normal production process, you will receive an e-mail notice when your article appears on Elsevier's online service ScienceDirect (www.sciencedirect.com). That e-mail will include the article's Digital Object Identifier (DOI). This number provides the electronic link to the published article and should be included in the posting of your personal version. We ask that you wait until you receive this e-mail and have the DOI to do any posting.

18.**Posting to a repository:** Authors may post their AAM immediately to their employer's institutional repository for internal use only and may make their manuscript publically available after the journal-specific embargo period has ended.

Please also refer to Elsevier's Article Posting Policy for further information.

19. **For book authors** the following clauses are applicable in addition to the above: Authors are permitted to place a brief summary of their work online only.. You are not allowed to download and post the published electronic version of your chapter, nor may you scan the printed edition to create an electronic version. **Posting to a repository:** Authors are permitted to post a summary of their chapter only in their institution's repository.

20. **Thesis/Dissertation**: If your license is for use in a thesis/dissertation your thesis may be submitted to your institution in either print or electronic form. Should your thesis be published commercially, please reapply for permission. These requirements include permission for the Library and Archives of Canada to supply single copies, on demand, of the complete thesis and include permission for Proquest/UMI to supply single copies, on demand, of the complete thesis. Should your thesis be published commercially, please reapply for permission.

Elsevier Open Access Terms and Conditions

Elsevier publishes Open Access articles in both its Open Access journals and via its Open Access articles option in subscription journals.

Authors publishing in an Open Access journal or who choose to make their article Open Access in an Elsevier subscription journal select one of the following Creative Commons user licenses, which define how a reader may reuse their work: Creative Commons Attribution License (CC BY), Creative Commons Attribution – Non Commercial - ShareAlike (CC BY NC SA) and Creative Commons Attribution – Non Commercial – No Derivatives (CC BY NC ND)

Terms & Conditions applicable to all Elsevier Open Access articles:

Any reuse of the article must not represent the author as endorsing the adaptation of the article nor should the article be modified in such a way as to damage the author's honour or reputation.

The author(s) must be appropriately credited.

If any part of the material to be used (for example, figures) has appeared in our publication with credit or acknowledgement to another source it is the responsibility of the user to ensure their reuse complies with the terms and conditions determined by the rights holder.

Additional Terms & Conditions applicable to each Creative Commons user license:

CC BY: You may distribute and copy the article, create extracts, abstracts, and other revised versions, adaptations or derivative works of or from an article (such as a translation), to include in a collective work (such as an anthology), to text or data mine the article, including for commercial purposes without permission from Elsevier

CC BY NC SA: For non-commercial purposes you may distribute and copy the article, create extracts, abstracts and other revised versions, adaptations or derivative works of or from an article (such as a translation), to include in a collective work (such as an anthology), to text and data mine the article and license new adaptations or creations under identical terms without permission from Elsevier

CC BY NC ND: For non-commercial purposes you may distribute and copy the article and include it in a collective work (such as an anthology), provided you do not alter or modify the article, without permission from Elsevier

Any commercial reuse of Open Access articles published with a CC BY NC SA or CC BY NC ND license requires permission from Elsevier and will be subject to a fee.

Commercial reuse includes:

- Promotional purposes (advertising or marketing)
- Commercial exploitation (e.g. a product for sale or loan)
- Systematic distribution (for a fee or free of charge)

Please refer to Elsevier's Open Access Policy for further information.

21. **Other Conditions**:

v1.7

Questions? customercare@copyright.com or +1-855-239-3415 (toll free in the US) or +1-978-646-2777.

Gratis licenses (referencing $0 in the Total field) are free. Please retain this printable license for your reference. No payment is required.

Copyright Permission for Fig. 1.7 (Chapter 1)

ELSEVIER LICENSE
TERMS AND CONDITIONS

Feb 09, 2015

This is a License Agreement between Hamed Asgari Moslehabadi ("You") and Elsevier ("Elsevier") provided by Copyright Clearance Center ("CCC"). The license consists of your order details, the terms and conditions provided by Elsevier, and the payment terms and conditions.

All payments must be made in full to CCC. For payment instructions, please see information listed at the bottom of this form.

Supplier	Elsevier Limited The Boulevard,Langford Lane Kidlington,Oxford,OX5 1GB,UK
Registered Company Number	1982084
Customer name	Hamed Asgari Moslehabadi
Customer address	Department of Mechanical Engineering, Saskatoon, SK S7N 5A9
License number	3564900430457
License date	Feb 09, 2015
Licensed content publisher	Elsevier
Licensed content publication	Materials Science and Engineering: A
Licensed content title	Effect of texture on high temperature deformation behavior at high strain rates in a Mg–3Al–1Zn alloy
Licensed content author	None
Licensed content date	15 October 2009
Licensed content volume number	523
Licensed content issue number	1-2
Number of pages	8
Start Page	304
End Page	311
Type of Use	reuse in a thesis/dissertation
Intended publisher of new work	other
Portion	figures/tables/illustrations
Number of figures/tables/illustrations	1
Format	both print and electronic

Are you the author of this Elsevier article?	No
Will you be translating?	No
Original figure numbers	Fig.8
Title of your thesis/dissertation	DYNAMIC MECHANICAL BEHAVIOR OF MAGNESIUM ALLOYS UNDER SHOCK LOADING CONDITIONS
Expected completion date	Jun 2015
Estimated size (number of pages)	200
Elsevier VAT number	GB 494 6272 12
Permissions price	0.00 USD
VAT/Local Sales Tax	0.00 USD / 0.00 GBP
Total	0.00 USD
Terms and Conditions	

INTRODUCTION

1. The publisher for this copyrighted material is Elsevier. By clicking "accept" in connection with completing this licensing transaction, you agree that the following terms and conditions apply to this transaction (along with the Billing and Payment terms and conditions established by Copyright Clearance Center, Inc. ("CCC"), at the time that you opened your Rightslink account and that are available at any time at http://myaccount.copyright.com).

GENERAL TERMS

2. Elsevier hereby grants you permission to reproduce the aforementioned material subject to the terms and conditions indicated.

3. Acknowledgement: If any part of the material to be used (for example, figures) has appeared in our publication with credit or acknowledgement to another source, permission must also be sought from that source. If such permission is not obtained then that material may not be included in your publication/copies. Suitable acknowledgement to the source must be made, either as a footnote or in a reference list at the end of your publication, as follows:

"Reprinted from Publication title, Vol /edition number, Author(s), Title of article / title of chapter, Pages No., Copyright (Year), with permission from Elsevier [OR APPLICABLE SOCIETY COPYRIGHT OWNER]." Also Lancet special credit - "Reprinted from The Lancet, Vol. number, Author(s), Title of article, Pages No., Copyright (Year), with permission from Elsevier."

4. Reproduction of this material is confined to the purpose and/or media for which permission is hereby given.

5. Altering/Modifying Material: Not Permitted. However figures and illustrations may be altered/adapted minimally to serve your work. Any other abbreviations, additions, deletions and/or any other alterations shall be made only with prior written authorization of Elsevier Ltd. (Please contact Elsevier at permissions@elsevier.com)

6. If the permission fee for the requested use of our material is waived in this instance, please be advised that your future requests for Elsevier materials may attract a fee.

7. Reservation of Rights: Publisher reserves all rights not specifically granted in the combination of (i) the license details provided by you and accepted in the course of this licensing transaction, (ii) these terms and conditions and (iii) CCC's Billing and Payment terms and conditions.

8. License Contingent Upon Payment: While you may exercise the rights licensed immediately upon issuance of the license at the end of the licensing process for the transaction, provided that you have disclosed complete and accurate details of your proposed use, no license is finally effective unless and until full payment is received from you (either by publisher or by CCC) as provided in CCC's Billing and Payment terms and conditions. If full payment is not received on a timely basis, then any license preliminarily granted shall be deemed automatically revoked and shall be void as if never granted. Further, in the event that you breach any of these terms and conditions or any of CCC's Billing and Payment terms and conditions, the license is automatically revoked and shall be void as if never granted. Use of materials as described in a revoked license, as well as any use of the materials beyond the scope of an unrevoked license, may constitute copyright infringement and publisher reserves the right to take any and all action to protect its copyright in the materials.

9. Warranties: Publisher makes no representations or warranties with respect to the licensed material.

10. Indemnity: You hereby indemnify and agree to hold harmless publisher and CCC, and their respective officers, directors, employees and agents, from and against any and all claims arising out of your use of the licensed material other than as specifically authorized pursuant to this license.

11. No Transfer of License: This license is personal to you and may not be sublicensed, assigned, or transferred by you to any other person without publisher's written permission.

12. No Amendment Except in Writing: This license may not be amended except in a writing signed by both parties (or, in the case of publisher, by CCC on publisher's behalf).

13. Objection to Contrary Terms: Publisher hereby objects to any terms contained in any purchase order, acknowledgment, check endorsement or other writing prepared by you, which terms are inconsistent with these terms and conditions or CCC's Billing and Payment terms and conditions. These terms and conditions, together with CCC's Billing and Payment terms and conditions (which are incorporated herein), comprise the entire

agreement between you and publisher (and CCC) concerning this licensing transaction. In the event of any conflict between your obligations established by these terms and conditions and those established by CCC's Billing and Payment terms and conditions, these terms and conditions shall control.

14. Revocation: Elsevier or Copyright Clearance Center may deny the permissions described in this License at their sole discretion, for any reason or no reason, with a full refund payable to you. Notice of such denial will be made using the contact information provided by you. Failure to receive such notice will not alter or invalidate the denial. In no event will Elsevier or Copyright Clearance Center be responsible or liable for any costs, expenses or damage incurred by you as a result of a denial of your permission request, other than a refund of the amount(s) paid by you to Elsevier and/or Copyright Clearance Center for denied permissions.

LIMITED LICENSE

The following terms and conditions apply only to specific license types:

15. **Translation**: This permission is granted for non-exclusive world **English** rights only unless your license was granted for translation rights. If you licensed translation rights you may only translate this content into the languages you requested. A professional translator must perform all translations and reproduce the content word for word preserving the integrity of the article. If this license is to re-use 1 or 2 figures then permission is granted for non-exclusive world rights in all languages.

16. **Posting licensed content on any Website**: The following terms and conditions apply as follows: Licensing material from an Elsevier journal: All content posted to the web site must maintain the copyright information line on the bottom of each image; A hyper-text must be included to the Homepage of the journal from which you are licensing at http://www.sciencedirect.com/science/journal/xxxxx or the Elsevier homepage for books at http://www.elsevier.com; Central Storage: This license does not include permission for a scanned version of the material to be stored in a central repository such as that provided by Heron/XanEdu.

Licensing material from an Elsevier book: A hyper-text link must be included to the Elsevier homepage at http://www.elsevier.com . All content posted to the web site must maintain the copyright information line on the bottom of each image.

Posting licensed content on Electronic reserve: In addition to the above the following clauses are applicable: The web site must be password-protected and made available only to bona fide students registered on a relevant course. This permission is granted for 1 year only. You may obtain a new license for future website posting.

17.**For journal authors:** the following clauses are applicable in addition to the above: Permission granted is limited to the author accepted manuscript version* of your paper.

***Accepted Author Manuscript (AAM) Definition:** An accepted author manuscript (AAM) is the author's version of the manuscript of an article that has been accepted for publication and which may include any author-incorporated changes suggested through the processes of submission processing, peer review, and editor-author communications. AAMs do not include other publisher value-added contributions such as copy-editing, formatting, technical enhancements and (if relevant) pagination.

You are not allowed to download and post the published journal article (whether PDF or HTML, proof or final version), nor may you scan the printed edition to create an electronic version. A hyper-text must be included to the Homepage of the journal from which you are licensing at http://www.sciencedirect.com/science/journal/xxxxx. As part of our normal production process, you will receive an e-mail notice when your article appears on Elsevier's online service ScienceDirect (www.sciencedirect.com). That e-mail will include the article's Digital Object Identifier (DOI). This number provides the electronic link to the published article and should be included in the posting of your personal version. We ask that you wait until you receive this e-mail and have the DOI to do any posting.

18.**Posting to a repository:** Authors may post their AAM immediately to their employer's institutional repository for internal use only and may make their manuscript publically available after the journal-specific embargo period has ended.

Please also refer to Elsevier's Article Posting Policy for further information.

19. **For book authors** the following clauses are applicable in addition to the above: Authors are permitted to place a brief summary of their work online only.. You are not allowed to download and post the published electronic version of your chapter, nor may you scan the printed edition to create an electronic version. **Posting to a repository:** Authors are permitted to post a summary of their chapter only in their institution's repository.

20. **Thesis/Dissertation**: If your license is for use in a thesis/dissertation your thesis may be submitted to your institution in either print or electronic form. Should your thesis be published commercially, please reapply for permission. These requirements include permission for the Library and Archives of Canada to supply single copies, on demand, of the complete thesis and include permission for Proquest/UMI to supply single copies, on demand, of the complete thesis. Should your thesis be published commercially, please reapply for permission.

Elsevier Open Access Terms and Conditions

Elsevier publishes Open Access articles in both its Open Access journals and via its Open Access articles option in subscription journals.

Authors publishing in an Open Access journal or who choose to make their article Open Access in an Elsevier subscription journal select one of the following Creative Commons user licenses, which define how a reader may reuse their work: Creative Commons Attribution License (CC BY), Creative Commons Attribution – Non Commercial - ShareAlike (CC BY NC SA) and Creative Commons Attribution – Non Commercial – No Derivatives (CC BY NC ND)

Terms & Conditions applicable to all Elsevier Open Access articles:

Any reuse of the article must not represent the author as endorsing the adaptation of the article nor should the article be modified in such a way as to damage the author's honour or reputation.

The author(s) must be appropriately credited.

If any part of the material to be used (for example, figures) has appeared in our publication with credit or acknowledgement to another source it is the responsibility of the user to ensure their reuse complies with the terms and conditions determined by the rights holder.

Additional Terms & Conditions applicable to each Creative Commons user license:

CC BY: You may distribute and copy the article, create extracts, abstracts, and other revised versions, adaptations or derivative works of or from an article (such as a translation), to include in a collective work (such as an anthology), to text or data mine the article, including for commercial purposes without permission from Elsevier

CC BY NC SA: For non-commercial purposes you may distribute and copy the article, create extracts, abstracts and other revised versions, adaptations or derivative works of or from an article (such as a translation), to include in a collective work (such as an anthology), to text and data mine the article and license new adaptations or creations under identical terms without permission from Elsevier

CC BY NC ND: For non-commercial purposes you may distribute and copy the article and include it in a collective work (such as an anthology), provided you do not alter or modify the article, without permission from Elsevier

Any commercial reuse of Open Access articles published with a CC BY NC SA or CC BY NC ND license requires permission from Elsevier and will be subject to a fee.

Commercial reuse includes:

- Promotional purposes (advertising or marketing)
- Commercial exploitation (e.g. a product for sale or loan)
- Systematic distribution (for a fee or free of charge)

Please refer to Elsevier's Open Access Policy for further information.

21. **Other Conditions**:

v1.7

Questions? customercare@copyright.com or +1-855-239-3415 (toll free in the US) or +1-978-646-2777.

Gratis licenses (referencing $0 in the Total field) are free. Please retain this printable license for your reference. No payment is required.

Copyright Permission for Manuscript # 1 (Chapter 2)

ELSEVIER LICENSE
TERMS AND CONDITIONS

Feb 08, 2015

This is a License Agreement between Hamed Asgari Moslehabadi ("You") and Elsevier ("Elsevier") provided by Copyright Clearance Center ("CCC"). The license consists of your order details, the terms and conditions provided by Elsevier, and the payment terms and conditions.

All payments must be made in full to CCC. For payment instructions, please see information listed at the bottom of this form.

Supplier	Elsevier Limited The Boulevard,Langford Lane Kidlington,Oxford,OX5 1GB,UK
Registered Company Number	1982084
Customer name	Hamed Asgari Moslehabadi
Customer address	Department of Mechanical Engineering, Saskatoon, SK S7N 5A9
License number	3564410556462
License date	Feb 08, 2015
Licensed content publisher	Elsevier
Licensed content publication	Materials & Design
Licensed content title	Texture evolution and dynamic mechanical behavior of cast AZ magnesium alloys under high strain rate compressive loading
Licensed content author	None
Licensed content date	September 2014
Licensed content volume number	61
Licensed content issue number	n/a
Number of pages	9
Start Page	26
End Page	34
Type of Use	reuse in a thesis/dissertation
Portion	full article
Format	both print and electronic

Are you the author of this Elsevier article?	Yes
Will you be translating?	No
Title of your thesis/dissertation	DYNAMIC MECHANICAL BEHAVIOR OF MAGNESIUM ALLOYS UNDER SHOCK LOADING CONDITIONS
Expected completion date	Jun 2015
Estimated size (number of pages)	200
Elsevier VAT number	GB 494 6272 12
Permissions price	0.00 USD
VAT/Local Sales Tax	0.00 USD / 0.00 GBP
Total	0.00 USD
Terms and Conditions	

INTRODUCTION

1. The publisher for this copyrighted material is Elsevier. By clicking "accept" in connection with completing this licensing transaction, you agree that the following terms and conditions apply to this transaction (along with the Billing and Payment terms and conditions established by Copyright Clearance Center, Inc. ("CCC"), at the time that you opened your Rightslink account and that are available at any time at http://myaccount.copyright.com).

GENERAL TERMS

2. Elsevier hereby grants you permission to reproduce the aforementioned material subject to the terms and conditions indicated.

3. Acknowledgement: If any part of the material to be used (for example, figures) has appeared in our publication with credit or acknowledgement to another source, permission must also be sought from that source. If such permission is not obtained then that material may not be included in your publication/copies. Suitable acknowledgement to the source must be made, either as a footnote or in a reference list at the end of your publication, as follows:

"Reprinted from Publication title, Vol /edition number, Author(s), Title of article / title of chapter, Pages No., Copyright (Year), with permission from Elsevier [OR APPLICABLE SOCIETY COPYRIGHT OWNER]." Also Lancet special credit - "Reprinted from The Lancet, Vol. number, Author(s), Title of article, Pages No., Copyright (Year), with permission from Elsevier."

4. Reproduction of this material is confined to the purpose and/or media for which permission is hereby given.

5. Altering/Modifying Material: Not Permitted. However figures and illustrations may be altered/adapted minimally to serve your work. Any other abbreviations, additions, deletions and/or any other alterations shall be made only with prior written authorization of Elsevier Ltd. (Please contact Elsevier at permissions@elsevier.com)

6. If the permission fee for the requested use of our material is waived in this instance, please be advised that your future requests for Elsevier materials may attract a fee.

7. Reservation of Rights: Publisher reserves all rights not specifically granted in the combination of (i) the license details provided by you and accepted in the course of this licensing transaction, (ii) these terms and conditions and (iii) CCC's Billing and Payment terms and conditions.

8. License Contingent Upon Payment: While you may exercise the rights licensed immediately upon issuance of the license at the end of the licensing process for the transaction, provided that you have disclosed complete and accurate details of your proposed use, no license is finally effective unless and until full payment is received from you (either by publisher or by CCC) as provided in CCC's Billing and Payment terms and conditions. If full payment is not received on a timely basis, then any license preliminarily granted shall be deemed automatically revoked and shall be void as if never granted. Further, in the event that you breach any of these terms and conditions or any of CCC's Billing and Payment terms and conditions, the license is automatically revoked and shall be void as if never granted. Use of materials as described in a revoked license, as well as any use of the materials beyond the scope of an unrevoked license, may constitute copyright infringement and publisher reserves the right to take any and all action to protect its copyright in the materials.

9. Warranties: Publisher makes no representations or warranties with respect to the licensed material.

10. Indemnity: You hereby indemnify and agree to hold harmless publisher and CCC, and their respective officers, directors, employees and agents, from and against any and all claims arising out of your use of the licensed material other than as specifically authorized pursuant to this license.

11. No Transfer of License: This license is personal to you and may not be sublicensed, assigned, or transferred by you to any other person without publisher's written permission.

12. No Amendment Except in Writing: This license may not be amended except in a writing signed by both parties (or, in the case of publisher, by CCC on publisher's behalf).

13. Objection to Contrary Terms: Publisher hereby objects to any terms contained in any purchase order, acknowledgment, check endorsement or other writing prepared by you, which terms are inconsistent with these terms and conditions or CCC's Billing and Payment terms and conditions. These terms and conditions, together with CCC's Billing and Payment terms and conditions (which are incorporated herein), comprise the entire

agreement between you and publisher (and CCC) concerning this licensing transaction. In the event of any conflict between your obligations established by these terms and conditions and those established by CCC's Billing and Payment terms and conditions, these terms and conditions shall control.

14. Revocation: Elsevier or Copyright Clearance Center may deny the permissions described in this License at their sole discretion, for any reason or no reason, with a full refund payable to you. Notice of such denial will be made using the contact information provided by you. Failure to receive such notice will not alter or invalidate the denial. In no event will Elsevier or Copyright Clearance Center be responsible or liable for any costs, expenses or damage incurred by you as a result of a denial of your permission request, other than a refund of the amount(s) paid by you to Elsevier and/or Copyright Clearance Center for denied permissions.

LIMITED LICENSE

The following terms and conditions apply only to specific license types:

15. **Translation**: This permission is granted for non-exclusive world **English** rights only unless your license was granted for translation rights. If you licensed translation rights you may only translate this content into the languages you requested. A professional translator must perform all translations and reproduce the content word for word preserving the integrity of the article. If this license is to re-use 1 or 2 figures then permission is granted for non-exclusive world rights in all languages.

16. **Posting licensed content on any Website**: The following terms and conditions apply as follows: Licensing material from an Elsevier journal: All content posted to the web site must maintain the copyright information line on the bottom of each image; A hyper-text must be included to the Homepage of the journal from which you are licensing at http://www.sciencedirect.com/science/journal/xxxxx or the Elsevier homepage for books at http://www.elsevier.com; Central Storage: This license does not include permission for a scanned version of the material to be stored in a central repository such as that provided by Heron/XanEdu.

Licensing material from an Elsevier book: A hyper-text link must be included to the Elsevier homepage at http://www.elsevier.com . All content posted to the web site must maintain the copyright information line on the bottom of each image.

Posting licensed content on Electronic reserve: In addition to the above the following clauses are applicable: The web site must be password-protected and made available only to bona fide students registered on a relevant course. This permission is granted for 1 year only. You may obtain a new license for future website posting.

17.**For journal authors:** the following clauses are applicable in addition to the above: Permission granted is limited to the author accepted manuscript version* of your paper.

***Accepted Author Manuscript (AAM) Definition:** An accepted author manuscript (AAM) is the author's version of the manuscript of an article that has been accepted for publication and which may include any author-incorporated changes suggested through the processes of submission processing, peer review, and editor-author communications. AAMs do not include other publisher value-added contributions such as copy-editing, formatting, technical enhancements and (if relevant) pagination.

You are not allowed to download and post the published journal article (whether PDF or HTML, proof or final version), nor may you scan the printed edition to create an electronic version. A hyper-text must be included to the Homepage of the journal from which you are licensing at http://www.sciencedirect.com/science/journal/xxxxx. As part of our normal production process, you will receive an e-mail notice when your article appears on Elsevier's online service ScienceDirect (www.sciencedirect.com). That e-mail will include the article's Digital Object Identifier (DOI). This number provides the electronic link to the published article and should be included in the posting of your personal version. We ask that you wait until you receive this e-mail and have the DOI to do any posting.

18.**Posting to a repository:** Authors may post their AAM immediately to their employer's institutional repository for internal use only and may make their manuscript publically available after the journal-specific embargo period has ended.

Please also refer to Elsevier's Article Posting Policy for further information.

19. **For book authors** the following clauses are applicable in addition to the above: Authors are permitted to place a brief summary of their work online only.. You are not allowed to download and post the published electronic version of your chapter, nor may you scan the printed edition to create an electronic version. **Posting to a repository:** Authors are permitted to post a summary of their chapter only in their institution's repository.

20. **Thesis/Dissertation**: If your license is for use in a thesis/dissertation your thesis may be submitted to your institution in either print or electronic form. Should your thesis be published commercially, please reapply for permission. These requirements include permission for the Library and Archives of Canada to supply single copies, on demand, of the complete thesis and include permission for Proquest/UMI to supply single copies, on demand, of the complete thesis. Should your thesis be published commercially, please reapply for permission.

Elsevier Open Access Terms and Conditions

Elsevier publishes Open Access articles in both its Open Access journals and via its Open Access articles option in subscription journals.

Authors publishing in an Open Access journal or who choose to make their article Open Access in an Elsevier subscription journal select one of the following Creative Commons user licenses, which define how a reader may reuse their work: Creative Commons Attribution License (CC BY), Creative Commons Attribution – Non Commercial - ShareAlike (CC BY NC SA) and Creative Commons Attribution – Non Commercial – No Derivatives (CC BY NC ND)

Terms & Conditions applicable to all Elsevier Open Access articles:

Any reuse of the article must not represent the author as endorsing the adaptation of the article nor should the article be modified in such a way as to damage the author's honour or reputation.

The author(s) must be appropriately credited.

If any part of the material to be used (for example, figures) has appeared in our publication with credit or acknowledgement to another source it is the responsibility of the user to ensure their reuse complies with the terms and conditions determined by the rights holder.

Additional Terms & Conditions applicable to each Creative Commons user license:

CC BY: You may distribute and copy the article, create extracts, abstracts, and other revised versions, adaptations or derivative works of or from an article (such as a translation), to include in a collective work (such as an anthology), to text or data mine the article, including for commercial purposes without permission from Elsevier

CC BY NC SA: For non-commercial purposes you may distribute and copy the article, create extracts, abstracts and other revised versions, adaptations or derivative works of or from an article (such as a translation), to include in a collective work (such as an anthology), to text and data mine the article and license new adaptations or creations under identical terms without permission from Elsevier

CC BY NC ND: For non-commercial purposes you may distribute and copy the article and include it in a collective work (such as an anthology), provided you do not alter or modify the article, without permission from Elsevier

Any commercial reuse of Open Access articles published with a CC BY NC SA or CC BY NC ND license requires permission from Elsevier and will be subject to a fee.

Commercial reuse includes:

- Promotional purposes (advertising or marketing)
- Commercial exploitation (e.g. a product for sale or loan)
- Systematic distribution (for a fee or free of charge)

Please refer to Elsevier's Open Access Policy for further information.

21. **Other Conditions**:

v1.7

Questions? customercare@copyright.com or +1-855-239-3415 (toll free in the US) or +1-978-646-2777.

Gratis licenses (referencing $0 in the Total field) are free. Please retain this printable license for your reference. No payment is required.

Copyright Permission for Manuscript # 2 (Chapter 3)

ELSEVIER LICENSE
TERMS AND CONDITIONS

Feb 08, 2015

This is a License Agreement between Hamed Asgari Moslehabadi ("You") and Elsevier ("Elsevier") provided by Copyright Clearance Center ("CCC"). The license consists of your order details, the terms and conditions provided by Elsevier, and the payment terms and conditions.

All payments must be made in full to CCC. For payment instructions, please see information listed at the bottom of this form.

Supplier	Elsevier Limited The Boulevard,Langford Lane Kidlington,Oxford,OX5 1GB,UK
Registered Company Number	1982084
Customer name	Hamed Asgari Moslehabadi
Customer address	Department of Mechanical Engineering, Saskatoon, SK S7N 5A9
License number	3564410724179
License date	Feb 08, 2015
Licensed content publisher	Elsevier
Licensed content publication	Materials Science and Engineering: A
Licensed content title	Effect of yttrium on the twinning and plastic deformation of AE magnesium alloy under ballistic impact
Licensed content author	None
Licensed content date	19 January 2015
Licensed content volume number	623
Licensed content issue number	n/a
Number of pages	12
Start Page	10
End Page	21
Type of Use	reuse in a thesis/dissertation
Portion	full article
Format	both print and electronic
Are you the author of this Elsevier article?	Yes
Will you be translating?	No

Title of your thesis/dissertation	DYNAMIC MECHANICAL BEHAVIOR OF MAGNESIUM ALLOYS UNDER SHOCK LOADING CONDITIONS
Expected completion date	Jun 2015
Estimated size (number of pages)	200
Elsevier VAT number	GB 494 6272 12
Permissions price	0.00 USD
VAT/Local Sales Tax	0.00 USD / 0.00 GBP
Total	0.00 USD
Terms and Conditions	

INTRODUCTION

1. The publisher for this copyrighted material is Elsevier. By clicking "accept" in connection with completing this licensing transaction, you agree that the following terms and conditions apply to this transaction (along with the Billing and Payment terms and conditions established by Copyright Clearance Center, Inc. ("CCC"), at the time that you opened your Rightslink account and that are available at any time at http://myaccount.copyright.com).

GENERAL TERMS

2. Elsevier hereby grants you permission to reproduce the aforementioned material subject to the terms and conditions indicated.

3. Acknowledgement: If any part of the material to be used (for example, figures) has appeared in our publication with credit or acknowledgement to another source, permission must also be sought from that source. If such permission is not obtained then that material may not be included in your publication/copies. Suitable acknowledgement to the source must be made, either as a footnote or in a reference list at the end of your publication, as follows:

"Reprinted from Publication title, Vol /edition number, Author(s), Title of article / title of chapter, Pages No., Copyright (Year), with permission from Elsevier [OR APPLICABLE SOCIETY COPYRIGHT OWNER]." Also Lancet special credit - "Reprinted from The Lancet, Vol. number, Author(s), Title of article, Pages No., Copyright (Year), with permission from Elsevier."

4. Reproduction of this material is confined to the purpose and/or media for which permission is hereby given.

5. Altering/Modifying Material: Not Permitted. However figures and illustrations may be altered/adapted minimally to serve your work. Any other abbreviations, additions, deletions

and/or any other alterations shall be made only with prior written authorization of Elsevier Ltd. (Please contact Elsevier at permissions@elsevier.com)

6. If the permission fee for the requested use of our material is waived in this instance, please be advised that your future requests for Elsevier materials may attract a fee.

7. Reservation of Rights: Publisher reserves all rights not specifically granted in the combination of (i) the license details provided by you and accepted in the course of this licensing transaction, (ii) these terms and conditions and (iii) CCC's Billing and Payment terms and conditions.

8. License Contingent Upon Payment: While you may exercise the rights licensed immediately upon issuance of the license at the end of the licensing process for the transaction, provided that you have disclosed complete and accurate details of your proposed use, no license is finally effective unless and until full payment is received from you (either by publisher or by CCC) as provided in CCC's Billing and Payment terms and conditions. If full payment is not received on a timely basis, then any license preliminarily granted shall be deemed automatically revoked and shall be void as if never granted. Further, in the event that you breach any of these terms and conditions or any of CCC's Billing and Payment terms and conditions, the license is automatically revoked and shall be void as if never granted. Use of materials as described in a revoked license, as well as any use of the materials beyond the scope of an unrevoked license, may constitute copyright infringement and publisher reserves the right to take any and all action to protect its copyright in the materials.

9. Warranties: Publisher makes no representations or warranties with respect to the licensed material.

10. Indemnity: You hereby indemnify and agree to hold harmless publisher and CCC, and their respective officers, directors, employees and agents, from and against any and all claims arising out of your use of the licensed material other than as specifically authorized pursuant to this license.

11. No Transfer of License: This license is personal to you and may not be sublicensed, assigned, or transferred by you to any other person without publisher's written permission.

12. No Amendment Except in Writing: This license may not be amended except in a writing signed by both parties (or, in the case of publisher, by CCC on publisher's behalf).

13. Objection to Contrary Terms: Publisher hereby objects to any terms contained in any purchase order, acknowledgment, check endorsement or other writing prepared by you, which terms are inconsistent with these terms and conditions or CCC's Billing and Payment terms and conditions. These terms and conditions, together with CCC's Billing and Payment terms and conditions (which are incorporated herein), comprise the entire agreement between you and publisher (and CCC) concerning this licensing transaction. In the event of any conflict between your obligations established by these terms and

conditions and those established by CCC's Billing and Payment terms and conditions, these terms and conditions shall control.

14. Revocation: Elsevier or Copyright Clearance Center may deny the permissions described in this License at their sole discretion, for any reason or no reason, with a full refund payable to you. Notice of such denial will be made using the contact information provided by you. Failure to receive such notice will not alter or invalidate the denial. In no event will Elsevier or Copyright Clearance Center be responsible or liable for any costs, expenses or damage incurred by you as a result of a denial of your permission request, other than a refund of the amount(s) paid by you to Elsevier and/or Copyright Clearance Center for denied permissions.

LIMITED LICENSE

The following terms and conditions apply only to specific license types:

15. **Translation**: This permission is granted for non-exclusive world **English** rights only unless your license was granted for translation rights. If you licensed translation rights you may only translate this content into the languages you requested. A professional translator must perform all translations and reproduce the content word for word preserving the integrity of the article. If this license is to re-use 1 or 2 figures then permission is granted for non-exclusive world rights in all languages.

16. **Posting licensed content on any Website**: The following terms and conditions apply as follows: Licensing material from an Elsevier journal: All content posted to the web site must maintain the copyright information line on the bottom of each image; A hyper-text must be included to the Homepage of the journal from which you are licensing at http://www.sciencedirect.com/science/journal/xxxxx or the Elsevier homepage for books at http://www.elsevier.com; Central Storage: This license does not include permission for a scanned version of the material to be stored in a central repository such as that provided by Heron/XanEdu.

Licensing material from an Elsevier book: A hyper-text link must be included to the Elsevier homepage at http://www.elsevier.com . All content posted to the web site must maintain the copyright information line on the bottom of each image.

Posting licensed content on Electronic reserve: In addition to the above the following clauses are applicable: The web site must be password-protected and made available only to bona fide students registered on a relevant course. This permission is granted for 1 year only. You may obtain a new license for future website posting.

17.**For journal authors:** the following clauses are applicable in addition to the above: Permission granted is limited to the author accepted manuscript version* of your paper.

***Accepted Author Manuscript (AAM) Definition:** An accepted author manuscript (AAM) is the author's version of the manuscript of an article that has been accepted for publication and which may include any author-incorporated changes suggested through the processes of submission processing, peer review, and editor-author communications. AAMs do not include other publisher value-added contributions such as copy-editing, formatting, technical enhancements and (if relevant) pagination.

You are not allowed to download and post the published journal article (whether PDF or HTML, proof or final version), nor may you scan the printed edition to create an electronic version. A hyper-text must be included to the Homepage of the journal from which you are licensing at http://www.sciencedirect.com/science/journal/xxxxx. As part of our normal production process, you will receive an e-mail notice when your article appears on Elsevier's online service ScienceDirect (www.sciencedirect.com). That e-mail will include the article's Digital Object Identifier (DOI). This number provides the electronic link to the published article and should be included in the posting of your personal version. We ask that you wait until you receive this e-mail and have the DOI to do any posting.

18.**Posting to a repository:** Authors may post their AAM immediately to their employer's institutional repository for internal use only and may make their manuscript publically available after the journal-specific embargo period has ended.

Please also refer to Elsevier's Article Posting Policy for further information.

19. **For book authors** the following clauses are applicable in addition to the above: Authors are permitted to place a brief summary of their work online only.. You are not allowed to download and post the published electronic version of your chapter, nor may you scan the printed edition to create an electronic version. **Posting to a repository:** Authors are permitted to post a summary of their chapter only in their institution's repository.

20. **Thesis/Dissertation**: If your license is for use in a thesis/dissertation your thesis may be submitted to your institution in either print or electronic form. Should your thesis be published commercially, please reapply for permission. These requirements include permission for the Library and Archives of Canada to supply single copies, on demand, of the complete thesis and include permission for Proquest/UMI to supply single copies, on demand, of the complete thesis. Should your thesis be published commercially, please reapply for permission.

Elsevier Open Access Terms and Conditions

Elsevier publishes Open Access articles in both its Open Access journals and via its Open Access articles option in subscription journals.

Authors publishing in an Open Access journal or who choose to make their article Open Access in an Elsevier subscription journal select one of the following Creative Commons user licenses, which define how a reader may reuse their work: Creative Commons Attribution License (CC BY), Creative Commons Attribution – Non Commercial - ShareAlike (CC BY NC SA) and Creative Commons Attribution – Non Commercial – No Derivatives (CC BY NC ND)

Terms & Conditions applicable to all Elsevier Open Access articles:

Any reuse of the article must not represent the author as endorsing the adaptation of the article nor should the article be modified in such a way as to damage the author's honour or reputation.

The author(s) must be appropriately credited.

If any part of the material to be used (for example, figures) has appeared in our publication with credit or acknowledgement to another source it is the responsibility of the user to ensure their reuse complies with the terms and conditions determined by the rights holder.

Additional Terms & Conditions applicable to each Creative Commons user license:

CC BY: You may distribute and copy the article, create extracts, abstracts, and other revised versions, adaptations or derivative works of or from an article (such as a translation), to include in a collective work (such as an anthology), to text or data mine the article, including for commercial purposes without permission from Elsevier

CC BY NC SA: For non-commercial purposes you may distribute and copy the article, create extracts, abstracts and other revised versions, adaptations or derivative works of or from an article (such as a translation), to include in a collective work (such as an anthology), to text and data mine the article and license new adaptations or creations under identical terms without permission from Elsevier

CC BY NC ND: For non-commercial purposes you may distribute and copy the article and include it in a collective work (such as an anthology), provided you do not alter or modify the article, without permission from Elsevier

Any commercial reuse of Open Access articles published with a CC BY NC SA or CC BY NC ND license requires permission from Elsevier and will be subject to a fee.

Commercial reuse includes:

- Promotional purposes (advertising or marketing)
- Commercial exploitation (e.g. a product for sale or loan)

- Systematic distribution (for a fee or free of charge)

Please refer to Elsevier's Open Access Policy for further information.

21. **Other Conditions**:

v1.7

Questions? customercare@copyright.com or +1-855-239-3415 (toll free in the US) or +1-978-646-2777.

Gratis licenses (referencing $0 in the Total field) are free. Please retain this printable license for your reference. No payment is required.

Copyright Permission for Manuscript # 3 (Chapter 4)

ELSEVIER LICENSE
TERMS AND CONDITIONS

Feb 08, 2015

This is a License Agreement between Hamed Asgari Moslehabadi ("You") and Elsevier ("Elsevier") provided by Copyright Clearance Center ("CCC"). The license consists of your order details, the terms and conditions provided by Elsevier, and the payment terms and conditions.

All payments must be made in full to CCC. For payment instructions, please see information listed at the bottom of this form.

Supplier	Elsevier Limited The Boulevard,Langford Lane Kidlington,Oxford,OX5 1GB,UK
Registered Company Number	1982084
Customer name	Hamed Asgari Moslehabadi
Customer address	Department of Mechanical Engineering, Saskatoon, SK S7N 5A9
License number	3564410877228
License date	Feb 08, 2015
Licensed content publisher	Elsevier
Licensed content publication	Materials Science and Engineering: A
Licensed content title	Experimental and simulation analysis of texture formation and deformation mechanism of rolled AZ31B magnesium alloy under dynamic loading
Licensed content author	None
Licensed content date	17 November 2014
Licensed content volume number	618
Licensed content issue number	n/a
Number of pages	13
Start Page	310
End Page	322
Type of Use	reuse in a thesis/dissertation
Intended publisher of new work	other

Portion	full article
Format	both print and electronic
Are you the author of this Elsevier article?	Yes
Will you be translating?	No
Title of your thesis/dissertation	DYNAMIC MECHANICAL BEHAVIOR OF MAGNESIUM ALLOYS UNDER SHOCK LOADING CONDITIONS
Expected completion date	Jun 2015
Estimated size (number of pages)	200
Elsevier VAT number	GB 494 6272 12
Permissions price	0.00 USD
VAT/Local Sales Tax	0.00 USD / 0.00 GBP
Total	0.00 USD
Terms and Conditions	

INTRODUCTION

1. The publisher for this copyrighted material is Elsevier. By clicking "accept" in connection with completing this licensing transaction, you agree that the following terms and conditions apply to this transaction (along with the Billing and Payment terms and conditions established by Copyright Clearance Center, Inc. ("CCC"), at the time that you opened your Rightslink account and that are available at any time at http://myaccount.copyright.com).

GENERAL TERMS

2. Elsevier hereby grants you permission to reproduce the aforementioned material subject to the terms and conditions indicated.

3. Acknowledgement: If any part of the material to be used (for example, figures) has appeared in our publication with credit or acknowledgement to another source, permission must also be sought from that source. If such permission is not obtained then that material may not be included in your publication/copies. Suitable acknowledgement to the source must be made, either as a footnote or in a reference list at the end of your publication, as follows:

"Reprinted from Publication title, Vol /edition number, Author(s), Title of article / title of chapter, Pages No., Copyright (Year), with permission from Elsevier [OR APPLICABLE SOCIETY COPYRIGHT OWNER]." Also Lancet special credit - "Reprinted from The Lancet, Vol. number, Author(s), Title of article, Pages No., Copyright (Year), with permission from Elsevier."

4. Reproduction of this material is confined to the purpose and/or media for which permission is hereby given.

5. Altering/Modifying Material: Not Permitted. However figures and illustrations may be altered/adapted minimally to serve your work. Any other abbreviations, additions, deletions and/or any other alterations shall be made only with prior written authorization of Elsevier Ltd. (Please contact Elsevier at permissions@elsevier.com)

6. If the permission fee for the requested use of our material is waived in this instance, please be advised that your future requests for Elsevier materials may attract a fee.

7. Reservation of Rights: Publisher reserves all rights not specifically granted in the combination of (i) the license details provided by you and accepted in the course of this licensing transaction, (ii) these terms and conditions and (iii) CCC's Billing and Payment terms and conditions.

8. License Contingent Upon Payment: While you may exercise the rights licensed immediately upon issuance of the license at the end of the licensing process for the transaction, provided that you have disclosed complete and accurate details of your proposed use, no license is finally effective unless and until full payment is received from you (either by publisher or by CCC) as provided in CCC's Billing and Payment terms and conditions. If full payment is not received on a timely basis, then any license preliminarily granted shall be deemed automatically revoked and shall be void as if never granted. Further, in the event that you breach any of these terms and conditions or any of CCC's Billing and Payment terms and conditions, the license is automatically revoked and shall be void as if never granted. Use of materials as described in a revoked license, as well as any use of the materials beyond the scope of an unrevoked license, may constitute copyright infringement and publisher reserves the right to take any and all action to protect its copyright in the materials.

9. Warranties: Publisher makes no representations or warranties with respect to the licensed material.

10. Indemnity: You hereby indemnify and agree to hold harmless publisher and CCC, and their respective officers, directors, employees and agents, from and against any and all claims arising out of your use of the licensed material other than as specifically authorized pursuant to this license.

11. No Transfer of License: This license is personal to you and may not be sublicensed, assigned, or transferred by you to any other person without publisher's written permission.

12. No Amendment Except in Writing: This license may not be amended except in a writing signed by both parties (or, in the case of publisher, by CCC on publisher's behalf).

13. Objection to Contrary Terms: Publisher hereby objects to any terms contained in any purchase order, acknowledgment, check endorsement or other writing prepared by you,

which terms are inconsistent with these terms and conditions or CCC's Billing and Payment terms and conditions. These terms and conditions, together with CCC's Billing and Payment terms and conditions (which are incorporated herein), comprise the entire agreement between you and publisher (and CCC) concerning this licensing transaction. In the event of any conflict between your obligations established by these terms and conditions and those established by CCC's Billing and Payment terms and conditions, these terms and conditions shall control.

14. Revocation: Elsevier or Copyright Clearance Center may deny the permissions described in this License at their sole discretion, for any reason or no reason, with a full refund payable to you. Notice of such denial will be made using the contact information provided by you. Failure to receive such notice will not alter or invalidate the denial. In no event will Elsevier or Copyright Clearance Center be responsible or liable for any costs, expenses or damage incurred by you as a result of a denial of your permission request, other than a refund of the amount(s) paid by you to Elsevier and/or Copyright Clearance Center for denied permissions.

LIMITED LICENSE

The following terms and conditions apply only to specific license types:

15. **Translation**: This permission is granted for non-exclusive world **English** rights only unless your license was granted for translation rights. If you licensed translation rights you may only translate this content into the languages you requested. A professional translator must perform all translations and reproduce the content word for word preserving the integrity of the article. If this license is to re-use 1 or 2 figures then permission is granted for non-exclusive world rights in all languages.

16. **Posting licensed content on any Website**: The following terms and conditions apply as follows: Licensing material from an Elsevier journal: All content posted to the web site must maintain the copyright information line on the bottom of each image; A hyper-text must be included to the Homepage of the journal from which you are licensing at http://www.sciencedirect.com/science/journal/xxxxx or the Elsevier homepage for books at http://www.elsevier.com; Central Storage: This license does not include permission for a scanned version of the material to be stored in a central repository such as that provided by Heron/XanEdu.

Licensing material from an Elsevier book: A hyper-text link must be included to the Elsevier homepage at http://www.elsevier.com . All content posted to the web site must maintain the copyright information line on the bottom of each image.

Posting licensed content on Electronic reserve: In addition to the above the following clauses are applicable: The web site must be password-protected and made available only

to bona fide students registered on a relevant course. This permission is granted for 1 year only. You may obtain a new license for future website posting.

17.**For journal authors:** the following clauses are applicable in addition to the above: Permission granted is limited to the author accepted manuscript version* of your paper.

***Accepted Author Manuscript (AAM) Definition:** An accepted author manuscript (AAM) is the author's version of the manuscript of an article that has been accepted for publication and which may include any author-incorporated changes suggested through the processes of submission processing, peer review, and editor-author communications. AAMs do not include other publisher value-added contributions such as copy-editing, formatting, technical enhancements and (if relevant) pagination.

You are not allowed to download and post the published journal article (whether PDF or HTML, proof or final version), nor may you scan the printed edition to create an electronic version. A hyper-text must be included to the Homepage of the journal from which you are licensing at http://www.sciencedirect.com/science/journal/xxxxx. As part of our normal production process, you will receive an e-mail notice when your article appears on Elsevier's online service ScienceDirect (www.sciencedirect.com). That e-mail will include the article's Digital Object Identifier (DOI). This number provides the electronic link to the published article and should be included in the posting of your personal version. We ask that you wait until you receive this e-mail and have the DOI to do any posting.

18.**Posting to a repository:** Authors may post their AAM immediately to their employer's institutional repository for internal use only and may make their manuscript publically available after the journal-specific embargo period has ended.

Please also refer to Elsevier's Article Posting Policy for further information.

19. **For book authors** the following clauses are applicable in addition to the above: Authors are permitted to place a brief summary of their work online only.. You are not allowed to download and post the published electronic version of your chapter, nor may you scan the printed edition to create an electronic version. **Posting to a repository:** Authors are permitted to post a summary of their chapter only in their institution's repository.

20. **Thesis/Dissertation**: If your license is for use in a thesis/dissertation your thesis may be submitted to your institution in either print or electronic form. Should your thesis be published commercially, please reapply for permission. These requirements include permission for the Library and Archives of Canada to supply single copies, on demand, of the complete thesis and include permission for Proquest/UMI to supply single copies, on demand, of the complete thesis. Should your thesis be published commercially, please reapply for permission.

- Promotional purposes (advertising or marketing)
- Commercial exploitation (e.g. a product for sale or loan)
- Systematic distribution (for a fee or free of charge)

Please refer to Elsevier's Open Access Policy for further information.

21. **Other Conditions**:

v1.7

Questions? customercare@copyright.com or +1-855-239-3415 (toll free in the US) or +1-978-646-2777.

Gratis licenses (referencing $0 in the Total field) are free. Please retain this printable license for your reference. No payment is required.

Copyright Permission for Manuscript # 4 (Chapter 5)

ELSEVIER LICENSE
TERMS AND CONDITIONS

Feb 08, 2015

This is a License Agreement between Hamed Asgari Moslehabadi ("You") and Elsevier ("Elsevier") provided by Copyright Clearance Center ("CCC"). The license consists of your order details, the terms and conditions provided by Elsevier, and the payment terms and conditions.

All payments must be made in full to CCC. For payment instructions, please see information listed at the bottom of this form.

Supplier	Elsevier Limited The Boulevard,Langford Lane Kidlington,Oxford,OX5 1GB,UK
Registered Company Number	1982084
Customer name	Hamed Asgari Moslehabadi
Customer address	Department of Mechanical Engineering, Saskatoon, SK S7N 5A9
License number	3564410985368
License date	Feb 08, 2015
Licensed content publisher	Elsevier
Licensed content publication	Materials & Design
Licensed content title	On dynamic deformation behavior of WE43 magnesium alloy sheet under shock loading conditions
Licensed content author	None
Licensed content date	November 2014
Licensed content volume number	63
Licensed content issue number	n/a
Number of pages	13
Start Page	552
End Page	564
Type of Use	reuse in a thesis/dissertation
Intended publisher of new work	other
Portion	full article
Format	both print and electronic
Are you the author of this Elsevier article?	Yes

Will you be translating?	No
Title of your thesis/dissertation	DYNAMIC MECHANICAL BEHAVIOR OF MAGNESIUM ALLOYS UNDER SHOCK LOADING CONDITIONS
Expected completion date	Jun 2015
Estimated size (number of pages)	200
Elsevier VAT number	GB 494 6272 12
Permissions price	0.00 USD
VAT/Local Sales Tax	0.00 USD / 0.00 GBP
Total	0.00 USD
Terms and Conditions	

INTRODUCTION

1. The publisher for this copyrighted material is Elsevier. By clicking "accept" in connection with completing this licensing transaction, you agree that the following terms and conditions apply to this transaction (along with the Billing and Payment terms and conditions established by Copyright Clearance Center, Inc. ("CCC"), at the time that you opened your Rightslink account and that are available at any time at http://myaccount.copyright.com).

GENERAL TERMS

2. Elsevier hereby grants you permission to reproduce the aforementioned material subject to the terms and conditions indicated.

3. Acknowledgement: If any part of the material to be used (for example, figures) has appeared in our publication with credit or acknowledgement to another source, permission must also be sought from that source. If such permission is not obtained then that material may not be included in your publication/copies. Suitable acknowledgement to the source must be made, either as a footnote or in a reference list at the end of your publication, as follows:

"Reprinted from Publication title, Vol /edition number, Author(s), Title of article / title of chapter, Pages No., Copyright (Year), with permission from Elsevier [OR APPLICABLE SOCIETY COPYRIGHT OWNER]." Also Lancet special credit - "Reprinted from The Lancet, Vol. number, Author(s), Title of article, Pages No., Copyright (Year), with permission from Elsevier."

4. Reproduction of this material is confined to the purpose and/or media for which permission is hereby given.

5. Altering/Modifying Material: Not Permitted. However figures and illustrations may be altered/adapted minimally to serve your work. Any other abbreviations, additions, deletions

and/or any other alterations shall be made only with prior written authorization of Elsevier Ltd. (Please contact Elsevier at permissions@elsevier.com)

6. If the permission fee for the requested use of our material is waived in this instance, please be advised that your future requests for Elsevier materials may attract a fee.

7. Reservation of Rights: Publisher reserves all rights not specifically granted in the combination of (i) the license details provided by you and accepted in the course of this licensing transaction, (ii) these terms and conditions and (iii) CCC's Billing and Payment terms and conditions.

8. License Contingent Upon Payment: While you may exercise the rights licensed immediately upon issuance of the license at the end of the licensing process for the transaction, provided that you have disclosed complete and accurate details of your proposed use, no license is finally effective unless and until full payment is received from you (either by publisher or by CCC) as provided in CCC's Billing and Payment terms and conditions. If full payment is not received on a timely basis, then any license preliminarily granted shall be deemed automatically revoked and shall be void as if never granted. Further, in the event that you breach any of these terms and conditions or any of CCC's Billing and Payment terms and conditions, the license is automatically revoked and shall be void as if never granted. Use of materials as described in a revoked license, as well as any use of the materials beyond the scope of an unrevoked license, may constitute copyright infringement and publisher reserves the right to take any and all action to protect its copyright in the materials.

9. Warranties: Publisher makes no representations or warranties with respect to the licensed material.

10. Indemnity: You hereby indemnify and agree to hold harmless publisher and CCC, and their respective officers, directors, employees and agents, from and against any and all claims arising out of your use of the licensed material other than as specifically authorized pursuant to this license.

11. No Transfer of License: This license is personal to you and may not be sublicensed, assigned, or transferred by you to any other person without publisher's written permission.

12. No Amendment Except in Writing: This license may not be amended except in a writing signed by both parties (or, in the case of publisher, by CCC on publisher's behalf).

13. Objection to Contrary Terms: Publisher hereby objects to any terms contained in any purchase order, acknowledgment, check endorsement or other writing prepared by you, which terms are inconsistent with these terms and conditions or CCC's Billing and Payment terms and conditions. These terms and conditions, together with CCC's Billing and Payment terms and conditions (which are incorporated herein), comprise the entire agreement between you and publisher (and CCC) concerning this licensing transaction. In the event of any conflict between your obligations established by these terms and

conditions and those established by CCC's Billing and Payment terms and conditions, these terms and conditions shall control.

14. Revocation: Elsevier or Copyright Clearance Center may deny the permissions described in this License at their sole discretion, for any reason or no reason, with a full refund payable to you. Notice of such denial will be made using the contact information provided by you. Failure to receive such notice will not alter or invalidate the denial. In no event will Elsevier or Copyright Clearance Center be responsible or liable for any costs, expenses or damage incurred by you as a result of a denial of your permission request, other than a refund of the amount(s) paid by you to Elsevier and/or Copyright Clearance Center for denied permissions.

LIMITED LICENSE

The following terms and conditions apply only to specific license types:

15. **Translation**: This permission is granted for non-exclusive world **English** rights only unless your license was granted for translation rights. If you licensed translation rights you may only translate this content into the languages you requested. A professional translator must perform all translations and reproduce the content word for word preserving the integrity of the article. If this license is to re-use 1 or 2 figures then permission is granted for non-exclusive world rights in all languages.

16. **Posting licensed content on any Website**: The following terms and conditions apply as follows: Licensing material from an Elsevier journal: All content posted to the web site must maintain the copyright information line on the bottom of each image; A hyper-text must be included to the Homepage of the journal from which you are licensing at http://www.sciencedirect.com/science/journal/xxxxx or the Elsevier homepage for books at http://www.elsevier.com; Central Storage: This license does not include permission for a scanned version of the material to be stored in a central repository such as that provided by Heron/XanEdu.

Licensing material from an Elsevier book: A hyper-text link must be included to the Elsevier homepage at http://www.elsevier.com . All content posted to the web site must maintain the copyright information line on the bottom of each image.

Posting licensed content on Electronic reserve: In addition to the above the following clauses are applicable: The web site must be password-protected and made available only to bona fide students registered on a relevant course. This permission is granted for 1 year only. You may obtain a new license for future website posting.

17.**For journal authors:** the following clauses are applicable in addition to the above: Permission granted is limited to the author accepted manuscript version* of your paper.

***Accepted Author Manuscript (AAM) Definition:** An accepted author manuscript (AAM) is the author's version of the manuscript of an article that has been accepted for publication and which may include any author-incorporated changes suggested through the processes of submission processing, peer review, and editor-author communications. AAMs do not include other publisher value-added contributions such as copy-editing, formatting, technical enhancements and (if relevant) pagination.

You are not allowed to download and post the published journal article (whether PDF or HTML, proof or final version), nor may you scan the printed edition to create an electronic version. A hyper-text must be included to the Homepage of the journal from which you are licensing at http://www.sciencedirect.com/science/journal/xxxxx. As part of our normal production process, you will receive an e-mail notice when your article appears on Elsevier's online service ScienceDirect (www.sciencedirect.com). That e-mail will include the article's Digital Object Identifier (DOI). This number provides the electronic link to the published article and should be included in the posting of your personal version. We ask that you wait until you receive this e-mail and have the DOI to do any posting.

18.**Posting to a repository:** Authors may post their AAM immediately to their employer's institutional repository for internal use only and may make their manuscript publically available after the journal-specific embargo period has ended.

Please also refer to Elsevier's Article Posting Policy for further information.

19. **For book authors** the following clauses are applicable in addition to the above: Authors are permitted to place a brief summary of their work online only.. You are not allowed to download and post the published electronic version of your chapter, nor may you scan the printed edition to create an electronic version. **Posting to a repository:** Authors are permitted to post a summary of their chapter only in their institution's repository.

20. **Thesis/Dissertation**: If your license is for use in a thesis/dissertation your thesis may be submitted to your institution in either print or electronic form. Should your thesis be published commercially, please reapply for permission. These requirements include permission for the Library and Archives of Canada to supply single copies, on demand, of the complete thesis and include permission for Proquest/UMI to supply single copies, on demand, of the complete thesis. Should your thesis be published commercially, please reapply for permission.

Elsevier Open Access Terms and Conditions

Elsevier publishes Open Access articles in both its Open Access journals and via its Open Access articles option in subscription journals.

Authors publishing in an Open Access journal or who choose to make their article Open Access in an Elsevier subscription journal select one of the following Creative Commons user licenses, which define how a reader may reuse their work: Creative Commons Attribution License (CC BY), Creative Commons Attribution – Non Commercial - ShareAlike (CC BY NC SA) and Creative Commons Attribution – Non Commercial – No Derivatives (CC BY NC ND)

Terms & Conditions applicable to all Elsevier Open Access articles:

Any reuse of the article must not represent the author as endorsing the adaptation of the article nor should the article be modified in such a way as to damage the author's honour or reputation.

The author(s) must be appropriately credited.

If any part of the material to be used (for example, figures) has appeared in our publication with credit or acknowledgement to another source it is the responsibility of the user to ensure their reuse complies with the terms and conditions determined by the rights holder.

Additional Terms & Conditions applicable to each Creative Commons user license:

CC BY: You may distribute and copy the article, create extracts, abstracts, and other revised versions, adaptations or derivative works of or from an article (such as a translation), to include in a collective work (such as an anthology), to text or data mine the article, including for commercial purposes without permission from Elsevier

CC BY NC SA: For non-commercial purposes you may distribute and copy the article, create extracts, abstracts and other revised versions, adaptations or derivative works of or from an article (such as a translation), to include in a collective work (such as an anthology), to text and data mine the article and license new adaptations or creations under identical terms without permission from Elsevier

CC BY NC ND: For non-commercial purposes you may distribute and copy the article and include it in a collective work (such as an anthology), provided you do not alter or modify the article, without permission from Elsevier

Any commercial reuse of Open Access articles published with a CC BY NC SA or CC BY NC ND license requires permission from Elsevier and will be subject to a fee.

Commercial reuse includes:

- Promotional purposes (advertising or marketing)
- Commercial exploitation (e.g. a product for sale or loan)

- Systematic distribution (for a fee or free of charge)

Please refer to Elsevier's Open Access Policy for further information.

21. **Other Conditions**:

v1.7

Questions? customercare@copyright.com or +1-855-239-3415 (toll free in the US) or +1-978-646-2777.

Gratis licenses (referencing $0 in the Total field) are free. Please retain this printable license for your reference. No payment is required.

Copyright Permission for Manuscript # 6 (Chapter 7)

ELSEVIER LICENSE
TERMS AND CONDITIONS

Mar 24, 2015

This is a License Agreement between Hamed Asgari Moslehabadi ("You") and Elsevier ("Elsevier") provided by Copyright Clearance Center ("CCC"). The license consists of your order details, the terms and conditions provided by Elsevier, and the payment terms and conditions.

All payments must be made in full to CCC. For payment instructions, please see information listed at the bottom of this form.

Supplier	Elsevier Limited The Boulevard,Langford Lane Kidlington,Oxford,OX5 1GB,UK
Registered Company Number	1982084
Customer name	Hamed Asgari Moslehabadi
Customer address	Department of Mechanical Engineering, Saskatoon, SK S7N 5A9
License number	3595480044238
License date	Mar 24, 2015
Licensed content publisher	Elsevier
Licensed content publication	Materials Science and Engineering: A
Licensed content title	Effect of grain size on High strain rate deformation of rolled Mg-4Y-3RE alloy in compression
Licensed content author	None
Licensed content date	1 May 2015
Licensed content volume number	633
Licensed content issue number	n/a
Number of pages	11
Start Page	92
End Page	102
Type of Use	reuse in a thesis/dissertation
Portion	full article
Format	both print and electronic
Are you the author of this Elsevier article?	Yes
Will you be translating?	No

Title of your thesis/dissertation	DYNAMIC MECHANICAL BEHAVIOR OF MAGNESIUM ALLOYS UNDER SHOCK LOADING CONDITIONS
Expected completion date	Jun 2015
Estimated size (number of pages)	200
Elsevier VAT number	GB 494 6272 12
Permissions price	0.00 USD
VAT/Local Sales Tax	0.00 USD / 0.00 GBP
Total	0.00 USD
Terms and Conditions	

INTRODUCTION

1. The publisher for this copyrighted material is Elsevier. By clicking "accept" in connection with completing this licensing transaction, you agree that the following terms and conditions apply to this transaction (along with the Billing and Payment terms and conditions established by Copyright Clearance Center, Inc. ("CCC"), at the time that you opened your Rightslink account and that are available at any time at http://myaccount.copyright.com).

GENERAL TERMS

2. Elsevier hereby grants you permission to reproduce the aforementioned material subject to the terms and conditions indicated.

3. Acknowledgement: If any part of the material to be used (for example, figures) has appeared in our publication with credit or acknowledgement to another source, permission must also be sought from that source. If such permission is not obtained then that material may not be included in your publication/copies. Suitable acknowledgement to the source must be made, either as a footnote or in a reference list at the end of your publication, as follows:

"Reprinted from Publication title, Vol /edition number, Author(s), Title of article / title of chapter, Pages No., Copyright (Year), with permission from Elsevier [OR APPLICABLE SOCIETY COPYRIGHT OWNER]." Also Lancet special credit - "Reprinted from The Lancet, Vol. number, Author(s), Title of article, Pages No., Copyright (Year), with permission from Elsevier."

4. Reproduction of this material is confined to the purpose and/or media for which permission is hereby given.

5. Altering/Modifying Material: Not Permitted. However figures and illustrations may be altered/adapted minimally to serve your work. Any other abbreviations, additions, deletions and/or any other alterations shall be made only with prior written authorization of Elsevier Ltd. (Please contact Elsevier at permissions@elsevier.com)

6. If the permission fee for the requested use of our material is waived in this instance, please be advised that your future requests for Elsevier materials may attract a fee.

7. Reservation of Rights: Publisher reserves all rights not specifically granted in the combination of (i) the license details provided by you and accepted in the course of this licensing transaction, (ii) these terms and conditions and (iii) CCC's Billing and Payment terms and conditions.

8. License Contingent Upon Payment: While you may exercise the rights licensed immediately upon issuance of the license at the end of the licensing process for the transaction, provided that you have disclosed complete and accurate details of your proposed use, no license is finally effective unless and until full payment is received from you (either by publisher or by CCC) as provided in CCC's Billing and Payment terms and conditions. If full payment is not received on a timely basis, then any license preliminarily granted shall be deemed automatically revoked and shall be void as if never granted. Further, in the event that you breach any of these terms and conditions or any of CCC's Billing and Payment terms and conditions, the license is automatically revoked and shall be void as if never granted. Use of materials as described in a revoked license, as well as any use of the materials beyond the scope of an unrevoked license, may constitute copyright infringement and publisher reserves the right to take any and all action to protect its copyright in the materials.

9. Warranties: Publisher makes no representations or warranties with respect to the licensed material.

10. Indemnity: You hereby indemnify and agree to hold harmless publisher and CCC, and their respective officers, directors, employees and agents, from and against any and all claims arising out of your use of the licensed material other than as specifically authorized pursuant to this license.

11. No Transfer of License: This license is personal to you and may not be sublicensed, assigned, or transferred by you to any other person without publisher's written permission.

12. No Amendment Except in Writing: This license may not be amended except in a writing signed by both parties (or, in the case of publisher, by CCC on publisher's behalf).

13. Objection to Contrary Terms: Publisher hereby objects to any terms contained in any purchase order, acknowledgment, check endorsement or other writing prepared by you, which terms are inconsistent with these terms and conditions or CCC's Billing and Payment terms and conditions. These terms and conditions, together with CCC's Billing and Payment terms and conditions (which are incorporated herein), comprise the entire agreement between you and publisher (and CCC) concerning this licensing transaction. In the event of any conflict between your obligations established by these terms and conditions and those established by CCC's Billing and Payment terms and conditions, these terms and conditions shall control.

14. Revocation: Elsevier or Copyright Clearance Center may deny the permissions described in this License at their sole discretion, for any reason or no reason, with a full refund payable to you. Notice of such denial will be made using the contact information provided by you. Failure to receive such notice will not alter or invalidate the denial. In no event will Elsevier or Copyright Clearance Center be responsible or liable for any costs, expenses or damage incurred by you as a result of a denial of your permission request, other than a refund of the amount(s) paid by you to Elsevier and/or Copyright Clearance Center for denied permissions.

LIMITED LICENSE

The following terms and conditions apply only to specific license types:

15. **Translation**: This permission is granted for non-exclusive world **English** rights only unless your license was granted for translation rights. If you licensed translation rights you may only translate this content into the languages you requested. A professional translator must perform all translations and reproduce the content word for word preserving the integrity of the article. If this license is to re-use 1 or 2 figures then permission is granted for non-exclusive world rights in all languages.

16. **Posting licensed content on any Website**: The following terms and conditions apply as follows: Licensing material from an Elsevier journal: All content posted to the web site must maintain the copyright information line on the bottom of each image; A hyper-text must be included to the Homepage of the journal from which you are licensing at http://www.sciencedirect.com/science/journal/xxxxx or the Elsevier homepage for books at http://www.elsevier.com; Central Storage: This license does not include permission for a scanned version of the material to be stored in a central repository such as that provided by Heron/XanEdu.

Licensing material from an Elsevier book: A hyper-text link must be included to the Elsevier homepage at http://www.elsevier.com . All content posted to the web site must maintain the copyright information line on the bottom of each image.

Posting licensed content on Electronic reserve: In addition to the above the following clauses are applicable: The web site must be password-protected and made available only to bona fide students registered on a relevant course. This permission is granted for 1 year only. You may obtain a new license for future website posting.

17. **For journal authors:** the following clauses are applicable in addition to the above:

Preprints:

A preprint is an author's own write-up of research results and analysis, it has not been peer-reviewed, nor has it had any other value added to it by a publisher (such as formatting, copyright, technical enhancement etc.).

Authors can share their preprints anywhere at any time. Preprints should not be added to or enhanced in any way in order to appear more like, or to substitute for, the final versions of articles however authors can update their preprints on arXiv or RePEc with their Accepted Author Manuscript (see below).

If accepted for publication, we encourage authors to link from the preprint to their formal publication via its DOI. Millions of researchers have access to the formal publications on ScienceDirect, and so links will help users to find, access, cite and use the best available version. Please note that Cell Press, The Lancet and some society-owned have different preprint policies. Information on these policies is available on the journal homepage.

Accepted Author Manuscripts: An accepted author manuscript is the manuscript of an article that has been accepted for publication and which typically includes author-incorporated changes suggested during submission, peer review and editor-author communications.

Authors can share their accepted author manuscript:

- – immediately
    - via their non-commercial person homepage or blog
    - by updating a preprint in arXiv or RePEc with the accepted manuscript
    - via their research institute or institutional repository for internal institutional uses or as part of an invitation-only research collaboration work-group
    - directly by providing copies to their students or to research collaborators for their personal use
    - for private scholarly sharing as part of an invitation-only work group on commercial sites with which Elsevier has an agreement
- – after the embargo period
    - via non-commercial hosting platforms such as their institutional repository
    - via commercial sites with which Elsevier has an agreement

In all cases accepted manuscripts should:

- – link to the formal publication via its DOI
- – bear a CC-BY-NC-ND license - this is easy to do
- – if aggregated with other manuscripts, for example in a repository or other site, be shared in alignment with our hosting policy not be added to or enhanced in any way to appear more like, or to substitute for, the published journal article.

Published journal article (JPA): A published journal article (PJA) is the definitive final record of published research that appears or will appear in the journal and embodies all value-adding publishing activities including peer review co-ordination, copy-editing, formatting, (if relevant) pagination and online enrichment.

Policies for sharing publishing journal articles differ for subscription and gold open access articles:

Subscription Articles: If you are an author, please share a link to your article rather than the full-text. Millions of researchers have access to the formal publications on ScienceDirect, and so links will help your users to find, access, cite, and use the best available version.

Theses and dissertations which contain embedded PJAs as part of the formal submission can be posted publicly by the awarding institution with DOI links back to the formal publications on ScienceDirect.

If you are affiliated with a library that subscribes to ScienceDirect you have additional private sharing rights for others' research accessed under that agreement. This includes use for classroom teaching and internal training at the institution (including use in course packs and courseware programs), and inclusion of the article for grant funding purposes.

Gold Open Access Articles: May be shared according to the author-selected end-user license and should contain a CrossMark logo, the end user license, and a DOI link to the formal publication on ScienceDirect.

Please refer to Elsevier's posting policy for further information.

18. **For book authors** the following clauses are applicable in addition to the above: Authors are permitted to place a brief summary of their work online only. You are not allowed to download and post the published electronic version of your chapter, nor may you scan the printed edition to create an electronic version. **Posting to a repository:** Authors are permitted to post a summary of their chapter only in their institution's repository.

19. **Thesis/Dissertation**: If your license is for use in a thesis/dissertation your thesis may be submitted to your institution in either print or electronic form. Should your thesis be published commercially, please reapply for permission. These requirements include permission for the Library and Archives of Canada to supply single copies, on demand, of the complete thesis and include permission for Proquest/UMI to supply single copies, on demand, of the complete thesis. Should your thesis be published commercially, please reapply for permission. Theses and dissertations which contain embedded PJAs as part of the formal submission can be posted publicly by the awarding institution with DOI links back to the formal publications on ScienceDirect.